# THE CRYSTAL GROWTH AND STRUCTURE

# OF SOME VANADIUM CARBON ALLOYS

by

J. BILLINGHAM, B.Sc.

A dissertation submitted

to the University of Warwick for

admission to the degree of

Doctor of Philosophy

School of Physics

January 1971.

# MEMORANDUM

This dissertation is submitted to the University of Warwick in support of my application for admission to the degree of Doctor of Philosophy. It contains an account of my own work performed at the School of Physics of the University of Warwick in the period October 1967 to October 1970 under the general supervision of Dr.M.H.Lewis. No part of it has been used previously in a degree thesis submitted to this or any other University. The work described in this thesis is the result of my own independent research except where specifically acknowledged in the text.

J. Billingham

JANUARY 1971

J. Billingham

# PUBLICATIONS.

Certain parts of the work reported in this thesis have been published, or are in the course of publication, in scientific journals as follows:-

(1) The paper "Order-Disorder Transformations in Vanadium Carbide" VII$^{th}$ Congrès International de Microscopie Électronique, Grenoble, Vol 2, 477, (1970), written with Dr.M.H.Lewis describes briefly some of the results presented in sections 4.3, 4.4, and 4.5 of this thesis.

(2) The paper "Dislocation Mechanisms for the Nucleation of Transformations in Vanadium Carbide" written with Dr.M.H.Lewis and based on section 4.4 of this thesis, is to be published shortly in Phil.Mag.

Further parts of the thesis may be submitted for publication elsewhere in due course.

## ACKNOWLEDGEMENTS

I should like to thank Professor A.J.Forty for making available to me the facilities of the laboratories at the School of Physics. I am extremely grateful to Dr.M.H.Lewis for his interest and advice throughout the course of this work, particularly with regard to the electron microscope studies and the preparation of this thesis. Furthermore I should like to thank all those members of the School of Physics who have been available for discussions on a variety of topics.

Thanks are also due to Mr.H.G.Ellacott and his workshop staff, particularly Messrs.E.C.Billington and A.F.Boyer, for their help in constructing the crystal growth apparatus.

My thanks are due to the Science Research Council for providing the financial support of a Research Studentship.

The help of Mrs. C.Allsopp in the preparation of the figures is gratefully acknowledged. Finally, I should like to thank my wife Heather, for her patience and encouragement throughout, and also for her care and attention in typing this thesis.

## ABSTRACT

The influence of ordering on the structure of vanadium carbon alloys has been studied using electron microscopy and electron diffraction. Within the nominally cubic (rocksalt) phase field of the vanadium carbon system non-stoichiometry occurs by the formation of carbon vacancies, and these have been shown to be always distributed in a non-random manner at low temperatures (below 1300°C). The cubic phase field has been shown to contain two ordered compounds both of which exist over a range of stoichiometry, and in addition a region exhibiting a form of short range order. The order-disorder temperature has been determined from metallographic changes occurring in quenched samples annealed at successively higher temperatures, and a revised equilibrium diagram proposed for this compositional region.

In order to produce the high purity single crystals of different composition required for this structural study, a floating zone melting apparatus has been designed and built to operate with r.f.heating under a positive pressure of ambient inert gas to reduce volatalisation losses. Crystal growth experiments using this apparatus are described.

The ordered compound $V_6C_5$ has been found to exist over a wide range of stoichiometry from $VC_{0.75}$ to $VC_{0.86}$. Two forms of ordered structure having monoclinic and trigonal symmetry are obtained, and duplex structures consisting of small highly faulted regions of both structures are obtained. Possible mechanisms and reasons for the formation of this type of structure are discussed. The alloys contain a high density of planar faults and these are analysed and discussed

in terms of possible fault vectors for the proposed structures. A long period superlattice is formed at high temperatures at compositions near to $VC_{0.84}$ whose formation is explained in terms of a crystallographic shear structure.

At higher carbon contents the cubic $V_8C_7$ compound exists from $VC_{0.87}$ to $VC_{0.90}$ and is characterised by a foam structure of anti-phase domain boundaries which have been analysed in terms of possible fault vectors. Both the cubic $V_8C_7$ and non-cubic $V_6C_5$ forms of ordered carbon atom arrangements are seen in alloys with intermediate compositions and the formation of such structures is discussed.

Above the order-disorder temperature and at lower carbon contents ($< VC_{0.75}$) the carbon atom arrangement indicates a form of short range order detectable by broad diffuse bands in diffraction patterns. Possible models for this type of structure are discussed. In addition these lower carbon alloys contain large numbers of intrinsic stacking faults bounded by Shockley partial dislocations. A dislocation mechanism is proposed whereby these faults are nuclei for the transformation to the $\zeta$-phase detected at lower carbon contents. This phase has a complex twelve layer metal-atom stacking sequence.

Finally an explanation for the formation and stability of the ordered compounds is given in terms of both electronic and structural considerations, and the possible role these structures might have on mechanical properties is discussed.

CONTENTS

# CHAPTER ONE

# INTRODUCTION

## 1.1 Non-Stoichiometry In Crystalline Materials

In the latter half of the 18th Century the Law of Definite or Constant Proportions was formulated by Proust who determined the composition of a large number of minerals and inorganic compounds in which the constituent elements were present in definite proportions, and usually in simple whole number ratios e.g. NaCl, $TiO_2$, $Al_2O_3$. Berthollet disputed this law at the time, claiming that elements could combine in varying proportions, and that substances which formed with definite proportions were merely special cases of the general rule. Shortly afterwards Dalton's work on the indivisibility of atoms seemed to verify Proust's ideas, and these became generally acceptable. This law remained a basic law of chemistry until the early part of the 20th Century when Kurnikow, in his studies of metallic phase equilibria, found a number of metallic compounds that were stable over a range of composition. He called these compounds 'Berthollides' which contrasted with compounds of constant compositions which he termed - 'Daltonides'. Although the name 'Berthollide' is still used in some of the Russian literature the term 'non-stoichiometric compound' is now almost universally used for such a material. Thus the term non-stoichiometric compound simply indicates that the compound is not made up of stoichiometric ratios of elements. In practice all crystalline inorganic compounds have a definite composition range of stability, called the

homogeneity range i.e. they are all non-stoichiometric to a greater or less extent; thus it is more correct to speak of non-stoichiometry in compounds rather than non - stoichiometric compounds.

Non-stoichiometry in crystals may be accommodated by the formation of structural defects. Such defects as the Schottky (vacancy), Frenkel (interstitial-vacancy pair), or substitutional types are present in varying proportions in all crystals of any temperature above absolute zero. Their concentration is dependent both on the energy of formation of the defect and on the temperature, and usually one type of defect predominates in any one system.

Thus if one considers a compound with Schottky defects i.e. vacant lattice sites, then the concentration of vacant sites of one species may be different from that of the other e.g. if the concentration of M vacancies is less than that of X vacancies in the compound MX, then metal atoms will be present in excess and the formula can be written as $MX_{1-x}$ when x is a measure of the excess of X vacancies over those of M.

In addition to the three main types of lattice defect there are three others that are theoretically possible but only one of which has so far been identified. These are the anti-Schottky defects which consist of equal numbers of M and X interstitials, a combination of inter - stitial and substitutional defects such that there are X interstitials and M atoms on X sites or M interstitials and X atoms on M sites, and thirdly a combination of sub - stitutional defects and vacancies such that M vacancies are

present and M atoms are also on X sites. This third possibility has been indentified[1] in the compound NiAl where Ni vacancies co-exist with Ni atoms on Al sites.

Using a statistical thermodynamic approach Schottky and Wagner[2] in 1930 showed that crystalline inorganic compounds were normally non-stoichiometric. Following this work extensive experimental evidence, especially X-ray diffraction work, indicated that non-stoichiometry was common in oxides, carbides, nitrides, borides, silicides and chalcogenides as well as in intermetallic compounds. A number of review papers covering this subject have been published including work on hydrides[3] intermetallic compounds[4], oxides and chalcogenides[5] and nitrides and carbides[6].

Non-stoichiometric compounds can be broadly divided into two types, one showing only very small deviation and the other gross departure from the ideal stoichiometric composition. Examples of the first type are alkali halides containing F-centres, $Cu_2O_{1-x}$, and $PbS_{1-x}$, in which the defects are usually detected by special techniques and can be considered as randomly distributed, so that the Schottky Wagner theory can apply. The second group covers gross departures from stoichiometry e.g. $TiC_{0.5}$ to $TiC_{1.0}$ and $TiO_{0.67}$ to $TiO_{1.26}$, and these materials contain large numbers of atoms with a different co-ordination from that existing in stoichiometric crystals, which could possibly lead to the formation of more stable structures. This is the type of compound with which this dissertation is concerned.

### 1.1.1. Structural Accommodation Of Gross Non-Stoichiometry

The intrinsic defect concentration, and therefore the ease of deviation from stoichiometry, can be affected by the type of chemical bonding in the compound, the relative size of the atoms or ions, and the variable valence of ions in ionic compounds. Generally covalent compounds show smaller deviations from stoichiometry than ionic or metallic compounds, and this can be attributed to the special directional properties of the bonds in these compounds. Naturally the greater the strength of the chemical bond the smaller in general will be the defect concentration. Interstitial atoms must be of such a size to be able to fit into an interstice without too great an expenditure of energy, and in the case of substitutional defects the size difference must not be too great for similar reasons. The transition metals which can exist in more than one valence state frequently form non-stoichiometric compounds since the electrons and holes can manifest themselves as changes in valence of the ion.

The existence of such large concentrations of defects as are present in oxides such as TiO leads to doubts concerning the thermodynamic stability of such structures with respect to other possible structures. These doubts are strengthened by the large numbers of ordered intermediate phases that have been discovered in recent years in phase diagrams previously reported to contain non-stoichiometric compounds with broad homogeneity ranges. This is especially true if the non-stoichiometric compound contains a metal of high atomic number and the original examination was by

X-ray diffraction techniques which will not readily reveal anomalies in the non-metal lattice (see section 4.3). The problem can only be properly considered in terms of the relative energies of the ordered and disordered structures at different temperatures. The defects in the crystal may attract each other thereby forming clusters, or repel one another which, when combined with the attractive forces between atoms, leads to ordering of the defects.

If a simple binary system consisting of A and B atoms is considered then at low temperature the most stable configuration is complete long range order with A and B atoms existing in different sublattices. As the temperature is increased the configurational entropy markedly increases, and more random atom arrangements are set up. In fact above a certain critical temperature (the order disorder temperature) the long range order is completely destroyed, and A and B atoms are arranged randomly throughout the crystal. However even in this so called 'disordered state' there is the possibility[7] of the existence of some order in the form of small microdomains. There is widespread experimental evidence[5] that many non-stoichiometric compounds are disordered at high temperature but form ordered compounds falling within the composition range on cooling. However the detection of ordered phases at lower temperature is often complicated by the requirement that long periods of heat treatment are necessary to develop the structure. Alternatively the non-stoichiometric compound may transform into two unrelated phases on annealing at low temperatures.

The Schottky-Wagner theory cannot be used to explain

results in systems with gross deviations from stoichiometry since an additional effect is present, namely the mod - ification of the structure with composition. No precise theory has been worked out but a general structural picture of the way in which the deviations occur can be given (following Wadsley[5]) in five broad categories:-

(1) Substitution.

This simply entails the substitution of one element M, on the lattice of the other X, and is common in intermetallic compound and chalcogenide systems.

(2) Interpolation

The introduction of an excess of one component M or X in a binary compound MX, is often called interstitial solid solution. Examples of this are interstitial compounds of metals, and interpolation of additional metal atoms between adjacent sheets of a layer structure in many chalcogenides

(3) Subtraction

In this case either M, X or both simultaneously,in unequal and variable amounts may be absent from the structure. Various oxide and carbide systems show examples of this type.

(4) Shear

This involves the removal of oxygen atoms from certain types of compound e.g. $TiO_2$ and $Nb_2O_5$ and compression of the structure along certain planes by a process known as 'crystallographic shear (8) '. Thus it is a special form of the subtraction case in which the vacant sites are ordered in a planar form resulting in

superlattices known as shear structures. In this process the cation co-ordination is unchanged but the anion co-ordination is increased to accommodate a reduced atom ratio of non-metal to metal. The sheets of atoms of changed co-ordination constitute boundaries between blocks of unchanged structure. In the simplest case all shear planes are parallel and regularly spaced, and a reduced oxide can be derived from a simple parent structure ($ReO_3$ or rutile types) by shear in one direction only. This enables a homologous series of structures (or Magneli phases[9]) to be identified with general formulae such as $Ti_nO_{2n-1}$[10] with n taking values from 4 to 10. In all cases the shear planes are arranged at regular intervals parallel to specific parent planes e.g. $(1\bar{2}1)$ rutile, and their separation increases with increasing n, When the shear planes are not ordered it is thought that they are possibly retained in a dis - ordered form which is difficult to recognise in the high temperature non-stoichiometric compound.

(5) Intergrowth

The parallel intergrowth of two phases of different composition can occur. The structures of the phases are usually closely related e.g. $Sr_2TiO_4$ consists of single perovskite like sheets interleaved with SrO (NaCl-type) sheets. Other examples are seen in the $BaO-TiO_2$ system.

In the present context the two most important classifications are subtraction and shear. In the transition metal carbon systems, treated in more detail in section 1.2, subtraction of the non-metal usually occurs to cause

deviation from stoichiometry; however, in the related oxide systems both metal and non-metal can be absent. Thus in TiO, which can exist from $TiO_{0.67}$ to $TiO_{1.26}$ all the titanium sites are filled at $TiO_{0.67}$ and 38% of the oxygen sites are vacant, while at $TiO_{1.26}$ all oxygen sites are occupied and 22% of the titanium sites are vacant . At the stoichiometric composition TiO approximately 15% of the sites on both sublattices are unoccupied.

The vacant lattice sites in both carbides and oxides may be ordered and result in the formation of a superlattice of carbon or oxygen atoms and vacancies. The metal atom sub-lattice may be retained with only small distortions in atom positions from that of the disordered structures.

### 1.1.2 Property Changes Accompanying Non-Stoichiometry

Certain properties of solid compounds such as chemical reactivity, mechanical strength, and electrical conductivity are strongly affected by the degree of non-stoichiometry. Most solid state reactions take place by the movement of lattice defects and hence the reactivity of a solid is expected to show strong dependence on both the direction and extent of non-stoichiometry. The most important class of reaction affected in this way for most solids is oxidation, and it is the non-stoichiometry of the reaction product that must be considered. During oxidation, if the oxide layer remains intact, further oxidation depends on the movement of metal atoms to the oxide-gas surface, or gas atoms to the metal surface. These diffusional type processes are accomplished by the movement of defects and are therefore strongly affected by the number of defects

present and hence by the non-stoichiometry. Sintering is another process which can be strongly affected, the rate of sintering normally increasing with deviation from stoichiometry. The extent of short range order in the system can also effect the reactivity, for example it is thought to play an important role in stress corrosion properties[11].

There is ample evidence that non-stoichiometry has an important effect on the mechanical properties of many compounds. The strength at high temperatures usually decreases as the deviation from stoichiometry increases, an effect which has been attributed[12] to the variation of lattice friction stress occurring when the composition and hence the bonding is altered. Thus increased deviation from stoichiometry produces a lowering of the yield strength in titanium carbide[13] and an increase in the creep rate of uranium dioxide[14]. Ashbee and Smallman[15] on the other hand found that non-stoichiometric rutile ($TiO_2$) had a yield strength which was an order of magnitude greater than that of the stoichiometric composition. The effect of non-stoichiometry on the mechanical properties of intermetallic compounds has been briefly reviewed by Westbrook[16].

Deviations from non-stoichiometry effect the electrical conductivity because the presence of anion vacancies or metal interstials in a compound, results in an excess number of electrons in the lattice and the crystal becoming an n-type conductor, or conversely metal vacancies or anion interstials lead to an excess number of holes and p-type conduction. Thus for example cadmium sulphide and zinc oxide are always n-type conductors due to the presence

of excess amounts of sulphur vacancies or zinc interstitials. The degree of conduction will vary with the extent of deviation from stoichiometry since the number of carriers is directly related to the number of defects which in turn determines the non-stoichiometry.

## 1.2 Non-Stoichiometry In Transition Metal Carbides

### 1.2.1 Phase Equilibria And Structures

The transition metal carbides have a number of interesting properties which include extremely high melting points, high hardness and resistance to chemical attack. These properties make them attractive as possible high temperature structural materials, but because of their extreme brittleness they may have to be incorporated in a composite structure. Their extremely high hardness is made use of in their more well known application as cutting materials. Their structures and phase relationships have been widely studied, and reviews have been published by Schwartzkopf and Kieffer[17] Goldschmidt[18] and Storms[19].

The carbides possess relatively simple crystal structures based on an arrangement of close packed transition metal atoms with carbon atoms positioned in the octahedral interstices. Deviations from stoichiometry can occur because not all octahedral interstices may be occupied by carbon atoms. Thus the carbides are subtraction compounds in the earlier classification (1.1.2).

Examination of the various reported equilibrium diagrams[20] (fig. 1.1) reveals many similarities, especially within any one group of elements in the periodic table.

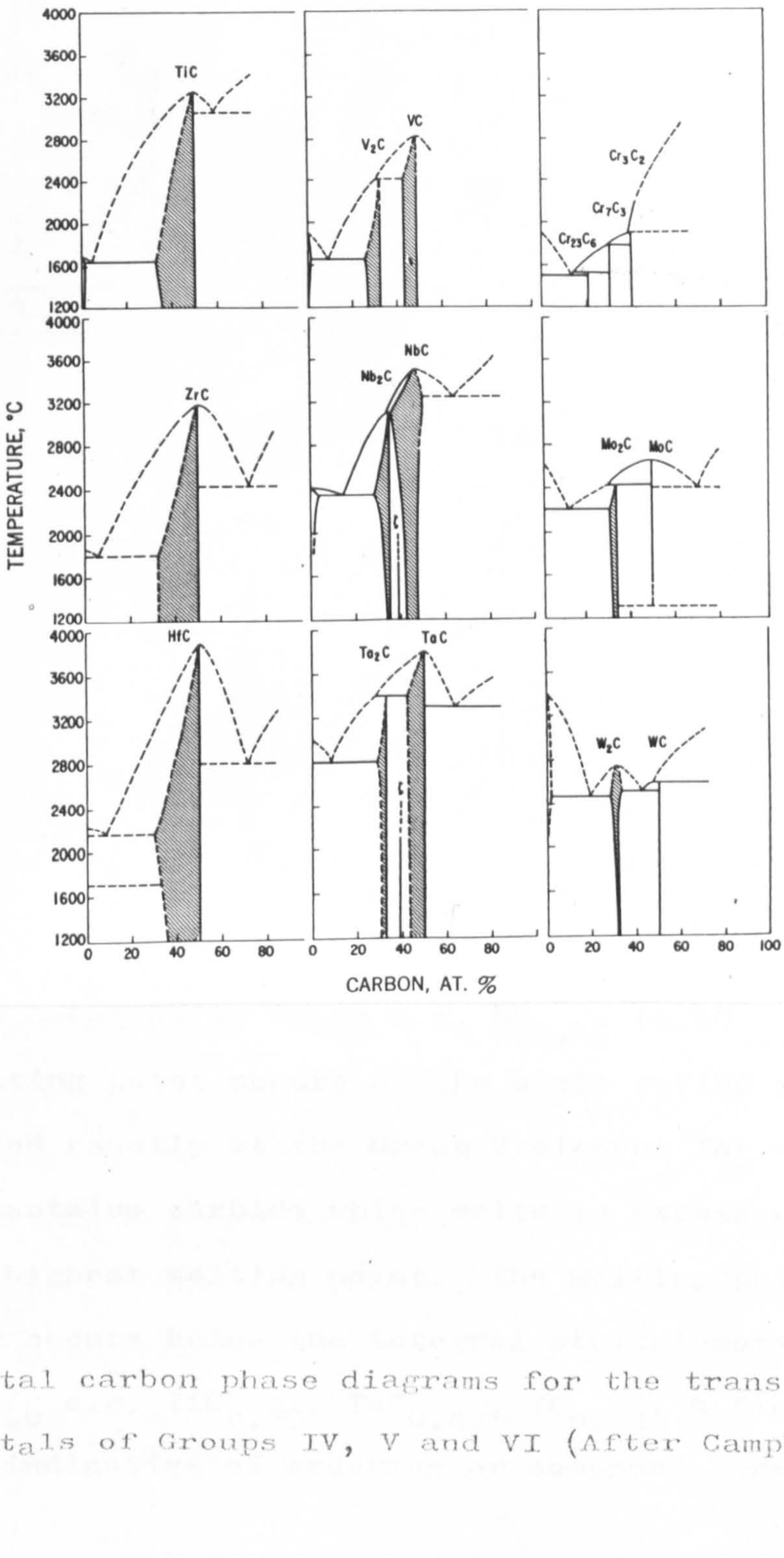


Fig. 1.1 Metal carbon phase diagrams for the transition metals of Groups IV, V and VI (After Campbell[20])

The most stable phase is always the one containing the highest amount of carbon which forms either at or below a composition corresponding to $MC_{1.0}$ and has a rock-salt structure with the metal and carbon atoms on face centred cubic sublattices. If another phase forms, it does so near the composition $MC_{0.5}$, with a structure which is close packed hexagonal if only the metal lattice is considered. Both of these phases can accommodate deviations from stoichiometry but the homogeneity range of the cubic mono-carbide phase (MC) is usually the most extensive. The carbon solubility in the body centred cubic structure at the metal rich end of the diagram is usually very small.

The most extensive homogeneity range is shown by the Group IV mono-carbides TiC, ZrC, and HfC, but no dicarbide phase is formed in these systems. Extremely high defect concentrations are possible in these alloys e.g. $TiC_{0.5}$ stable at high temperatures has only half the octahedral interstices occupied and a defect concentration of 25%. The Group V elements have a less extensive mono-carbide homogeneity range usually from approximately $MC_{0.70}$ to $MC_{1.0}$, but in addition form a hexagonal dicarbide which usually has a much narrower homogeneity range e.g. $MC_{0.45}$ to $MC_{0.50}$.

The maximum melting point occurs at the sixth period within any one Group and usually at the Group V element for any one period. Thus tantalum carbide which melts in excess of 4000°C has the highest melting point. The melting point maximum usually occurs below the integral stoichiometric composition $MC_{1.0}$ e.g. $TiC_{0.87}$, $TaC_{0.82}$, $VC_{0.83}$, a factor which is often indicative of ordering or compound formation

in the solid state. It is interesting to note that the integral stoichiometric value $MC_{1.0}$ is rarely reached, the maximum discrepancy being shown by the Group V carbides, and VC in particular which terminates at $VC_{0.89}$. The reason for this behaviour is not known although it is possibly associated with the electronic structure. Lye[21] was able to explain this on the basis of band structure calculations which showed that at $VC_{0.89}$ the bonding states of the d-band are completely occupied. The addition of further carbon atoms to the alloy merely contributes electrons to anti-bonding d-states and hence favours the formation of graphite as an additional phase.

The Group VI carbides are generally less stable than those of the other Groups and can form additional compounds at compositions corresponding to $M_{23}C_6$, $M_7C_3$, $M_5C_3$ and $M_3C_2$. Only slight similarities occur between molybdenum and tungsten carbide, and none between these and chromium. In spite of its lower stability the hardness of tungsten carbide is high enough to ensure widespread use in the hard-metal industry when associated with cobalt.

Deviations from stoichiometry are always caused by defects in the carbon sublattice and never by metal interstitials, but the remaining carbon atoms may take up ordered arrangements. This leads to the formation of super-lattice lines in diffraction patterns. In the case of titanium and vanadium these should be detectable in X-ray diffraction patterns, but for all the heavier transition metals neutron or electron diffraction experiments are required in order to detect the superlattice and ordered

carbon arrangement. The vanadium and titanium carbide systems have been widely studied using X-ray diffraction techniques and although order has been reported in the vanadium carbide system, both in the mono-carbide and dicarbide phase fields (see section 1.3 for more detail) no order was found in titanium carbide. The neutron diffraction experiments of Gorbunov et al.[22] also indicated that random carbon atom arrangements existed throughout the whole titanium mono-carbide phase field. Recently however Goretzki[23] using the same technique, has found ordered carbon atom arrangements in both the titanium and zirconium carbide systems, and Zubkov et al.[24] in niobium and tantalum mono-carbides. Other ordered arrangements have been found in the dicarbide phase fields of the vanadium[25], niobium[25] tantalum[26a] and molybdenum[26b] systems.

### 1.2.2 Structural Notation

Parthé and Yvon[27] recently suggested a new notation for describing the crystal structures of the close packed transition metal carbides based on the structural features of the phases. This was in order to counteract confusion in the present literature due mainly to the use of Greek prefixes to denote different phases, which has led to the same phase being given a different prefix by different authors, or different phases being given the same prefix. The proposed notation consists of the Jagodzinski-Wyckoff[28] symbol for the stacking sequence of the close packed metal atom layers, followed by the space group of the compound to distinguish between different arrangements of the carbon atoms in the octahedral interstices.

Five different stacking variations can be distinguished for the transition metal atoms in the close packed carbides. These stacking sequences can be represented as in fig. 1.2 by describing the structures with hexagonal unit cells and showing the atom arrangements in the $(11\bar{2}0)$ plane. The stacking sequence of the hexagonal metal layers can be described by the Jagodzinski- Wyckoff symbols[28]: h for $T_2C$, hcc, and hhc for $T_3C_2$, hhcc for $T_4C_3$, and c for TC. These symbols form the first part of the proposed Parthé and Yvon notation.

The number of octahedral interstices in any close packed structure is equal to the number of atoms, and does not depend on which way the hexagonal metal layers are stacked. Thus it might be expected that all carbides would have the maximum composition TC but phase diagram studies have shown that it is only in the case of metal stacking c (i.e. TC) that all the octahedral interstices can be filled, and even in this case there are exceptions e.g. VC which extends only to $VC_{0.89}$. All other stacking sequences contain unoccupied interstitial sites and the compositions for maximum carbon content are $T_2C$, $T_3C_2$, and $T_4C_3$ as shown in fig. 1.2. Thus the stacking symbol also indicates the highest possible carbon content for each form of stacking. If one considers the interactions between atoms it is not unreasonable that there exists a restriction on the occupation of the octahedral interstices by carbon atoms that depends on the stacking of the metal atom layers. In particular if two interstices are located directly above one another in the $(11\bar{2}0)$ plane then only one site will be occupied, the

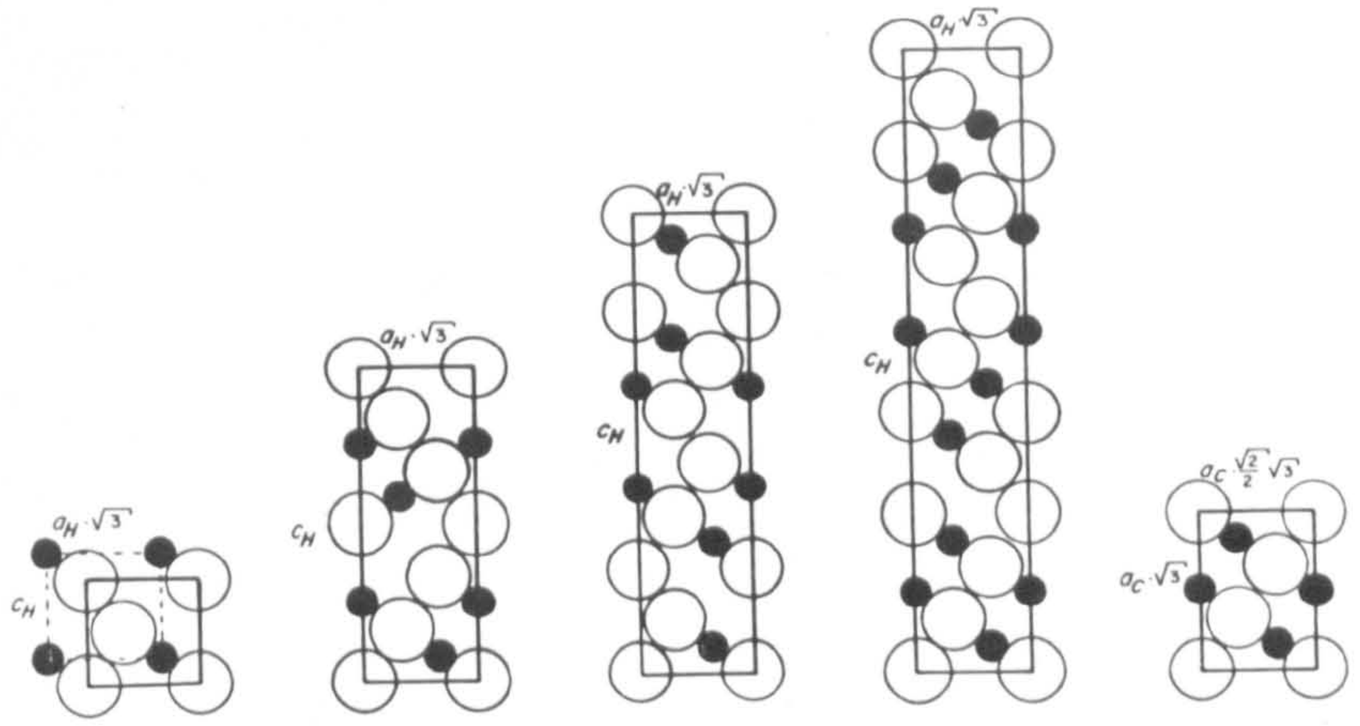


| | | | | | |
|---|---|---|---|---|---|
| Theoretical carbide composition with highest carbon content | $T_2C$ | $T_3C_2$ | $T_3C_2$ | $T_4C_3$ | TC |
| Symbol of metal layer stacking after Jagodzinski-Wyckoff | *h* | *hcc* | *hhc* | *hhcc* | *c* |

Fig. 1.2 Stacking variations of hexagonal metal atom layers in the close packed transition metal carbides. Metal atoms (large open circles) are shown in their arrangement in the $(11\bar{2}0)$ plane of the corresponding hexagonal unit cells. The carbon atoms are represented by small black circles.

other remaining unoccupied (this happens with every h stacking of the metal layers). Neutron diffraction experiments have shown that this rule holds universally for the close packed transition metal carbides, and this can in fact be used to calculate compositions of hypothetical close packed carbide phases after making assumptions concerning the metal atom layer stacking.

The second part of the poposed notation is the Schoenfies space group symbol, since for a given metal layer stacking and carbon content a number of different structures can be formed depending on how the interstices are filled by the carbon atoms. Parthé and Yvon have listed all the possible structure types for disordered and ordered carbon atom arrangements in all the different metal atom stacking variations. Thus for 'h' metal atom stacking there are six different carbide structures, and for 'c' stacking only one type if all carbon interstices are occupied. However most cubic close packed metal atom carbides can exist with carbon deficiency[19], and at least four defect structures in 'c' type stacking have been determined at the present time[27]. Most NaCl defect type structures follow the rule that alternate carbon layers are full and defects only occur in the carbon layers between them. Thus to describe these structures it is usually only to indicate the carbon atom arrangement in the defect containing layers.

## 1.3 Non-Stoichiometry In The Vanadium-Carbon System

There have been a number of recent experimental determinations of the vanadium carbon equilibrium diagram by Storms and McNeal (1962)[29], Adelsberg and Cadoff (1968)[30] and Rudy et al.(1968)[31]. The main difference between them was that Storms and McNeal reported peritectic melting of the VC phase whereas both later investigations reported a congruent melting point and consequently the formation of a eutectic between the mono-carbide and graphite. These later phase diagrams are shown in fig. 1.3. The phase diagram is similar to that of the other Group V transition metal carbides in having a cubic VC phase field with wide deviation from stoichiometry with a much smaller deviation in the hexagonal $V_2C$ phase field. The cubic VC phase melts at approximately 2650°C and extends from $VC_{0.72}$ to $VC_{0.88}$ at 1000°C and over a wider range at higher temperatures. The extent to which the composition of the upper phase boundary deviates from the $VC_{1.0}$ ratio is unusually high compared with the other carbides. The $V_2C$ hexagonal phase is found between $VC_{0.47}$ and $VC_{0.50}$ at 1000°C and again over a considerably wider range at higher temperatures. Carbon solubility in the metal is small, being less than 1% at 1000°C.

Another phase reported in this system is the $\zeta$-phase reported initially by Storms and McNeal[29], and more recently by Rudy et al.[25] and Yvon and Parthé[32] which is analogous to the intermediate compounds reported for the niobium carbon[33] and tantalum carbon systems[34.35]. The structure of this phase has only recently been determined

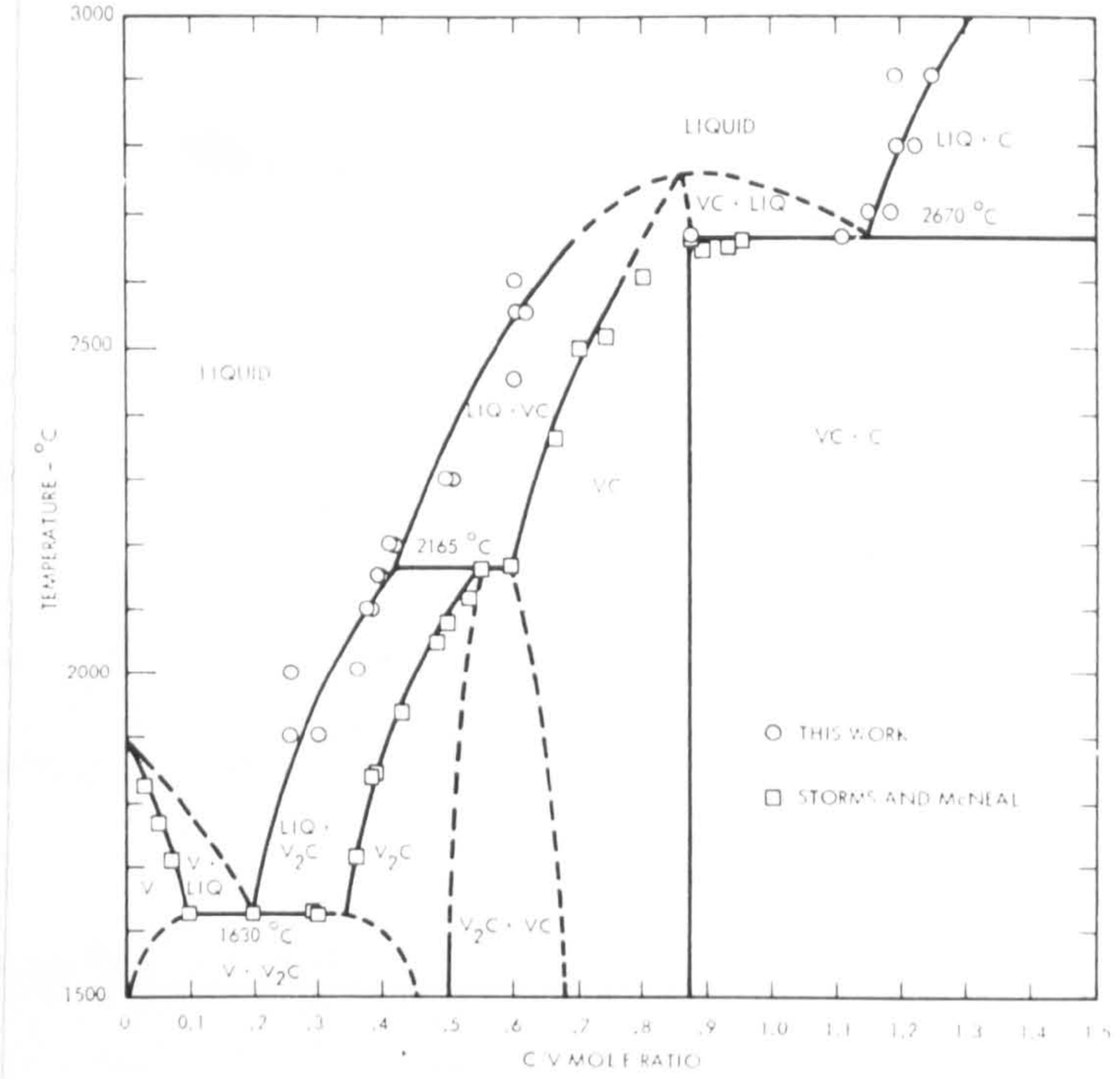


(a)

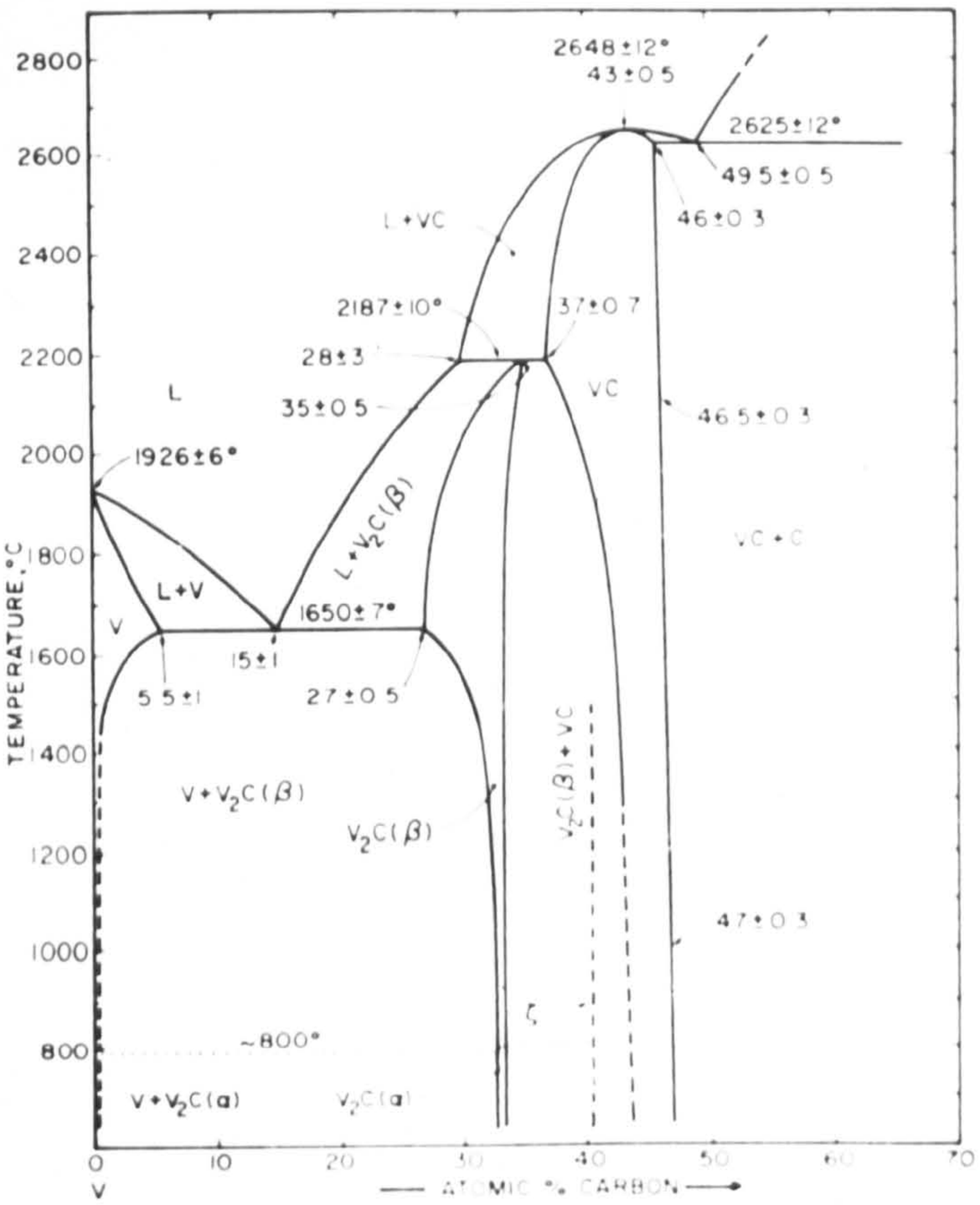


(b)

Fig. 1.3 Vanadium carbon phase diagram.

(a) After Adelsberg and Cadoff[30]

(b) After Rudy et al.[31]

and its homogeneity range with respect to composition and temperature is still not accurately known.

Ordering of the carbon sublattice has been reported throughout the phase diagram including compositions in both of the main carbide phase fields. In addition at very low carbon concentrations the electron microscope study of Thomas and Villagrana[36] indicated a compound $V_{64}C$ formed by an ordered distribution of the interstitial atoms in the octahedral positions in the metal lattice. A similar phase has also been reported by the same workers in the tantalum carbon system[37].

The hexagonal divanadium carbide($\beta$) which has a disordered carbon sublattice and is stable at high temperature is reported to transform at approximately 800°C into an orthorhombic ($\alpha$) modification which is associated with ordering in the carbon sub-lattice[25]. Russian workers[38] indicated that trace impurities of oxygen and nitrogen had an important effect in facilitating the hexagonal to orthorhombic phase change, and there still exists some discrepancies with respect to the exact structure of the ordered phase and to its mode of transformation.

In the mono-carbide phase field the nuclear magnetic resonance studies of Froidevaux and Rossier[39] indicated that the carbon sub-lattice exhibited order throughout the entire composition range. In addition Alyamovski et al.[40] studied infra-red absorption spectra and concluded that strong short range order was present at compositions $VC_{0.86}$ and $VC_{0.75}$ in the mono-carbide region, and $VC_{0.49}$ in the dicarbide phase field.

A cubic superlattice was identified at $VC_{0.88}$ by de Novion et al.[41] using X-rays. It was confirmed by Kordes[42] and Alyamovski et al.[43] that at this composition the material should be described in terms of a cubic unit cell with a parameter twice that of the rock-salt unit cell and a composition corresponding to $V_8C_7$. The composition and temperature limits within which this phase is stable were not determined by any of the investigators who mainly used X-ray diffraction techniques to examine pressed and sintered material. According to the Parthé and Yvon notation the structure type is described as a c $(o^6)$ $V_8C_7$ type and the space group is $P4_332$. It is interesting that this structure is the irregular case when defects occur in every layer as apposed to the more usual case when they occur only in alternate layers. Fig. 1.4(a) (after Parthé and Yvon) shows the carbon atom arrangement in $V_8C_7$ contrasted with that in hypothetical $VC_{1.0}$ by considering the projection on the hexagonal base plane, whereas in fig. 1.4(b) the model of de Novion et al. showing the vacancy distribution in the double cell of $V_8C_7$, is compared with the standard NaCl or B1-type structure of VC.

At $VC_{0.84}$, Venables et al.[44] using a combination of electron diffraction and nuclear magnetic resonance techniques showed that the superlattice symmetry became hexagonal (trigonal) due to the ordered arrangement of the carbon atoms, and exhibited a domain structure which was visible under polarised light and electron microscope examination. The structure type was c $(C_3^2)$ $V_6C_5$ type using the Parthé and Yvon notation (fig. 1.5). $V_6C_5$ can be viewed

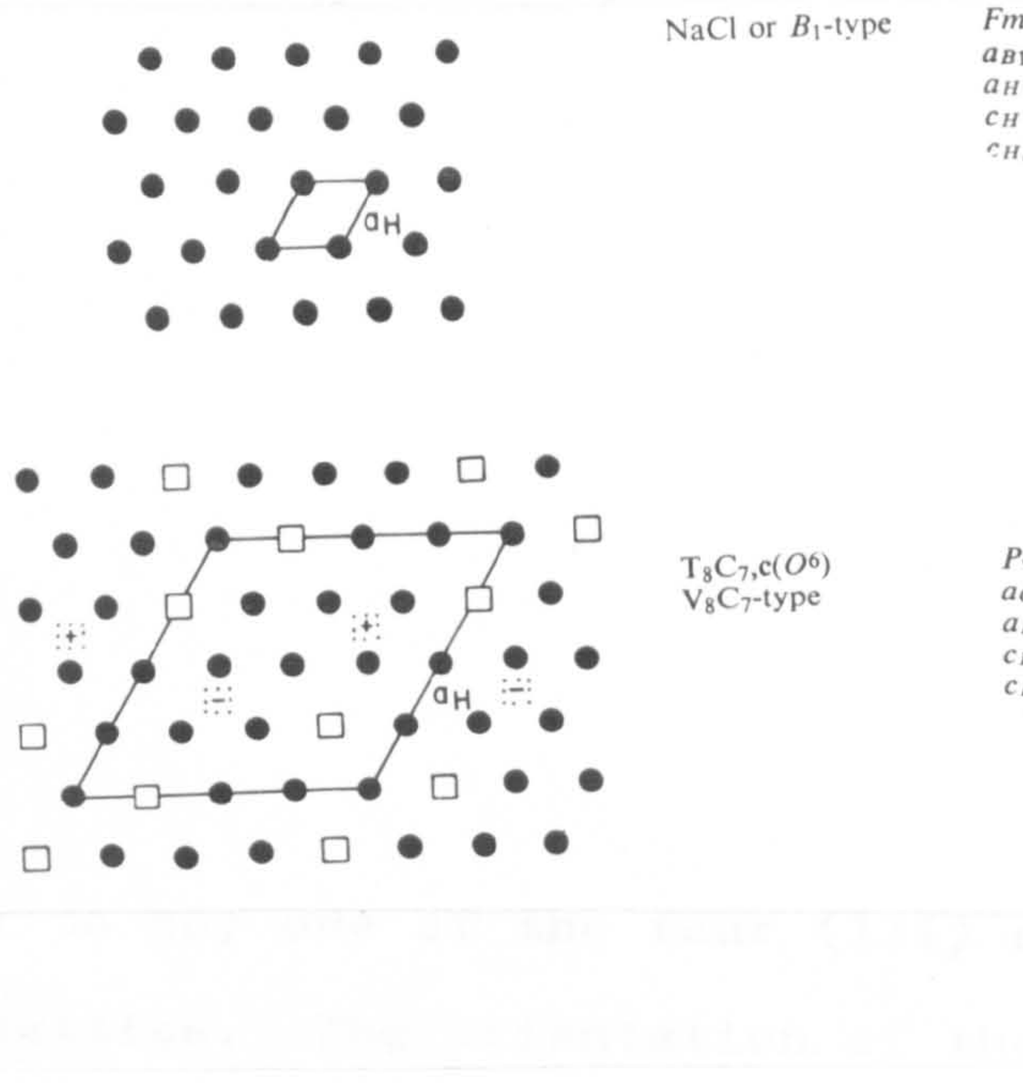


Fig. 1.4 Structure of $V_8C_7$

(a) After Parthé and Yvon[27] showing atom arrangement on alternate carbon atom layers.

(b) Model of superlattice double cell de Novion et al.[41] Only the carbon vacancies are shown in the super - structure.

(c) NaCl structure. VC of hypothetical $VC_{1.0}$ composition.

in terms of two interpenetrating sub-lattices; a vanadium atom lattice which is essentially face centred cubic with some small distortion, and a hexagonal superlattice containing all the carbon atoms. The domain structure results because the c-axis of the superlattice can be oriented parallel to any one of the four ⟨111⟩ directions in the vanadium sublattice. The orientation of the super - lattice with respect to the parent lattice is -

$$\langle 00.1\rangle_{SL} \parallel \langle 111\rangle_{PL}$$
$$\langle 10.0\rangle_{SL} \parallel \langle 112\rangle_{PL}$$

The length of the c-axis corresponds to six complete {111} layers of atoms in the cubic lattice, and the a-axis to the carbon-carbon (or metal-metal) atom spacing in the ⟨112⟩ direction of the parent unit cell.

The model of Venables et al. for the proposed structure is illustrated in fig. 1.5.(2) from which it can be seen that carbon vacancies occur in an ordered manner on alternate {111} carbon atom planes in the structure. Each vacant carbon atom site in a partially full plane is separated from its nearest neighbour vacant sites by the atom separation in the ⟨112⟩ direction in the close packed plane. Thus each vanadium atom in the adjacent {111} planes has its co-ordination modified so that it is in contact with the carbon atom vacancy in its first nearest neighbour environment, and the resulting atom ratio corresponds to the composition $V_6C_5$.

An alternative way of viewing this structure is by considering $V_6C_5$ as a trigonal ordered compound with space group $P3_1$ or $P3_2$. The structure is then built up of

(1)

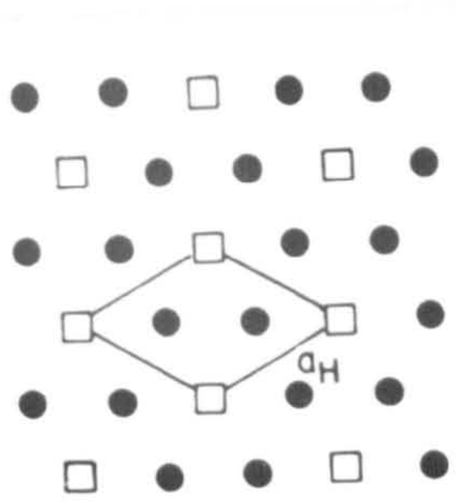


$T_6C_5$, $c(C_3^2)$
$V_6C_5$-type

(2)

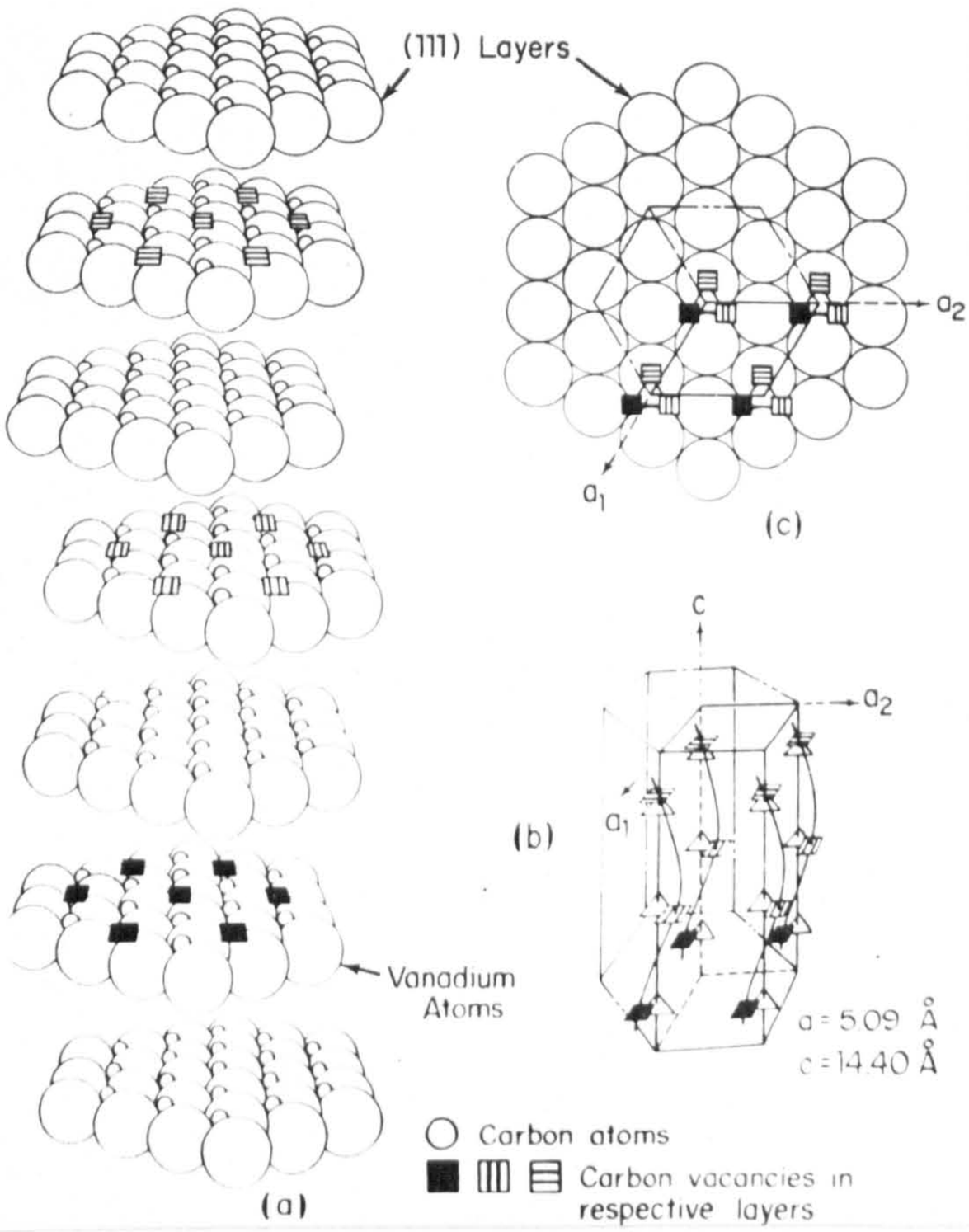


Fig. 1.5 Structure of $V_6C_5$

(1) After Parthé and Yvon[27]. Carbon atom arrangement on alternate carbon atom layers.

(2) After Venables et al.[44] (a) depicts atom arrangement on close packed {111} planes whereas (c) and (b) show how vacancy positions spiral about trigonal unit cell c-axis.

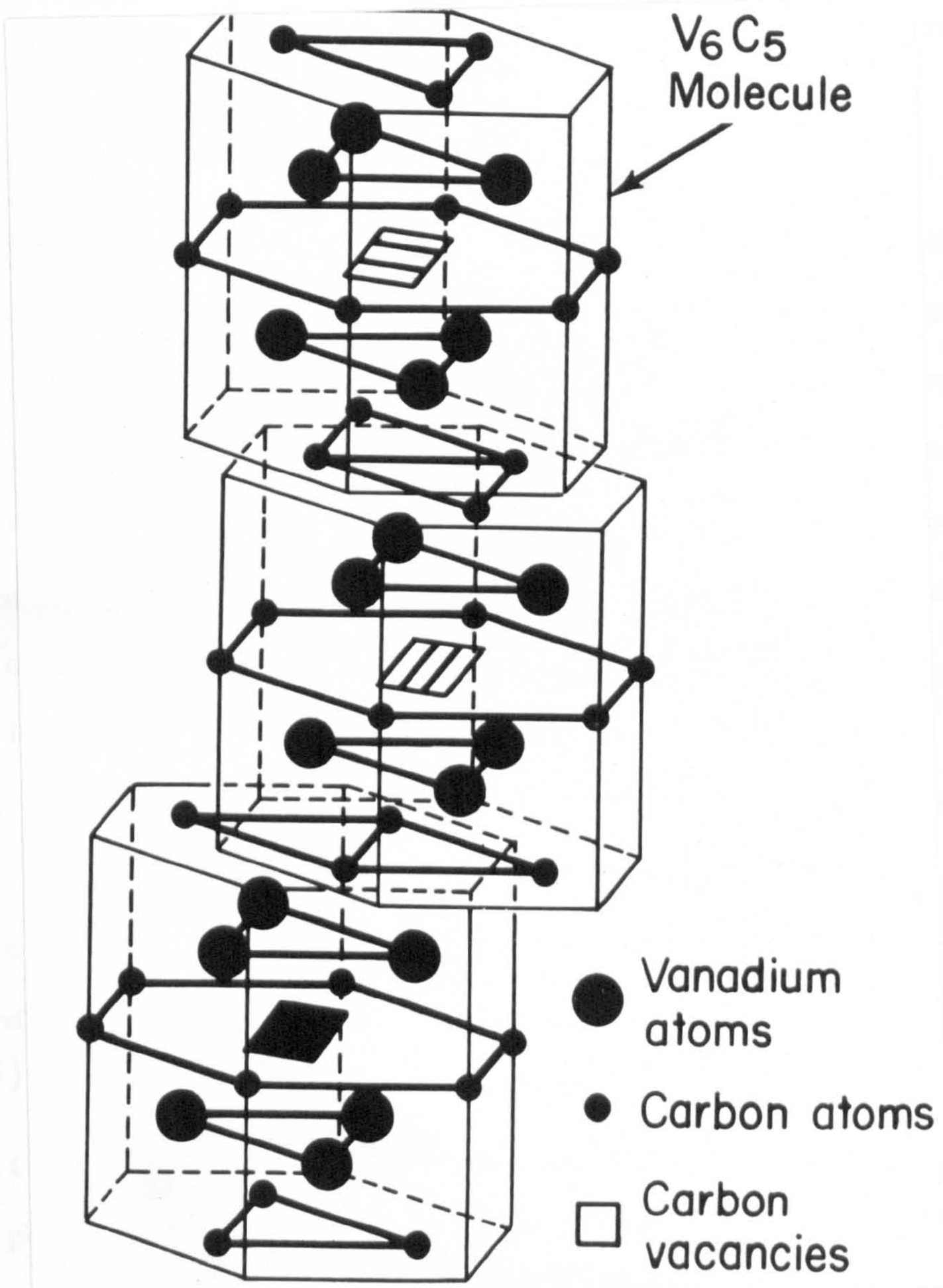


Fig. 1.6 Structure of $V_6C_5$ considered as ordered trigonal compound with space group $P3_1$ or $P3_2$. Right hand spiral form shown although left hand form is equally possible. After Venables et al.[44]

molecules consisting of six vanadium atoms and five carbon atoms and each complete unit cell contains nine molecules (fig. 1.6). The complete structure consists of chains of molecules that spiral about a direction parallel to the c-axis of the unit cell. Both right hand and left hand spiral rotations are possible $P3_1, P3_2$. The domain structure arises because the direction of the spiral axis (the trigonal unit cell axis) may vary in different crystal regions.

The deformation behaviour of vanadium mono-carbide has been shown[45] to be strongly dependent on composition. Thus the greatest high temperature strength is shown by an alloy of composition $VC_{0.84}$ whereas $VC_{0.75}$ and $VC_{0.88}$ are both considerably weaker. This has been attributed to the formation of the ordered compound $V_6C_5$ at this composition ($VC_{0.84}$). The strength is considerably improved by the addition of small amounts of boron which precipitate as vanadium diboride in a finely dispersed form throughout the matrix[45]. In TiC the precipitation of $TiB_2$ was shown to be preferentially nucleated on dislocation nodes[46] and thus held out possibilities of further strengthening by suitable heat treatment schedules.

## 1.4 Aim Of The Present Work

In the vanadium carbon system the work of Froidevaux and Rossier[39] and Parthé and Yvon[32] indicated that other ordered phases might be formed in addition to $V_6C_5$ studied by Venables et al.[44] and $V_8C_7$ by de Novion et al.[41]. Three important questions then arise; how is the structural form of order affected by variations in composition and temperature, by what mechanism do these ordering reactions

take place, and how do the ordered structures affect the mechanical properties.

It was decided to study a range of alloys chosen from within the mono-carbide phase field of the vanadium carbon system in an attempt to answer some of these questions. A study of this kind requires a number of high purity crystals each of known and constant composition for its successful completion. The vanadium carbon system chosen for its structural anomalies, has an additional advantage over the other transition metal carbides for this work since it is more amenable experimentally to crystal growth studies because it has the lowest melting point of all the Group IV and V transition metal carbides (2650°C).

In addition to close control of composition the total impurity content must be kept as low as possible since it is known that impurities can affect reactions of this kind[38]. The presence of grain boundaries, which might modify the diffusion behaviour of the constituent atoms and the distribution of impurity atoms, is also detrimental. For these reasons a planned programme of single crystal growth was undertaken which would additionally provide useful samples for any subsequent deformation studies.

An outline of possible crystal growth techniques and a description of the apparatus used is given in Chapter 2,and the experimental details of a crystal growth programme presented in Chapter 3. The results of a simultaneous electron microscopic and electron diffraction study of the phase structure of alloys with compositions

throughout the entire mono-carbide phase field of the vanadium carbon system, is described in Chapter 4 and forms the major part of this dissertation. Finally in Chapter 5 a correlation is made of the phase structures, previously identified in Chapter 4, for variations in composition and temperature.

## REFERENCES


1. A.J.Bradley and A.Taylor, Proc.Roy.Soc.,A159,56 (1937)
2. W.Schottky and C.Wagner, Z.physik.Chem.(Leipzig) B11, 163, (1930)
3. G.G.Libowitz, in "Non-Stoichiometric Compounds",(R.Gould, ed.) adv.chem,series., 39 (1963)
4. J.H.Westbrook,"Intermetallic Compounds" (Wiley,New York, 1967)
5. A.D.Wadsley, in "Non-Stoichiometric Compounds", (L.Mandelcorn ed.Academic Press,New York,1964)
6. J.Bénard, Inst.interm.chim,Solvay Counseil chim.,Brussels, 1956, 83 (1956).
7. J.M.Cowley,J.Austr.Inst.Met., 11 258 (1966)
8. A.D.Wadsley, Revs.Pure and Appl.Chem.(Australia)5,165,(1955)
9. A.Magnéli,Acta Cryst., 6 495, (1953)
10. S.Andersson and L.Johnberg. Ark.Kemi.21 413 (1963).
11. J.B.Cohen,J.Mater.Sci., 4 1012, (1969)
12. G.E.Hollox,Mat.Science Eng., 3 121,(1968)
13. W.S.Williams,J.Appl.Phys., 35 1329, (1964)
14. W.M.Armstrong and W.R.Irvine, J.Nuclear.Mat. 9,1, (1963)
15. K.H.G.Ashbee and R.E.Smallman,Proc.Roy.Soc., A274,195(1963)
16. J.H.Westbrook,"Mechanical Properties Of Intermetallic Compounds", (Wiley, New York, 1960)
17. P.Schwartskopf and R.Kieffer,"Refractory Hard Metals", (Macmillan,London, 1953)
18. H.J.Goldschmidt, "Interstitial Alloys",(Butterworths, London 1967)
19. E.K.Storms,"The Refractory Carbides",(Academic Press, New York, 1967)

20. I.E.Campbell, in "High Temperature Materials and Technology" eds., I.E.Campbell and E.M.Sherwood, (Wiley, New York 1967).

21. R.G.Lye, Private communication in J.D.Venables PhD. thesis University Of Warwick, 1970.

22. N.S.Gorbunov, N.A.Shishakov, and C.G.Saidkov, Izv.Akad. Nauk.SSSR, 11, 2093, (1961)

23. H.Goretzki, Phys.Stat.Sol., 20, K141, (1967)

24. V.G.Zubkov, L.B.Dubrovskaya, P.V.Gel'd, Y.A.Tskhai and Y.A.Dorafeev, Dokl.Akad.Nauk.SSSR, 184, 874, (1969)

25. E.Rudy and C.E.Brukl, J.Am.Ceram.Soc., 50, 265, (1967)

26a. A.L.Bowman, Acta.Cryst. 19, 6, (1965)

26b. A.L.Bowman, Acta.Cryst. 21, 670, (1966)

27. E.Parthé and K.Yvon, Acta.Cryst. B26, 153, (1970)

28. H.Jagodzinski, Acta.Cryst., 7, 17, (1954)

29. E.K.Storms and R.J.McNeal, J.Phys.Chem., 66, 1401, (1962)

30. L.M.Adelsberg, and L.H.Cadoff, J.Am.Ceram.Soc., 51, 213, (1968)

31. E.Rudy, S.Windisch and C.E.Brukl, Planseever, 16, 3, (1968)

32. K.Yvon and E.Parthé, Acta.Cryst. B26, 149, (1970)

33. G.Brauer and R.Lesser, Z.Metallk., 50, 8, (1959)

34. W.F.Brizes and J.M.Tobin, J.Am.Ceram.Soc., 50, 115, (1967)

35. G.Brauer and R.Lesser, Z.Metallk., 49, 622, (1958)

36. G.Thomas and R.E.Villagrana, Acta.Met. 14, 1633, (1966)

37. G.Thomas and R.E.Villagrana, Phys.Stat.Sol., 2, 499, (1965)

38. S.I.Alyamovskii, G.P.Shveikin, P.V.Gel'd and N.M.Volkova, Russ.J.Inor.Chem., 12, 301, (1967)

39. C.Froidevaux and D.Rossier, J.Phys.Chem.Solids, 28, 1197, (1967)

40. S.I.Alyamovskii, G.P.Shveikin, P.V.Gel'd, Russ.J.Inor. Chem. 12, 915, (1967).

41. C.H.de Novion, R.Lorenzelli and P.Costa,C.R.Acad. Sci., Paris, 263, 775, (1966)

42. D.Kordes, Phys.Stat.Sci., 26, K103, (1968)

43. S.I.Alyamovskiĭ, G.P.Shveikin, P.V.Gel'd, and E.M.Shchetnikov Russ.J.Inor.Chem., 13, 472, (1968)

44. J.D.Venables, D.Kahn and R.G.Lye, Phil.Mag., 18 177 (1968)

45. R.G.Lye,G.E.Hollox and J.D.Venables, Proceedings Of The International Symposium on "Anisotropy in Single-Crystal Refractory Compounds", Dayton, June 1967

46. J.D.Venables, Phil.Mag., 16, 143, (1967)

# CHAPTER TWO

## THE DESIGN OF A SUITABLE CRYSTAL GROWTH APPARATUS

The reasons why large high purity single crystals of vanadium carbide are required for this study have already been outlined in the previous Chapter. This present Chapter deals briefly with several possible ways of producing such material and discusses in detail the techniques chosen for the present study - floating zone melting. The necessary design features of a suitable apparatus are presented.

### 2.1 Methods Of Producing Single Crystals Of Transition Metal Carbides

Most of the early investigations concerning refractory carbides were carried out on poorly characterised material that was usually prepared by the compaction and sintering of relatively impure powders. More recently[1,2,3] efforts have been made to produce high purity single crystals of these materials to allow a more accurate evaluation of their potential for use as high temperature structural materials. This work is hindered by the extremely high melting temperatures required (2650° to 4000°C) and the expense of the raw materials.

Numerous methods for crystal growth are available which can be broadly divided into four groups: (a) growth from the melt, (b) growth from solution, (c) growth from a vapour phase, and (d) growth in the solid state. Each of these methods has advantages and disadvantages when applied to the transition metal carbides.

2.1.1 Growth From The Melt

This method offers the best possibility for producing large single crystals at reasonable growth rates. In all modifications of this technique, the melt is held at a temperature slightly above the melting point while the crystallising solid is held just below the melting point. The major difficulty associated with this method is the attainment of the very high temperature required i.e. 2650°C to 4000°C. A number of other serious difficulties in the present context include: possible changes in stoichiometry due to the wide homogeneity range of monocarbide phases arising from selective depletion of one or other of the components of the carbide due to the high vaporisation rates, and the inducement of high thermal stresses during melting and cooling resulting in high defect concentrations and possible fracture of the product crystal.

Growth from the melt contained in a crucible is the oldest established method of melt growth. Two tech - niques are available, the Bridgman-Stockbarger method where a crucible containing the completely molten charge is solidified from one end by movement through a temperature gradient, or the zone method where a small molten zone is passed along the charge. A further method which also involves a crucible is the Czochralski technique where a crystal is 'pulled' from the molten charge contained in the crucible.

In the case of materials which melt at over 2000°C such as the carbides, there is extreme difficulty in providing crucibles that do not react with the melt and

cause contamination. Thus methods that do not use crucibles must be used. The absence of a crucible has the added advantage that there is no liquid-crucible interface for causing heterogeneous nucleation, and no strains set up due to differential thermal expansion between the crucible and the crystal. Two techniques are available - the Verneuil and the floating zone techniques.

The Verneuil technique has been used to grow a wide variety of high melting point materials including transition metal carbides[4]. In this process the material, usually in the form of a powder, falls from a hopper through the heat source and arrives molten on the surface of the growing crystal. A wide variety of heating sources are used including oxy-hydrogen flames in the flame fusion process, and electron-beam or arc-image heating in more refined methods. However with these methods the attainment of the necessary temperatures, with the associated control of the atmosphere to prevent vaporisation losses is difficult. Other methods of heating which are more amenable to atmosphere control such as electric-arc discharge and induction coupled plasma heating have been used[5].

The floating zone technique has recently been applied to growing single crystals of transition metal carbides[1,2]. In this technique a molten zone is passed along a solid rod of crystal, the molten zone being supported mainly by surface tension forces. A number of heating methods have been used to produce the molten zone but R.F. induction heating is most frequently used. The provision of a facility for atmosphere control is compatible with this

means of heating, but the material must be present initially in the form of a solid rod instead of in the more widely available powder form which is used in the Verneuil technique. The method can be modified slightly to melt poor conductors or insulators by making use of the fact that these usually become conducting in the liquid phase. In this case the specimen is surrounded by a moveable conducting susceptor which indirectly heats the specimen to its melting point, and then the susceptor is removed and direct heating is used for the zoning process.

2.1.2 Growth From Solution

The growth of crystals from homogeneous solutions, using either seed crystals of relying on spontaneous nucleation, is a well established technique which has been used for many high melting point materials such as rutile ($TiO_2$) and alumina ($Al_2O_3$)[6]. This technique is useful for growing crystals of high perfection at convenient working temperatures well below the melting point of the materials. It is also useful for the growth of materials which undergo structural transitions at temperatures near to their melting points but above the growth temperatures from solution (e.g.$BaTiO_3$). Crystallisation is induced by cooling the system or by allowing the solvent to evaporate, and the nucleation is usually spontaneous although some attempts have been made to utilise seed crystals. The main advantages of this method are the comparatively low temperatures required, the high quality of crystals that are obtainable and the ease of doping with suitable elements if required. The attendant disadvantages are the risk of contamination from the solvent

constituent elements or from the crucible, and the excessive spontaneous nucleation which severely limits the size of crystal obtainable.

The choice of a suitable solvent is of primary importance to this technique since any solvent must satisfy the following requirements; adequate solubility of the constituent elements of the crystal and variation of solubility with temperature, sufficiently low melting point, absence of compound formation between crystal components and solvent, no chemical reaction with the crucible material, low vapour pressure, and low solubility of solvent materials in the crystal. A number of solvent materials have been found for the transition metal carbide crystals including aluminium and iron. Thus Bartlett and Halden[5] prepared single crystals of tantalum carbide by growth from an aluminium melt contained in an alumina crucible, but they found that the extremely slow growth rates and the inability to control spontaneous nucleation prevented them from obtaining crystals larger than 0.2 mm.

This growth technique was not attempted for the research described here because of the difficulty in producing large crystals suitable for an analysis of micro-structure and mechanical properties.

### 2.1.3 Growth From The Vapour Phase.

The vapour transport technique offers several advantages common with the solution technique. Thus growth at temperatures below the melting point is possible but the process is usually slow. The preparation of high purity carbides by the Van Arkel process has been used for many

years. In this technique[7] a halide of the metal is normally reacted with hydrogen and a hydro-carbon to deposit the carbide on a hot surface. The method in common with the previous one, suffers from low growth rates and difficulties in preventing random crystal nucleation, and was therefore considered unsuitable for the current investigation.

2.1.4 Growth From The Solid State.

Large single crystals can be produced by strain annealing treatments on polycrystalline solid rods using a technique which has been well established for metal crystals[8]. It is found that subsequent annealing of material given a critical amount of plastic strain (usually in the range 2 to 5 %) can result in the formation of a few abnormally large grains. This process is known as secondary recrystalisation or coarsening, and differs from primary recrystallisation and grain growth, which normally occurs on annealing where the distribution of grain sizes throughout the crystal is nearly uniform. When the process is suitably controlled good quality single crystals can be produced. The process of secondary recrystallisation is still not completely understood but certain factors which are known to be important are the presence of a dispersed phase and of a preferred crystallographic orientation for grains formed by primary recrystallisation.

Fleischer and Tobin[9] have produced large single crystals of a number of refractory carbides utilising this technique. They firstly produced fine grained carbide crystals by a direct reaction of the liquid transition metals

with graphite and used a subsequent annealing treatment to homogenise the carbon content throughout the sample. Deformation at 2000° to 2500°C to give critical strains in the range 5 to 10% was followed by annealing for up to 25 hours at temperatures of 2500° to 3000°C which resulted in the formation of single crystals. Crystals of TiC, ZrC, HfC, NbC and TaC were produced in this way. It is interesting to note that frequently single crystals of VC were produced following the initial homogenising treatment, and no strain anneal experiments were carried out on this material.

The greatest difficulty associated with this technique is the controlled production of crystals with varying degrees of non-stoichiometry, since this can only be achieved by varying the times of the initial direct reaction process and then homogenising by long annealing treatments. The use of pressed and sintered rods instead of directly reacted material, was reported to give inferior results due to embrittlement problems associated with gaseous contamination during the long anneals at high temperature.

Because of this difficulty in easily varying the composition of the material, and the fact that the necessary complex and costly high temperature annealing and deformation equipment was not available, this method was not studied.

The foregoing brief review of available crystal growth techniques has indicated several possible ways of producing single crystals of the transition metal carbides. Thus most of these carbides have been produced by the Verneuil[4], strain anneal[9], or floating zone techniques[1,2]. In the present study large single crystals of vanadium

carbide with varying degrees of non-stoichiometry are required, and the need for close control of composition favours melt growth over the strain anneal technique. The necessity to provide a facility to reduce vanadium vaporisation losses during the growth process[10] seriously complicates the apparatus required, especially the heating facility. Thus neither a simple flame fusion Verneuil apparatus nor an electron-beam heated floating zone apparatus working in vacuum can be used.

## 2.2 Zone Melting Apparatus.

The choice of a floating zone technique for the growth of vanadium carbide was made on the basis of the factors outlined above, and the availability of an apparatus designed originally for the Czochralski crystal growth process, (fig 2.1), which could be suitably modified for the present research programme, and a 30 kw.r.f. generator. The important features of an apparatus suitable for zone melting vanadium carbide are listed below and shown diagrammatically in fig. 2.2.

(1) accurate and closely controllable coupled axial movement of the specimen grips over a range of speeds.

(2) independent rotational control for one of the specimen grips to reduce transverse temperature and compositional gradients during crystal growth.

(3) accurate permanent alignment of the upper and lower specimen grips.

(4) a continuously variable heating source capable of melting a small volume of sample.

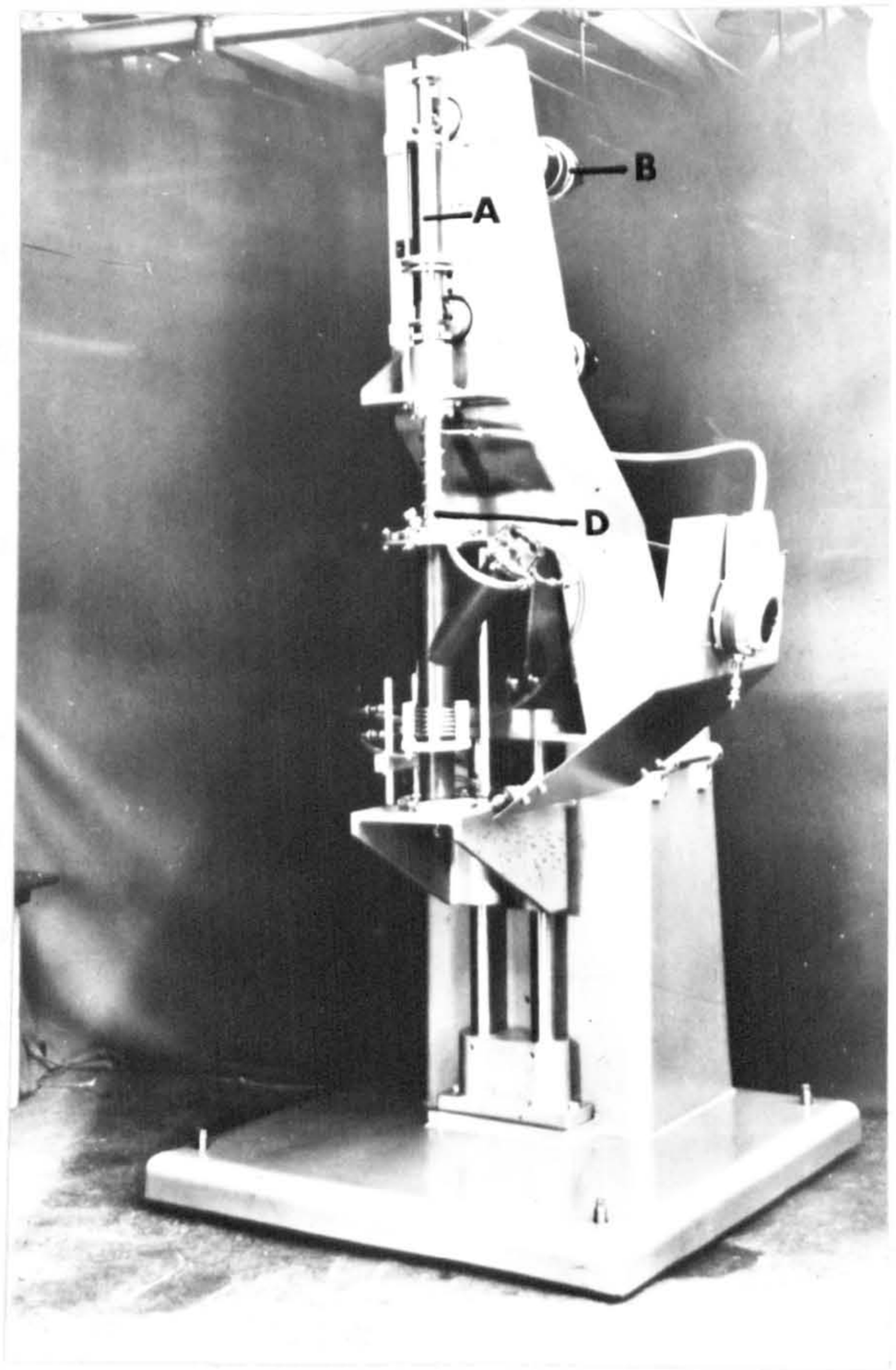


FIG. 2.1.

CZOCHRALSKI CRYSTAL GROWTH APPARATUS.

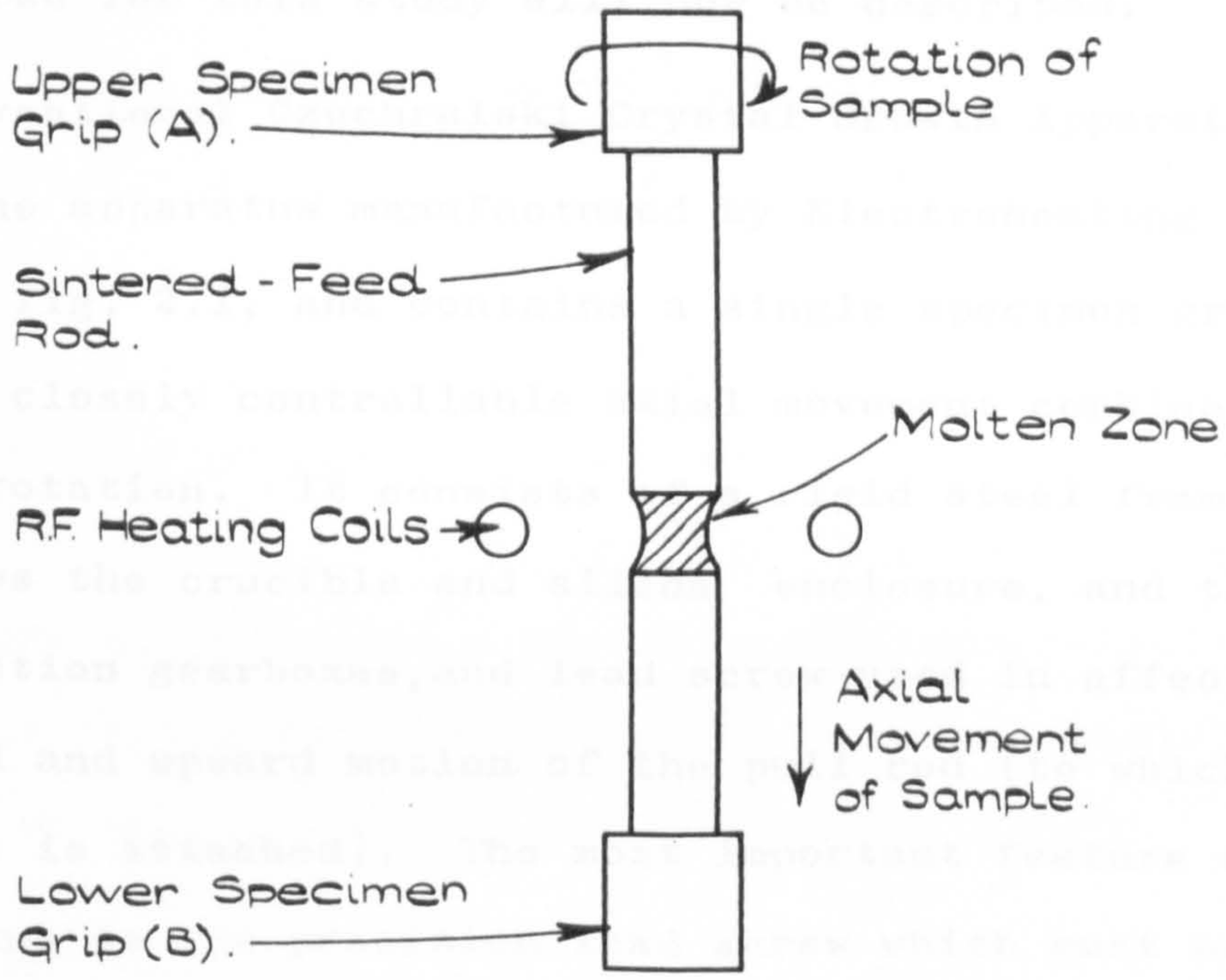


FIG. 2.2.

FLOATING ZONE MELTING ARRANGEMENT.

(5) accurate independent control over the axial movement of the sintered feed rod, relative to the movement of the zone along it, to compensate for density changes occurring during melting and solidification of the sintered feed rod (which has less than 100% theoretical density).

(6) a means of controlling and operating the furnace atmosphere at positive pressures of the ambient gas (up to 20 atmospheres pressure) to reduce vanadium vaporisation losses. The working chamber associated with this must in addition allow for good visibility during the growth process, and easy access for assembling and dismantling experiments.

(7) provision of 'afterheater' and radiation shielding facilities to reduce thermal stresses set up during the cooling of the solidified crystal.

A description of the Czochralski apparatus and the modifications required for this study will now be described.

### 2.2.1 Conventional Czochralski Crystal Growth Apparatus

The apparatus manufactured by Electroheating Ltd., is shown in fig. 2.1, and contains a single specimen grip which has a closely controllable axial movement combined with a means of rotation. It consists of a rigid steel frame which carries the crucible and silica enclosure, and the motors, reduction gearboxes, and lead screw used in affecting a controlled and upward motion of the pull rod (to which the seed crystal is attached). The most important feature of this apparatus is the precision lead screw which must be capable of controlled and stable movement over a range of

speeds. Thus the stainless steel lead screw 'A' can be driven at a pulling rate in the range 6mm per hour to 600mm per hour by means of the servo motor 'B'acting through a gearbox. A similar motor and gearbox control the rotation mechanism over the normal range 0.5 to 350 r.p.m.

In the production of good quality single crystals, fluctuations in growth rate must be avoided since these affect compositional variations and impurity distribution at the growing interface. This criterion is best achieved with a slow stable growth rate. To this end the motors are designed to maintain a set speed independent of temperature and supply voltage fluctuations, and are normally run only at slow speeds to minimise vibration. However, full speed in each direction is available by means of an over-riding switch in the controller 'C' to allow for fast positioning of the pull-rod during the setting up procedure at the begining of the crystal growth process.

The sample is usually heated indirectly by placing it in a conducting crucible, which is heated by direct r.f. induction by surrounding the sample with a water-cooled copper work coil connected to the radio-frequency generator. The power output can be varied manually up to a maximum of 30 kw at 450 kc/s by adjustment of the continuously variable r.f. output transformer. A 57 kVA saturable reactor is used to control the output voltage of the generator at any desired value in the working range and to ensure close maintenance of output voltage irrespective of supply variations.

### 2.2.2 Modification Of Czochralski Crystal Growth Apparatus

The Czochralski pull-rod was made the upper specimen grip (A in fig. 2.2) and this was coupled to the lower grip (B in fig. 2.2) via two platforms connected together by long steel supports. These can be seen clearly in the photograph of the apparatus shown in fig. 2.3. Thus movement of the lead screw was followed by the two platforms, and hence via the intermediate connections by the two specimen grips. The long steel supports moved through p.t.f.e. alignment bushes to ensure accurate alignment of the upper and lower platforms, and hence the upper and lower specimen grips. In this way both grips were driven from the accurately controllable lead screw arrangement of the existing Czochralski apparatus and the rotational facility was not impaired.

(a) Independent Axial Feed Rod Control

The growth of single crystals from sintered rods poses problems due to shrinkage of the material on melting and solidification, which necessitates independent means of moving the growing crystal relative to the sintered feed rod. In the present experiments the sintered rods had 90% theoretical density such that zoning involved a 10% reduction in volume. A separate motor drive and lead screw similar in action to those on the original Czochralski apparatus were designed to allow independent close control of the movement of the bottom of the feed rod into the molten zone. The necessary motor, gears and lead screw device were attached to an aluminium platform below the main pressure chamber as shown in fig. 2.4. This whole assembly plus its controller

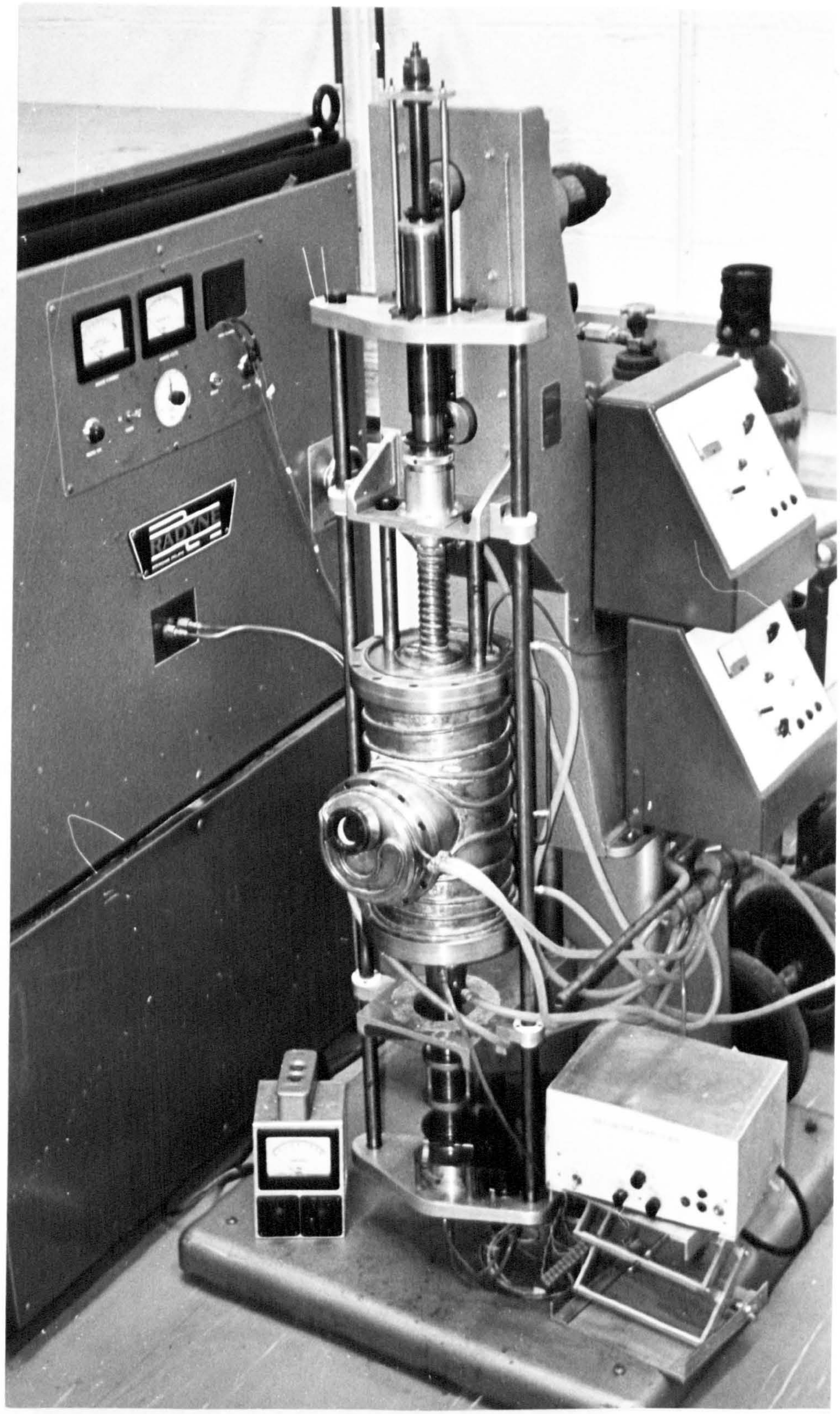


Fig. 2.3 Modified floating zone melting apparatus.

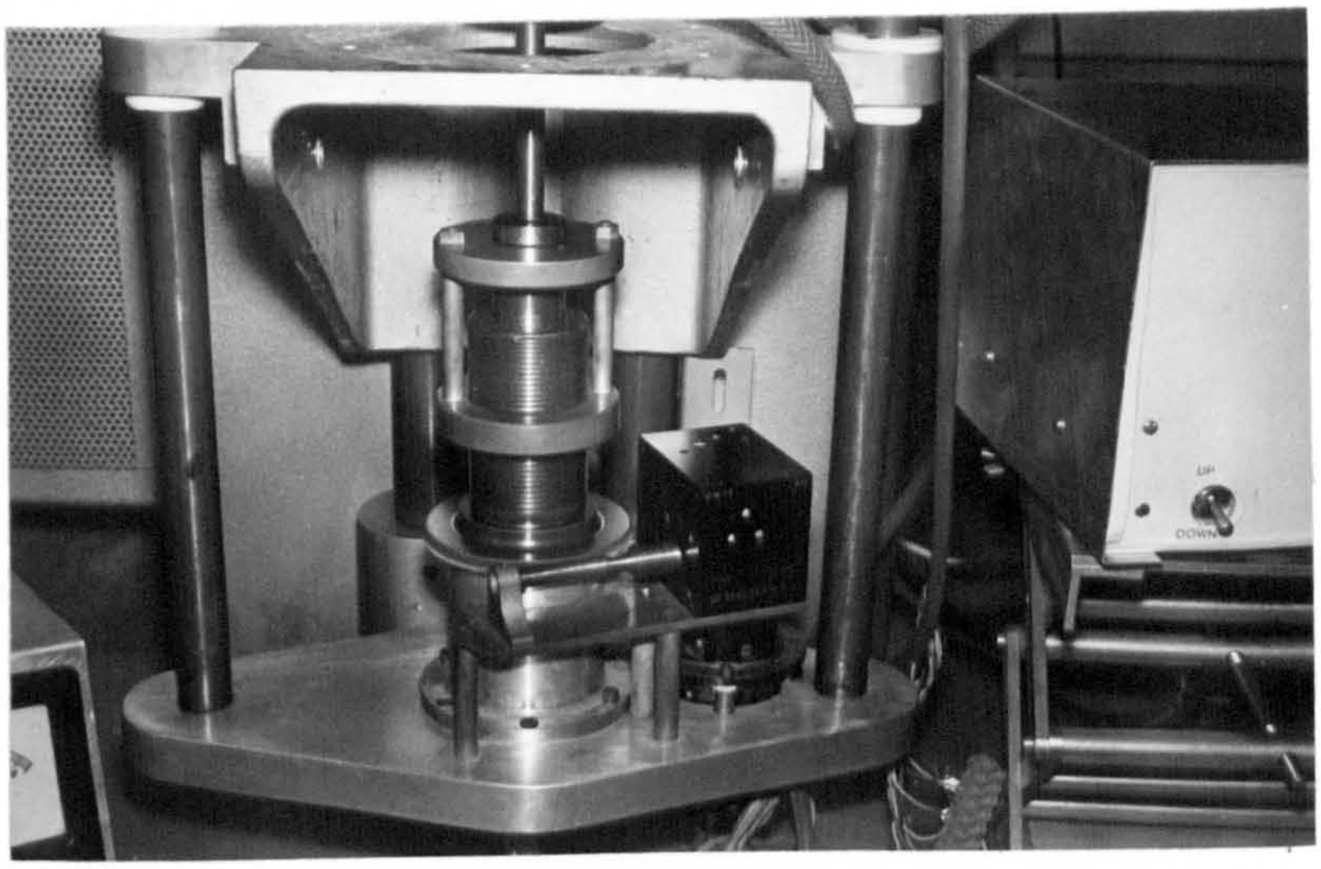

Fig. 2.4 Lead screw and gearbox for independent axial movement of bottom pull rod.

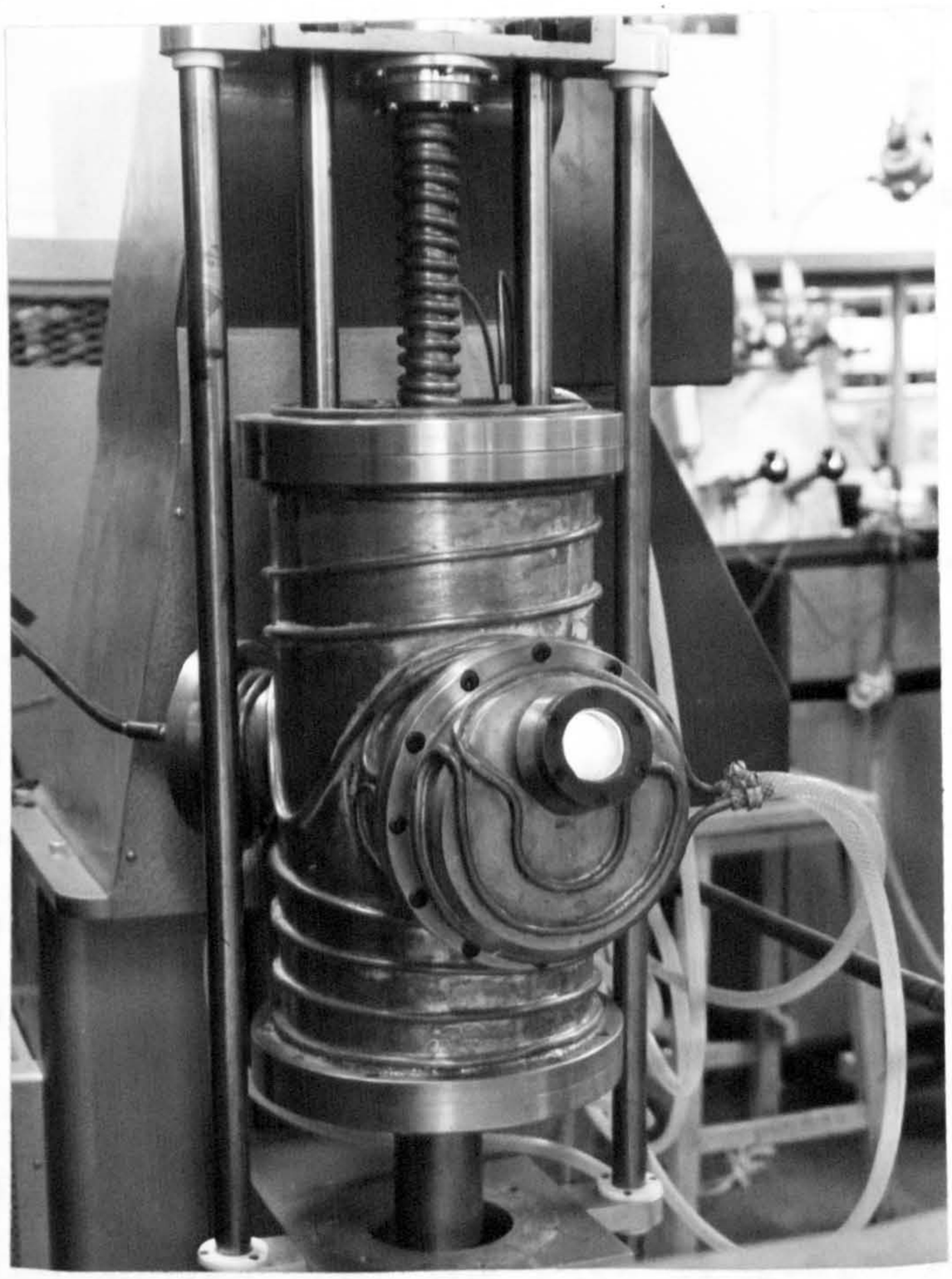

Fig. 2.5 Stainless steel water cooled pressure chamber.

can be seen in fig. 2.3. The movement is controllable in both directions over a range of speeds 0.5 to 20 mm per hour. The movement in the opposite direction is sometimes used if the zone becomes unstable due to temperature or compositional fluctuations.

The whole of this drive mechanism must be attached to the bottom of the feed rod and driven at the same speed as the sample through the heating coil, thus care was taken in selecting all the materials used because the entire weight of this drive assembly, the two platforms and the long supports has to be borne by the lead screw. Thus steel tubes were used instead of rods, which gave an additional advantage in that the long lengths involved were available with a closer uniformity of size control. The platforms were made of aluminium, and a lightweight electric motor and gear box were chosen. In view of the extra weight borne by the lead screw in this modified apparatus the bearing in the lead screw housing was strengthened by including a stouter angular contact bearing.

(b) Furnace Atmosphere Control

Storms[10] reported that vanadium was lost preferentially when certain compositions of vanadium carbide were heated at elevated temperatures. The work of Wenkus et al.[2] showed that boron loss from certain refractory metal borides could be substantially reduced by the incorporation of a positive inert gas pressure above the melt; indeed without some means of affecting this control the production of crystals of controlled composition is impossible. He showed that the rate of evaporation decreased

approximately at $1/\sqrt{P}$ where P is the ambient pressure of inert gas, and the rate controlling step is diffusion through a boundary layer. Precht and Hollox[1] also used this technique to give closer control of stoichiometry in growing titanium and vanadium carbide by the floating zone technique using a commercially available zone melting apparatus manufactured by Lepel. The atmospheres used in these experiments were either pure argon, a 5% hydrogen - argon mixture or pure helium. The former gas resulted in arcing problems during the zoning operation due to its low ionisation potential but no such problems were reported with either of the other atmospheres.

In the present work argon was used initially on economic grounds during the commissioning of the apparatus, but in all later experiments helium was used. Helium was preferred to the cheaper gas mixture because it contains lower oxygen and nitrogen impurity levels and is readily available.

The apparatus was designed to operate at ambient pressures up to 20 atmospheres and consisted of a welded stainless steel chamber which could be attached to the existing crystal puller together with the necessary pressure controls. The chamber itself (fig. 2.5) is made of $\frac{1}{4}$ inch thick stainless steel and is $8\frac{1}{2}$ inches diameter and 16 inches long. Two ports have been welded to the main structure, one to provide adequate visability of the melting process and the other an inlet for the electrical power leads. The water cooled copper pipes brazed to the outside of the structure serve to cool the apparatus during crystal growth.

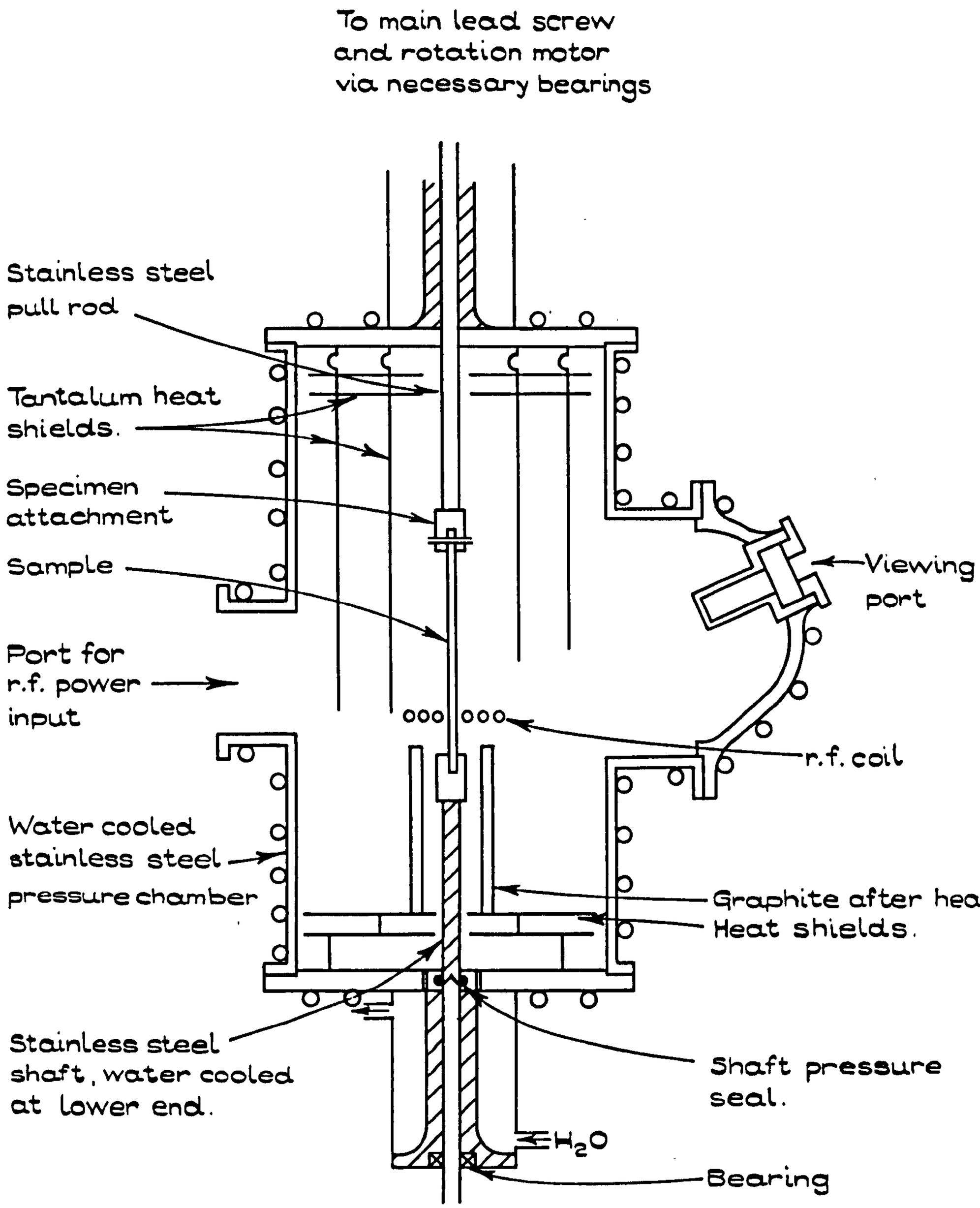


FIG. 2.6.

DIAGRAM OF CRYSTAL GROWTH APPARATUS.

A detailed diagram of this chamber is given in fig. 2.6.

A number of safety valves are incorporated in the pressure system which are designed to release the pressure in the working chamber if it exceeds a certain set value (fig. 2.7). In addition to their safety function these valves serve as a means of maintaining a constant pressure during crystal growth. In operation the main regulator valve is adjusted so that the valves are constantly leaking gas i.e. the pressure is just in excess of the safety 'blow-off' value. Thus experiments can easily be carried out at constant pressures of 5,10 or 20 atmospheres, or at any pressure within these limits if adjustments to the main regulator valve are made.

The chamber was made of sufficient size to enable adequate radiation shielding and 'after heating' facilities to be included if required, and to ensure that the outer body did not seriously overheat. The provision of adequate viewing facilities was also of prime importance.

The use of high pressures meant that all joints between removable sections of the apparatus had to be carefully designed. Pressure tight joints were obtained by bolting sealing plates to the main body with conventional rubber 'O' ring seals as shown in fig. 2.6. The water cooling on the chamber prevented overheating of these 'O' rings and this was a major contribution to their operating success. The sealing of the window assembly in the viewing port is shown in greater detail in fig. 2.8. 'Spectrosil' * a synthetic fused silica was chosen for the window material because it had high spectral emissivity over a wide range

* Supplied by Thermal Syndicate Ltd., Wallsend, Northumberland

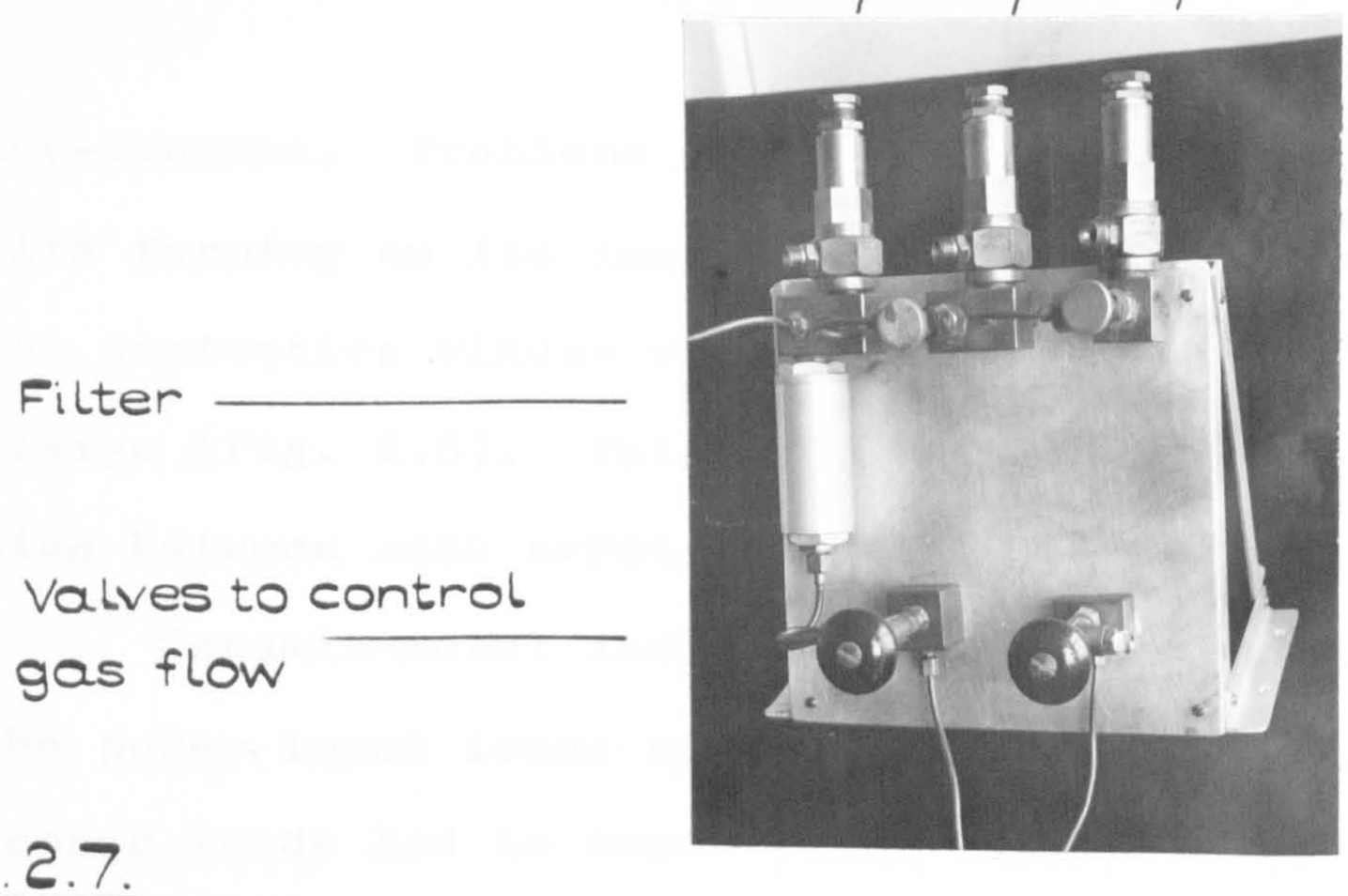


FIG. 2.7.

ARRANGEMENT OF PRESSURE CONTROLS.

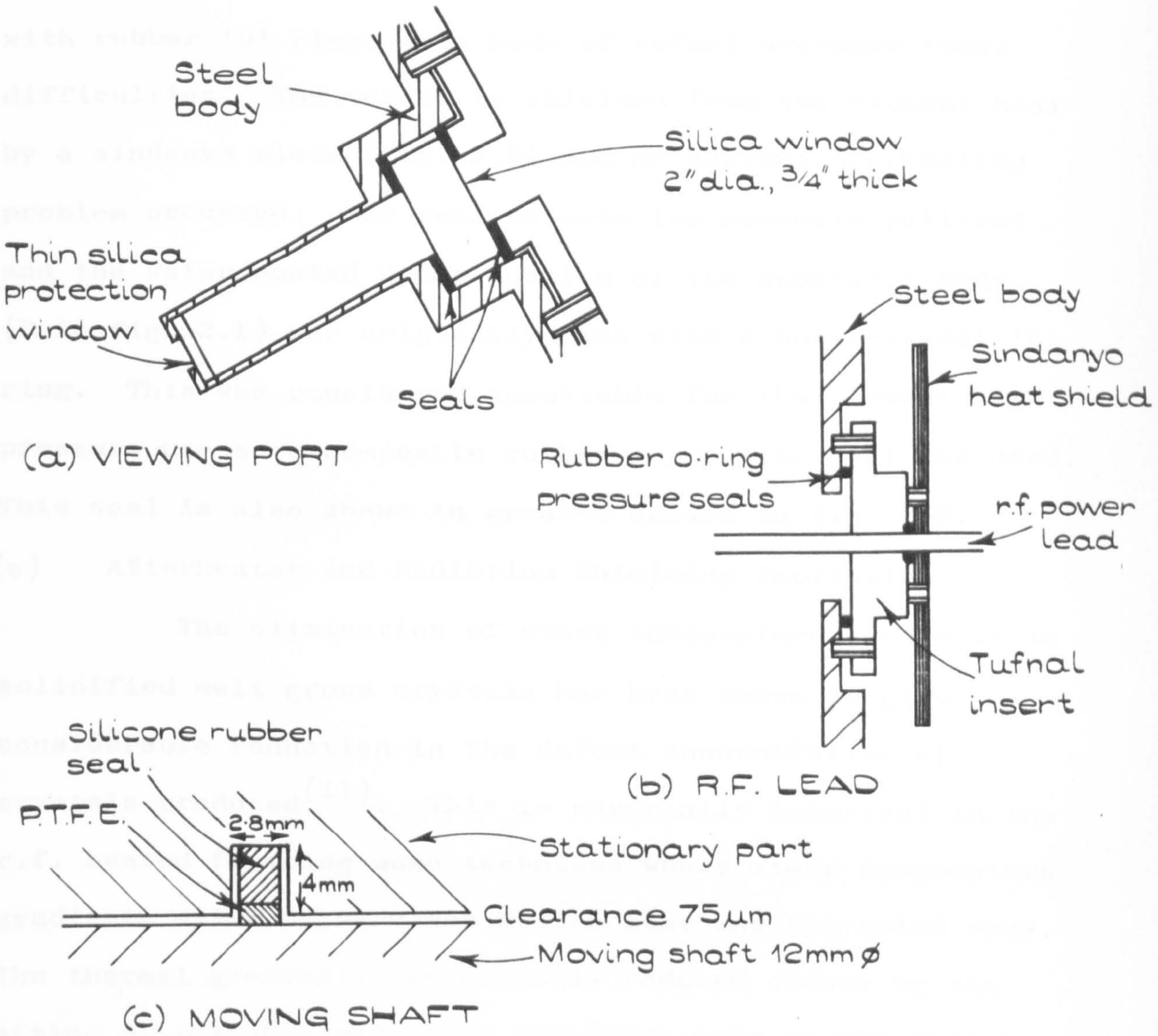


FIG. 2.8.

PRESSURE SEALS.

of wave-lengths. Problems were encountered with evaporation deposits forming on its inner surface and a much smaller section protective window was therefore incorporated into the design (fig. 2.8). This could be easily removed for cleaning between each crystal growing operation.

Ceramic-metal insulated seals were initially used for the power imput leads but the wide separation of the two copper leads led to imput power losses which in certain cases prevented melting taking place. The use of a design incorporating much less widely separated leads which sealed with rubber 'O' rings to a body of tufnol overcame these difficulties. The tufnol is shielded from the radiant heat by a sindanyo plate (fig. 2.8) and no serious overheating problem occurred. The seal between the moveable pull-rod and the water cooled upper portion of the apparatus body (D in fig. 2.1) was originally made with a conventional 'O' ring. This was considered unsuitable for the present high pressure use so a composite rubber - p.t.f.e. seal was used. This seal is also shown in greater detail in fig. 2.8.

(c) Afterheater And Radiation Shielding Facilities

The elimination of steep temperature gradients in solidified melt grown crystals has been shown to give considerable reduction in the defect concentration of crystals produced[11]. This is especially important in the r.f. heated floating zone technique where steep temperature gradients exist between the molten zone and the solid rods. The thermal gradients are normally reduced either by the siting of suitable radiation shielding near to the molten zone, or by the provision of an afterheater. The latter

usually consists of a suitable susceptor of tantalum or graphite which is positioned near to the r.f. work coil and is induction heated to some suitable intermediate temperature. It is usually sited on the side of the coil where the growing crystal is positioned, although in very brittle materials some form of pre-heating is also included because cracking could lead to coupling problems. Radiation shielding, which is usually tantalum, molybdenum or stainless steel depending on the temperature, serves the dual purpose of reducing thermal gradients and preventing the inner surface of the furnace chamber from overheating (see fig. 2.6).

The conventional Czochralski crystal puller is designed to operate with the pull rod moving slowly upwards as in normal melt growth by this technique. However, with this arrangement and the condition that good viewing facilities of the molten zone are essential, the siting of a suitable afterheater is difficult. Early experiments using this arrangement with no afterheater resulted in the production of single crystal material that was severely cracked due to steep thermal gradients. Thermal cracking was reduced by positioning a tantalum radiation shield close to the zone by suspending it from the roof of the furnace chamber. This was not entirely successful because the need for ensuring adequate vision of the molten zone meant that a vertical gap existed between the molten zone and the radiation shielding and this limited the shielding effect. Modification of the design of the r.f. coil to reduce thermal gradients was also attempted and is discussed later in

section 3.2. In view of these difficulties the apparatus was later modified to allow slow controlled growth movement with the feed rod moving downwards through the work coil. With this arrangement a graphite susceptor, that was split horizontally to allow easier assembly of the apparatus, provided an afterheater that reduced thermal cracking (see section 3.2). This is shown in fig. 2.6.

(d) Means Of Attaching Specimens

The expense and difficulty of fabrication of these materials demands that maximum usage be made of the sintered rod material. However, in view of the temperatures involved in sample preparation care must be taken in designing suitable specimen holders which fill the dual role of allowing maximum usage of crystal while assuring that minimum contamination occurs. A less important third criterion is to ensure a more gradual longitudinal thermal gradient along the sintered rod.

In normal Czochralski growth the specimen is attached to a stainless steel or molybdenum rod by means of a clamping arrangement, but this method would lead to serious contamination problems in the growth of carbides. The method chosen for the carbides is to join the top of the sintered rod to a graphite holder by means of a tantalum pin and to attach this graphite holder to the pull rod end by means of a stainless steel holder. The holes in the sintered rod were produced by spark machining or by ultrasonic drilling using a dispersion of carborundum powder in water. The former process is preferred due to its far greater speed of operation, and less need for constant

supervision. A large number of graphite holders were available with varying specimen hole sizes to allow small variations in feed rod diameter to be accommodated. The bottom of the feed rod was ground flat and placed in the flat bottomed specimen hole in the bottom graphite holder (fig. 2.9). Graphite was chosen as the holder material because it could withstand the high temperature involved (up to 1500°C), would not cause serious contamination, and would reduce longitudinal thermal gradients by coupling to the r.f. field.

Fig. 2.9 Means of attaching sintered carbide rod to apparatus pull rods via. graphite holders.

## REFERENCES


1. W.Precht and G.E.Hollox, J.Crystal Growth,3 ,818 (1968)
2. J.F.Wenkus, J.S.Haggerty and D.W.Lee,Tech.Report.AFML-TR-68-228, Sept. 1968.
3. A.D.Kieffer, Linde Co., private communication in paper by W.S.Williams and R.D.Schaal,J.Appl.Phys.,33 955, (1962)
4. R.W.Bartlett,F.A.Halden and J.W.Fowler,Rev.Sci.Instrum., 38, 1313 (1967)
5. R.W.Bartlett and F.A.Halden,Stanford Research Institute NASA-49 (19), June 1967
6. R.C.Linares, J.Appl.Phys., 33 1749 (1962)
7. T.Takahashi,K.Sugiyama and H.Itoh,J.Electrochem.Soc.,117, 541,(1970)
8. K.T.Aust in "The Art And Science Of Growing Crystals", edited J.J.Gilman (John Wiley, New York, 1963)
9. L.R.Fleischer and J.M.Tobin, Proceedings of Third International Symposium on High Temperature Technology, Asilomar,California 1967 (Butterworths,London, 1969)
10. E.K.Storms "The Refractory Carbides",(Academic Press, New York, 1967)
11. B.Cockayne and J.D.Ridley, J.Sci.Instrum., 41 647 (1964)

# CHAPTER THREE

## GROWTH OF SINGLE CRYSTALS.

In this chapter a description is given of the growth of single crystals of vanadium carbide with varying degrees of non-stoichiometry. Section 3.1 deals with the preliminary formation of sintered rods from high purity powder material, while the floating zone melting experiments to produce the single crystals are discussed in section 3.2. Finally in the third section, the characterisation of the 'as-grown' crystals by chemical analysis and optical micro-structural examination is reported.

### 3.1 Preparation Of Pressed And Sintered Rods

High purity vanadium and vanadium carbide powders were thoroughly blended to produce mixtures with differing carbon to vanadium atomic ratios. The high purity powders were obtained from - New Metals and Chemicals Ltd., and Polaron M.R.C.Ltd., typical analyses being given in Table - 3.1.

The powders were encapsulated in rubber containers produced by dipping glass formers into a solution of 'Revultex' * and allowing the coating to dry thoroughly. The size of the samples produced in this way could be varied by adjusting the size of the glass formers used, but most of the samples were of round section 10-12 mm in diameter and up to 140 mm in length.

* Obtained from Bellman, Ivey and Carter Ltd., West Wimbledon, London.

TABLE 3.1.

ANALYSIS OF STARTING MATERIALS.

| ELEMENT | VANADIUM. | VAN. CARBIDE | VAN. CARBIDE |
|---|---|---|---|
| | New Metals & Chemicals Ltd. | | Polaron M.R.C. |
| | | ANALYSIS | |
| Vanadium | 99.1 | 81.45 | 81.5 |
| Carbon | 0.04 | 18.3 | 18.3 |
| Free Carbon | | 0.6 | 0.7 |
| Oxygen | 0.57 | 0.15 | 0.04 |
| Nitrogen | 0.08 | 0.05 | 0.05 |
| Iron | 0.17 | 0.05 | - |
| Silicon | 0.11 | - | - |
| Aluminium | 0.02 | - | - |

The samples were isostatically pressed at room temperature at a pressure of 78 kg/mm $^2$ . This work was carried out using hydrostatic pressure in a special oil filled steel chamber at the - B.S.A. Group Research Centre, Birmingham. The maximum dimension which could be pressed in this apparatus was 150 mm and most of the samples were of approximately this size. Some difficulty in retaining the straightness of long samples was experienced but this was partially overcome by excercising closer control over the range of powder sizes in the original mixtures, especially by greatly reducing the proportion of very fine powders in the mixtures. The most satisfactory results were obtained

when a powder size range of- 150 mesh + 400 mesh was used in the alloy preparation ( - 150 + 400 mesh size ≡ 50 - 100 μm). Additional control of specimen straightness was achieved by encasing the rubber bags containing the powder in wire mesh shields which prevented serious distortion occurring.

The production of sound pressed compacts was found to be strongly dependent on the composition of the mixtures. The compositions at low carbon to vanadium ratios ( $< 0.7$) pressed satisfactorily into sound even compacts, but as the carbon to vanadium ratio increased the difficulty in obtaining satisfactory compacts increased. This was probably due to the beneficial binding action of the vanadium metal which was present in much larger amounts at the lower carbon to vanadium ratio compositions. This binding action was more effective because of the smaller size range of the vanadium powder ( $< 40$ μm) and the fact that it was much softer than the vanadium carbide powder. At carbon to vanadium ratios of $> 0.75$ the samples either formed a series of small cylinders or did not bind together at all.

The problem of unsatisfactory cold isostatic pressing of powders can be overcome either by adding a material to the powders to act as a binding agent, or by simultaneously pressing and heating the samples. Both of these processes can lead to some contamination, the former from the difficulty in subsequently completely removing the binding agent, and the latter from contact with the specimen container during the hot pressing operation. However, the former process is relatively simple and inexpensive to carry

out, whereas the latter is extremely difficult and expensive.

A number of easily removable binder materials were used unsuccessfully before some success was achieved by the use of paraffin wax. The wax was dissolved in trich - lorethylene and the resulting solution mixed with the blended powder mixture which was subsequently dried in an oven and packed in the container in the usual manner. The percentage of wax added to the powder was usually in the range 2 to 5% with the highest percentages used for the highest carbon to vanadium ratio mixtures. In this manner sound pressed compacts were obtained with compositions throughout the cubic vanadium carbide phase field. The wax could be largely removed from the pressed samples by heating them slowly to 400°C in a vacuum furnace containing a cold trap to collect the wax which is driven off as a vapour from the samples. Any wax that is not removed by this operation is subsequently lost during the high temperature vacuum sintering treatment.

At this stage of the process the pressed samples had densities of approximately 80% of the theoretical values but were still very fragile and had to be handled carefully to prevent breakages. In order to achieve a more uniform product for subsequent zone melting and facilitate handling, the samples were sintered for 1 to 2 hours in vacuum at temperatures corresponding to 0.6 - 0.7 Tm where Tm is the absolute melting temperature (cf 1600°to 1800°C depending on composition). Contamination was minimised by supporting the samples in a graphite holder and working at a vacuum level of 1-10 x $10^{-5}$ torr. The samples were heated by r.f.

induction in a water-cooled high vacuum chamber. The temperature was measured through a viewing port with an optical pyrometer. The density of the samples increased during sintering to 80 to 90% of the theoretical value, and although the samples were still brittle they could be handled with much less care. The pressing and sintering details of the samples are listed in Table 3.2.

TABLE 3.2.

| Initial Composition | % of Paraffin wax as binding agent | Sintering Temperature °C | Approx. Melting Temperature °C | Diameter mm | Length mm |
|---|---|---|---|---|---|
| VC 0.84 | 3 | 1700 | 2740 | 9 | 105 |
| VC 0.81 | 2 | 1700 | 2700 | 8 | 103 |
| VC 0.78 | 2 | 1660 | 2650 | 9 | 110 |
| VC 0.73 | - | 1660 | 2580 | 9 | 103 |
| VC 0.65 | - | 1600 | 2350 | 9 | 52 |
| VC 0.52 | - | 1470 | 2165 | 7 | 83 |
| VC 0.47 | - | 1400 | 2050 | 7 | 92 |
| VC 0.43 | - | 1330 | 1950 | 10 | 97 |

Small variations in the diameter of the pressed and sintered samples produced in this way caused some later difficulties in the control of the zone melting process. Machining of the sample was difficult because of the fragility of the pressed samples, and the combination of extremely high hardness (approximately 2,000 Hv) and brittleness of the sintered material. These latter obstacles could be overcome by using the centreless grinding process where the sample is not rigidly held but is revolved by a soft supporting wheel against two grinding wheels impregnated with diamond powder. Using this process samples with a smooth surface and a close uniformity of diameter could be produced.*

3.2 Crystal Growth.

The major problem associated with crystal growth proved to be the designing of a suitable radio frequency induction coil which would allow melting at all compositions of vanadium carbide, and yet give a stable zone configuration. In order to form a stable molten zone between two solid rods two criteria must be satisfied. Firstly, sufficient power must be introduced into a limited volume to balance heat losses when the surface is at a temperature exceeding the melting point, and secondly, zone stability must be achieved which depends in a complex manner upon zone length, diameter and shape as a function of the radii of the two solid bars between which it is suspended.

*This work was kindly carried out by -
Alfred Herbert Ltd., Coventry.

Surface tension is the principal force supporting a molten zone and equating this force to the hydrostatic pressure can give information concerning the size, shape, and stability of the molten zone.[1] The maximum length of zone which can be supported by its own surface tension increases linearly with rod radius for small radii and approaches a limit at larger radii. An important factor in aiding zone stability is to use an upper rod of larger diameter than the bottom[2]. The crystal growth apparatus is designed to allow relative movement of the unmelted sintered rod into the molten zone to compensate for density changes during melting. However, it was found that more satisfactory operation could be achieved by taking advantage of the above information and allowing the crystal to solidify with a smaller diameter than the sintered feed rod material which was not of theoretical density.

The distribution of heat generated in the bar by induced currents depends on the coil configuration, the relative position of the bar surface to each of the coil elements, the r.f. frequency, and the specific resistivity of the material. The rate of which heat is lost depends upon a number of properties of the material e.g. melting point, thermal conductivity and emissivity and on the surroundings of the zone. A large amount of heat is reflected back into the zone by the close proximity of the coil in these experiments, and in addition from the tantalum radiation shielding which is also included in the melting chamber. However, acting in opposition to the need for effective radiation shielding is the criterion that an

unrestricted view of the molten zone is required.

Several coil configurations were investigated empirically during the course of the work to overcome specific problems. A single turn coil used in part of the early work was not capable of coupling sufficient power into the sample to melt the highest melting point alloys. Attempting to increase the power coupled into the specimen, by reducing the clearance between coil and sample, led to severe arcing problems between the molten sample and the deposits of vanadium which condense on the coil, following evaporation from the melt. The diameter of the coil adopted was a compromise dictated by these two problems. The most satisfactory coil configuration was found to be a three turn concentric coil as shown in fig. 3.1 which gave stable molten zones at all compositions.

Most of the crystal growth experiments were carried out with the zone moving down the polycrystalline rod as this was the standard direction of adjustable movement of the lead screw in the crystal growth apparatus. However, in addition to being contrary to normal zone melting practice, this led to problems in the siting of a satisfactory 'after heater' to reduce the tendency for thermal cracking. This was partially overcome by having a single turn coil above the three turn concentric melting coil which led to a lowering of the temperature gradient above the melt and a reduction in the cracking of the crystals. An obvious draw-back of this downward direction of zone travel is that any escaping gasses tend to rise in the melt and accumulate at the upper edge of the molten zone where solidification is

Fig.3.1 R.F. coil assembly used in zone melting experiments.

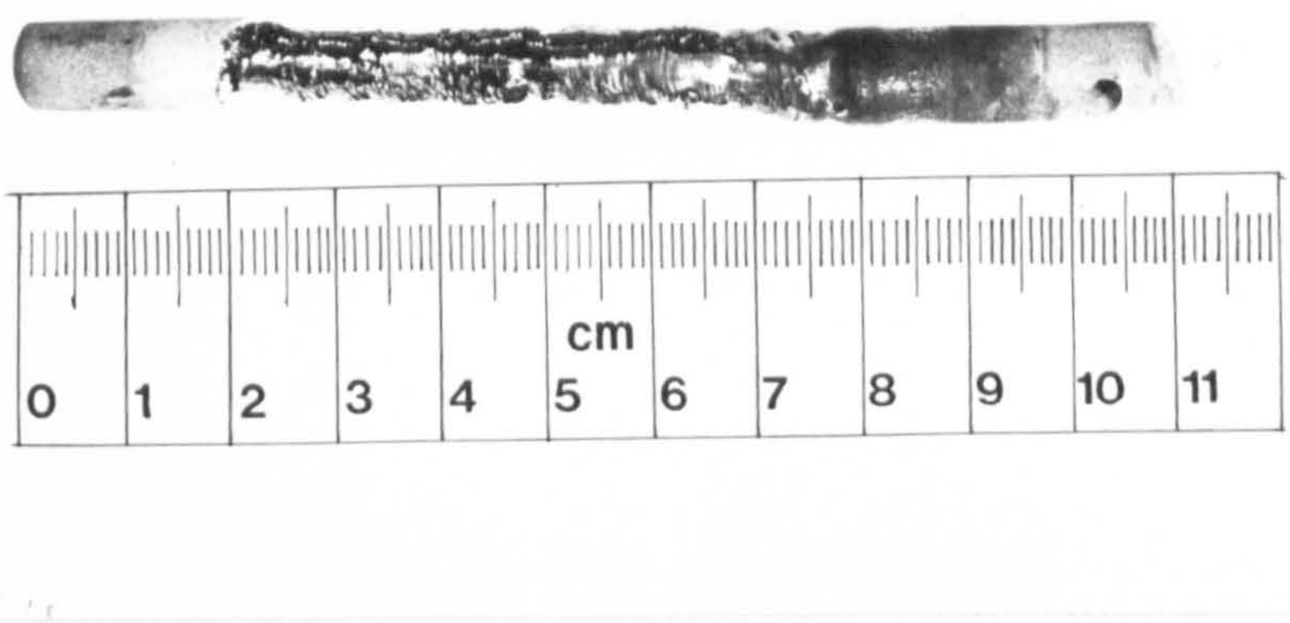


Fig. 3.2 Typical zoned crystal nominal composition $VC_{0.84}$. The sintered feed rod material can be clearly seen. Approximately 40 mm of the zoned length was single crystal material.

taking place, and thus produce instabilities in the growth process. The apparatus was therefore modified in order to allow zone travel in either direction by inserting the necessary switching and control devices in the electrical circuit controlling the motor operating the movement of the main lead screw. Later crystal growth experiments were therefore conducted with the zone moving up the sintered sample, which led to the production of a more stable zone and also allowed the installation of a graphite 'after - heater' to reduce thermal gradients (fig. 2.6).

The melting chamber was evacuated and flushed out with helium three times prior to filling to a working pressure during the experiment. The r.f. power was slowly increased until a molten zone was initiated in the sintered rod, and thereafter minor adjustments were made to the power imput to control zone stability. The sintered rod was then moved through the r.f. coil at a constant speed of approximately 10 mm per hour. The onset of single crystal formation was found to occur after a short distance of two or three zone lengths travel (approximately 20 or 30 mm) and the samples were usually zoned for lengths varying between 40 and 80 mm. Occasionally, the build up of deposit became so severe that arcing led to a premature finish to the experiment, and to obviate this problem and also the extreme length of the experiment, a faster zoning speed of 20 mm per hour was used initially for approximately one hour and thereafter normal zone speeds were used. The specimen was slowly cooled at the end of the zoning experiment to reduce thermal cracking. The crystals produced were several centimetres

long and approximately 10 mm in diameter an example being shown in fig. 3.2. The composition and size of all crystals grown are given in Table 3.3.

TABLE 3.3

| Initial Composition. | Length of Crystal zoned mm | Direction of Zone travel | Comments |
|---|---|---|---|
| $VC_{0.90}$ * | 41 | Downward | Single crystal - badly cracked. |
| $VC_{0.84}$ (1) | 25 | Downward | " " |
| $VC_{0.84}$ (2) | 53 | Downward | Single crystal - some cracking. |
| $VC_{0.81}$ (1) | 52 | Downward | Overun occurred but a short length of single crystal obtained. |
| $VC_{0.81}$ (2) | 42 | Downward | Contained a small central poly crystalline area indicating incomplete melting. |
| $VC_{0.81}$ (3) | 54 | Downward | Single crystal. |
| $VC_{0.78}$ (1) | 54 | Downward | Single crystal. |
| $VC_{0.78}$ (2) | 58 | Upward | Single crystal. |
| $VC_{0.73}$ (1) | 40 | Downward + | Large polycrystals. |
| $VC_{0.73}$ (2) | 69 | Upward + | Single crystal. |
| $VC_{0.65}$ | 43 | Downward + | Polycrystalline. |
| $VC_{0.52}$ | 12 | Downward | Polycrystalline |
| $VC_{0.47}$ | 40 | Downward | Polycrystalline. |
| $VC_{0.43}$ | 75 | Upward + | Polycrystalline. |

* Purchased as sintered rod from Polaron M.R.C.

+ Zone levelling experiments.

It is known that in order to produce long crystals of constant longitudinal composition, a condition of zone levelling must be set up when the composition of solid melting into the zone is equal to that depositing from the zone. This can be achieved by either substantially increasing the length of zone travel, or by adjusting the composition of the initial molten zone. Thus for example rods of constant composition $VC_{0.78}$ could be produced by forming a molten zone initially in a rod of composition $VC_{0.70}$ (refer to equilibrium diagram fig. 1.3). Experiments of this type were carried out to produce long samples of composition $VC_{0.72}$ and $VC_{0.80}$ as shown in Table 3.3. In addition attempts to produce single crystals of the compound $V_2C$, which forms by a peritectic reaction, were also carried out using these ideas of zone levelling proposed by Mason and Cook[3], but were unsuccessful in producing single crystals.

## 3.3 Characterisation Of Crystals

### 3.3.1 Chemical Analysis

Chemical analyses for vanadium and carbon were carried out at various points along selected grown crystals.* A sample weight of 0.1 gm was used for each determination which consisted of a thin transverse slice of crystal. The results are presented in Table 3.4

* Analyses were carried out by Mr. P. Stables at - B.S.A. Group Research Centre, Birmingham.

TABLE 3.4

CHEMICAL ANALYSIS OF AS-GROWN SINGLE CRYSTALS

| Nominal Starting Composition | Analyses measured as C/V mole ratios | | | | | | | | |
|---|---|---|---|---|---|---|---|---|---|
| | Distance of analysis sample from initial molten zone $_{min}$ | | | | | | | | |
| | Sintered rod | 0 | 10 | 20 | 30 | 40 | 50 | 60 | 70 |
| VC 0.90 | 0.87 | 0.89 | | 0.90 | 0.87 | | | | |
| VC 0.84(1) | | | 0.86 | | 0.84 | | | | |
| VC 0.84(2) | | 0.85 | 0.85 | | | 0.86 | | | |
| VC 0.81(3) | | | 0.80 | | | 0.80 | 0.83 | | |
| VC 0.78(1) | | | 0.80 | | | | 0.80 | | |
| VC 0.78(2) | | | 0.78 | | | | 0.77 | 0.63 | |
| VC 0.73(1) | | | 0.75 | | 0.73 | | | | |
| VC 0.73(2) | 0.74 | | 0.73 | | 0.72 | | | 0.73 | 0.35 |
| VC 0.65 | | | | 0.65 | | | | | |

A correlation between the determined compositions and the optical microstructure and phase equilibria relationships, is given in section 3.3.

Gas fusion analyses were carried out to determine the oxygen, nitrogen, and hydrogen content of the 'as-grown' crystals, but widely scattered results were obtained as indicated in Table 3.5. Low results were obtained on solid

TABLE 3.5

GAS ANALYSIS OF ALLOYS

| Nominal Composition | Approximate distance from initial zone (mm) | Analyses ppm | | |
|---|---|---|---|---|
| | | Oxygen | Nitrogen | Hydrogen |
| | | 120 | 200 | 19 |
| VC 0.90 | 40 | 90 | 115 | 15 |
| | | 76 | 115 | 14 |
| VC 0.84 | 10 | 586 | 150 | 12 |
| VC 0.84 | 40 | 5066 | 100 | 47 |
| VC 0.78 | 10 | 9251 | 80 | 67 |
| VC 0.78 | 50 | 10417 | 80 | 92 |
| VC 0.73 | 60 | 2510 | 200 | 91 |

samples which did not completely dissolve in the molten platinum bath, but the high results obtained when powdered material was used to overcome this dissolution problem are suspect due to the ease of contamination with oxygen during room temperature storage. In view of these complications it is difficult to decide whether the reported figures have any value, but it may be significant that the sum of the vanadium and carbon chemical analyses invariably gave answers of less than 100%. It is thought likely that the oxygen levels in the samples could be of the order of a few thousand p.p.m. whereas the nitrogen and hydrogen levels are probably much lower of the order of 100 to 200 p.p.m. This contamination probably occurred either in the room

temperature blending of the powders or during the drying process following addition of the binding agent.

### 3.3.2 Microstructure Of Crystals

The microstructures of all the crystals produced were examined using conventional metallographic techniques. Thin slices of material were removed at selected points along the length of the crystal using either a 'Capco' diamond cut-off saw, or a Servomet spark machine. Materials with high melting points, and poor electrical conductivity such as vanadium carbide ($2680^{o}C$, resistivity approximately 600 $\mu$ ohm m ) are usually not amenable to the spark machining process, but these alloys machined satisfactorily and more-over high rates of material removed were possible. This was thought to be due to the brittle nature of the alloys which allowed local fragmentation of the material under the action of the spark. Thus faster rates of removal than with most metals could be achieved, but when these very high rates of removal were used the material cracked. For this reason, most of the operations were carried out at much slower rates corresponding to range 5 or 6 on the conventional Servomet spark machine.

Cutting with the diamond impregnated cut-off wheel also caused difficulties with cracking of the material, and for this reason was rarely used.

The cut sections were mounted in an epoxy resin and polished, using standard metallurgical techniques, on silicon carbide grinding papers, and nylon cloths impregnated with diamond paste. The sections were etched prior to examination in a Zeiss 'Ultraphot' optical microscope using

both reflected and polarised light. The etch normally used, consisted of 3 parts nitric acid, $1\frac{1}{2}$ parts acetic acid and 1 part hydrofluoric acid.

The zone melting technique for single crystal growth depends on the preferential growth of one grain from the polycrystalline region constituting the initially solidified zone. This process is illustrated in fig.3.3 which shows the transition during the growth process from a sintered polycrystalline porous feed rod sample to a fully dense single crystal. Unless the material is a pure metal or a congruently melting compound, compositional variations will occur on melting which is the basis for conventional zone refining techniques. If a solid rod of for example composition $VC_{0.78}$ is melted the initial solid depositing should have a composition of $VC_{0.83}$ under equilibrium melting conditions (fig.1.3). As the solidification process continues, the vanadium content of the solidifying material increases progressively until a condition of zone levelling is set up, when the composition of the solidifying rod is the same as that which is melting into the zone i.e. $VC_{0.78}$. Under these conditions, the solidifying material will be of approximately constant composition and the final zone to solidify should have a composition of $VC_{0.70}$ and should contain both the cubic VC and hexagonal $V_2C$ carbides.

These ideas are shown to be substantially correct by observing compositional and microstructural changes along a crystal of nominal composition $VC_{0.78}$. Chemical analyses (Table 3.4) indicated that the composition after 10 and 50 mm zone travel respectively was $VC_{0.78}$ and $VC_{0.77}$, whereas the

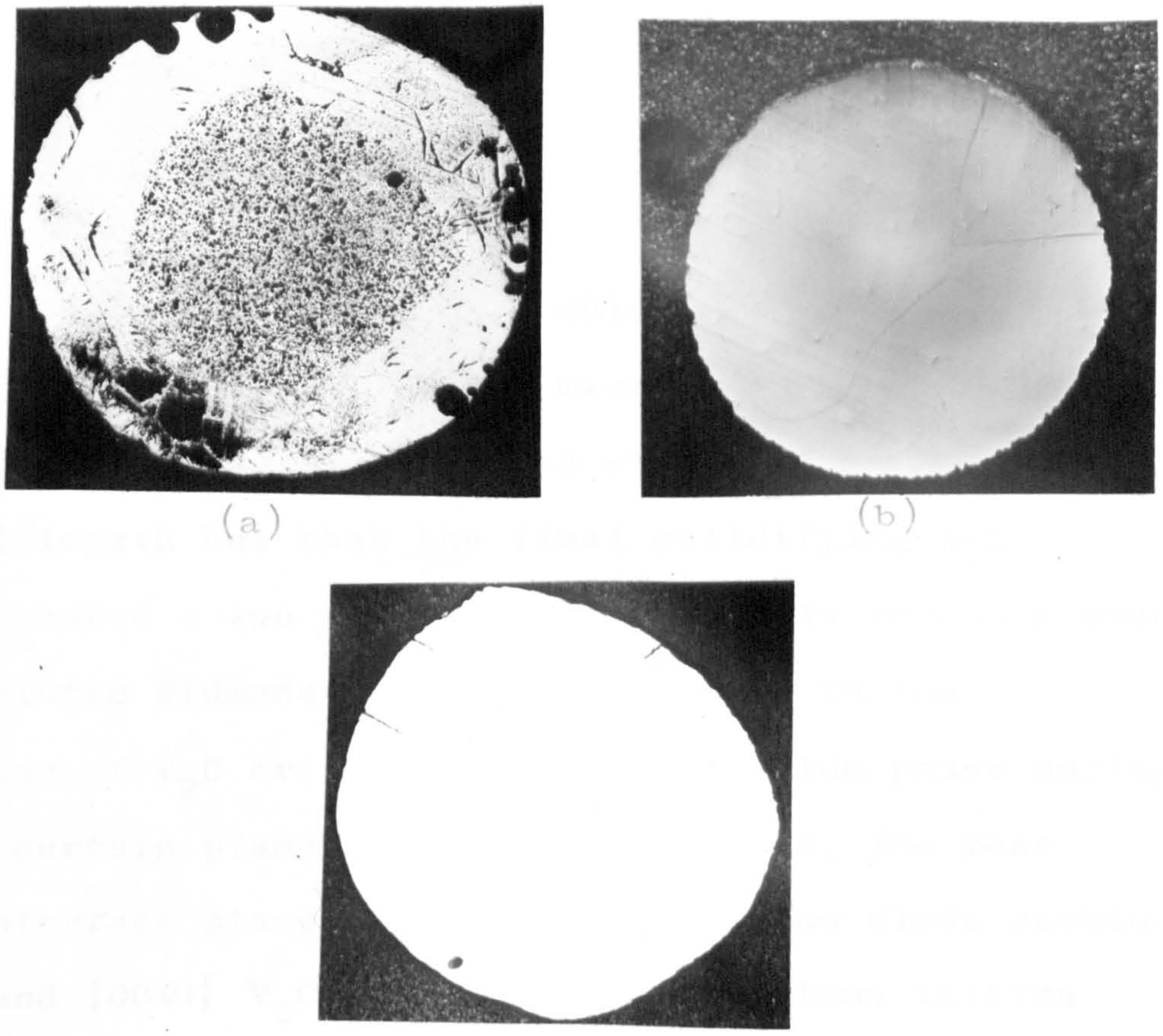

(a) (b) (c) x4

Fig. 3.3 Showing transition from polycrystalline to single crystal (a) initial molten zone (b) 15 mm zoned (c) 25 mm zoned.

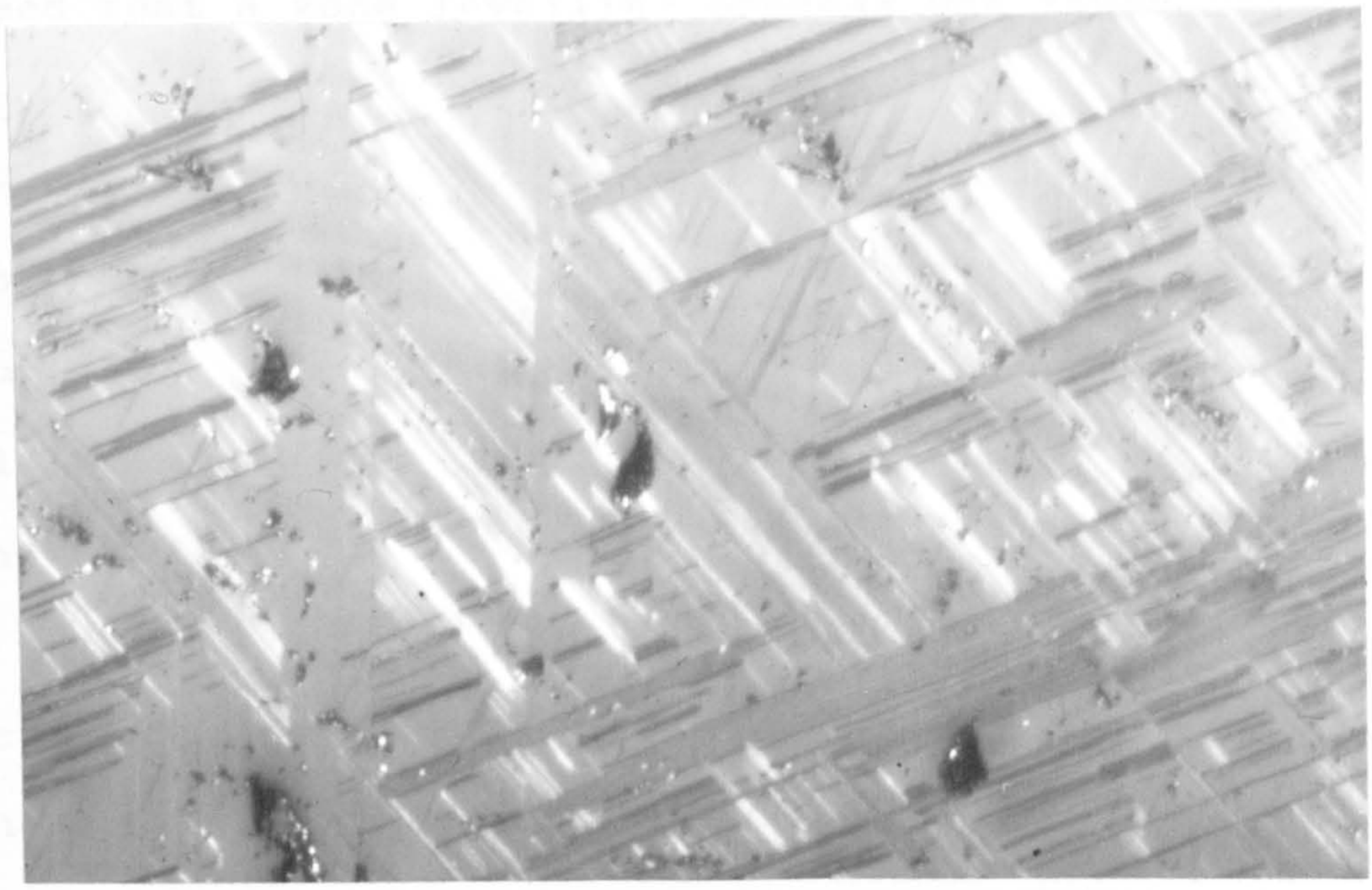

Fig. 3.4 Two phase Widmanstätten structure consisting of platelets of $V_2C$ or $\zeta$-$VC_{1-x}$ in a matrix of VC. Final solidifying zone of rod of starting composition $VC_{0.78}$. Viewed under polarised light. x200

final zone composition was $VC_{0.63}$ which is well within the VC plus $V_2C$ phase field. Optical micrographs indicated that this alloy exhibited a single phase structure over most of the crystal length but that the final solidifying zone (fig. 3.4) showed a two phase structure. This region showed a characteristic Widmanstätten structure due to the precipitation of $V_2C$ or possibly $\zeta$-$VC_{1-x}$ carbide phase during cooling on certain planes in the VC structure. The most probable interface planes are likely to be the close packed {111} VC and {0001} $V_2C$ planes which have close lattice matching.

Metallographic examination of the structure in the vicinity of the final solidifying zone is also useful in determining the approximate composition of the sample if it can be assumed that a zone levelling process has taken place. Thus an alloy of nominally $VC_{0.90}$ is found on examination to be single phase over the majority of its zoned length but the final solidifying zone also contains graphite in the microstructure (fig. 3.5). The estimated composition of the final zone is $VC_{0.97}$, which if zone levelling has occurred would indicate an alloy composition of approximately $VC_{0.88}$, which is in reasonable agreement with the chemical analyses ranging from $VC_{0.87}$ to $VC_{0.90}$.

The alloys all showed longitudional compositional variations as expected from zone melting theories outlined briefly above, but few transverse compositional variations were detected. In the $VC_{0.75}$ alloy, the presence of the Widmanstätten phase was less pronounced in the surface layers than at the centre of the crystal indicating a compositional variation. However it is possible that this

x 150

Fig.3.5 Final zone microstructure of alloy with nominal starting composition $VC_{0.90}$. Graphite is present in the microstructure.

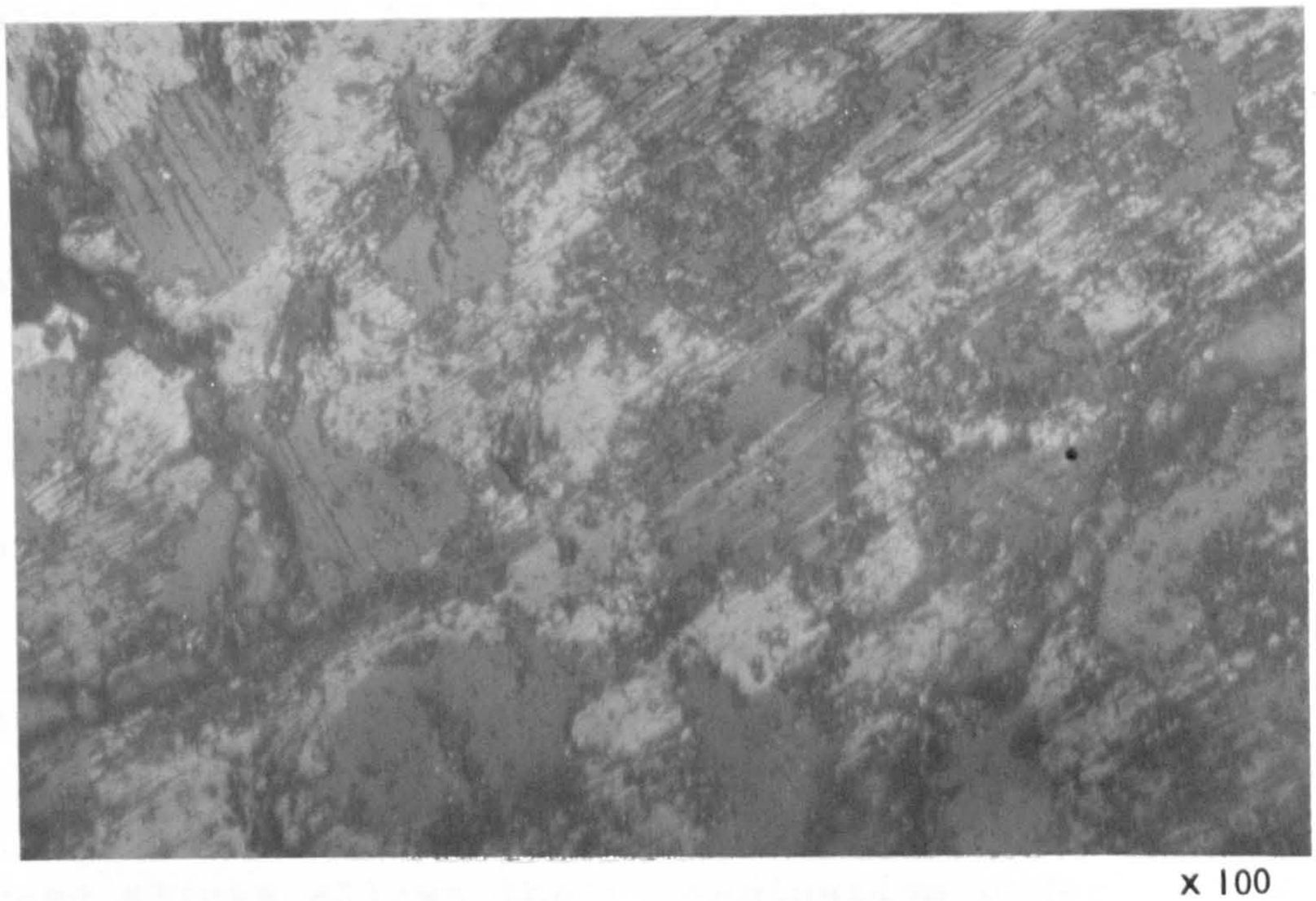

x 100

Fig,3.6 Two phase microstructure in $VC_{0.52}$ alloy. The two phases are $V_2C$ and VC. Viewed under polarised light.

effect could be due to the increased cooling rate near to the surface rather than to a compositional effect.

Single crystals of alloys in the monocarbide phase field ranging in composition from $VC_{0.78}$ to $VC_{0.90}$ were produced. At all other compositions investigated two phase polycrystalline structures were formed.

The $VC_{0.73}$ alloy consisted of large polycrystals of single phase $VC_{1-x}$ in which $V_2C$ or $\zeta-VC_{1-x}$ carbide had precipitated during cooling in a Widmastätten form similar to that shown in fig. 3.4. At lower carbon contents two phase structures were obtained as shown in fig. 3.6. The presence of $V_2C$ in these alloys can be detected by examination with polarised light because it is strongly birefringent due to its hexagonal structure e.g. see fig. - 3.4 or fig. 3.6.

The presence of strongly oriented phases formed during cooling can also be detected in these lower carbon content alloys. Thus fig. 3.7 shows an oriented precipitate in the $VC_{1-x}$ matrix of an alloy showing the characteristic appearance of peritectic solidification. This micro - structure is seen in the final solidifying zone of the $VC_{0.65}$ alloy and consists of primary $VC_{1-x}$ phase containing the strongly oriented $V_2C$ or $\zeta-VC_{1-x}$ carbides, surrounded by a two phase structure of $V_2C$ in which further $VC_{1-x}$ has formed during the cooling.

The presence of an anisotropic superlattice in some of these alloys allows their examination under polarised light conditions when the differently oriented domains in the single phase material are revealed. The domain structure is only observed if a cleaved or highly

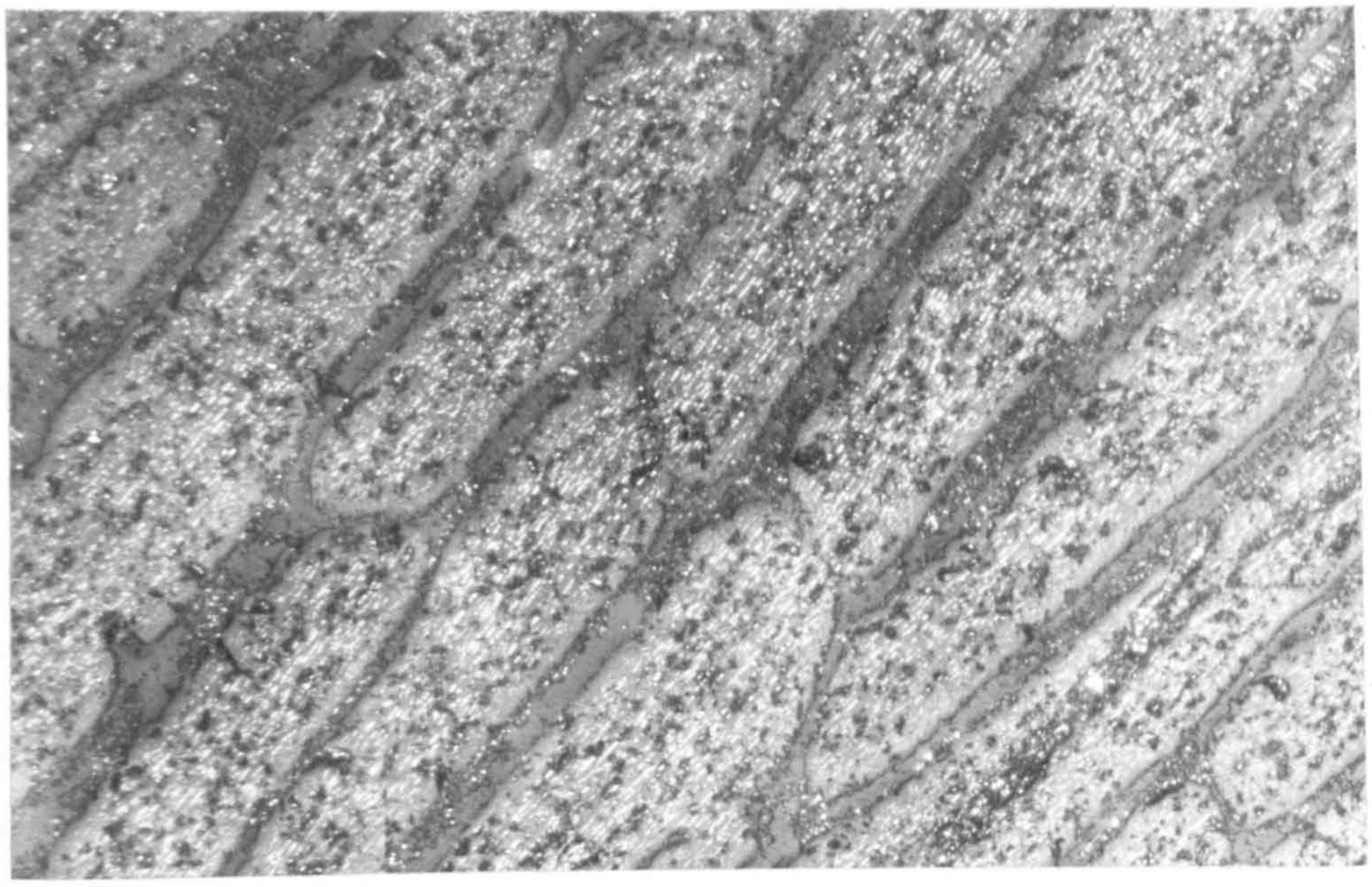

×150

Fig. 3.7 Oriented precipitates formed during cooling in final zone region of $VC_{0.65}$ alloy. Structure shows peritectic solidification of primary $VC_{1-x}$ and inter-dendritic areas of $V_2C$. Viewed under polarised light.

× 200

Fig. 3.8 Domain structure in a $VC_{0.81}$ alloy. Photograph of a polished surface viewed under polarised light.

polished surface is examined (fig. 3.8). The identification of these domains serves as a useful indication of the alloy composition because previous investigators[4] had reported their existance at $VC_{0.83}$ and their absence at $VC_{0.75}$ and $VC_{0.88}$. This technique is also useful for revealing the presence of grain boundaries which are otherwise difficult to detect in these single phase materials.

The final zone of the $VC_{0.90}$ sample contained a highly oriented phase in addition to the VC and graphite phases. This took the form of angular precipitates (fig.3.9) which strongly resemble the 'Mondrian' precipitates reported by Williams[5] in titanium carbide. These were originally thought to be due to graphite, but later work by Williams[6] and Venables[7] indicated that they were probably titanium boride platelets, which could be formed with boron impurity - levels as low as 200 p.p.m. The zone refining nature of the present crystal growth method would tend to concentrate such an impurity into the final zone, and such levels are possible. No positive identification of this phase was made in the present work, and the formation of a new vanadium carbon phase precipitating at low temperatures cannot be ruled out.

Examination of the final zone structure for other alloy compositions revealed similar oriented two phase structures. However, these alloys are expected to contain $V_2C$ or $\zeta$-$VC_{1-x}$ carbides as a second phase in the final zone region, and this is also known to form in a strongly oriented manner[8]. The response of these carbide phases to the acid etches used is similar to that of the borides so unambiguous identification is impossible.

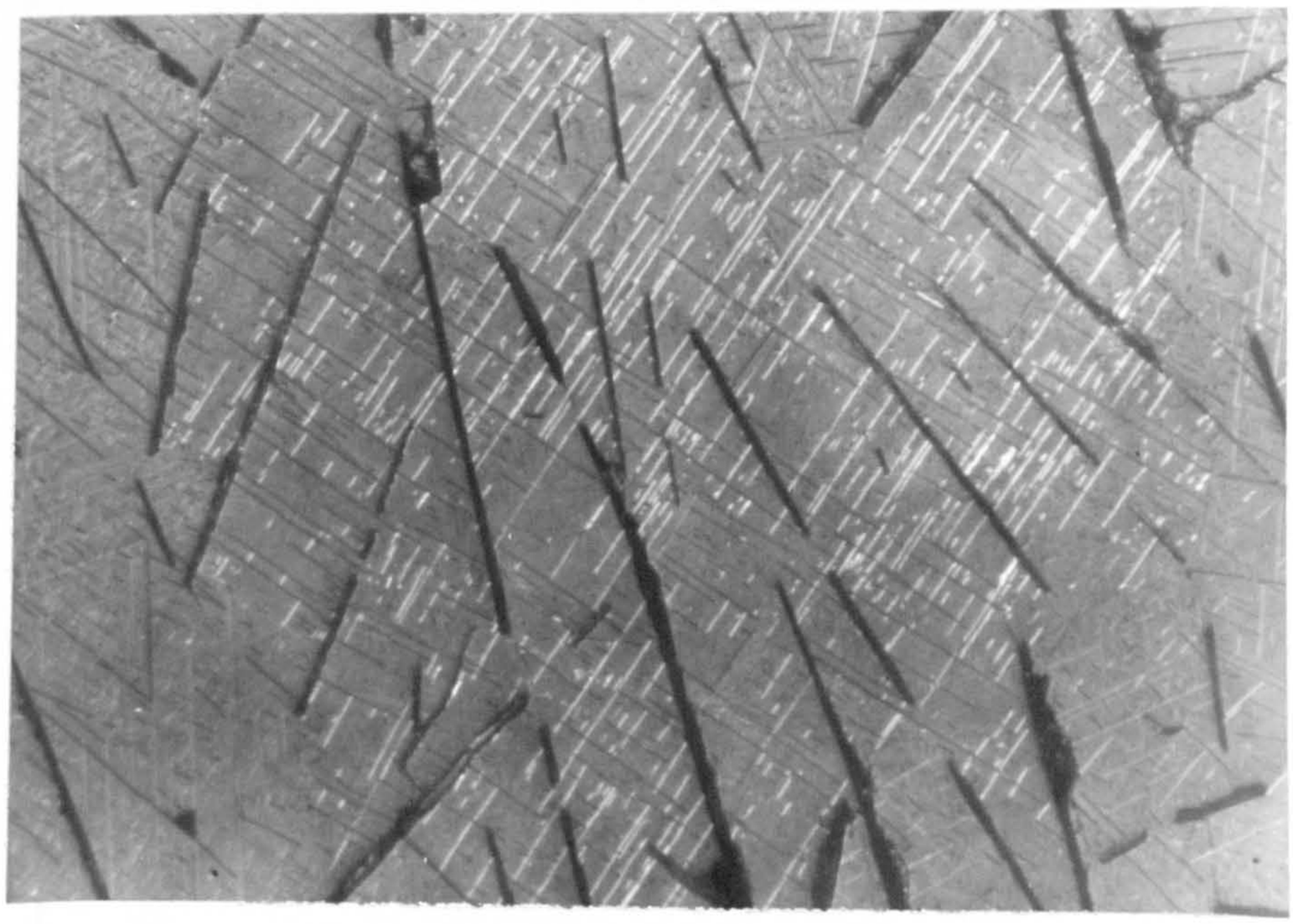

x150

Fig. 3.9 Oriented precipitate in final solidifying zone of $VC_{0.90}$

### 3.3.3 Density Determinations

Density determinations were made on material in the pressed, sintered, and 'as grown' conditions. A pycnometric method was used with ethylene dibromide of specific gravity 2.17 at 20°C as the liquid. Table 3.6 shows the results for all the samples examined.

TABLE 3.6

DENSITY OF SAMPLES

| Nominal Composition | Density of Material ($kg/m^3 \times 10^{-3}$) | | |
|---|---|---|---|
| | Pressed | Sintered | As-Grown |
| VC 0.90 | - | 5.08 | 5.66 |
| VC 0.84 | 5.02 | | 5.64 |
| | | | 5.65 |
| VC 0.81 | 4.89 | 5.06 | 5.64 |
| | 5.11 | | 5.64 |
| | | | 5.64 |
| | | | 5.63 |
| VC 0.78 | 5.02 | 5.17 | 5.61 |
| | | 4.90 | 5.63 |
| | | | 5.62 |
| | | | 5.63 |
| VC 0.73 | 4.67 | 5.04 | 5.62 |
| | | 5.05 | 5.63 |
| | | | 5.64 |
| VC 0.65 | | | 5.65 |
| VC 0.52 | 5.10 | | 5.53 |
| VC 0.47 | | 5.32 | 5.74 |
| | | | 5.81 |
| VC 0.45 | 5.22 | 5.34 | 5.74 |
| | 5.31 | | |

Storms[9] reports the X-ray density of the VC phase as 5.649 at both phase boundaries ($VC_{0.88}$ and $VC_{0.72}$) with a minimum value of 5.607 at a composition of $VC_{0.78}$. The density of the $V_2C$ phase is reported as 5.665 at $VC_{0.50}$. The values agree broadly with the present results and indicate that a measurement of density alone cannot be used as a simple check on composition variation. However the density measurement provides a simple means of verifying the soundness of the grown crystal by comparison with known values for sintered and fully dense material.

## REFERENCES


1. W.G.Pfann "Zone Melting" (John Wiley,New York,1959).
2. P.H.Keck, M.Grun, and M.L.Polk, J.Appl.Phys.,24(1953)1469
3. D.R.Mason and J.S.Cook,Ibid.32,475 (1961)
4. J.D.Venables, Private communication,University of Warwick.
5. W.S.Williams, J.Appl.Phys. 32, 552 (1961)
6. W.S.Williams, Trans.Met.Soc.AIME, 236, 211 (1966)
7. J.D.Venables, Phil.Mag., 16, 143 (1967)
8. L.M.Adelsberg and L.H.Cadoff,J.Am.Ceram.Soc., 51,213(1968)
9. E.K.Storms, "The Refractory Carbides",(Academic Press, New York, 1967)

# CHAPTER FOUR

## EXAMINATION OF THE VANADIUM CARBIDE PHASE FIELD

In this Chapter the microstructures and phase transformations occurring in the vanadium monocarbide phase field are examined. The experimental techniques used are discussed in section 1, and the 'as-grown' crystals examined in section - 2. In the following sections, the phase field is sub-divided according to composition and structure, and the alloys examined as a function of heat treatment temperature. Section - 3 deals with alloys containing the ordered $V_8C_7$ superlattice whereas section 4 examines alloys near to the $V_4C_3$ composition. Alloys based on the ordered $V_6C_5$ compound are described in section 5, and finally in section 6 alloys containing both $V_6C_5$ and $V_8C_7$ are discussed.

### 4.1 Experimental Techniques

#### 4.1.1 Specimen Preparation For Electron Microscopy

As outlined in section 3.2 and 3.3 single crystals were obtained with compositions ranging from $VC_{0.72}$ to $VC_{0.90}$ i.e. effectively covering the whole of the monocarbide phase field. Transverse slices, approximately 1mm thick, were cut from these crystals by spark machining at such points as to ensure that the material was single phase and of known composition.

Vanadium carbide is an electrical conductor and therefore can be thinned, prior to electron microscope examination by electropolishing techniques. The standard p.t.f.e. holder method, which uses samples in the form of 3mm diameter discs, was found to be the most suitable for this material. The discs were prepared from the thin slices

of material by spark machining using a copper tube as the work tool.

The structures of the alloys were examined both in the 'as-grown' state, and after various equilibrating vacuum heat treatments. These were carried out on discs of selected material in a resistance heated horizontal tube vacuum furnace. Vacuum levels throughout the annealing treatments were better than $1 \times 10^{-5}$ torr. The discs were cooled rapidly in an attempt to maintain the equilibrium structure characteristic of the annealing temperature.

Electropolishing was carried out at room temperature in a 5% solution of sulphuric acid in methanol at approximately 20 volts. Polishing was continued until the first perforation appeared in the centre of the disc specimen, which was washed in methanol and dried. The samples could subsequently be stored in air at room temperature without deterioration.

### 4.1.2 Electron Microscopy

The polished samples were examined in a JEM 7 or JEM 200 electron microscope operating at 100 and 200 kv respectively and both equipped with $30^{o}$ tilting stages.

In transmission electron microscopy the image can be formed when either the transmitted beam (bright field image) or the diffracted beam (dark field image) passes through a small aperture in the objective lens. The objective aperture can be translated in a plane perpendicular to the electron beam direction , and is either positioned axially to intersect the main beam or non-axially to include any of the numerous possible diffracted beams. The dark field

technique has been widely used in this work and will therefore be described in more detail.

The quality of the image obtained by displacing the aperture in the simple way described above and observing the image with a non-axial diffracted beam is poor. In addition it falls off rapidly as the distance of the diffracted beam from the axial position increases ( i.e. as the order of reflection increases) due mainly to increased spherical aberration of the objective lens. For high resolution work a method of tilting the illumination must be employed so that the diffracted beam passes axially down the microscope column. This is known as the 'gun-tilt' or 'beam-tilt' method and the simple technique is referred to as 'aperture displacement'.

In the 'gun-tilt' method the incident beam is deflected electromagnetically by means of two coils so that a selected diffracted beam passes along the optic axis. It is possible in this way to tilt the beam so that any diffracted beam can pass along the axis. The technique has additional advantages because greater resolution is possible, because the inelastically scattered beams make a smaller contribution to the image and therefore chromatic aberration is reduced. Furthermore the association of certain regions in the structure (often of extremely small size) with certain diffracted beams can be made because of the enhanced contrast in these regions when imaged with the particular diffracted beam. Thus by examination in a number of such diffracted beams the regions in the microstructure giving rise to particular diffracted spots can be identified.

In practice gun-tilting is often difficult and time consuming especially if a large number of reflections are to be examined. Thus preliminary searching experiments are usually carried out using the displaced aperture technique, and precise analyses, when these are indicated, by using the gun-tilt method. The image forming ray makes an angle of twice the Bragg angle with the optic axis in displacement dark field images, and this leads to large spherical aberration in the image. If the accelerating voltage of the microscope is increased the Bragg angles will be correspondingly smaller, and the dark field images of correspondingly better quality. Sahashi[1] has shown that at high voltage (>500 kv) aberrations are much reduced, and are almost negligable at 1000 kv for low order reflections, enabling high resolution images to be obtained simply and quickly by the displaced aperture technique. Noticeable improvements in the dark field displaced aperture images have been obtained for low order reflections on changing from 100 to 200 kv accelerating potentials. The techniques described have been used in an analysis of the structure throughout the vanadium-carbon phase field described in the following sections.

## 4.2 Structure Of 'As-Grown' Crystals

Optical microscope examination (section 3.3.2) had indicated that the monocarbide phase field could be broadly divided into three regions based on microstructural appearance and composition. Intermediate compositions near to $VC_{0.83}$ were characterised by the presence of a domain structure when viewed under polarised light conditions

(see fig. 3.8) which was absent in alloys of both higher and lower carbon contents. Lower carbon content alloys ($VC_{0.73}$) often contained a small amount of second phase in the microstructure which had presumably formed by a solid state reaction during cooling (see fig. 3.4). The third region consisted of alloys near to the upper carbide graphite boundary which showed no distinguishing features in a single phase structure. Graphite was however present in some of the alloys of highest carbon content.

Electron microscope examination of the alloys confirmed that this preliminary division of the phase field was justified, and the electron diffraction patterns supported this conclusion. Thus at intermediate compositions long range order was detectable with diffraction patterns consistent[2] with the presence of $V_6C_5$ (fig. 4.2.1) whereas at higher carbon contents the presence of an ordered superlattice which was different from $V_6C_5$ was indicated by the diffraction evidence (fig. 4.2.2). At lower carbon contents no long range order was detected.

Some samples especially those within the intermediate composition range, showed a variety of structural differences within narrow compositional limits. Thus quite marked differences in the size of the long range ordered domains, and in the substructure within the domains, were obtained. Some alloys contained a high proportion of striations within domains, which led to profuse streaking in the diffraction patterns (fig.4.2.3) whereas others contained fewer striations or small regions entirely free from striations The possibility of another form of order being present in

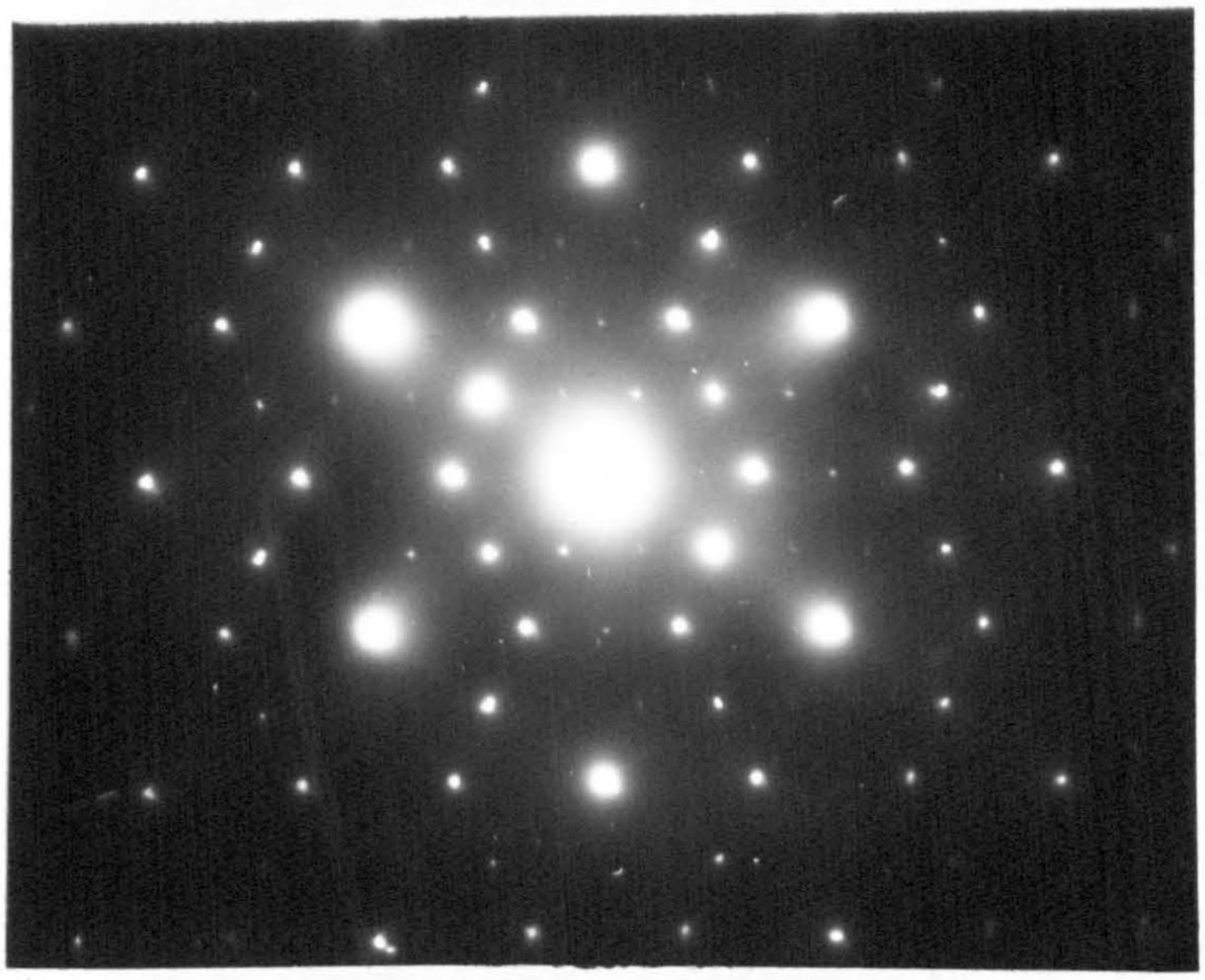

Fig. 4.2.1 Diffraction pattern from $VC_{0,81}$ alloy. 110 pattern consistent with presence of $V_6C_5$ superlattice.

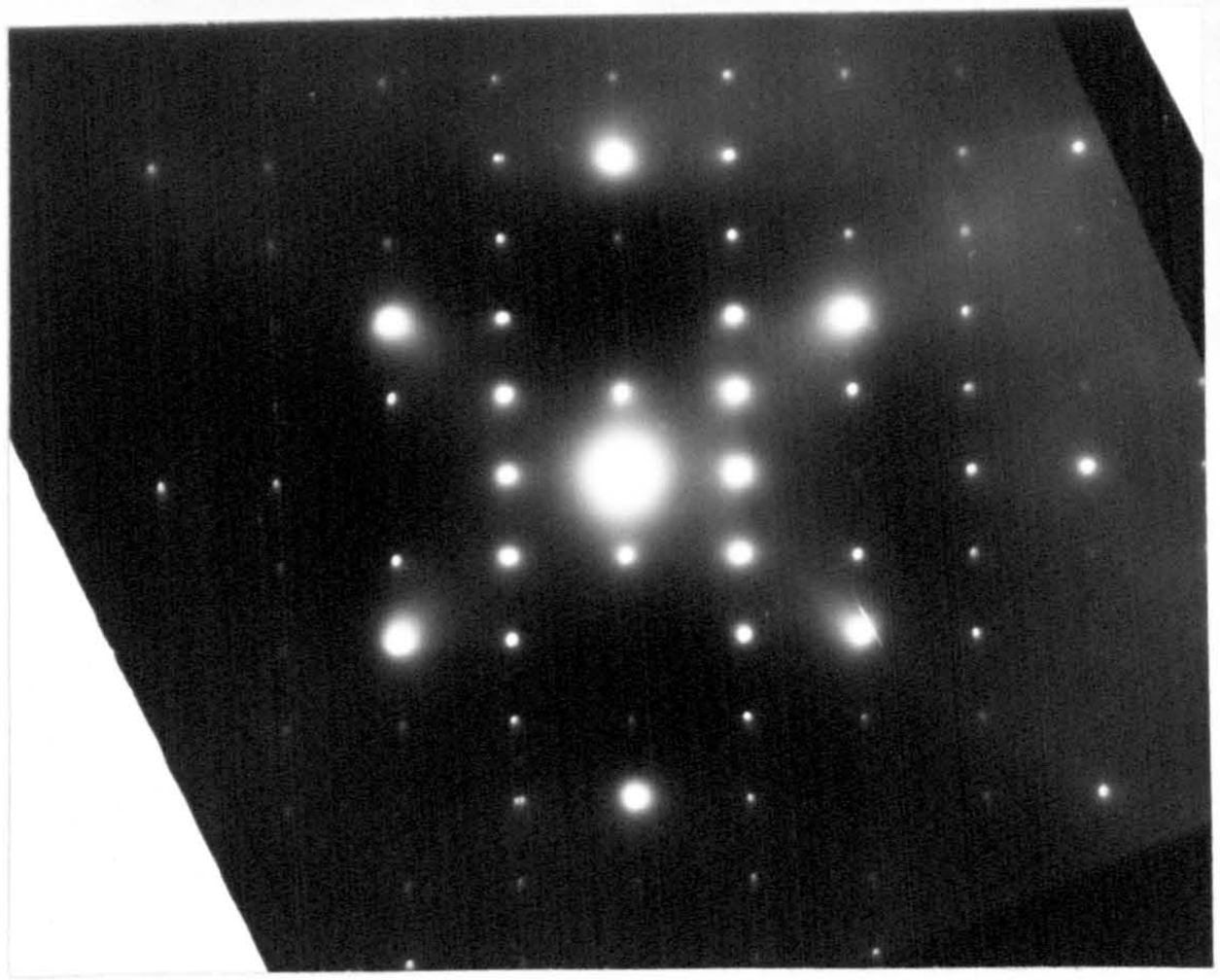

Fig. 4.2.2 Diffraction pattern from $VC_{0.89}$ alloy. 110 pattern containing superlattice spots not consistent with the presence of $V_6C_5$.

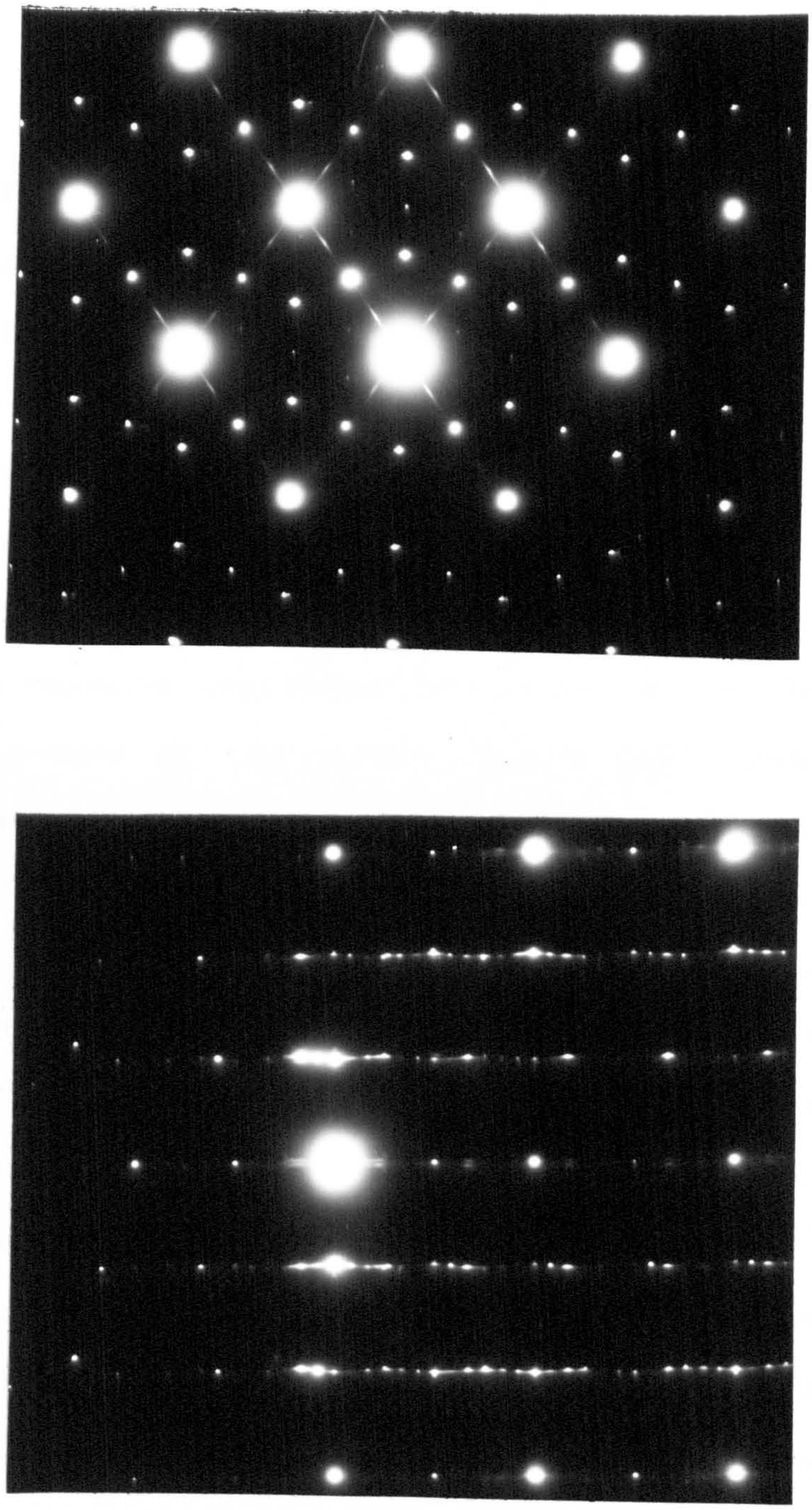

Fig. 4.2.3 Diffraction patterns from $VC_{0.81}$ alloys showing profuse streaking in addition to the superlattice spots.

this composition range perhaps only within a certain temperature range, was indicated by the appearance of extra spots in certain diffraction patterns.

These variations indicated that very small compositional changes corresponding to c/v ratios of approximately 0.2 were having a profound effect on the structure. However, it is known that different parts of the 'as-grown' single crystals receive different heat-treatments and cooling rates because of the method chosen for crystal growth. Thus these heat treatment differences could also possibly account for some of the observed structural variations. In view of this it was decided to anneal the samples under standard conditions prior to examination, in an attempt to obtain near equilibrium structures to aid the correlation of microstructure and composition.

In the following sections 4.3 to 4.6 the relationship between structure and composition in the vanadium monocarbide phase-field will be discussed in greater detail. The effect of temperature on the structural stability will also be considered.

## 4.3 The $V_8C_7$ Superlattice

### 4.3.1 Electron Diffraction

The X-ray work of de Novion et al [3] had shown that an ordered structure existed at a composition of $VC_{0.88}$ and this had been confirmed by Russian workers[4]. The structure of the ordered phase was reported as cubic with a unit cell approximately twice that of the parent rocksalt structure and the vacancy positions as outlined in section -

1.3 and fig. 1.4. The calculated 'd' spacings for this superlattice are shown in Table 4.3.1 below.

TABLE 4.3.1

| h.k.l. | d in Å | Intensity |
|---|---|---|
| 110 | 5.894 | VW |
| 111 | 4.812 | VW |
| 210 | 3.727 | W |
| 222 (111 primary) | 2.406 | VS |
| 320 | 2.311 | W |
| 400 (200 primary) | 2.083 | VS |
| 520-432 | 1.548 | W |
| 440 (220 primary) | 1.473 | VS |
| 622 (311 primary) | 1.256 | S |
| 630-542 | 1.242 | W |
| 444 (222 primary) | 1.203 | W |

Electron diffraction patterns obtained from alloys in the composition range $VC_{0.87}$ to $VC_{0.90}$ are shown in fig.-4.3.1 for specimens in which the electron beam is nearly parallel to ⟨100⟩ ⟨110⟩ ⟨111⟩ and ⟨112⟩ directions. Accompanying each photograph are the predicted diffraction patterns from the superlattice of de Novion et al and their

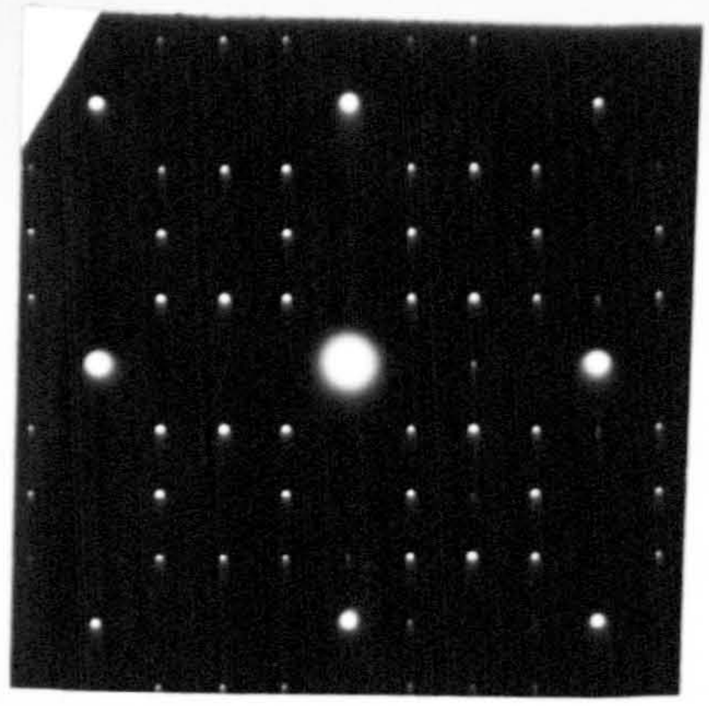

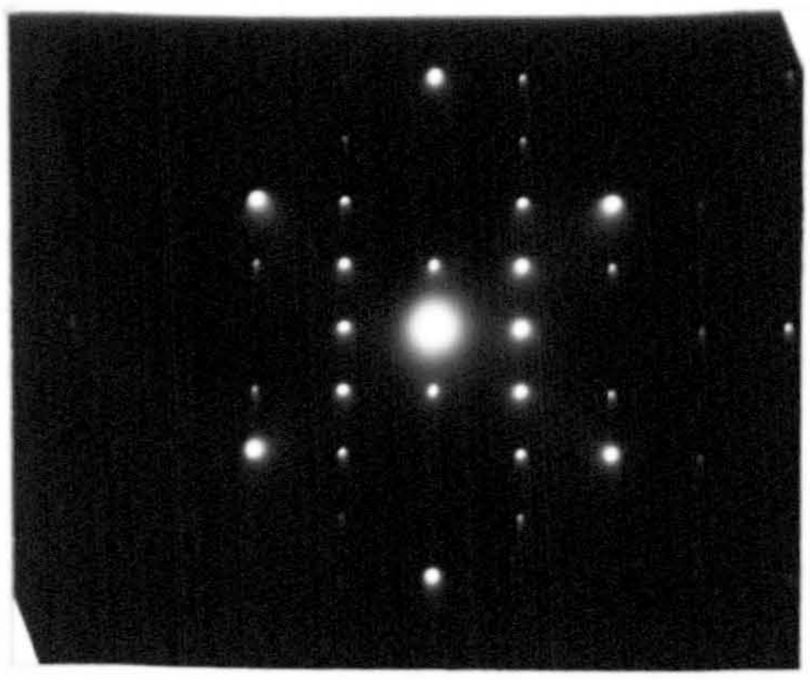

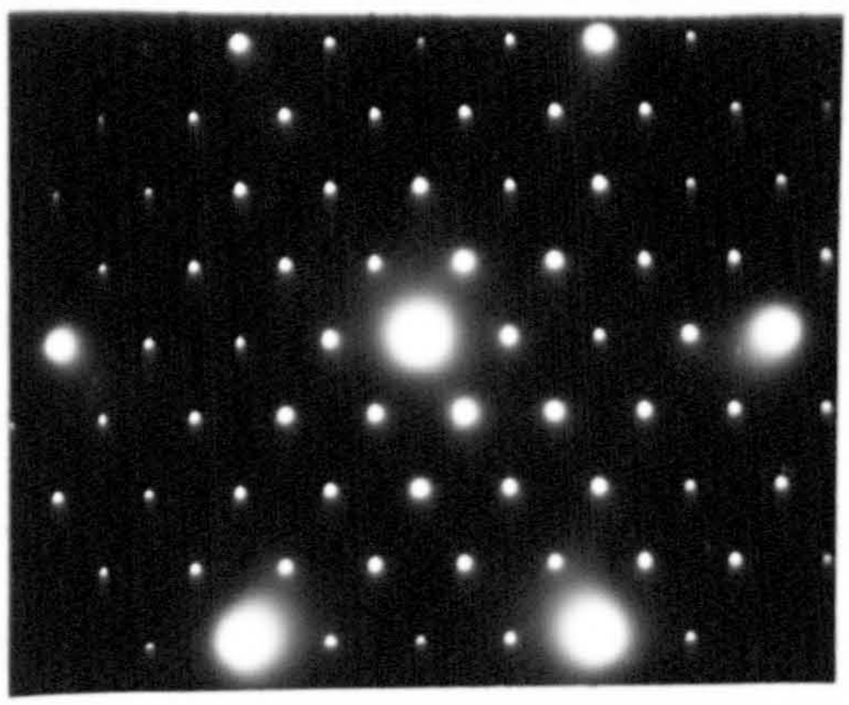

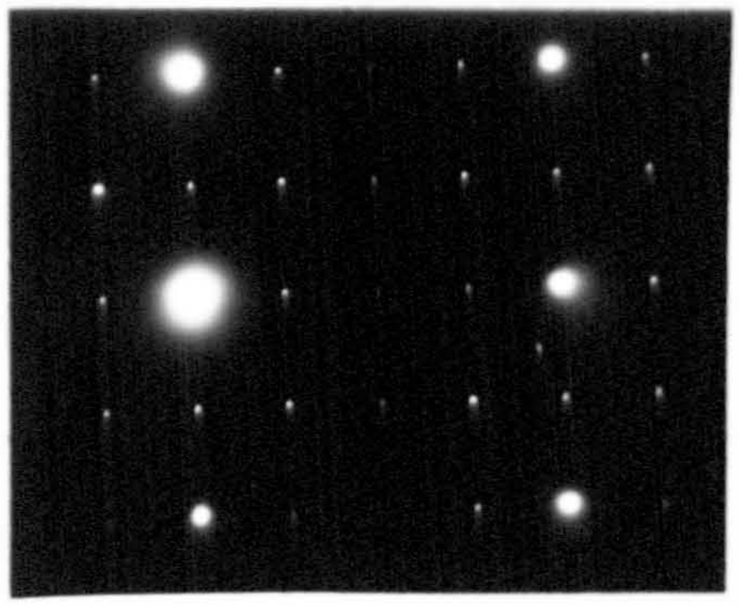

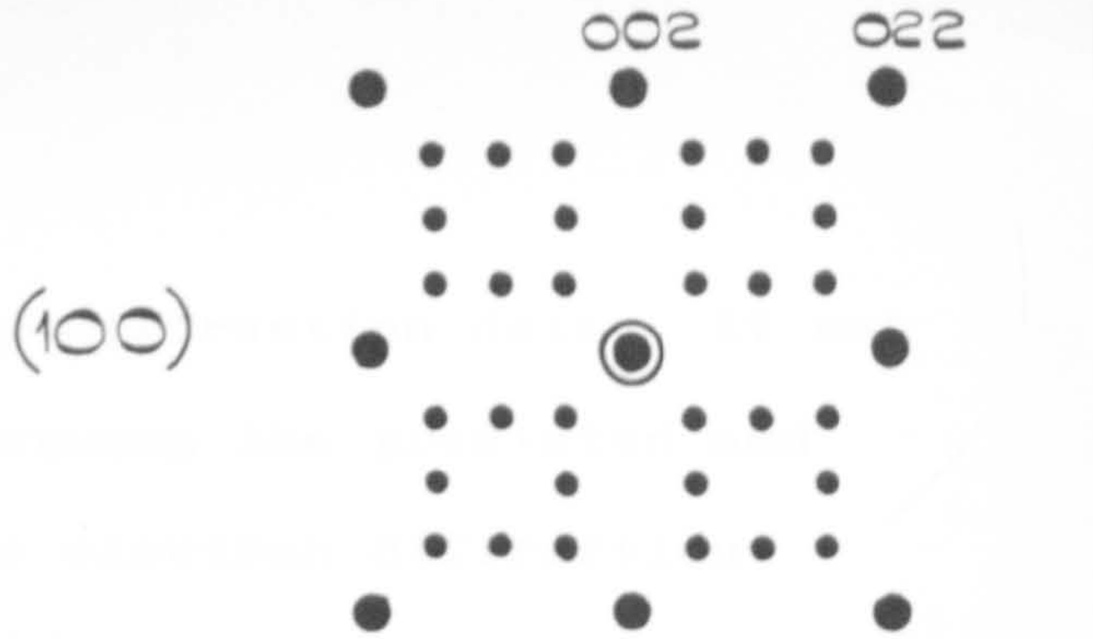


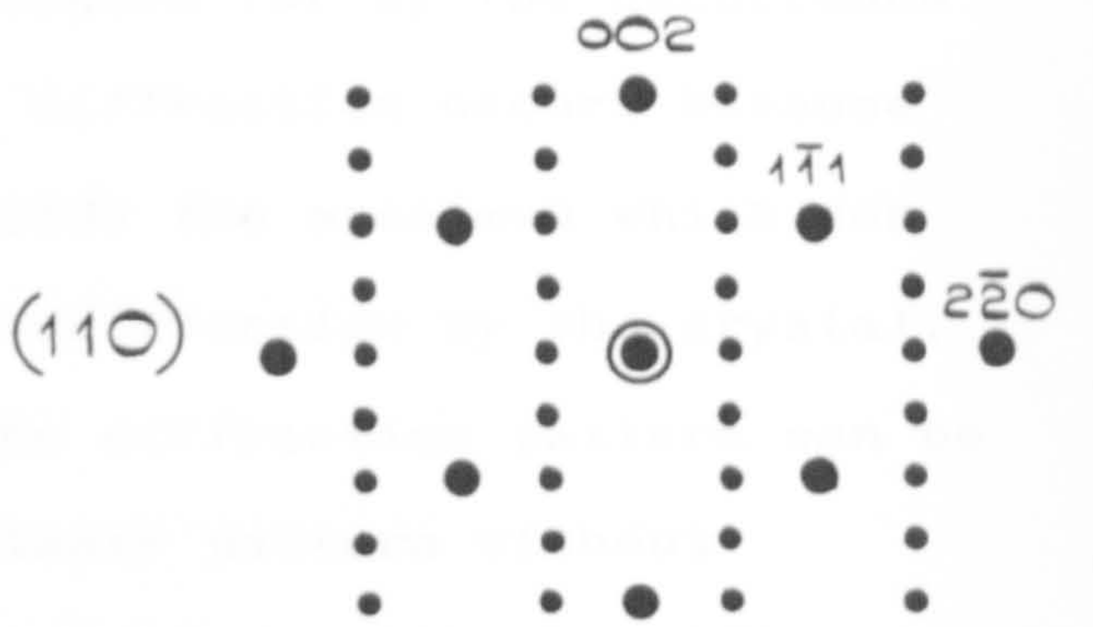


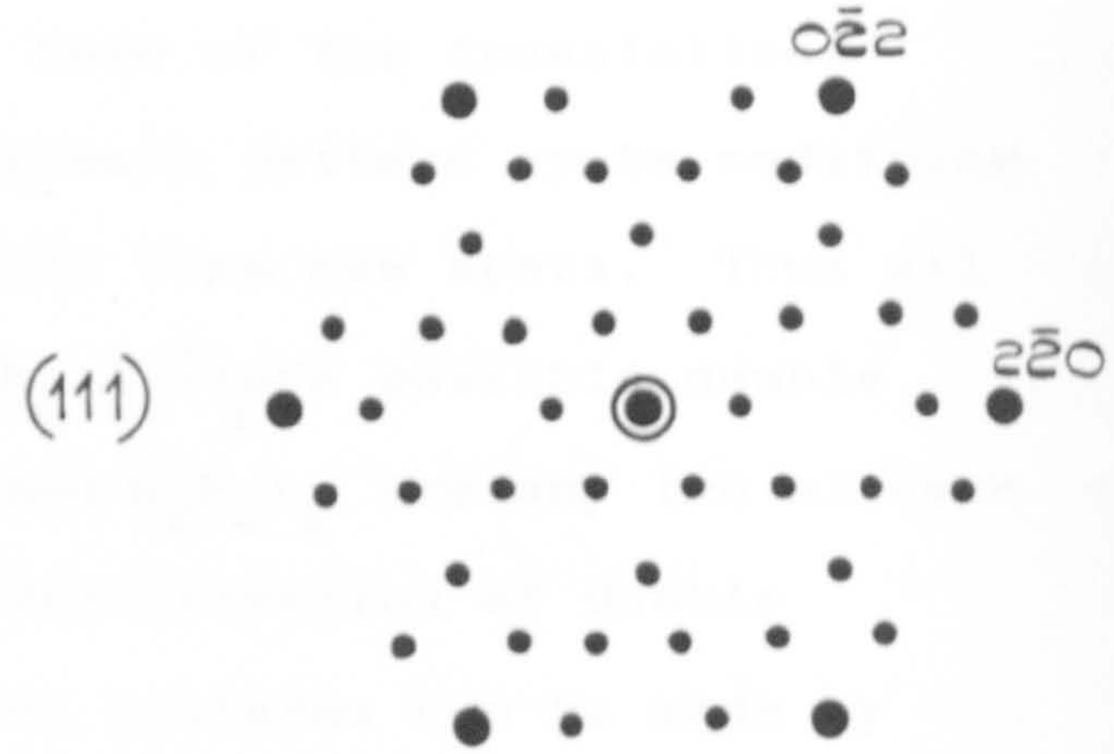


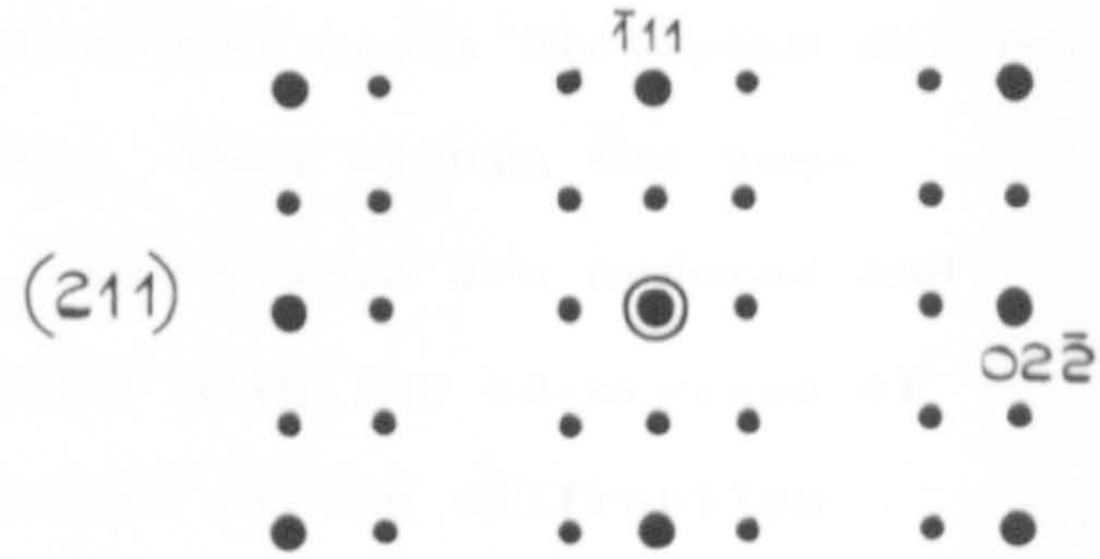


Fig. 4.3.1.

DIFFRACTION PATTERNS FROM $VC_{0.89}$.
ON THE RIGHT ARE THE PREDICTED PATTERNS
FOR THE $V_8C_7$ SUPERLATTICE (de Novion et al.[3]).

- PRIMARY LATTICE SPOTS.
- SUPERLATTICE SPOTS.

experimentally determined X-ray diffraction data. It can be seen that broad agreement between the predicted and actual data is obtained but the electron diffraction patterns contain a number of extra spots. All of these extra spots can however be accounted for by the occurrence of double diffraction. Double diffraction occurs because diffracted beams are formed inside the specimen which can act as new sources for further diffraction by the crystal. The resulting extra spots in the diffraction pattern can be obtained by translating the primary pattern without rotation so that the origin corresponds with the diffraction spots of the primary pattern. Some of the translations will coincide with existing primary pattern spots modifying their intensities but others will form new spots. Thus all spots of the form $h_1 \pm h_2, k_1 \pm k_2, l_1 \pm l_2$ are possible double diffraction spots where $h_1 k_1 l_1$ and $h_2 k_2 l_2$ are any two allowed primary spots. The positive identification of double diffraction spots in diffraction patterns can be made by tilting the sample about a reciprocal lattice vector containing the spots, when double diffraction spots disappear whereas true diffraction spots do not. Thus within the composition range $VC_{0.87}$ to $VC_{0.90}$ the alloys are ordered and the diffraction data is consistent with the occurrence of the $V_8C_7$ superlattice. Examination of the diffraction patterns from samples annealed in the temperature range $600^{o}$ to $1200^{o}C$ were identical to those described above although some microstructural changes did occur (see section 4.3.5).

### 4.3.2 Domain Structure

Ordering usually occurs as a nucleation and growth process from a disordered matrix, with the two phases often sharing a common lattice with relatively small distortions . The dimensions of the ordered unit cell are often multiples of the disordered cell. The ordered phase is characterised by specific atoms occupying a specific sublattice of the crystal, but there is no reason why any particular sublattice should be chosen from the many available by the nucleating ordered phase. Thus separately nucleated domains will grow and eventually touch each other, forming a metastable structure of anti-phase domains just like the grains in a polycrystalline material. Between each domain there may exist an anti-phase boundary (A.P.B.) or 'out of step' relationship. The shape of the boundaries is determined by the condition that the total boundary energy should be a minimum. Thus if the A.P.B. energy is anisotropic a rearrangement of the boundaries will occur so that they lie parallel to low energy planes. In order that such a system be stable and fill space without the domains combining and consuming each other there must be at least four different possible types of domain [5]. This condition is determined by the number of sublattices available and the symmetry of the ordered structure. Thus in practice the formation of such a 'foam structure' of domains is possible in all common ordered structures except for the β-brass type ($B_2$ type superlattice) in which only two types of domain are possible.

If two parts of a crystal can be derived one from

the other by means of a translation defined by a lattice vector of the disordered crystal, but not of the ordered crystal, the interface between two such parts is known as an anti-phase boundary (A.P.B.). There are two possible types of anti-phase at such a domain boundary, one where the vector lies in the plane of the boundary and the other where the vector does not lie in the plane of the boundary. These are described by Marcinkowski [6] as anti-phase vectors of the first and second kind respectively. One difference between them is that the production of an anti-phase of the first kind does not create a nett change in wrong nearest neighbours across the boundary, while the removal of a plane of atoms, which is required for the out of step of the second kind, means that an increase in the number of wrong nearest neighbours across the boundary is produced. Thus these two types of anti-phase have different A.P.B. energies, the first type being of lower energy. In one dimensional long period superlattices in f.c.c. alloys (discussed later in section - 4.5.4) the anti-phase is always of the first kind. The general relationship can be expressed in the following way. If the anti-phase domain boundary is characterised by $\{h\,k\,l\}$ and the out of step vector $\langle u\,v\,w\rangle$ then for the first kind of anti-phase -

$$hu + kv + lw = 0 \qquad (1)$$

whereas for the second kind of anti-phase

$$hu + kv = lw \neq 0 \qquad (2)$$

Fisher and Marcinkowski [7] have shown that the stacking faults contrast theory developed by Wholan and Hirsch [8] can be extended to the case of anti-phase

boundaries in superlattices because the images of both types of defect are due to phase contrast. An A.P.B. is characterised by a constant displacement vector $\underline{R}$, and the contrast is determined by the phase changes $\alpha = 2\pi \underline{g}.\underline{R}$ occurring when the electrons traverse the defect ($\underline{g}$ is the reciprocal lattice vector for the operating reflections). Thus the intensity distribution associated with electron waves will consist of alternate light and dark fringes for certain values of $\alpha$, and the fault vector $\underline{R}$ can be determined using an analysis of $\underline{g}.\underline{R}$ and by noting the invisibility of fringes in certain reflections. Care must be excercised in this type of analysis because the extinction distance $\xi$ may be large compared with the foil thickness, when fringes will be absent. The extinction distance is given by the expression

$$\xi = \frac{\pi a_o^3 \cos\theta}{\lambda} \frac{1}{F} \qquad (3)$$

where $\lambda$ is the relativistically corrected wave length of the electrons, and F is the structure factor for a unit cell of edge length $a_o$ associated with a reflection $\underline{g}$ and can be written as

$$F = \sum_j f_j \exp(-2\pi i \underline{g}.\underline{r}_j) \qquad (4)$$

where $f_j$ is the atomic scattering factor associated with the $j^{th}$ atom located at $r_j$ in the unit cell.

Ordered structures usually exhibit two well defined types of reflection characterised by the structure factors

$$F_f = (f_A + f_B) \qquad (5)$$

$$F_s = S(f_A - f_B) \qquad (6)$$

where the subscripts f and s refer to the fundamental and superlattice reflections, S is the long range order parameter

of Bragg and Williams[9] which has a value of 1 for a fully ordered alloy and 0 for a disordered alloy, and $f_A$ and $f_B$ are the atomic scattering factors for atoms A and B in the alloy AB. These equations indicate that the structure factor associated with a superlattice reflection is much smaller than that of a fundamental reflection, and therefore from equation 3 the corresponding extinction distance is relatively large. These distances are usually in excess of 2000Å and therefore the fringe spacing observed at A.P.B's corresponds to a depth periodicity of approximately 1000Å near the exact Bragg condition, which is typically the thickness of the thin foils for microstructural examination. Thus the contrast usually consists of a single dark or bright region rather than as a set of fringes characteristic of stacking faults[8].

The intensity of the superlattice reflections is given

$$I \propto |F|^2 \propto S^2 (f_A - f_B)^2 \qquad (7)$$

and examination shows that this will be extremely weak if the degree of order is small, or if the atomic scattering factors of the elements involved are similar e.g. Cu Zn. The intensity of the fundamental reflections will be much greater since the structure factor terms involved are additive i.e.

$$I \propto |F|^2 \propto S^2 (f_A + f_B)^2 \qquad (8)$$

The original theory of Fisher and Marcinkowski[7] did not include the effect of anomalous absorption, but later workers[10a,10b] have considered the effect both of different absorption parameters, and of deviation from the

Bragg reflecting position, on the image profiles for a number of values of the phase angle ($\frac{\pi}{10}$, $\frac{2\pi}{3}$ and $\pi$). Many beam dynamical calculations of the effect of systematic multiple reflections on the image profiles have also been reported[11].

Examination of the proposed structure for $V_8C_7$ indicated that anti-phase boundaries with fault vectors of the type $^a/4\ \langle 110\rangle$ and $^a/12\ \langle 112\rangle$ are possible (see fig. 4.3.2). Table 4.3.2 lists values of a calculated for these possible fault vectors in various reflections, which can be used to facilitate an analysis of R.

TABLE 4.3.2

| hkl | R | a | R | a |
|---|---|---|---|---|
| $110_s$ | | $\pm\ \pi\ ,\ 0$ | | $\pm\frac{\pi}{3}\ \ \frac{\pi}{2}\ ,\ 0$ |
| $111_s$ | | $\pm\ \pi\ ,\ 0$ | | $\pm\frac{\pi}{3}, \pm\frac{2\pi}{3}\ ,\ 0$ |
| $210_s$ | | $\pm\ \frac{\pi}{2}\ \frac{\pm 3\pi}{2}, \pm\ \pi$ | | $\pm\frac{5\pi}{6}, \pm\frac{\pi}{6}\ \pm\frac{\pi}{2}\ ,0$ |
| $220_s$ | $\frac{a}{4}\langle 110\rangle$ | $\pm\ \pi\ ,\ 0$ | $\frac{a}{12}\langle 112\rangle$ | $\pm\ \pi\ , \pm\frac{\pi}{3}, \pm\frac{2\pi}{3}\ ,\ 0$ |
| $222_m$ | | 0 | | $\pm\frac{4\pi}{3}, \pm\frac{2\pi}{3}\ ,\ 0$ |
| $400_m$ | | 0 | | $\pm\frac{2\pi}{3}, \pm\frac{4\pi}{3}$ |
| $330_s$ | | $\pm\frac{3\pi}{2}\ ,\ 0$ | | $\pm\frac{3\pi}{2}\ , \pm\frac{\pi}{2}, \pm\ \pi\ , 0$ |
| $440_m$ | | 0 | | $\pm\frac{4\pi}{3}, \pm\frac{2\pi}{3}\ ,\ 0$ |

Inspection shows that it should be possible to distinguish between the two types of fault by examination in 222, 400, or 440 reflections since faults of the type $^a/4\ \langle 110\rangle$ should be invisible for all reflections of this type.

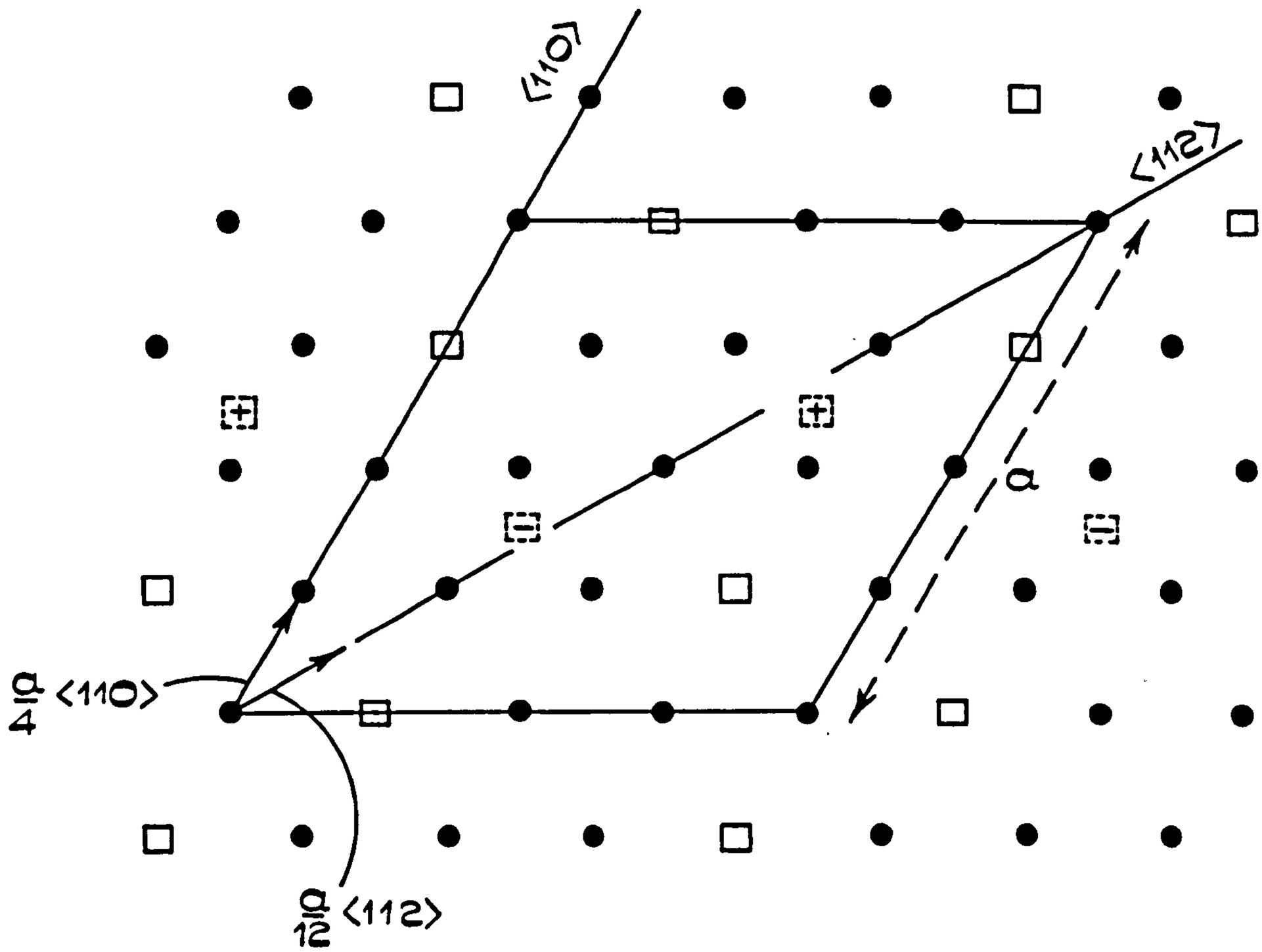


FIG. 4.3.2.

POSSIBLE ANTI-PHASE VECTORS IN THE $V_8C_7$ SUPERLATTICE. PROJECTION OF CARBON ATOMS ON CLOSE PACKED {111} PLANES. THE VANADIUM ATOMS ARE NOT SHOWN.

● OCCUPIED CARBON ATOM SITE

□ UNOCCUPIED CARBON ATOM SITE.

[+] [−] UNOCCUPIED ATOM SITES IN {111} PLANE ABOVE AND BELOW REFERENCE PLANE.

### 4.3.3 Microstructural Observations

All alloys in the composition range $VC_{0.87}$ to $VC_{0.90}$ exhibited a 'foam structure' of ordered domains under suitable imaging conditions (fig. 4.3.3). If a large number of superlattice reflections could contribute to the image, such as when the electron beam was parallel to a prominent zone axis, then the anti-phase boundaries were clearly outlined and contained a number of fringes. However, imaging under normal two-beam conditions with a superlattice reflection operating revealed the boundaries as single light or dark bands as predicted in section 4.3.2 above (fig 4.3.4) The domain boundaries did not show any strong tendancy to lie parallel to any particular crystallographic plane. An analysis of the fault vectors following Table 4.3.2 indicates that the fault vectors are of the type $^{a}/4\ \langle 110\rangle$ since no fringes were seen with 222, 400 or 440 reflections operating. The shape of the domains and the formation of a character - istic foam structure are consistent with a multiplicity of vectors of the type $^{a}/4\ \langle 110\rangle$ .

The dark field analysis of such structures is complicated by the presence of large numbers of double diffraction spots and by the close proximity of the spots. The double diffraction spots can be identified by tilting about a reciprocal lattice vector containing these spots when they should disappear but with the present conditions this is experimentally very difficult to accomplish. The dark field micrographs shown in fig. 4.3.5 illustrate extinction for certain A.P.B's with the indicated operating reflections. All analyses are consistent with anti-phase vectors of the type $^{a}/4\ \langle 110\rangle$

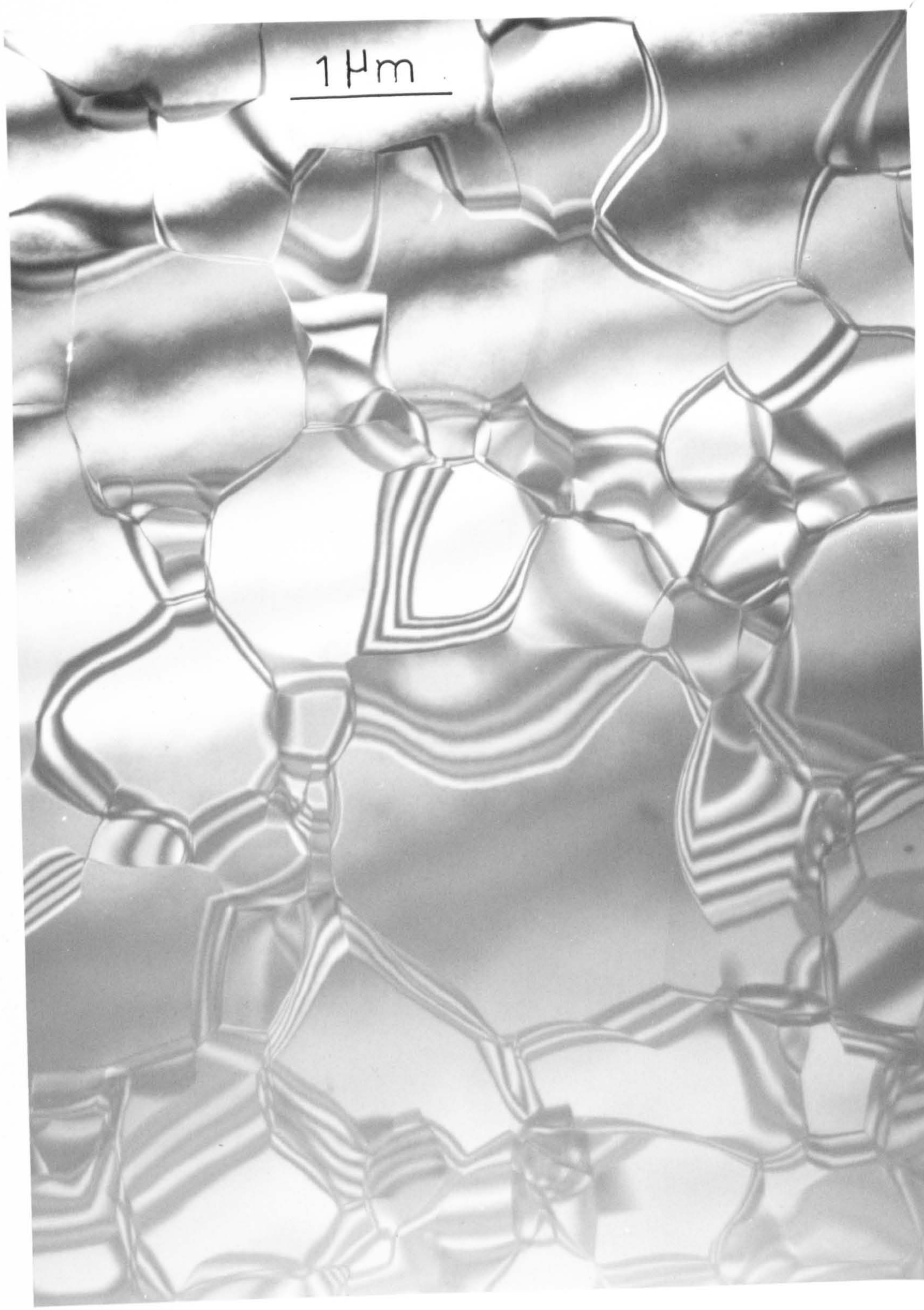


FIG. 4.3.3.

FOAM STRUCTURE OF A.P.B's IN VC0·87:-

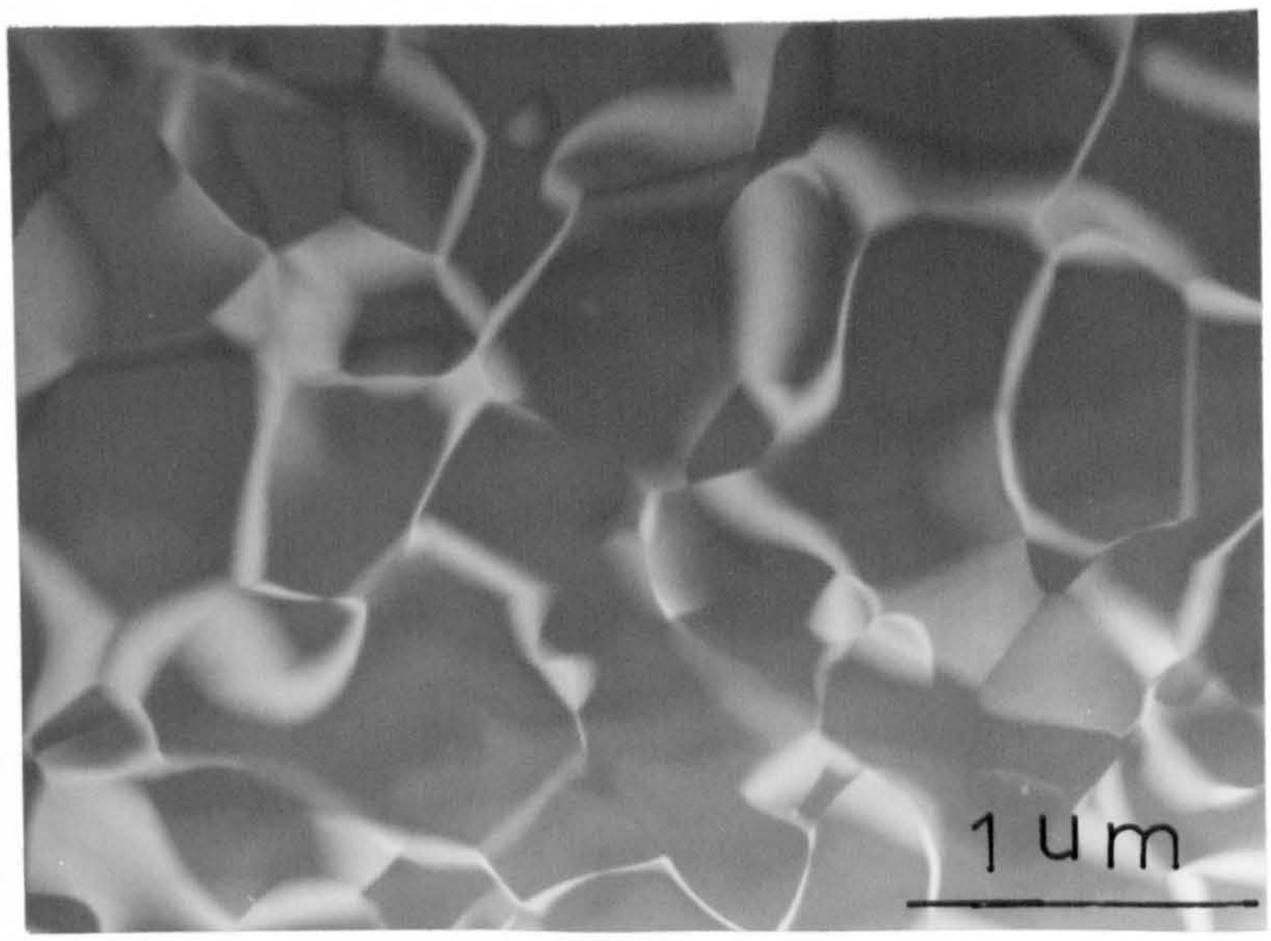


Fig.4.3.4 A.P.B's in $VC_{0.89}$ alloys imaged under two beam conditions with a strong superlattice operating reflection.

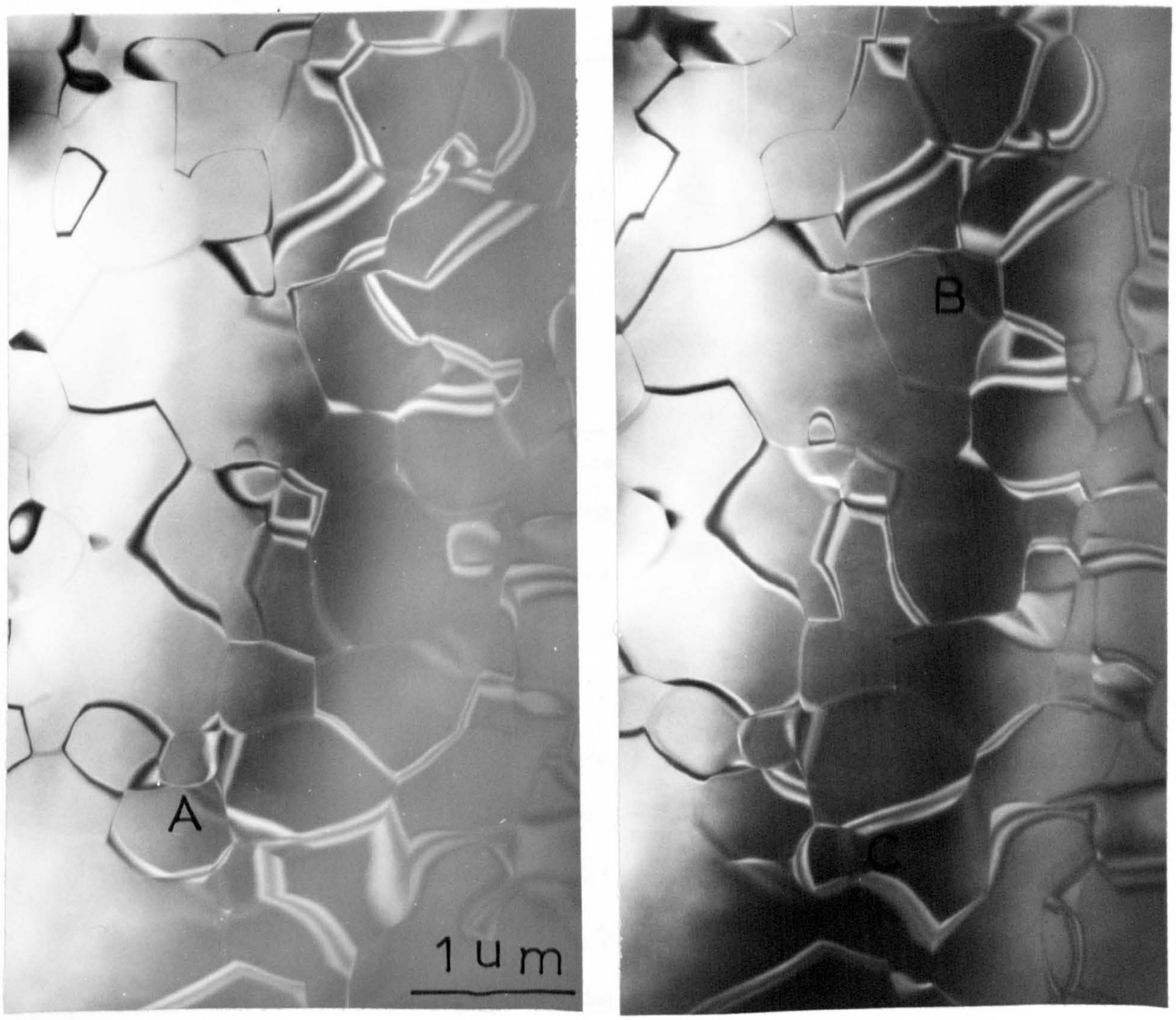


Fig.4.3.5 Dark field micrographs of A.P.B's taken with (a) $1\bar{1}1$ and (b) $\bar{1}11$ operating reflections. Note extinctions at A,B and C.

### 4.3.4 Dislocations In $V_8C_7$

In addition to the thermal A.P.B's discussed in the previous section other A.P.B's can be formed by the passage of a dislocation through an ordered structure. It is energetically feasible for dislocations to pass through ordered structures in pairs (known as super-dislocations) and of necessity the region between the dislocations is an A.P.B. In the $V_8C_7$ structure the possible types of dis - locations are listed in Table 4.3.3. (with reference to the vanadium sublattice).

TABLE 4.3.3

| Type of Dislocation | Disordered | Ordered $V_8C_7$ |
|---|---|---|
| Perfect | $a/2$ $\langle 110 \rangle$ | $a'/4$ $\langle 110 \rangle$ |
| Shockley partial | $a/6$ $\langle 112 \rangle$ | $a'/12$ $\langle 112 \rangle$ |
| Frank partial | $a/3$ $\langle 111 \rangle$ | $a'/6$ $\langle 111 \rangle$ |

where a' is lattice parameter of $V_8C_7$ structure

During examination of the $V_8C_7$ alloys, few dis - locations were seen except in isolated subgrain boundaries (fig. 4.3.6). Such dislocations were paired and had Burgers vectors of the same sign as evidenced by the black and white oscillations at the ends of adjacent dislocations being the same[12] as would be expected for super-dislocations. Under suitable imaging conditions A.P.B's could be seen between the paired dislocations fig. 4.3.7 which also shows A.P.B's terminating on dislocations in the boundary.

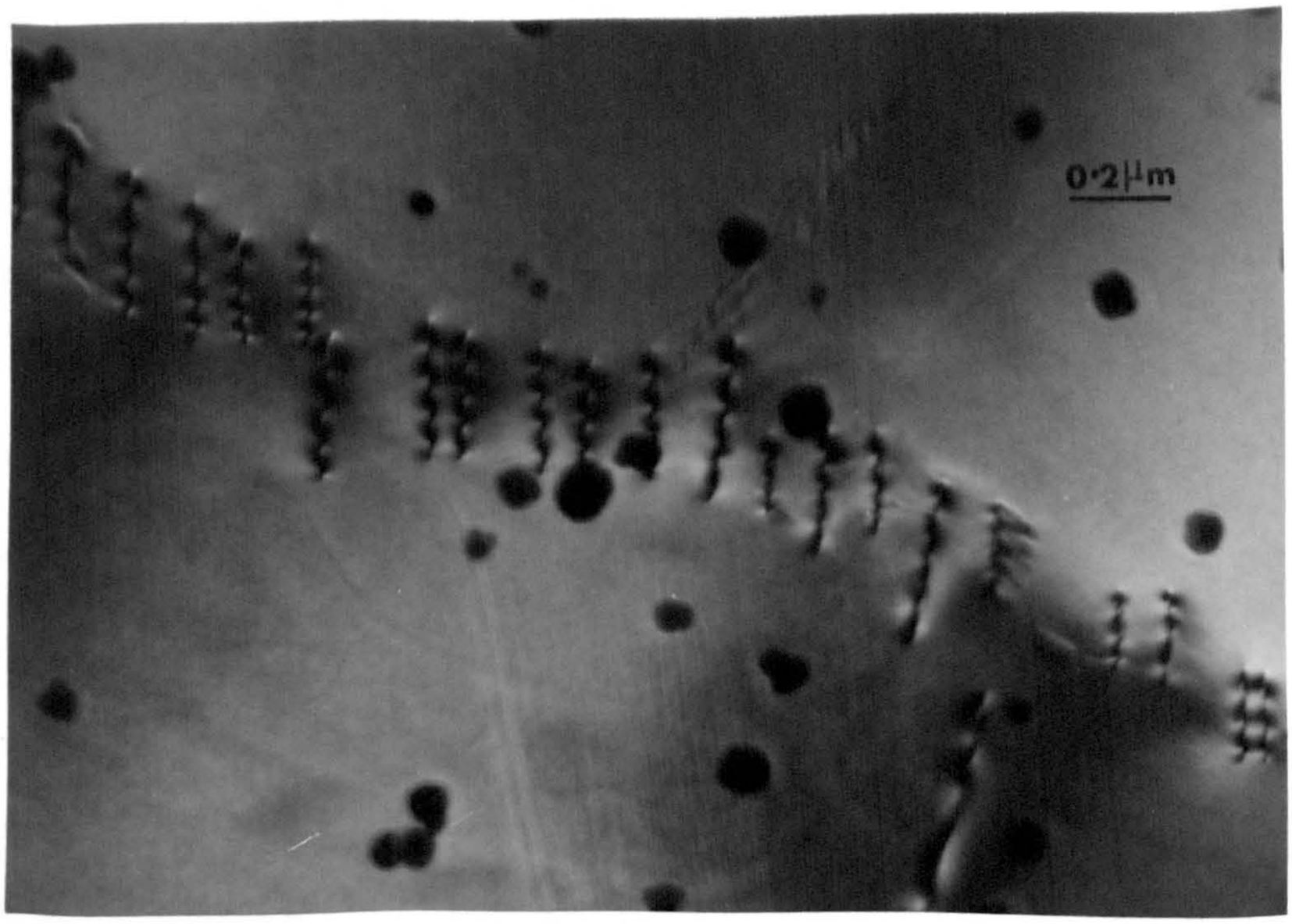


Fig. 4.3.6 Paired dislocations in $V_8C_7$. Note similar black and white oscillations at ends of adjacent dislocations

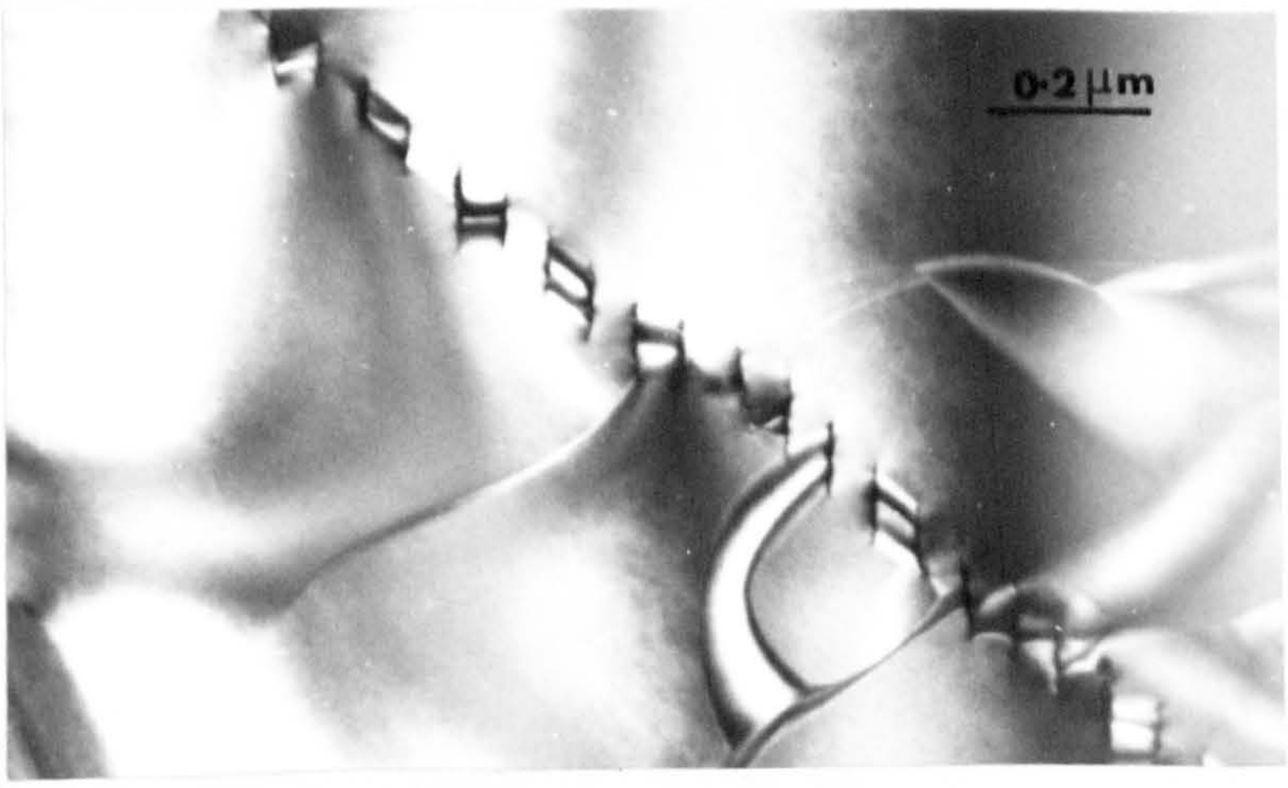


Fig. 4.3.7 Showing A.P.B's between paired dislocations in sub-grain boundary in $VC_{0.90}$.


Fig. 4.3.8 Straight A.P.B's in $VC_{0.90}$.

Occasionally very long straight A.P.B's were seen (fig. 4.3.8) which are usually indicative of dislocation produced boundaries as opposed to the more irregularly shaped thermal A.P.B. composing the 'foam structure'.

### 4.3.5 Order Disorder Critical Temperature For $V_8C_7$

The effect of heat treatment on the ordered structure was investigated by examining samples annealed for 100 hours in the temperature range 700 to 1200°C. No change in the 'foam structure' or in the diffraction patterns was seen following such treatments at temperatures up to 1070°C. However, following 1130° and 1200°C treatments a marked reduction in the domain size was detected. Since the samples were rapidly cooled during these treatments, to ensure the examination of near equilibrium structures, it was thought that the small domain size was a consequence of quenching from the disordered state at an insufficient rate to suppress the ordering reaction. Thus the order disorder temperature of the alloys $VC_{0.87}$ to $VC_{0.90}$ is likely to be in the temperature range 1070°C to 1130°C. This is in approximate agreement with some Russian work[13] where a break in the curve relating enthalpy and temperature occurred at 1120°C in a $VC_{0.92}$ alloy. Examination of an alloy in the 'hot stage' of the 100 kv electron microscope up to the maximum stage operating temperature of 1000°C failed to produce any change in the microstructure or diffraction pattern.

## 4.4 Lower Carbon Alloys ($^{C}/_{V} < 0.75$)

### 4.4.1 Electron Diffraction

No long range order was detectable in diffraction patterns from 'as-grown' alloys in the composition range $VC_{0.70}$ to $VC_{0.75}$ but they were characterised by the presence of diffuse intensity bands (fig. 4.4.1). The occurrence of such diffraction effects indicates that the carbon atom distribution is not completely random in these alloys, and moreover the fact that intensity maxima occur at $\frac{1}{2}\ \frac{1}{2}\ \frac{1}{2}$ positions (with respect to the f.c.c. reciprocal lattice) means that the arrangement of carbon atoms is different on alternate {111} planes. The diffraction effects are not modified by heat treating the alloys and are thought to represent a stable equilibrium state for the system which will subsequently be referred to as the S-state. Similar diffuse banding has been seen by Bell[14] in VO and TiN, by Hollox and Venables[15] in TiC-VC alloys, and by Watanabe et al.[16] in TiO where it was attributed to the presence of a form of short range order.

Comparison of the diffraction patterns with those associated with the fully ordered $V_6C_5$ compound reported at $VC_{0.84}$ indicates that the bands intersect prominent reciprocal lattice vectors close to long range order spot positions e.g. $\frac{1}{2}\ \frac{1}{2}\ \frac{1}{2}$, $\frac{2}{3}\ \frac{2}{3}$ o (fig. 4.4.1 ) . When discussing this compound (and its relationship with the parent lattice) it is often helpful to use indices referred to the cubic parent lattice because indices for the superlattice are multiples of this. This does lead to the use of fractional indices but these are retained for convenience. However, as

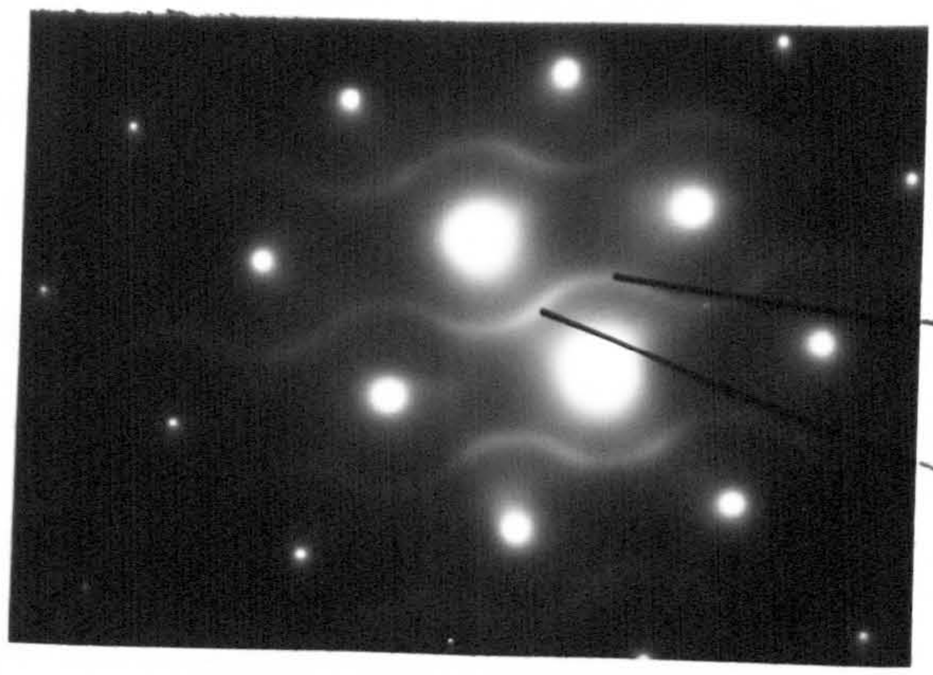


(á) 110 pattern

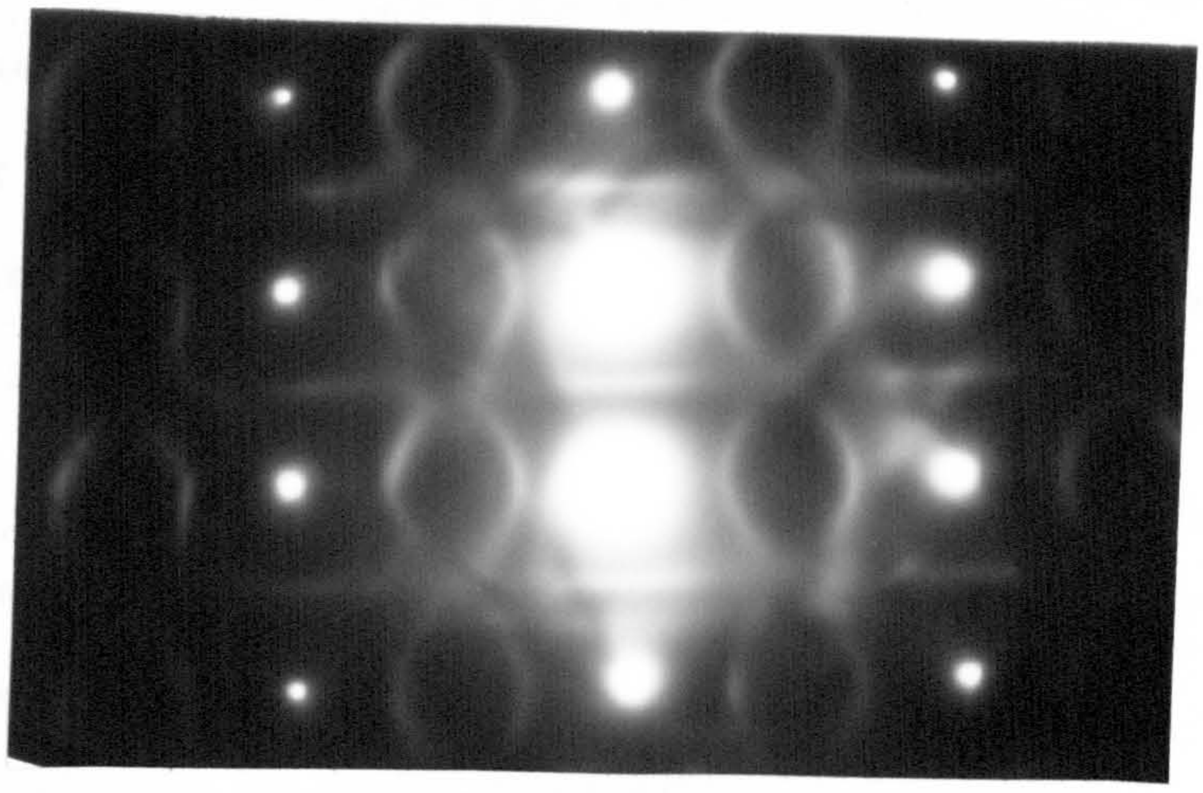

(b) 112 pattern

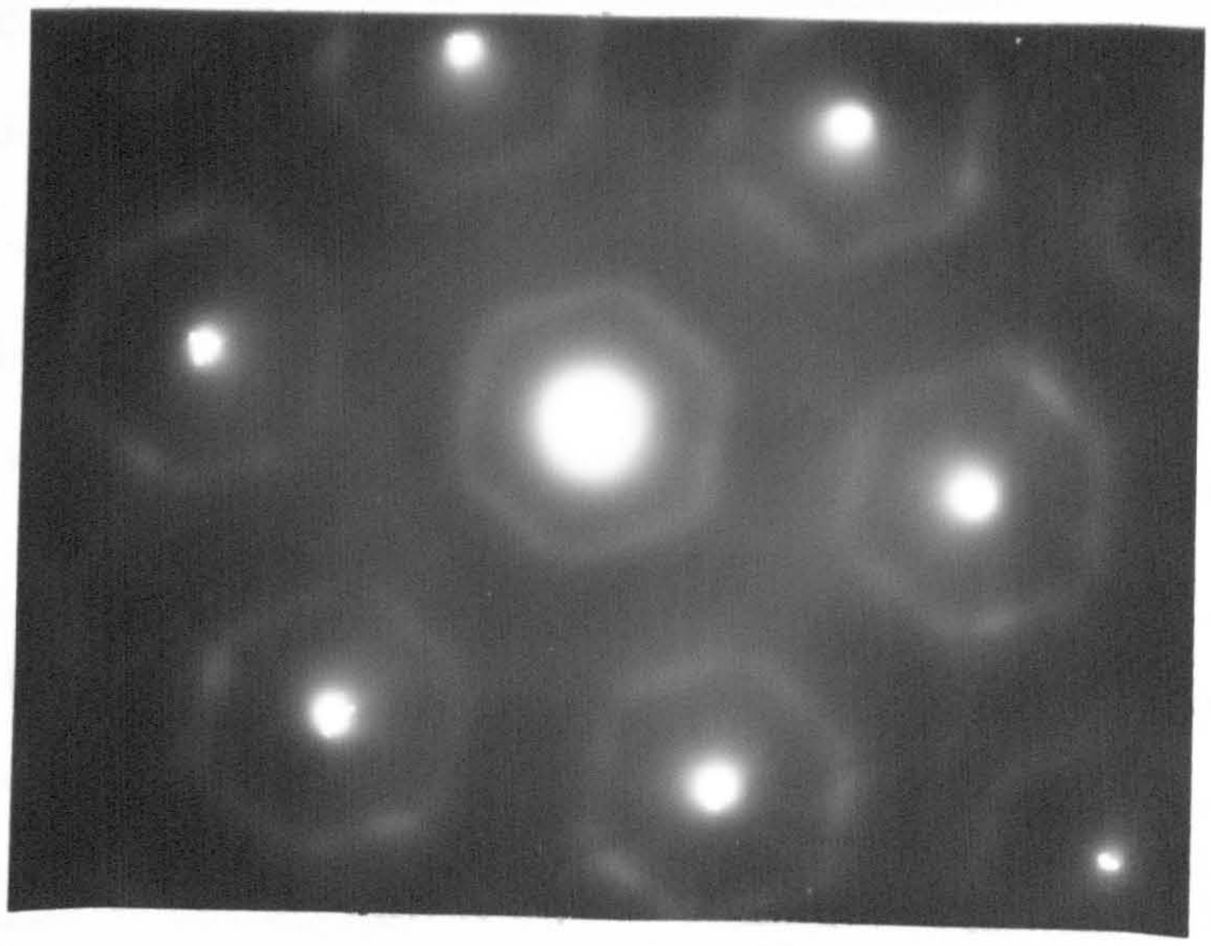

(c) 111 pattern

Fig. 4.4.1 Diffuse intensity bands in diffraction patterns from alloys in the composition range $VC_{0.70}$ to $VC_{0.75}$.

in other systems, such as the nickel molybdenum system investigated by Ruedl et al.[17], the position where the diffuse regions intersects the reciprocal lattice vector does not exactly coincide with the position of the long range order spots which subsequently form (e.g. $\frac{2}{3}$ $\frac{2}{3}$ o).

Beam heating experiments in the electron microscope did result in the formation of long range order spots. This was originally thought to be a heat treatment effect due to the rise in temperature of the sample, but extensive annealing experiments (up to 200 hours on 'as-grown' material before electropolishing) at temperatures in the range of $600^{o}$ to $1200^{o}$C failed to reproduce the long range order. A more likely explanation is that vanadium evaporation occurred at the high temperature generated by the beam heating, which resulted in an effective local increase in carbon content, thereby adjusting the composition into a region of the phase field where long range ordered phases were stable. This was confirmed in later experiments when an alloy of composition $VC_{0.72}$ was severely beam heated, and developed long range order spots consistent with the presence of the ordered compound $V_8C_7$ i.e. the composition had been locally adjusted to $VC_{0.87}$ or above. Similar compositional changes have been observed by Hollox[18] in beam heated samples.

4.4.2 Microstructure

Optical metallography had indicated that at $VC_{0.75}$ the material was single phase but that precipitates of either $V_2C$ or $\zeta$ - $VC_{1-x}$ formed at slightly lower carbon contents e.g. $VC_{0.72}$ (see section 3.3.2). These observations

were confirmed in the electron microscope examination of the 'as-grown' material.

At $VC_{0.75}$ the alloy was single phase with few distinguishing features and exhibited banding in the diffraction pattern as outlined above. One possible explanation of the diffuse banding is that it is associated with the presence of extremely small long range ordered domains. Very careful examination of high resolution dark field images, obtained by tilting the beam so that the objective aperture was filled with the maximum intensity region of the diffuse bands, failed to detect the presence of small ordered domains.

At slightly lower carbon contents e.g. $VC_{0.73}$ large numbers of fringed faults were observed (fig. 4.4.2). The fringe contrast obtained with the faults is similar to that associated with stacking faults in f.c.c. materials in which the phase angle $\alpha$ for electrons changes by $\pm 2\pi/3$ when traversing the fault plane. It is different from that associated with the usual type of anti-phase boundary for which $\alpha = \pi$ . Thus the fringes are symmetric in bright and asymmetric in dark field, and additional fringes form at the centre of the faults as the foil thickness increases. Diffraction patterns associated with these faulted regions contained only spots associated with the face centred cubic vanadium carbide phase, no precipitate or superlattice spots could be detected.

It can be shown by trace analysis of different sections that all the faults lie on {111} planes. Thus in a foil with a [110] normal (such as seen in fig. 4.4.3)

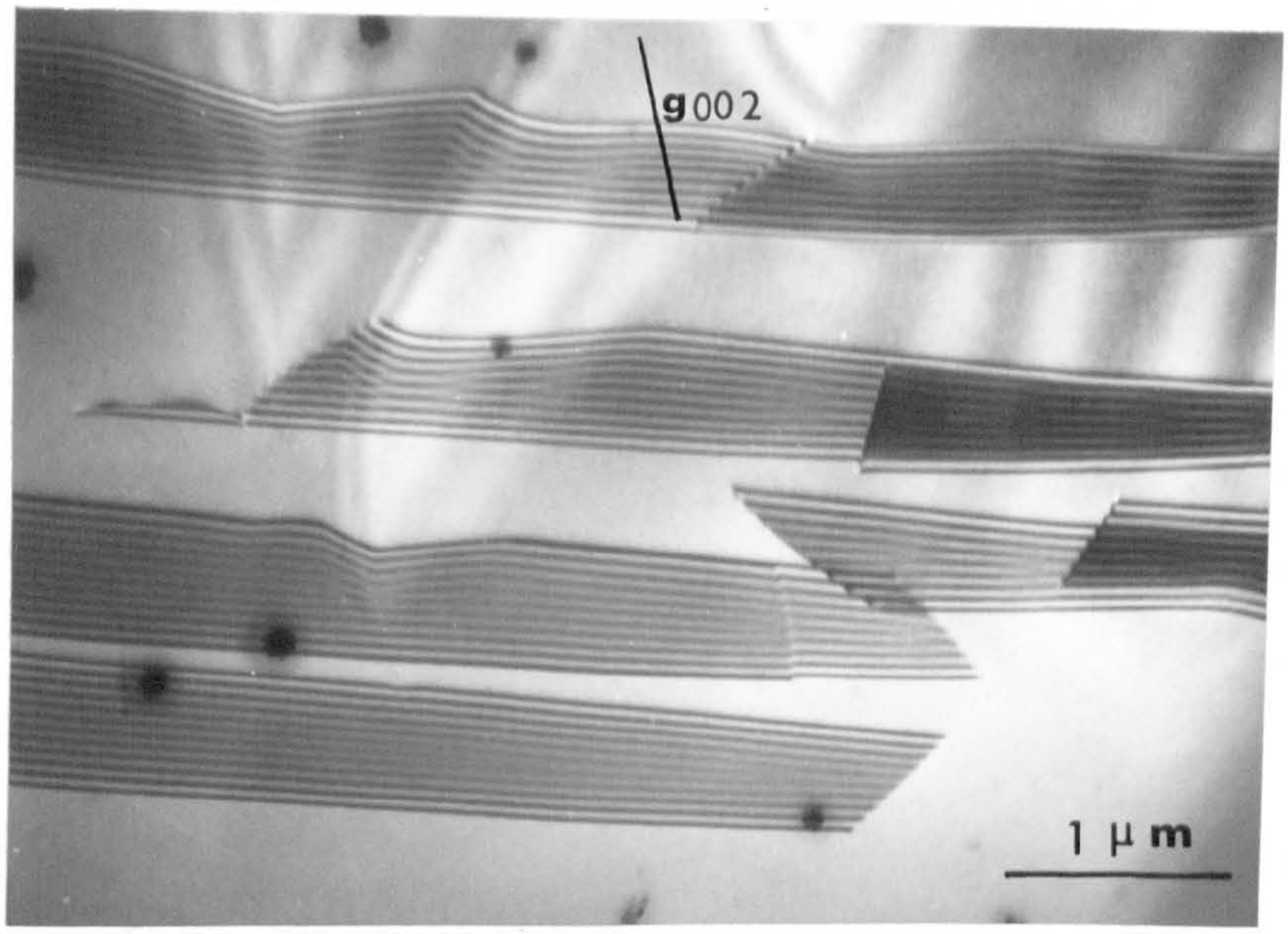


Fig. 4.4.2 Large number of faults in $VC_{0.73}$ alloy.

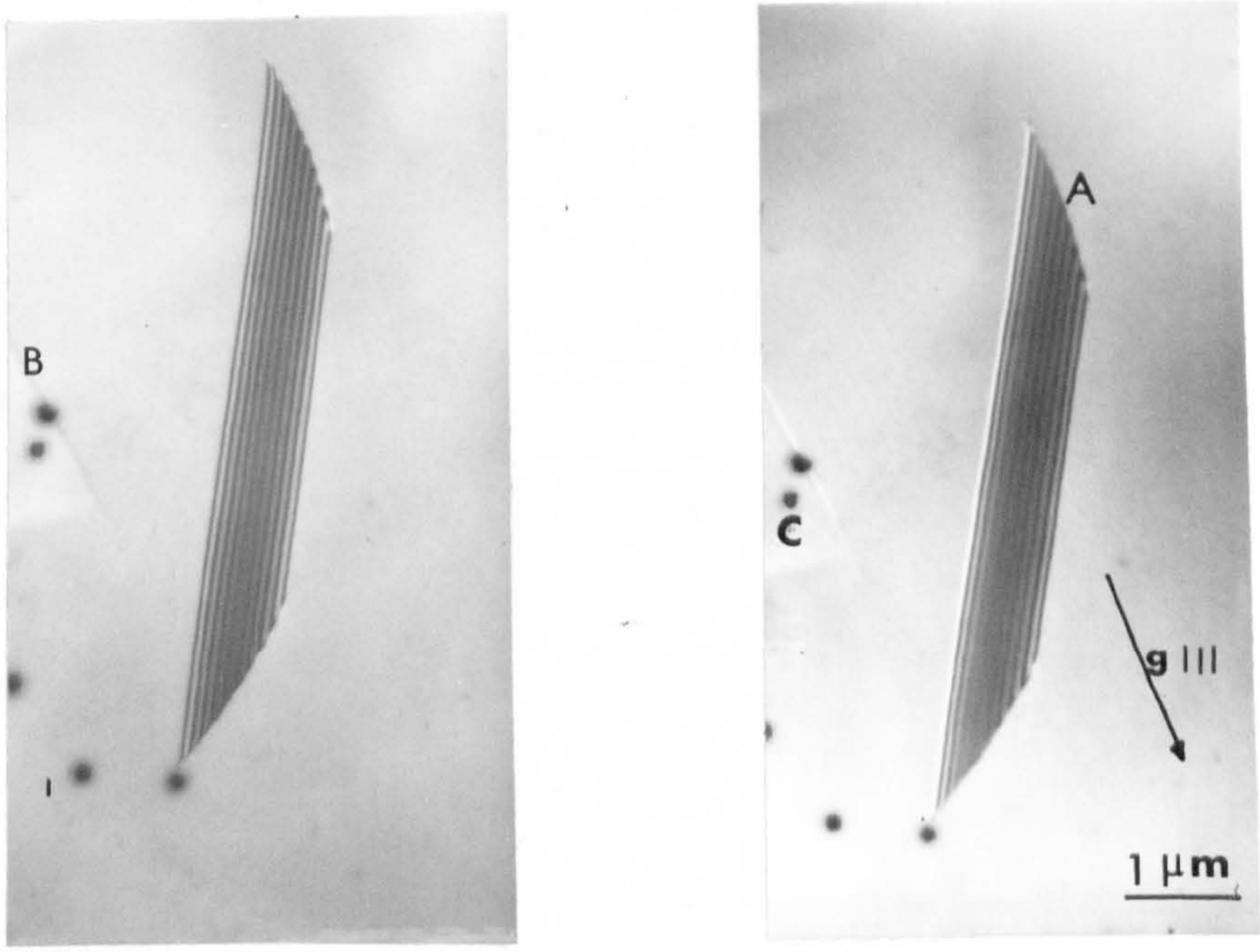


(a) (b)

Fig. 4.4.3 Bright (a) and dark field (b) images of a single stacking fault in $VC_{0.73}$. The fault is of the intrinsic type.

faults on (111) and $(11\bar{1})$ planes are readily visible (for example see A) because they lie at $55^{o}$ to the electron beam. The faults lying on the $(\bar{1}11)$ and $(1\bar{1}1)$ planes are seen edge on since these planes are parallel to the electron beam (e.g. at B). The fringe invisibility criteria demonstrated by the faults, viz invisibility for $\underline{g}$ = 220 and 113 and contrast for $\underline{g}$ = 111 and 002, is consistent with a fault vector $R = \pm \frac{1}{3}[111]$ characteristic of a stacking fault in the metal atom sublattice on {111} planes.

The origin of stacking fault contrast in the electron microscope depends on the phase change introduced into the electron wave in traversing the fault[19]. Complete dynamical calculations with the effects of absorption have been considered, and allow the nature of the faults to be determined. Thus Hashimoto et al.[20] showed that as a result of absorption the nature of the outermost fringes in the bright field image were determined only by the sign of the phase angle $\alpha$. On a positive print these fringes are light if $\alpha$ is positive i.e. $\alpha < \pi$, and dark if $\alpha$ is negative i.e. $2\pi \geq \alpha > \pi$. Thus if the sign of $\alpha$ and the sense $\underline{g}$ with respect to the fault plane are known then the sense of the fault vector $\underline{R}$ can be determined. Gevers et al.[21] have further simplified this procedure whereby the nature of the faults can be determined simply from examination of the dark field image and the diffraction pattern, regardless of the inclination of the fault. The bright and dark field images of a large single fault are shown in fig. 4.4.3 for a 111 reflection. The rule of Gevers indicates that the fault is intrinsic. A large number of faults were examined and all

were found to be of the same type.

As well as the large extended faults, some much smaller faults were also visible (see for example **c** in fig. 4.4.3). The contrast exhibited by these faults indicated that they were of similar type to the larger faults. Certain samples contained numbers of overlapping faults which complicates the fringe patterns obtained[22] e.g. two closely spaced intrinsic faults have similar fringe profiles to an extrinsic fault. The partial dislocations bounding faults on {111} planes in f.c.c. lattices can be either of the Frank or Shockley types with Burgers vectors $^{a}/_{3}\langle 111\rangle$ or $^{a}/_{6}\langle 112\rangle$ respectively. It is possible to distinguish between these by careful examination of the visibility criteria with a number of different operating reflections. A foil with a (110) orientation is suitable for such an analysis and in order to avoid complications due to overlapping effects[22] it is most suitable to choose a large single fault for examination.

Considering a fault lying on a (111) plane then possible Burgers vectors are $^{a}/_{6}[\bar{2}11]$, $^{a}/_{6}[1\bar{2}1]$ and $^{a}/_{6}[11\bar{2}]$ for Shockley dislocations and $^{a}/_{3}[111]$ for a Frank dislocation. Table 4.4.1 (taken from Hirsch et al.[19]) lists the values of $g.b$ for these Burgers vectors and four possible operating reflections for a $[1\bar{1}0]$ direction parallel to the electron beam. A partial for which $g.b = 0$ or $\pm \frac{1}{3}$ is predicted to be invisible whereas one for which $g.b = \pm \frac{2}{3}$ or $\pm 1$ is predicted to be visible.

TABLE 4.4.1

| Reflection | b | Shockley $^1/6[\bar{2}11]$ | Shockley $^1/6$ $[1\bar{2}1]$ | Shockley $^1/6$ $[11\bar{2}]$ | Frank $^1/3$ [111] |
|---|---|---|---|---|---|
| $\bar{1}$ 11 | | $^2/3$ | $-^1/3$ | $-^1/3$ | $^1/3$ |
| 1 $\bar{1}$ 1 | | $-^1/3$ | $^2/3$ | $-^1/3$ | $^1/3$ |
| 0 0 2 | | $^1/3$ | $^1/3$ | $-^2/3$ | $^2/3$ |
| 2 $\bar{2}$ 0 | | - 1 | + 1 | 0 | 0 |

Fig. 4.4.4 illustrates the visibility criteria obtained from dislocations bounding a single fault in a $VC_{0.73}$ alloy. Dislocations are visible in images formed with a $2\bar{2}0$ reflection and invisible for 002 reflection which is consistent with the behaviour of the first two dislocations in the table, and indicates that the dis - locations are of the Shockley and not the Frank type. However, an edge dislocation can give rise to contrast even if $g.b = 0$ because it produces a displacement normal to the slip plane and in order to ensure complete invisibility the parameter m must also be zero ( $m = g.b \wedge u$ where u is unit vector along the positive direction of the dislocation line). Silcock and Tunstall[23] examined the contrast from Frank dislocations under conditions where $g.b = 0$ and $m \simeq 0.2$ and obtained characteristic 'spotty contrast'. This type of contrast is very different from the contrast obtained here with $g.b = 0$ i.e. $2\bar{2}0$ reflection. In addition the contrast obtained varies with orientation (fig. 4.4.4(b)) which is inconsistent with $\underline{b} = \frac{1}{3}$ [111] where the two dislocation segments would be symmetrically oriented with respect to

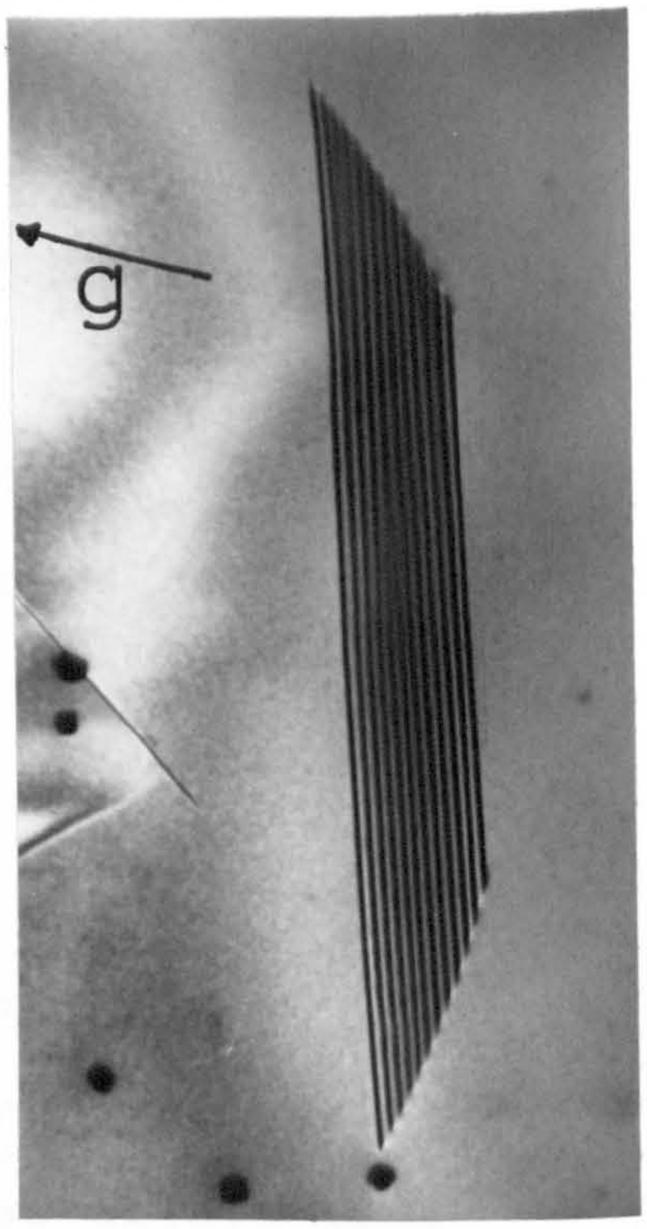


(a) 002

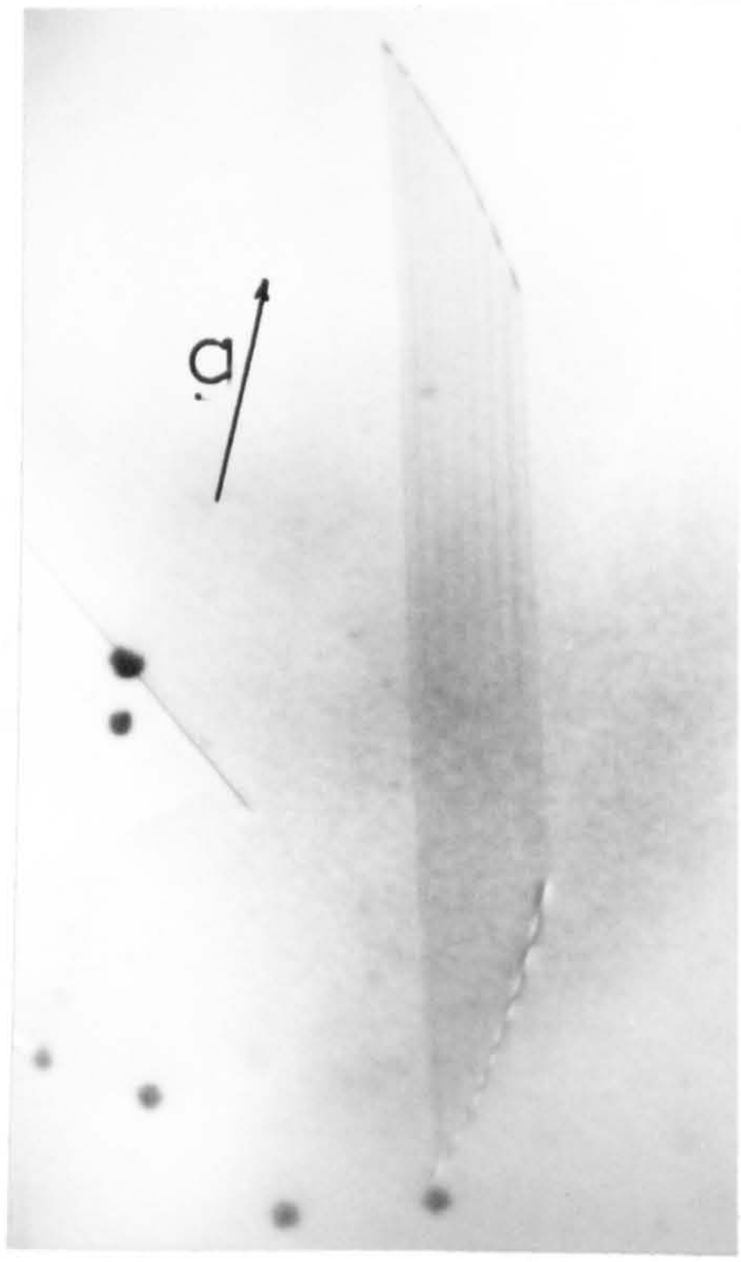


(b) 220

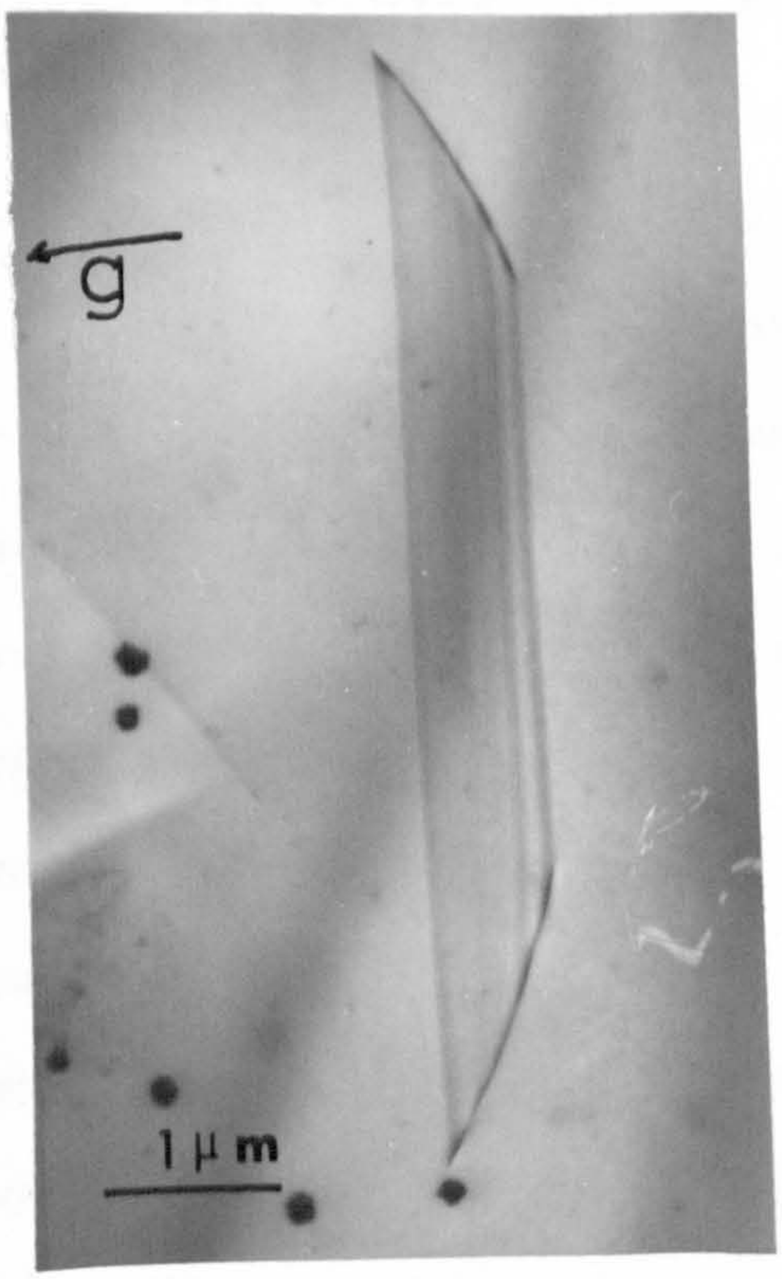


(c) $\bar{1}13$

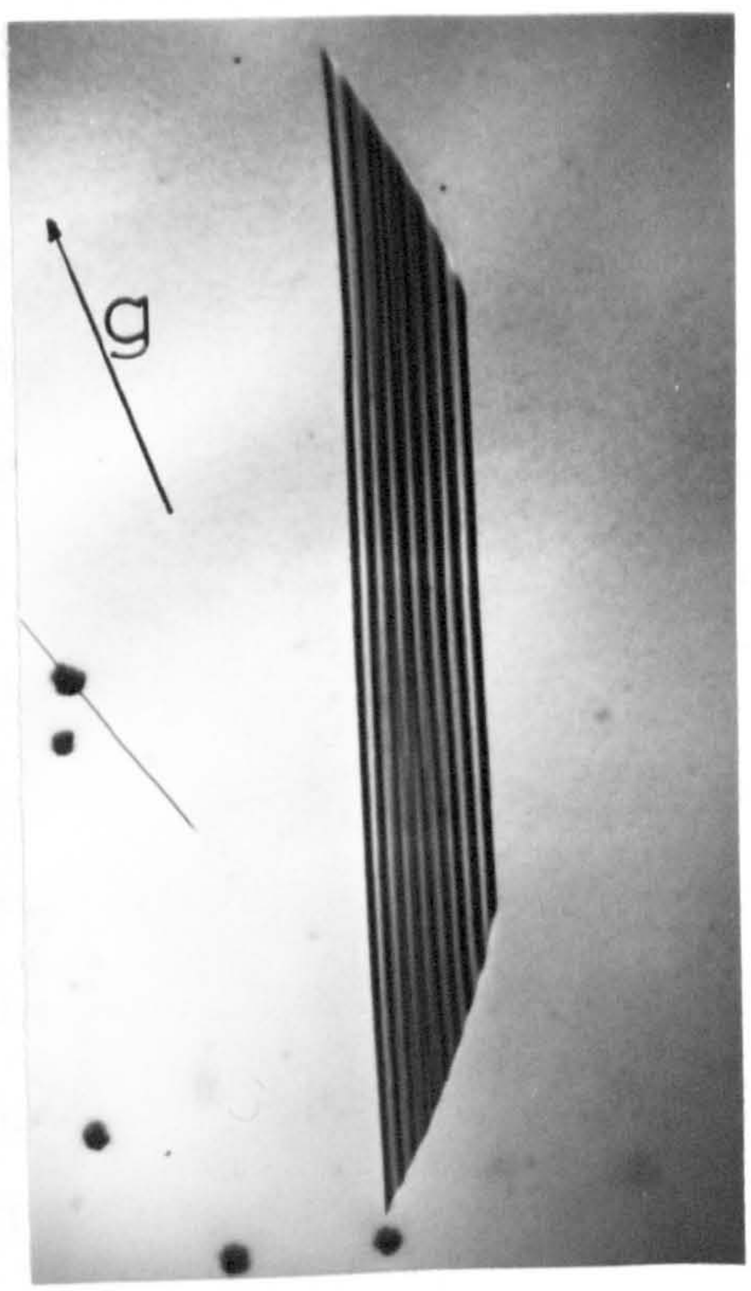


(d) $\bar{1}11$

Fig. 4.4.4 Single stacking fault in $VC_{0.72}$ imaged with indicated operating reflections.

both $\underline{b}$ and $\underline{g}$ $2\bar{2}0$.

The reversal in visibility from $\bar{1}11$ to $1\bar{1}1$ reflectionsdistinguishes between the two remaining Shockley partial dislocations and for this particular case $b = {}^{a}/6[\bar{2}11]$. Other analyses confirm that the dislocations are always of similar type.

The dislocations in transition metal carbides are usually undissociated[24] indicating a high stacking fault energy. This is tue of all compositions above $VC_{0.75}$ in these alloys i.e. as the alloy becomes more nearly stoichiometric. However, within this narrow compositional range the stacking fault energy is obviously drastically reduced because the faults are often widely extended. Stacking faults have been observed previously in cubic carbides by Martin et al.[25] in tantalum carbide at similar compositions to the present observations, and by Venables[26] in titanium carbide of nearly stoichiometric composition. In the latter case the faults were only present in boron doped (100ppm) crystals, and were,of the extrinsic type whereas in the former case intrinsic faults were formed in $TaC_{0.75}$ of high purity. The extrinsic faults were nuclei for subsequent titanium boride precipitation. The present crystals are of high purity and are expected to contain boron levels much lower than those in Venables sample (of the order of a few ppm). The stacking faults were seen in a number of crystals all grown within the narrow composition range $VC_{0.72}$ to $VC_{0.75}$ and were not seen at any other alloy composition. Since all the starting powder materials were similar, the possibility of boron being associated with the faults in a

nucleation mechanism for vanadium boride preciptation appears extremely unlikely. According to zone melting theory any boron present in the alloy should be concentrated in the final zone, and as discussed briefly in section 3.3 evidence for precipitation of additional phases was seen in this region (see for instance fig. 3.9 ). Electron microscope examination of such regions did show evidence for boride precipitation but the form of the precipitation process (extremely small precipitates) differed markedly from the present microstructures containing the stacking faults.

4.4.3 Formation Of Other Ordered Phases

Examination of alloys of lower carbon content indicated that the fault density increases with decrease in carbon content, and the microstructures develop an appear - ance characteristic of Widmanstätten precipitates on {111} planes (fig. 4.4.5). At this stage the preparation of thin sections for electron microscopy is difficult due to differential electropolishing effects between precipitate and matrix. Techniques based on cleaving small regions from the samples also proved largely unsuccessful

In view of the inability to conclusively confirm the existance of $\zeta$ phase by electron diffraction, a number of samples were examined by powder X-ray diffraction tech - niques. The patterns were indexed and the calculated d - spacings compared with published values[27] for vanadium carbide (VC), divanadium carbide ($V_2C$) and zeta phase ( $\zeta$ )[28]. The results are shown in Table 4.4.2 (all values are in $\mathring{A}$ and intensity values are estimated, the strongest lines are underlined).

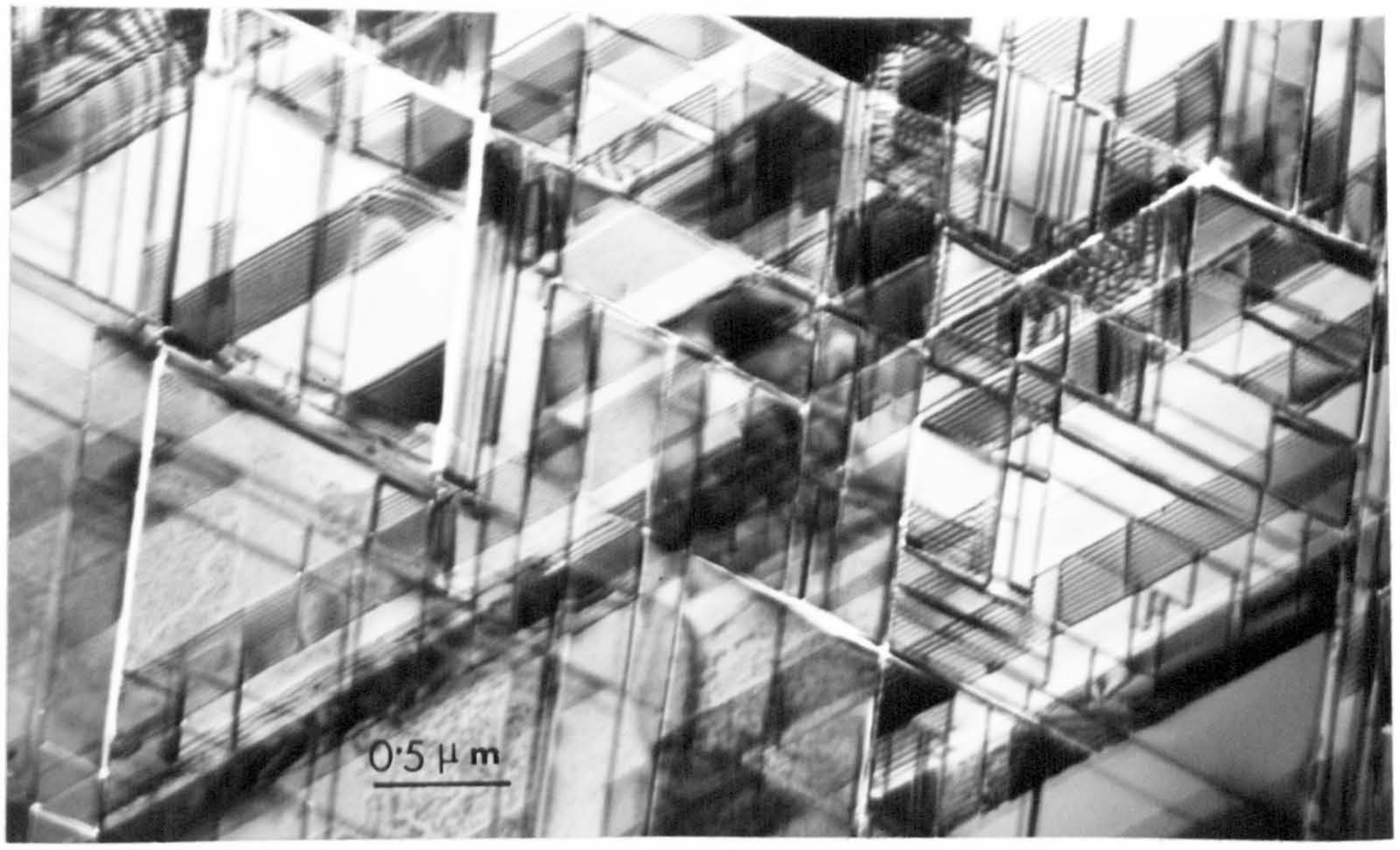


Fig.4.4.5 Widmanstätten precipitates in a vanadium carbide VC matrix in a $VC_{0.65}$ alloy.

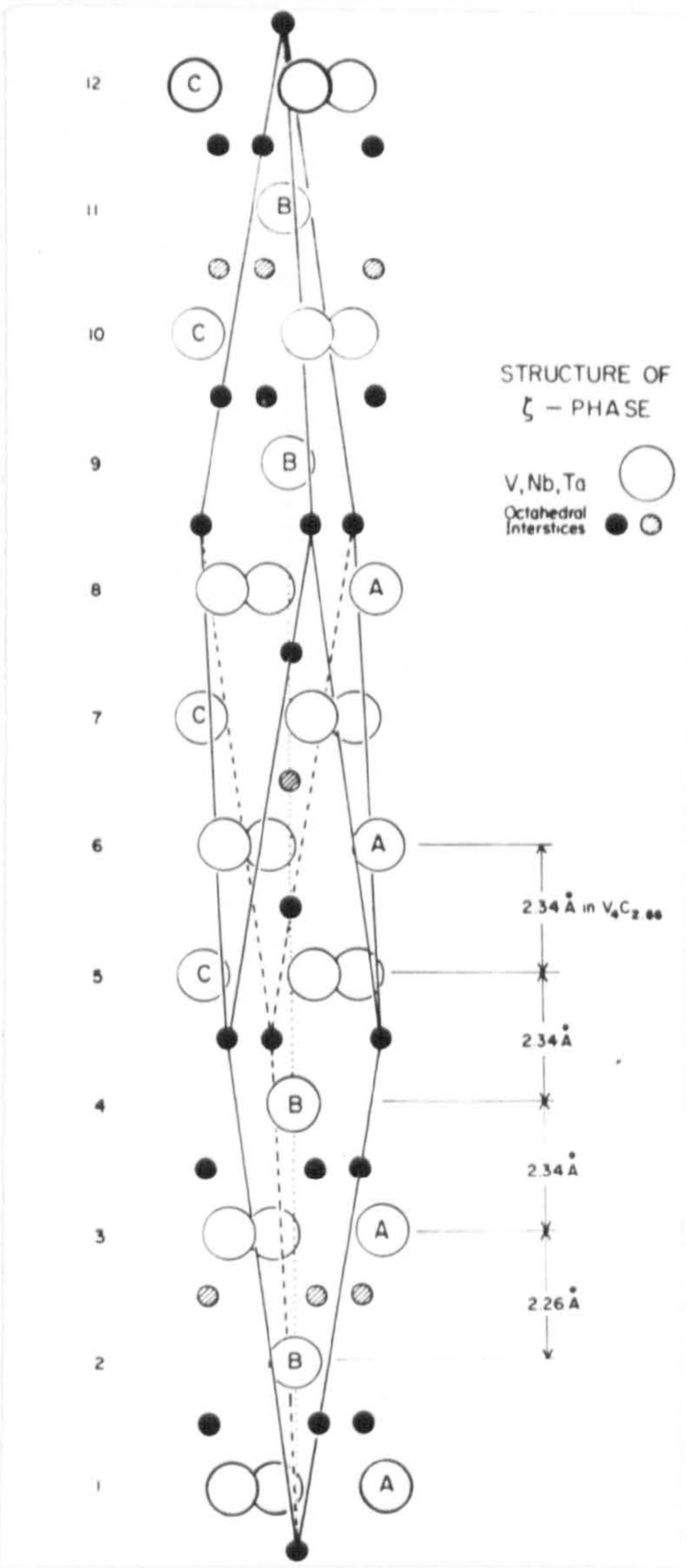


Fig.4.4.6 The structure of ζphase after Yvon and Parthe[28] For maximum carbon content the composition of the ζ phase is $T_4C_3$. In this case the 3(b)positions indicated by small shaded circles are not occupied.

TABLE 4.4.2

| Sample. $VC_{0.65}$ annealed 1000°C | Intensity | ζ-phase | VC | $V_2C$ |
|---|---|---|---|---|
| | | | | 2.50 (W) |
| | | 2.52 (W) | | |
| 2.47 | W | 2.48 (W) | | |
| 2.38 | M | 2.37 (W) | 2.40(VS) | |
| | | 2.32 (VS) | | |
| 2.30 | VS | 2.30 (VS) | | 2.28 (W) |
| 2.20 | W | | | 2.19 (VS) |
| 2.14 | VS | 2.13 (VS) | | |
| 2.06 | M | | 2.08(VS) | |
| | | 2.04 (M) | | |
| 1.86 | W | 1.87 (M) | | |
| | | 1.79 (W) | | |
| | | | | 1.69 (S) |
| | | 1.63 (W) | | |
| 1.56 | W | 1.56 (M) | | |
| 1.46 | VS | 1.46 (VS) | 1.47 (M) | 1.45 (S) |
| | | 1.37 (S) | | 1.30 (S) |
| 1.36 | | | | |
| 1.28 | | | | |
| 1.23 | | 1.26 (S) | 1.25 (M) | |

The composition shows that this sample $VC_{0.65}$ contained an appreciable amount of ζ-phase associated with a much smaller amount of cubic VC phase. The hexagonal $V_2C$ phase was either completely absent or present in extremely small quatities, a result disagreeing with Yvon and Parthé[28] who found that the three phases were always present in all

samples examined. However, their samples were produced by hot pressing powder mixtures in graphite dies, and the formation of the $\zeta$-phase occurred on the existing VC or $V_2C$ phase, and moreover was favoured by the presence of $V_2C$. Other samples with comparable compositions and heat treatments gave similar results but no precise details of the extent of the possible $\zeta$-phase field with respect to composition and temperature limits could be made. However, the presence of $\zeta$-phase was confirmed in alloys of $VC_{0.65}$ composition showing the Widmanstätten type precipitate structure in the electron microscope.

An analysis of the observed defect structure suggests a dislocation mechanism for the nucleation of transformations principally involving a modification of the stacking sequence for the vanadium atom sublattice.

As outlined in Chapterl, the cubic VC phase is replaced at lower carbon content by a structure with c.p. hexagonal metal atom stacking $V_2C$. Yvon and Parthé[28] have recently determined the structure of an intermediate compound of approximate composition $V_4C_3$, and termed the $\zeta$-phase, as trigonal (space group $R\bar{3}m$) which corresponds to the metal atom layer stacking sequence h h c c. Their X-ray diffraction analysis failed to identify any ordering in the carbon vacancy distribution. Recent electron diffraction work by Martin[29] on tantalum carbide indicates that in this system the carbon atom arrangement in the $\zeta$-phase is ordered.

Comparison of the metal atom arrangement in the $V_2C$ and $\zeta$-phase structures shows that they may be considered

as cubic structures with differently arranged stacking fault distributions. Thus $V_2C$ is equivalent to a structure with intrinsic faulting on alternate {111} layers of the cubic stacking sequence, and $\zeta$-phase to faulting on every fourth layer of the cubic sequence resulting in 12 close packed layers in the unit cell (fig. 4.4.6). The arrangement of atoms in {111} planes of the perfect face centred cubic structure of vanadium carbide may be written as -

A γ B α C β A γ B α C β A ....

where following Frank and Nicholas[30] the stacking sequence of the carbon atom planes are designated by Greek letters - γ α β and the vanadium atom planes by Roman letters - A B C. For the non-stoichiometric structure some of the octahedral sites will remain vacant and the electron diffraction patterns from $VC_{0.75}$ indicate a departure from random selection of these sites. An intrinsic fault in this perfect system may be written -

A γ B α C β A γ B α A γ B α C β A ....

Fault formation may occur by the motion of a Shockley partial dislocation in the metal atom sublattice which results in a relative displacements of the crystal parts above and below the fault of $^{a}/_{6}\ \langle 11\bar{2} \rangle$ on {111} planes. This will result in the sequence B α A indicative of the incorporation of a layer of carbon atoms in tetrahedral sites. Two mechanisms are possible for avoiding this unfavourable sequence. The first is the condensation of the non-stoichiometric carbon vacancies in the fault plane to eliminate the tetrahedral co-ordinated atom layer resulting in the sequence

... A γ B □ A γ B ...

(Where □ represents an unoccupied layer)

which is characteristic of the compound $V_2C$. An alternative method of retaining the favoured octahedral co-ordination for the carbon atoms is given by the sequence

A γ B α C β A γ B γ A γ B α C β A ....

This sequence cannot form by the simple shear motion of partial dislocations. It may however be formed via a mechanism derived from the suggested dissociation of dislocations in cubic transition metal carbides by Kelly and Rowcliffe[31]. This is analogous to the process of 'synchro-shear' developed by Kronberg[32] for corundum ($\alpha$-$Al_2O_3$) and involves the motion of carbon atoms in interstices at the core of a Shockley dislocation in a direction at 60° to that for the metal atoms. This dislocation mechanism is equivalent to the hypothetical process of an independent translation of the tetrahedral layer into a new octahedral layer after the formation of an intrinsic fault in the f.c.c. vanadium atom structure.

The first mechanism may be applied to the trans-formation from the non-stoichiometric VC to $V_2C$ having the stacking sequence;

A γ B □ A γ B □ A γ B □ ....

This sequence may be produced from the cubic carbide by the glide of Shockley partial dislocations of similar Burgers vector on alternate close packed vanadium layers and the diffusion of carbon vacancies to the dislocation core. The expansion of the Shockley dislocation is then controlled by the diffusion rate of carbon atoms in vanadium carbide structure. The first part of this process, involving the f.c.c. to h.c.p. transformation is analogous to the poly-

morphic shear transformation found in cobalt[33] and has been proposed by Thomas[34] to explain a similar trans - formation in an aluminium silver alloy.

A transformation to the ζ phase which involves a more complex metal stacking sequence may occur by a similar partial dislocation mechanism but in this case the shear must occur on every fourth {111} vanadium atom layer to produce the h h c c stacking sequence. If carbon atom vacancies are ordered, and occur preferentially in the plane of shear involved in the transformation, then the mechanism becomes similar to that for $V_2C$. However, carbon vacancy ordering has not been detected in the ζ phase by Yvon and Parthé[28] and the most likely mechanism for the transform- ation then must involve the 'synchro-shear' motion of the carbon atoms at the core of the partial dislocations producing the vanadium atom stacking modification. The resulting structure may be described by the sequence -

AγBγ̲AγBαCβAβ̲CβAγBαCα̲BαC .....

in which the octahedral layers produced by 'synchro-shear' are underlined. The ζ phase composition dictates that less than $\frac{3}{4}$ of the octahedral sites are occupied by carbon atoms, and since the tendency to ordered occupancy is retained in the cubic matrix carbide phase, it is possible that this also occurs in the ζ phase. The small volume of ζ phase in thin sections precludes the detection of diffraction effects similar to that observed in fig. 4.4.1 for the cubic matrix.

The ζ phase has also been detected in the niobium[35] and tantalum carbon systems[36,37], and in the latter system

intrinsic stacking faults have been reported at $TaC_{0.75}$ by Martin et al.[25]. Stacking faults have also recently been observed by Bell and Lewis[38] in vanadium and titanium mononitrides near to the phase boundary with the lower nitride phase. Hence it is probable that the mechanisms suggested here for the phase transformation from the cubic vanadium carbide to lower carbides with modified metal atom stacking sequences are applicable to all Group V transition metal carbides and nitrides.

.....

## 4.5 The Intermediate Composition Range $VC_{0.75}$ to $VC_{0.86}$

### 4.5.1 The Superlattice With Trigonal Symmetry

As outlined in section 4.1 the alloys within this composition range were ordered and showed a domain structure and diffraction patterns similar to those reported by Venables et al.[2] at $VC_{0.84}$. The primary vanadium carbide patterns remained unaltered throughout the structure but a different superlattice pattern was associated with each separate domain. All types of patterns reported by these workers were seen (fig. 4.5.1) together with some additional patterns in sections with ⟨112⟩ orientation which are discussed in a later section. Imaging in dark field with a number of different reflections allows all the domains to be identified with particular orientations of the super - lattice unit cell with respect to the parent lattice (fig. 4.5.2). According to Venables et al.[2] this arises because the 'c' direction of the trigonal unit cell of the superlattice (refer Chapter 1) can be oriented in a number

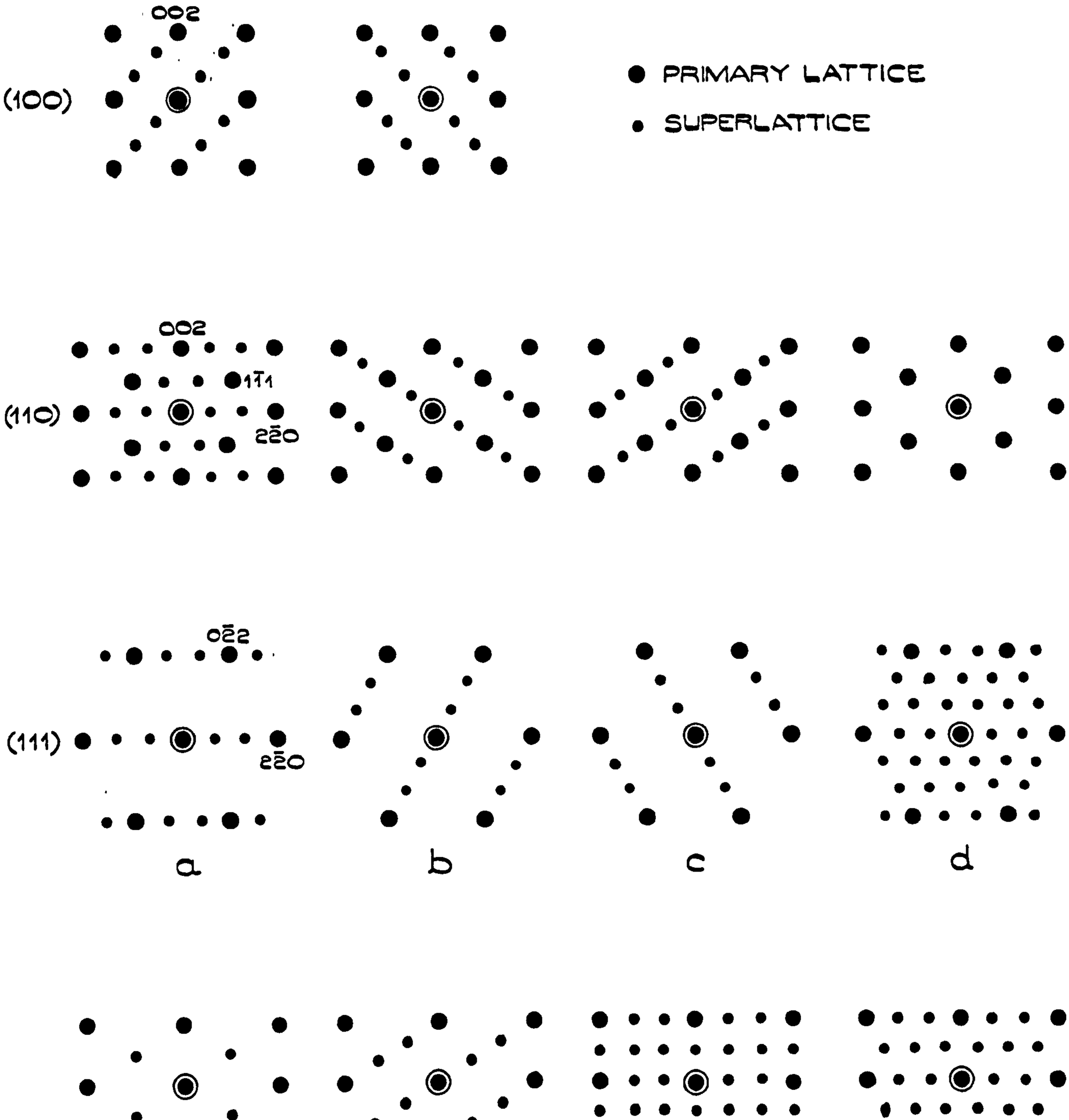


FIG. 4.5.1.

SELECTED AREA DIFFRACTION PATTERNS OBTAINED FROM DOMAINS WITH INDICATED ORIENTATIONS, IN ALLOYS IN COMPOSITION RANGE $VC_{0.75}$ TO $VC_{0.86}$.

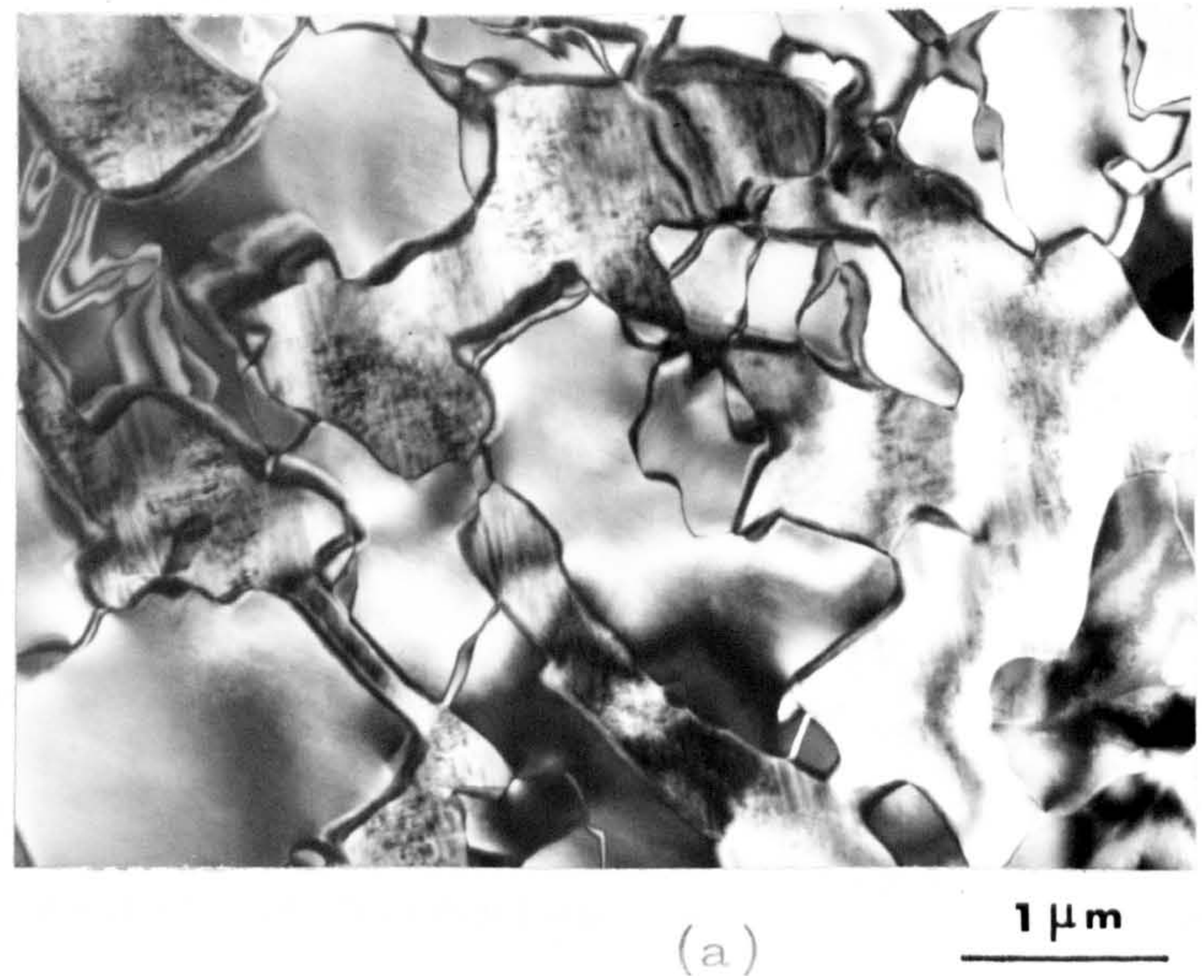


(a)

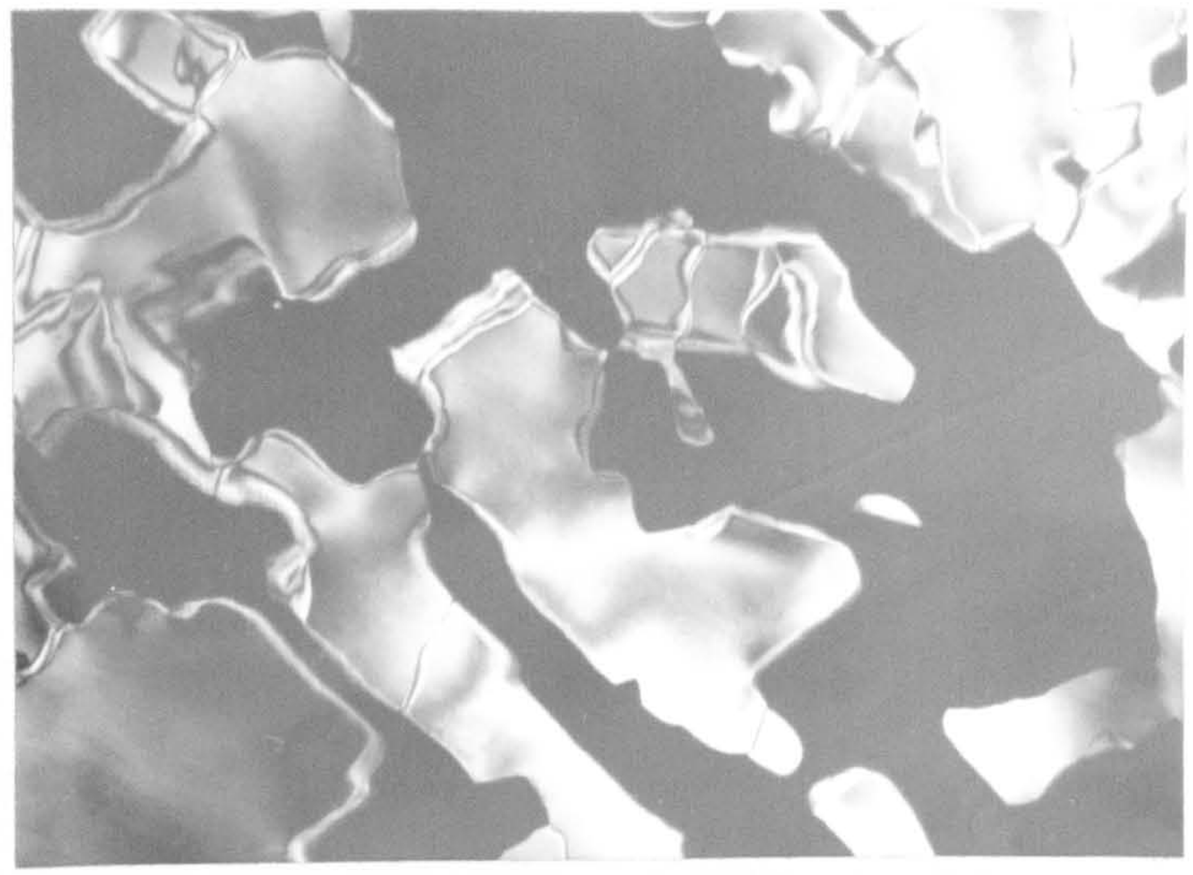

$\frac{1}{2}(111)$

(b)

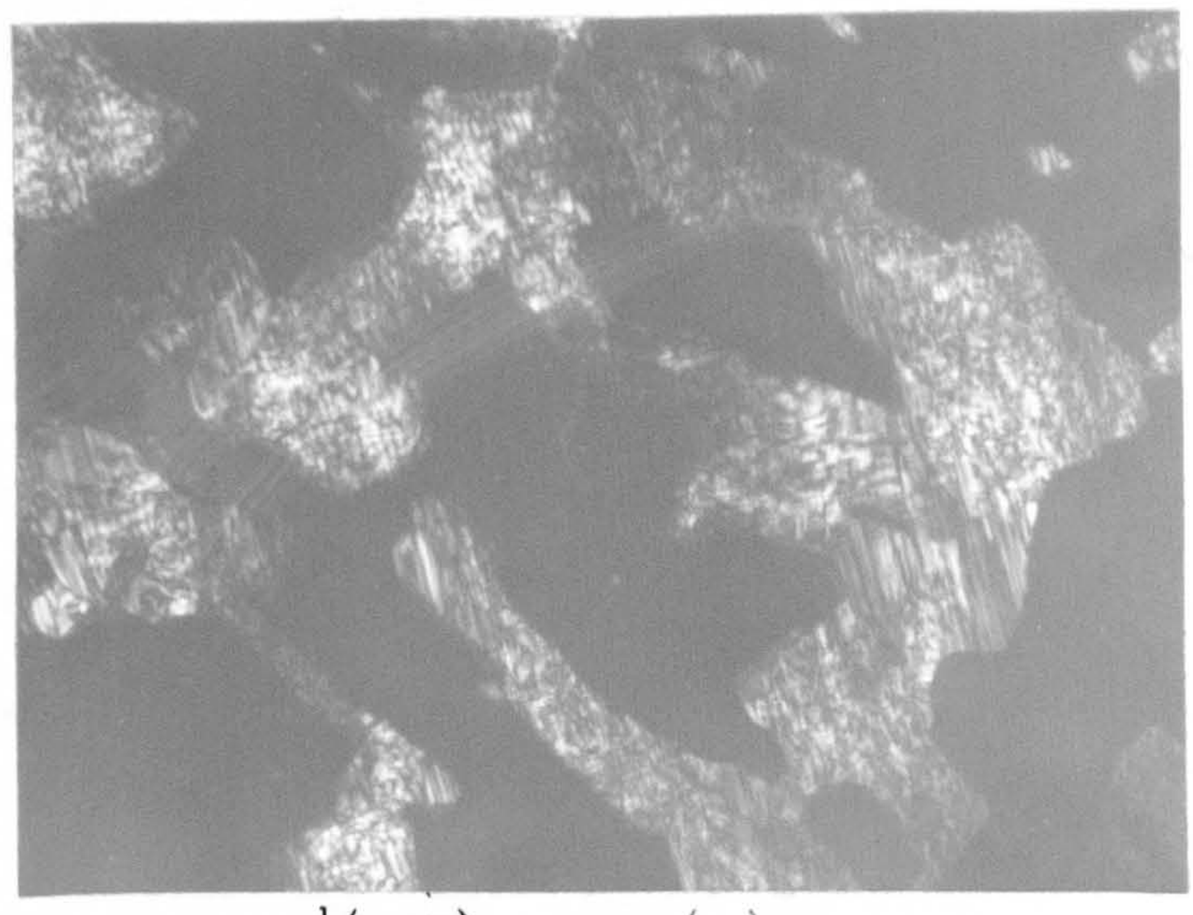

$\frac{1}{3}(220)$ (c)

Fig. 4.5.2 Superlattice domains in $VC_{0.84}$ alloy. Dark field micrographs (b) and (c) enable different domains to be associated with different orientations of superlattice unit cell with respect to the parent lattice.

of ways with respect to the parent lattice i.e. along the four possible ⟨111⟩ directions. The boundaries between domains were examined and found to be of the δ - type[39] where the contrast arises from slight differences between the diffracting vectors in both parts of the crystal.

Consideration of the model of Venables et al.[2] for the superstructure of $V_6C_5$ (see Chapter 1) indicates a number of possible anti-phase vectors. Fig. 4.5.3(a) shows schematically the carbon atom and vacancy positions in a partially filled carbon atom layer on a {111} plane (or basal plane) of perfectly ordered $V_6C_5$. Possible anti-phase vectors associated with translations within this basal plane by a vector equal to the carbon-carbon atom distance are shown in the diagram. In addition to this set of vectors further displacements are possible by similar translations between adjacent carbon-carbon atom layers as indicated schematically in fig. 4.5.3(b). These will be referred to as a non-basal set of fault vectors.

An analysis of the visibility criteria for these two sets of anti-phase vectors is presented in Table 4.5.1 for a (111) basal plane of the superlattice and a number of possible operating reflections. The A.P.B's associated with these fault vectors as expected, show no contrast for normal parent lattice reflections e.g. 111, 220 etc.

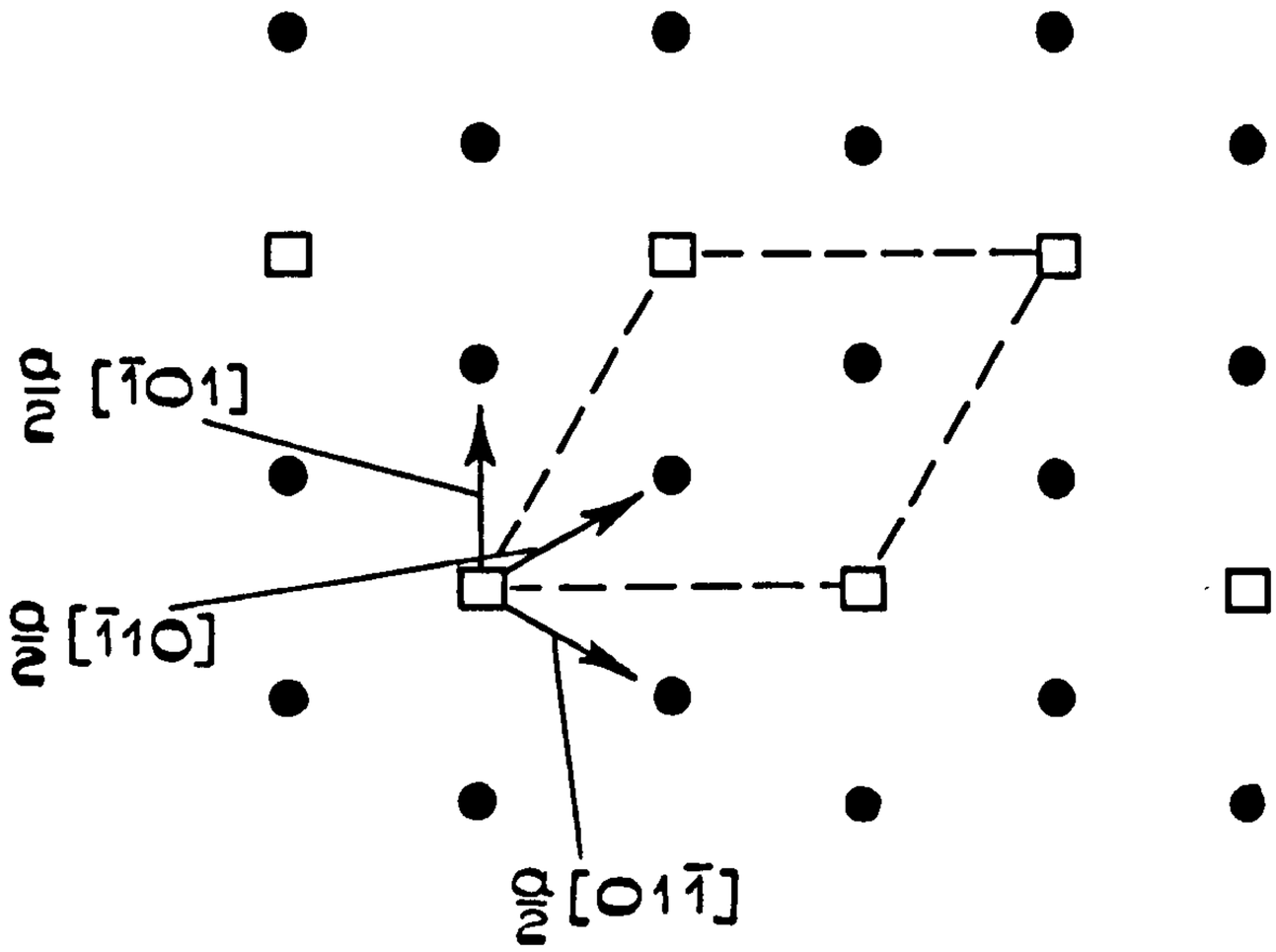


(a) BASAL PLANE ANTIPHASE VECTORS

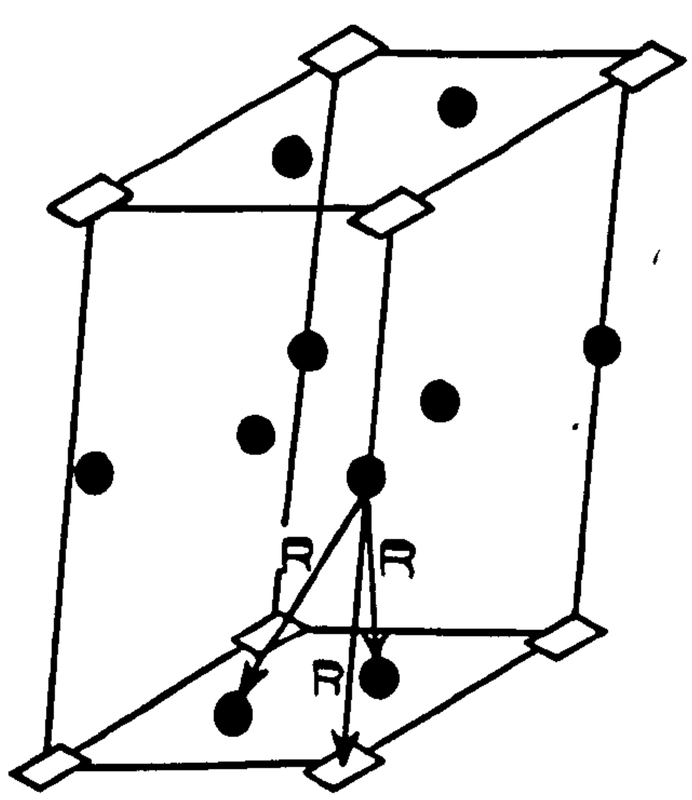


Partially filled layer.

Full layer

Partially filled layer.

(b) NON BASAL PLANE ANTIPHASE VECTORS.
$R = \frac{a}{2}\langle 110 \rangle$

FIG. 4.5.3.

POSSIBLE ANTIPHASE VECTORS IN THE $V_6C_5$ SUPERLATTICE.

● CARBON ATOM

□ VACANT SITE

ONLY CARBON ATOM SITES SHOWN.

TABLE 4.5.1.

| Operating Reflections | Phase angle $\alpha$ | | | | | |
|---|---|---|---|---|---|---|
| | R (basal set) | | | R (non-basal set) | | |
| | $\frac{a}{2}[1\bar{1}0]$ | $\frac{a}{2}[10\bar{1}]$ | $\frac{a}{2}[01\bar{1}]$ | $\frac{a}{2}[101]$ | $\frac{a}{2}[110]$ | $\frac{a}{2}[011]$ |
| $\frac{1}{2}$ 111 | 0 | 0 | 0 | $\pi$ | $\pi$ | $\pi$ |
| 111 | 0 | 0 | 0 | 0 | 0 | 0 |
| $\frac{1}{3}$ $2\bar{2}0$ | $-\frac{4}{3}\pi$ | $\frac{2}{3}\pi$ | $-\frac{2}{3}\pi$ | $\frac{2}{3}\pi$ | 0 | $-\frac{2}{3}\pi$ |
| $\frac{1}{2}$ $\bar{3}11$ | 0 | 0 | 0 | $\pi$ | $\pi$ | $\pi$ |
| $\frac{1}{3}$ $\bar{3}11$ | $-\frac{4}{3}\pi$ | $-\frac{4}{3}\pi$ | 0 | $-\frac{2}{3}\pi$ | $-\frac{2}{3}\pi$ | $\frac{2}{3}\pi$ |
| $\bar{3}11$ | 0 | 0 | 0 | 0 | 0 | 0 |

Distinction between a basal and non-basal set of anti-phase vectors can be made by examination in suitable $\frac{1}{2}\ \frac{1}{2}\ \frac{1}{2}$, and $\frac{2}{3}\ \frac{2}{3}\ 0$ reflections, when no contrast should be obtained in all reflections of the type $\frac{1}{2}\ \frac{1}{2}\ \frac{1}{2}$ for the basal set, or in a particular $\frac{2}{3}\ \frac{\bar{2}}{3}\ 0$ for the non-basal set. In addition to the vectors listed in this table, two further sets composed of R vectors of the type $^{a}/6\ \langle 112\rangle$ are possible (one set is shown in fig. 4.5.1). However, as in the case previously considered for possible anti-phase vectors in the $V_8C_7$ superlattice (section 4.3), these give contrast with matrix reflections since they represent stacking faults in the vanadium sublattice, and because this type of contrast behaviour is not obtained, they will not be considered further.

The large amount of substructure present caused elongation of diffraction spots in reciprocal space, which complicated analysis of diffraction data. The substructure is mainly composed of large numbers of closely spaced faults whose number is considerably reduced by annealing at elevated temperatures (above 800°C),which enables the faults to be analysed. The annealing confers the additional benefit of removing effects due to prior heat treatment and cooling rate variations

Two types of A.P.B can be distinguished: very straight boundaries which are usually closely spaced and present in large numbers, and irregularly shaped boundaries which are much less frequent. The straight A.P.B's can be identified with the basal plane fault vectors following Table 4.5.1, by examination with suitable $\frac{1}{2}\ \frac{1}{2}\ \frac{1}{2}$ super-lattice reflections. Thus fig. 4.5.4 shows both types of A.P.B's in an ordered domain of $V_6C_5$ with an extinction for the straight A.P.B's occurring with a $\frac{1}{2}\ \frac{1}{2}\ \frac{1}{2}$ operating reflection (fig. 4.5.4 (a), and extinction of the irregular boundary with a particular $\frac{2}{3}\ \frac{\bar{2}}{3}\ 0$ reflection (fig. 4.5.4(b)). The irregular A.P.B's can therefore be associated with the non-basal set of anti-phase vectors. The irregular type of A.P.B are thought to form during the growth of the ordered domains from the disordered matrix when the domain interface crosses a dislocation present in the disordered structure which has a component of its Burgers vector not lying in the basal plane. They could also possibly occur by the impingement of two growing ordered regions which have the same orientation of c-axis and a carbon atom

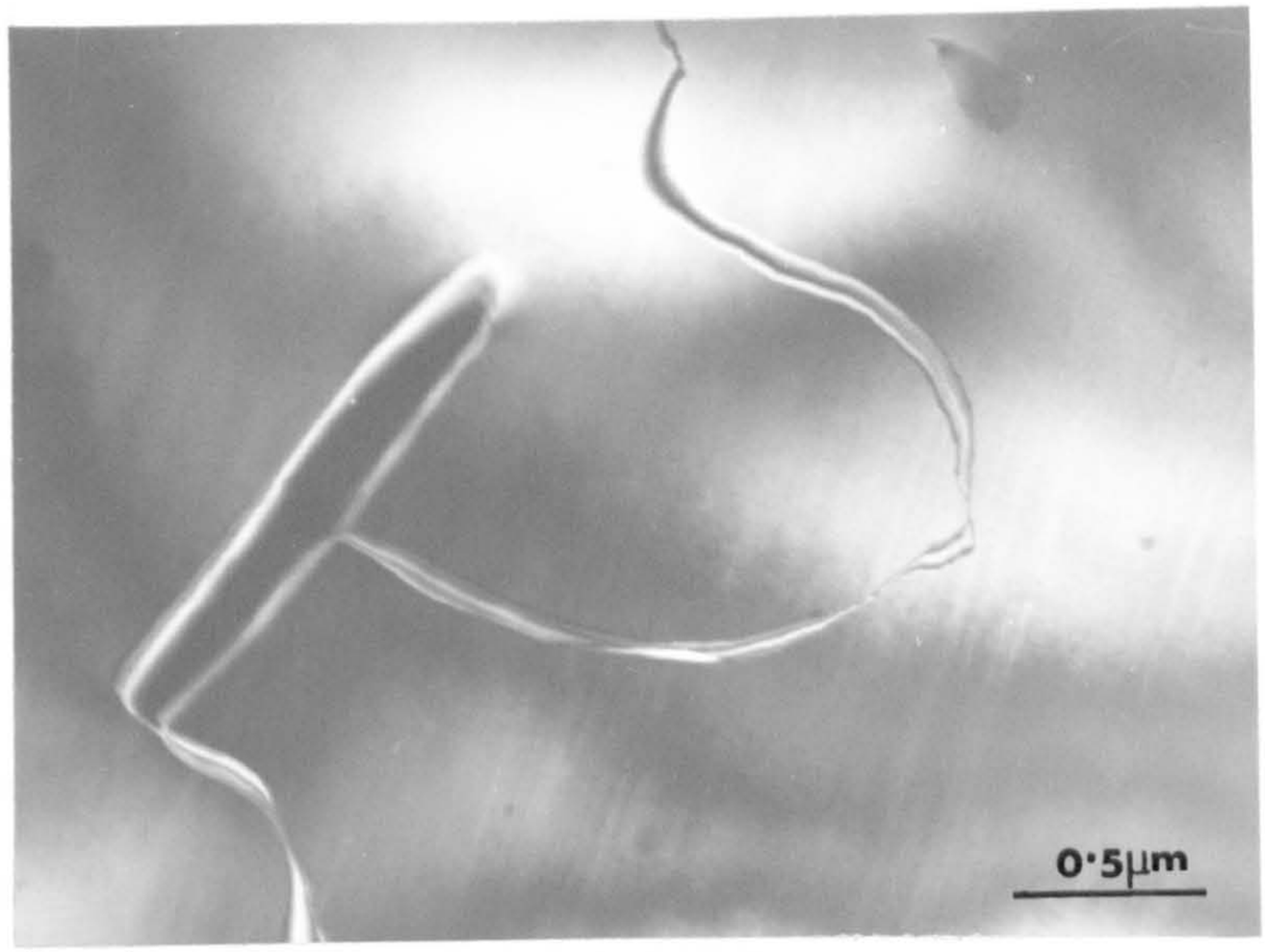


(a)

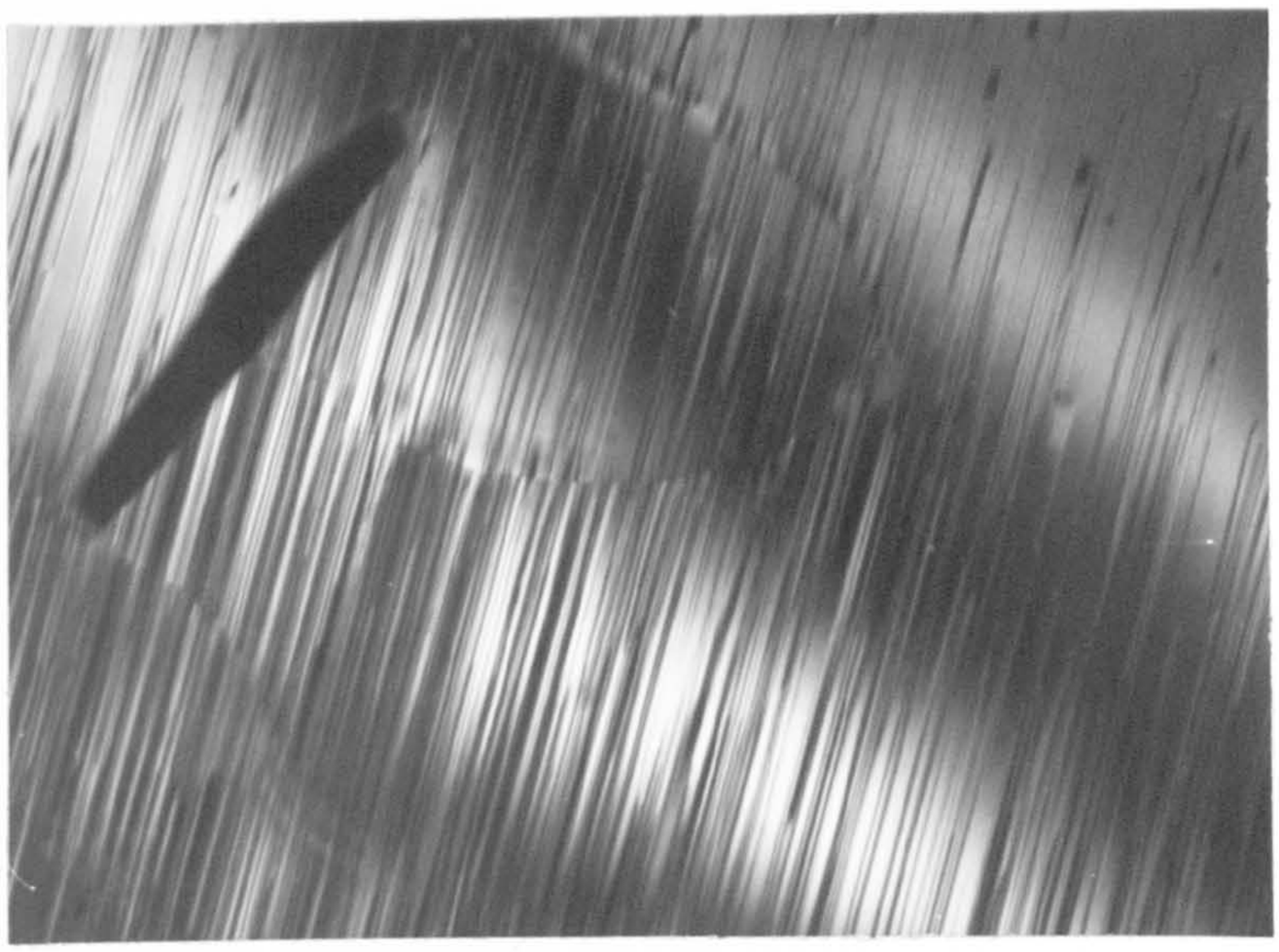

(b)

Fig. 4.5.4 Extinction for both types of A.P.B. in $VC_{0.83}$ alloy. Fig. (a) shows extinction for straight boundaries (basal type) and fig.(b) for irregular boundary (non-basal type).

arrangement relatively displaced as shown in fig. 4.5.3(b). The extremely large numbers, close proximity and accurate alignment of the straight A.P.B's precludes their formation by this means. The diffraction patterns formed by such faulted structures are highly streaked, but they show a constant direction of streaking indicating that growth accidents are not responsible for fault formation. Fig.4.5.5. shows an example of the basal plane faults in a $VC_{0.84}$ alloy annealed for 100 hours at 800°C. In certain regions the straight A.P.B's are seen to be cross linked. The irregular type usually completely traverse a superlattice domain or terminate on grown-in dislocations within the domain interior, (fig.4.5.6).

The differences in contrast within the domains in sections with 110 orientation (fig. 4.5.2) can now be explained in terms of the two types of fault vector. Basal planes either lie parallel to the electron beam, allowing resolution of the fine structure, or at 55° to it when they show a mottled form of contrast. Dark field images with a $\frac{1}{2}\ \frac{1}{2}\ \frac{1}{2}$ operating reflection show mainly uniform contrast in those domains with the basal plane parallel to the beam since g.R is zero for the basal vectors, but some irregular A.P.B's do show contrast (see fig. 4.5.2(b)) since g.R is non zero for these faults. If the operating reflection is $\frac{2}{3}\ \frac{\bar{2}}{3}$ 0 the domains with basal planes at 55° to the electron beam show contrast but in this case g.R is usually non zero for both types of faults and the mottled contrast shown in fig. 4.5.2(c) is obtained.

The numbers of the irregular types of faults are substantially less than those of the straight type and hence

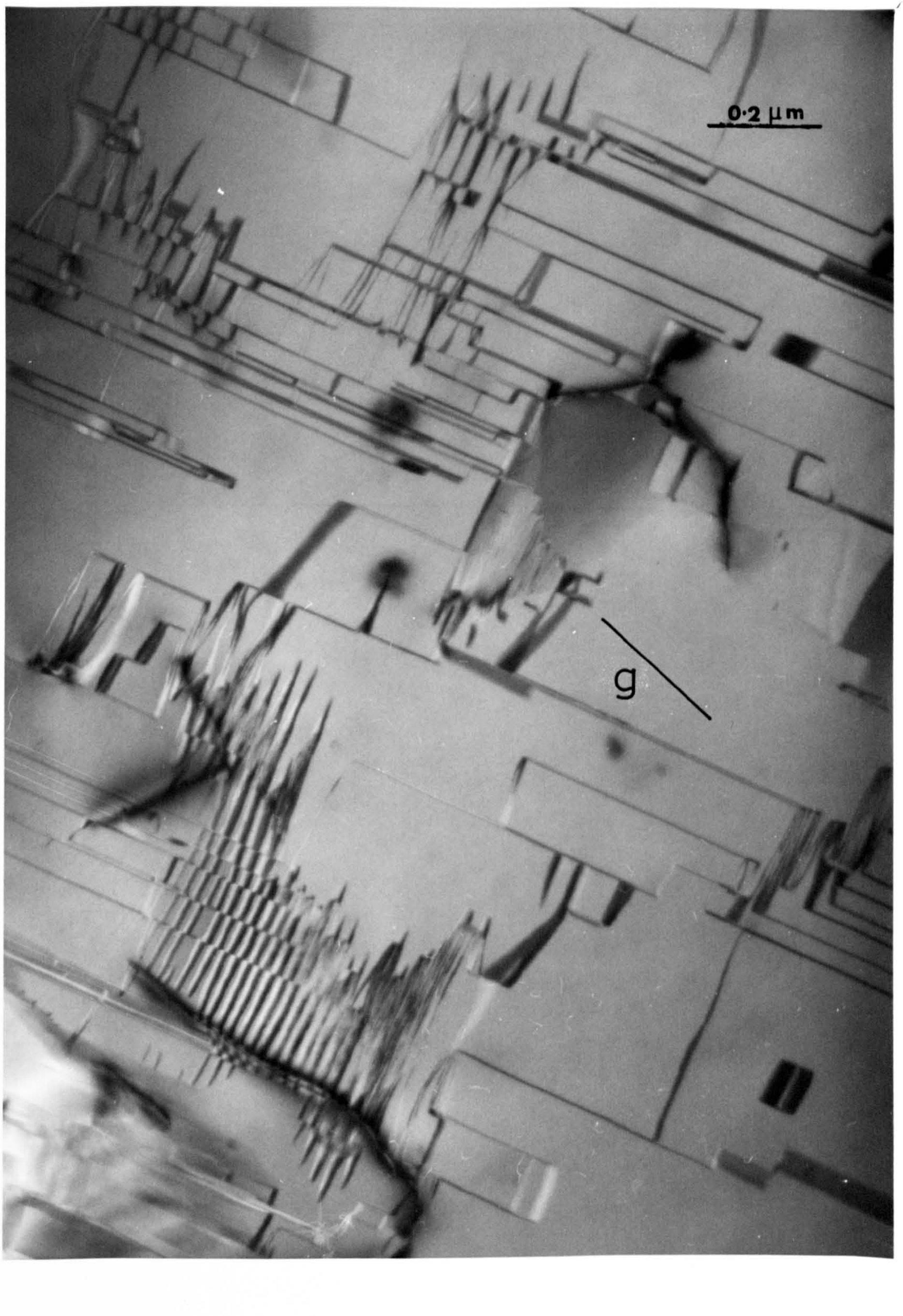


FIG. 4.5.5.

$VC_{0.85}$ ANNEALED 100 HRS. AT 800°C SHOWING BASAL PLANE FAULTS.

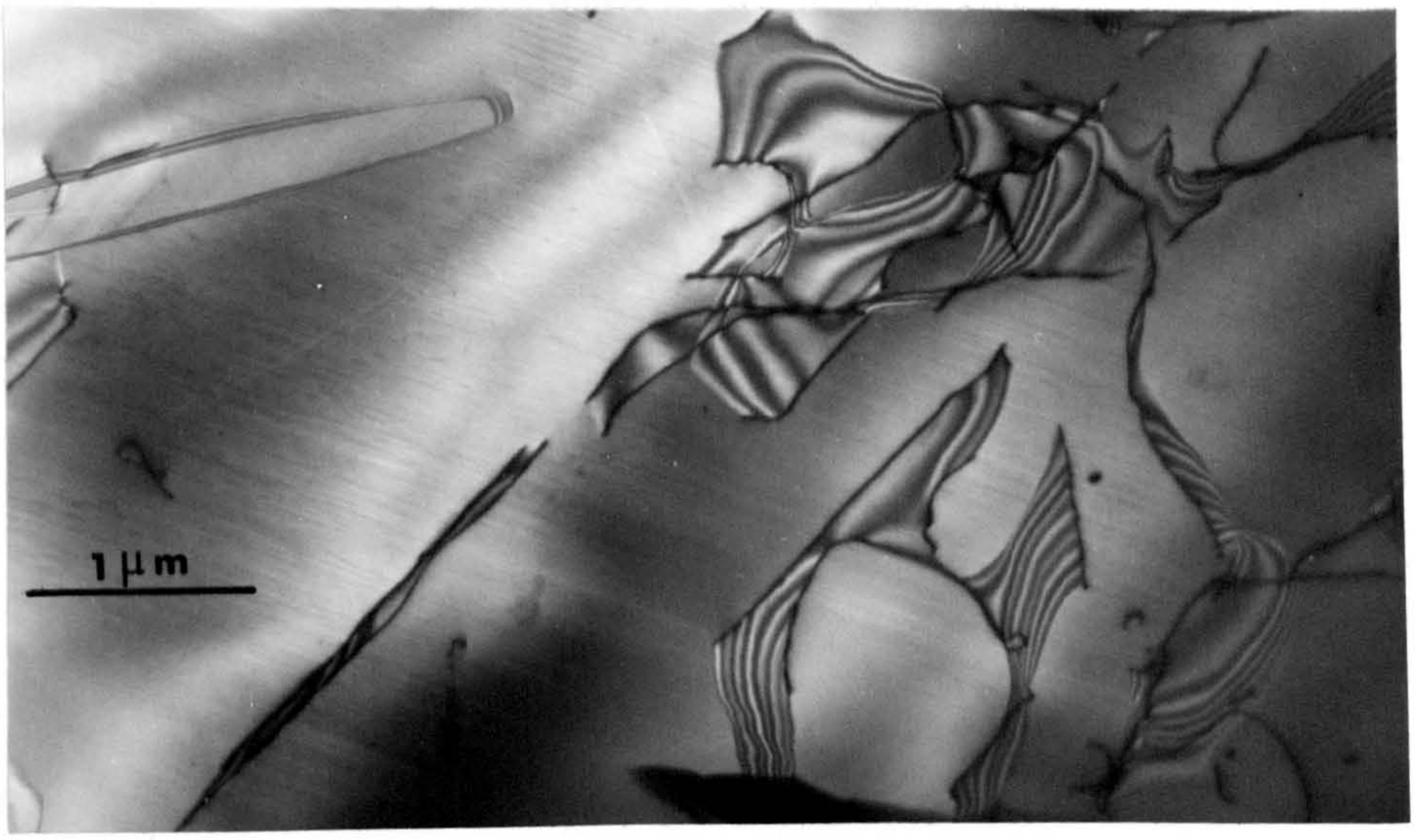


Fig. 4.5.6 Irregular A.P.B's in $VC_{0.81}$. The A.P.B's terminate at grown-in dislocations within the superlattice domain interior or completely traverse the domains.

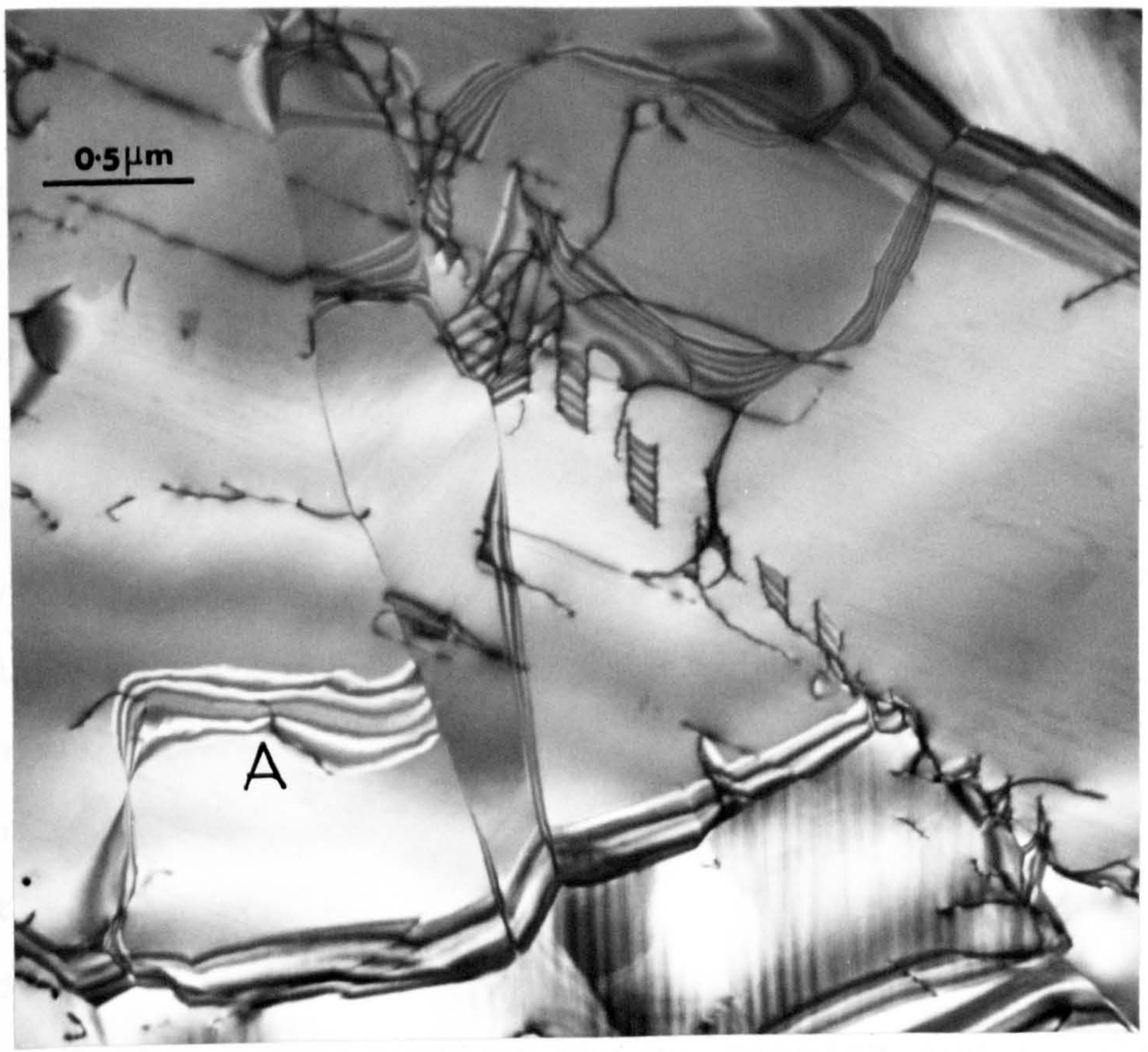


Fig. 4.5.7 Showing A.P.B's associated with paired dislocations in a sub-grain boundary in a $VC_{0.81}$ alloy. An irregular A.P.B. terminating at a grown-in dis - location within the interior of a superlattice domain can be clearly seen (A).

the substructure within the domains is largely composed of faults whose anti-phase vectors lie in the basal plane of the superlattice unit cell. This is also indicated by the corresponding diffraction patterns which show streaking in ⟨111⟩ directions indicating thin faulted regions on {111} planes, or on the basal plane of the superlattice.

### 4.5.2 Dislocation in Ordered $V_6C_5$

As discussed in section 4.3.5 dislocations can move through ordered structures in pairs, the region between them constituting an anti-phase region. Such arrangements are seen occasionally in sub-grain boundaries fig. 4.5.7 or attached to grown-in dislocations within the ordered domains (e.g. see A in fig. 4.5.7). This latter type are the non-basal A.P.B's discussed above. No dislocations can be seen associated with the straight A.P.B's. The majority of the dislocations seen in the alloys were not associated with obvious A.P.B. as outlined above indicating that the superlattice paired dislocations were very closely spaced. These references are to dislocations having a non-basal component of Burgers vector because the presence of such large numbers of A.P.B's parallel to the basal plane rendered any analysis of such structure extremely difficult.

Large numbers of dislocations were occasionally seen in heat treated alloys which had presumably formed during the deformation produced by the heating and cooling e.g. fig. 4.5.8 shows dislocation loops, dipoles and tangles in a $VC_{0.84}$ alloy heated in 1800°C and cooled rapidly. Few dislocation pairs could be resolved and the ease with which they cross domain boundaries indicates that they were formed

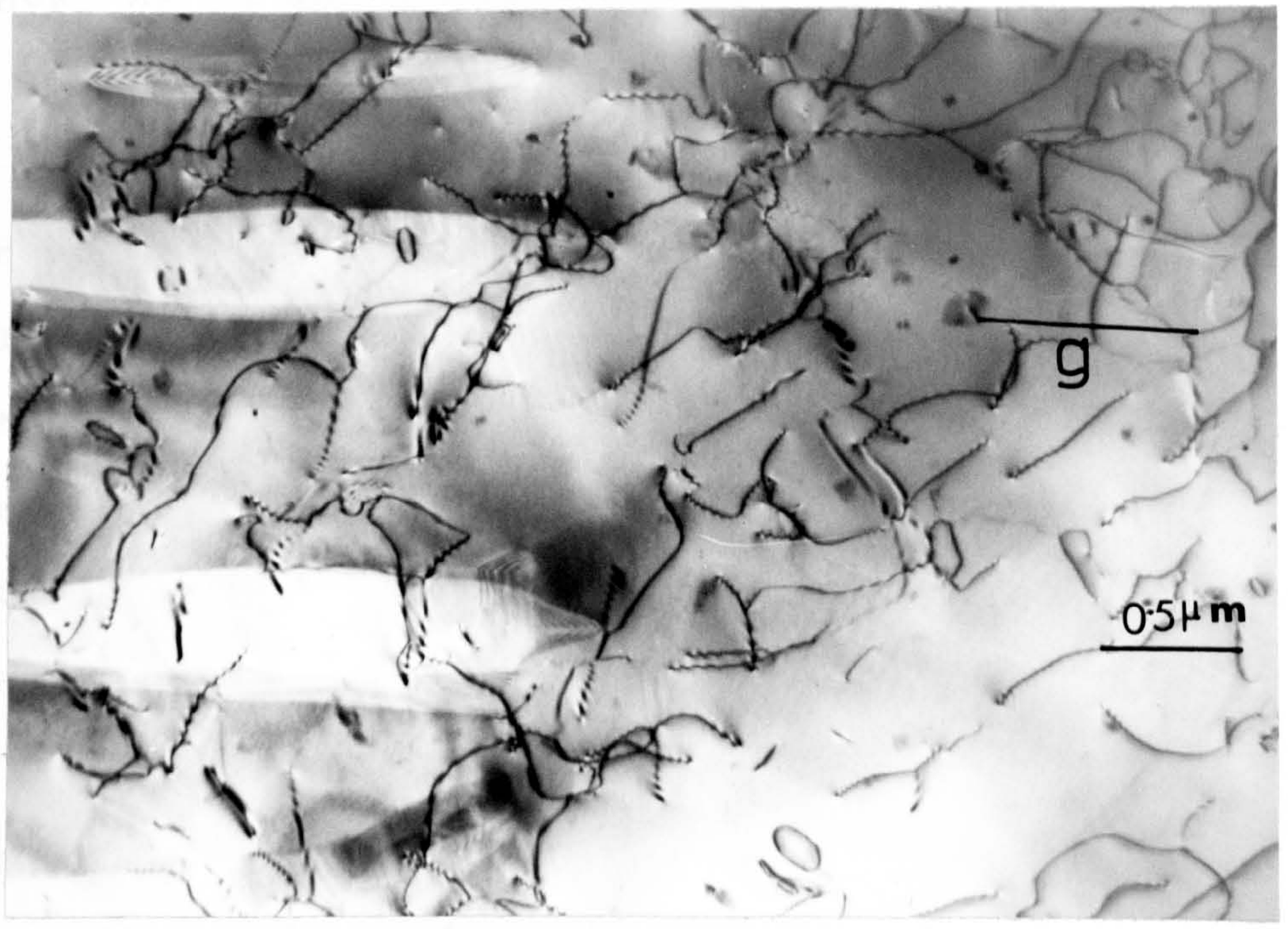


Fig. 4.5.8 Large numbers of dislocations in $VC_{0.84}$ alloy heated to 1800°C and rapidly cooled. Dislocation loops, dipoles and tangles can be seen.

above the ordering temperature. This type of dislocation structure has been previously reported in TiC[24] annealed at high temperatures which has a disordered NaCl structure. Both the number and arrangement of the dislocations varied with carbon content. Within this composition range dis - locations were more common than in the higher carbon content ($V_8C_7$) alloys, or in the lower carbon alloys ($< VC_{0.75}$) where they were mostly of the Shockley partial type and associated with stacking faults. Dislocations often acted as favoured sites for domain nucleation.

The recently developed weak beam technique of Cockayne et al.[40] was used in an attempt to resolve super-lattice dislocation pairs, and to examine dislocation arrangements in highly complex microstructures. This tech-nique relies on examination of the crystal set at an orientation a long way from a Bragg reflecting condition (i.e. $|Sg|$ the deviation parameter in very large) when the beam is only weakly excited in the crystal and the intensity of the image is very low. However, along a dislocation line the regions of high strain close to the core can bend the lattice planes into the reflecting condition. The image produced at such a dislocation has a relatively strong narrow peak, which allows individual images of closely spaced dislocations to be seen.

Fig. 4.5.9 shows the advantage of this technique for examining ordered alloys containing complex structures including domain boundaries, planer defects, and dislocations. The weak beam micrograph was taken in the 200 reflection with the 600 reflection satisfied (this row of systematic


(a)

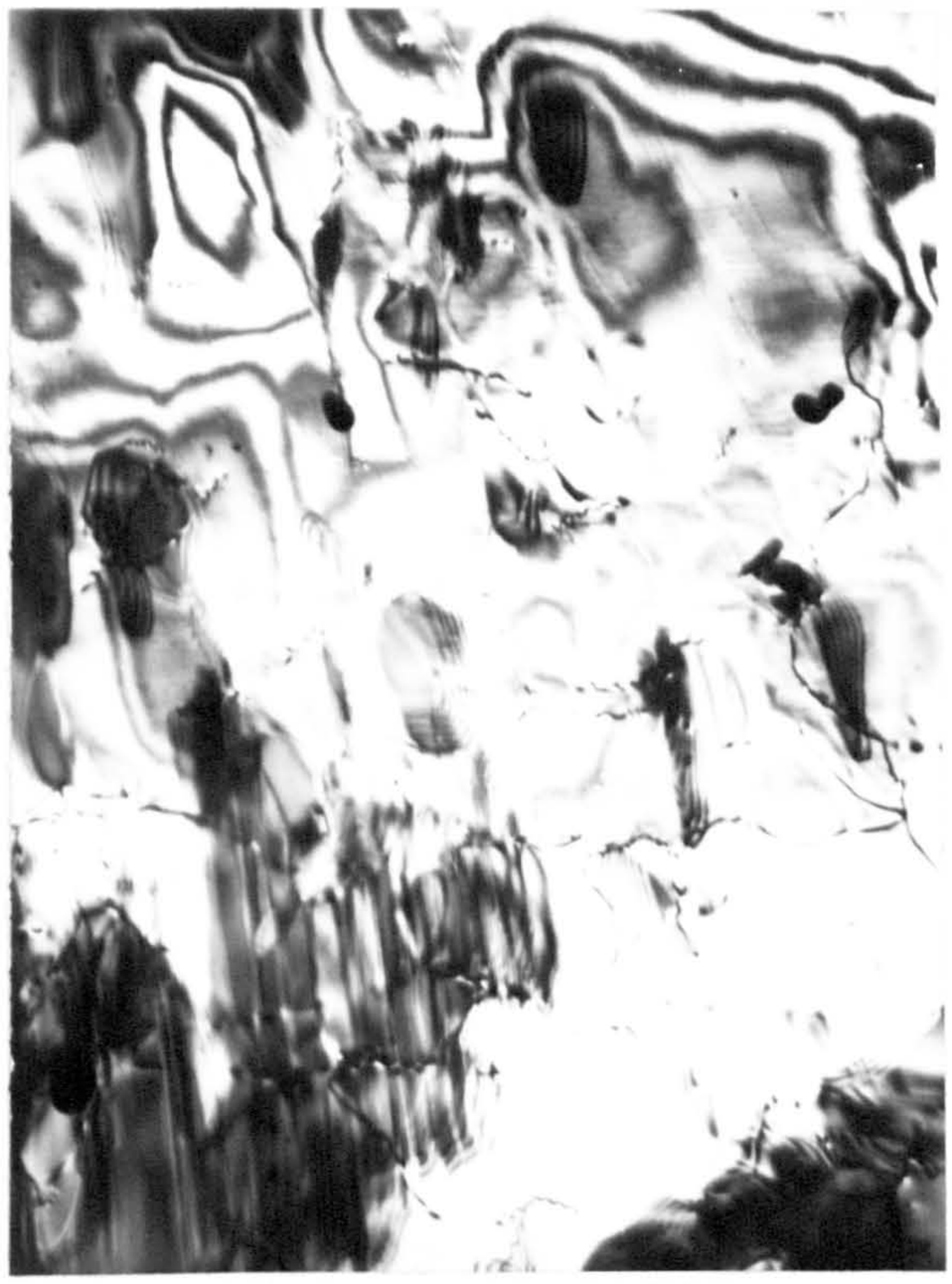

(b)


(c)

(d)

Fig. 4.5.9 Figs.(a) and (b) illustrate the improvement brought about by using the weak beam technique (fig.a) to examine complex microstructures containing dislocations,domain boundaries etc. In fig.(c) and (d) the clarity of the dislocation images when using this technique (c) compared to the normal technique (d) is shown. The dislocation pairs cannot however be resolved.

reflections contains no superlattice reflections so no complications can arise from A.P.B. contrast), and isolates the contrast due to the dislocations. The normal two-beam bright field image showing the complex structure is included for comparison purposes. The clarity of the weak beam dislocation image compared to the highly strained contrast normally produced in the two-beam bright field image is clearly demonstrated in the further micrographs in fig.4.5.9, but the paired dislocations are still unresolved. This work was not continued because a high resolution specimen stage for the electron-microscope with a suitable tilting attachment was not available.

### 4.5.3 A Superlattice With Monoclinic Symmetry

Diffraction patterns from alloys within this composition range contained additional spots in certain reciprocal lattice sections which were not consistent with the proposed trigonal $V_6C_5$ superlattice. Thus fig. 4.5.10 shows such a pattern with a ⟨112⟩ direction parallel to the electron beam, in a $VC_{0.84}$ alloy annealed at 800°C. The 112 reciprocal lattice sections for trigonal $V_6C_5$ are shown in fig. 4.5.1 for comparison. Examination of all other highly symmetric reciprocal lattice sections failed to reveal any additional spots not accounted for by the trigonal structure. However, in certain 110 reciprocal lattice sections, regions of crystal were examined which were associated with diffraction patterns showing no superlattice spots i.e. apparently disordered regions. Tilting the foil and examining such regions in other orientations showed that they were ordered, and tilting to a 112 section showed

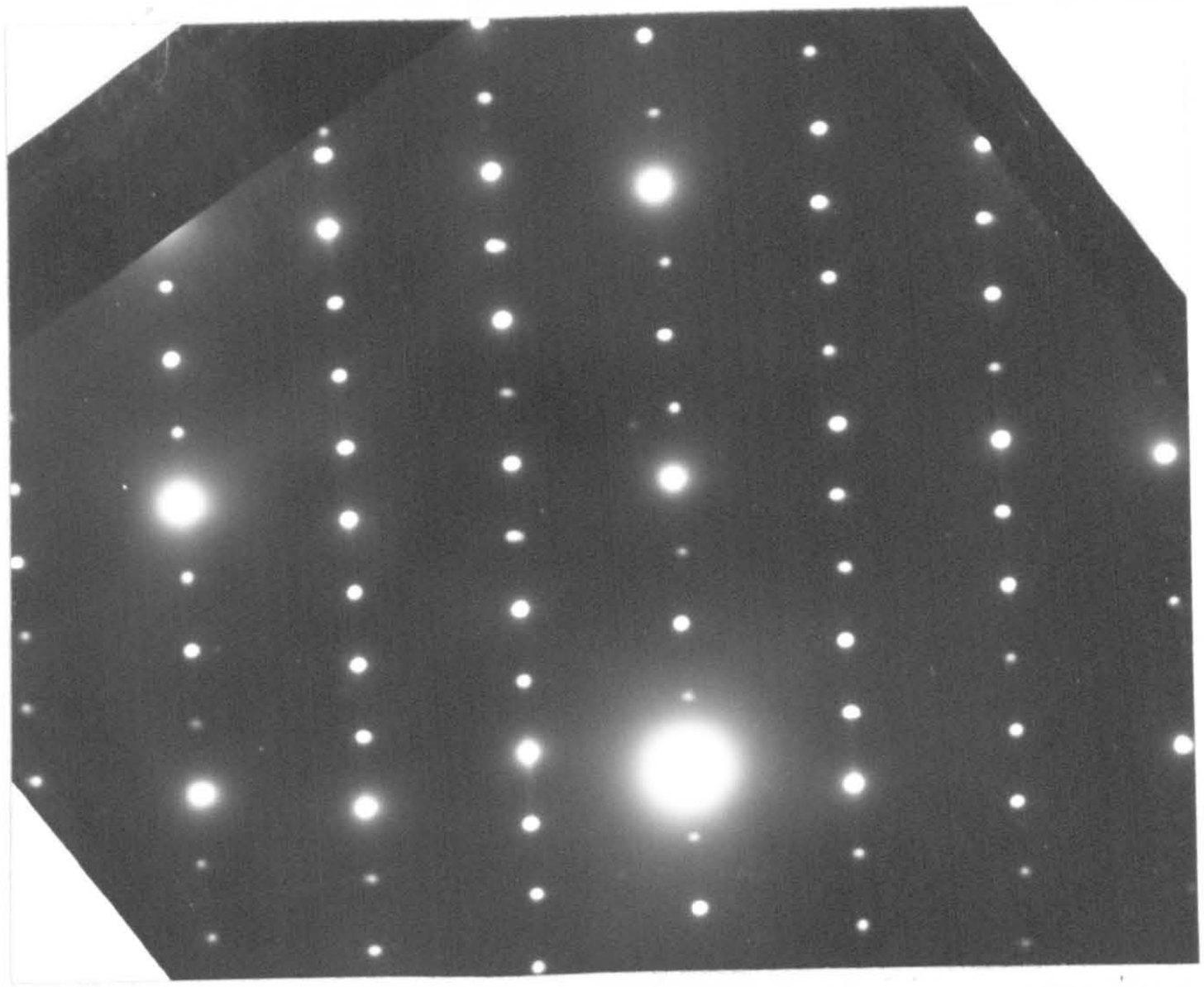

Fig. 4.5.10 $VC_{0.84}$ alloy annealed 100 hrs. at 800°C . 112 diffraction pattern from small region of microstructure.

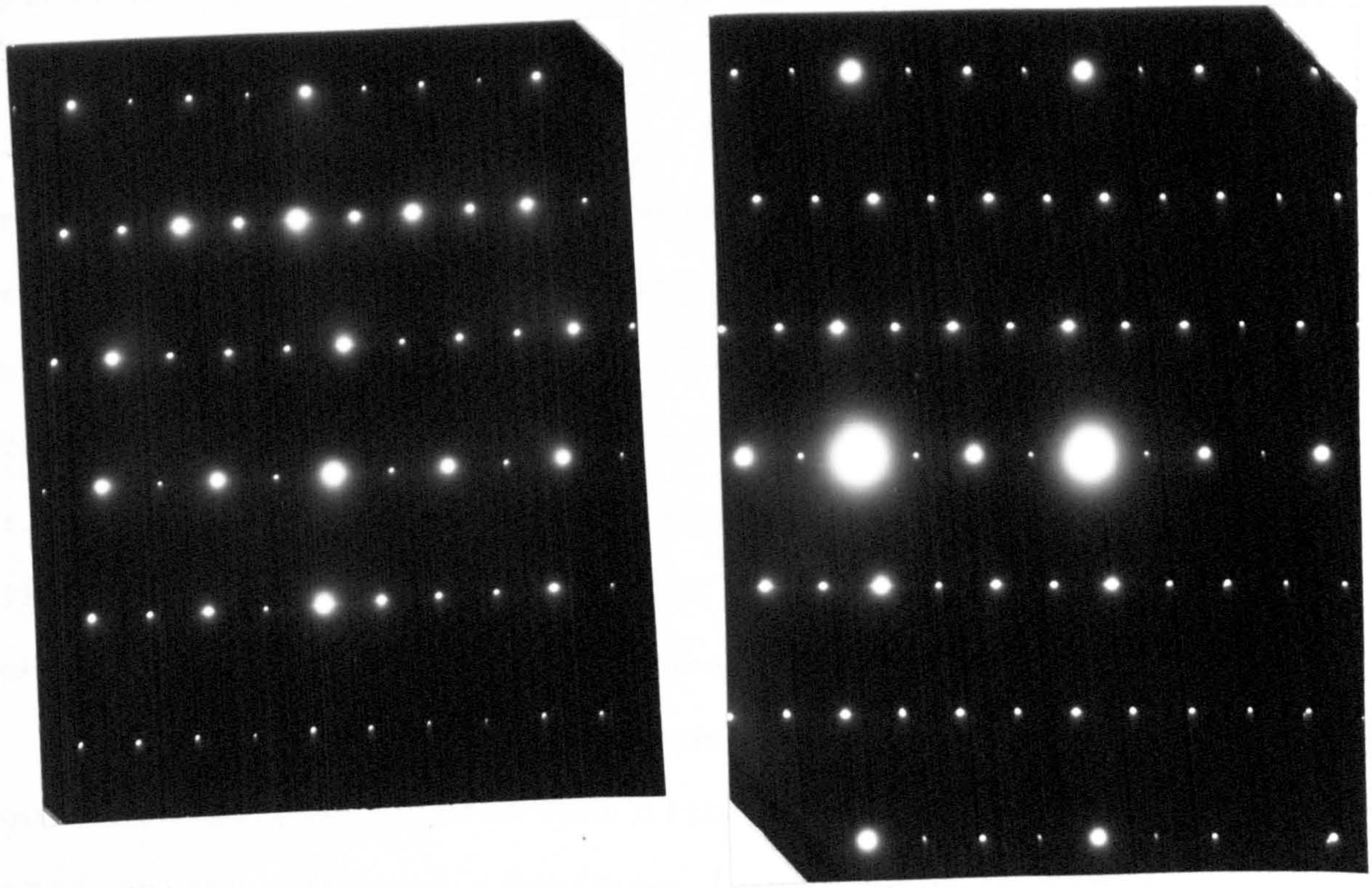

(a) (b)

Fig. 4.5.11 Twin related forms of 112 diffraction patterns obtained from adjacent regions of $VC_{0.84}$ alloy annealed at 1070°C.

that they were associated with the type of pattern shown in fig. 4.5.10. Twin forms of this pattern were sometimes obtained in adjacent regions of crystal (fig. 4.5.11).

The trigonal structure of $V_6C_5$ is formed by ordering of carbon vacancies on alternate {111} layers in such a way that the vanadium atoms have one carbon vacancy in the nearest neighbour environment. The precise details of the vacancy arrangement were postulated to account for the nuclear magnetic resonance spectra of this compound[2] which indicated that all the vanadium atoms were on sites which have one carbon vacancy in the nearest neighbour shell. The vacancy arrangement in the perfectly ordered trigonal $V_6C_5$ compound as shown in fig. 1.5, forms a spiral arrangement around the c - axis of the trigonal unit cell in successive layers. If however (as shown in fig. 4.5.12) a translation in the basal plane occurs in every third carbon atom layer containing vacancies (by the vector $\tau$ shown in the diagram), then the symmetry of the structure is altered. Moreover the vanadium atom co-ordination is unchanged by such a process i.e. each vanadium still has one carbon vacancy in its nearest neighbour environment, and therefore such an arrangement is still in agreement with the N.M.R. structural work.

The structure arising from such a shearing process is outlined in fig. 4.5.12 and although it is closely related to the trigonal structure (refer also to fig. 4.5.3) it has monoclinic symmetry. Thus a comparison of the structures shows that within the layers they are identical, and it is only in the positioning of the third vacancy

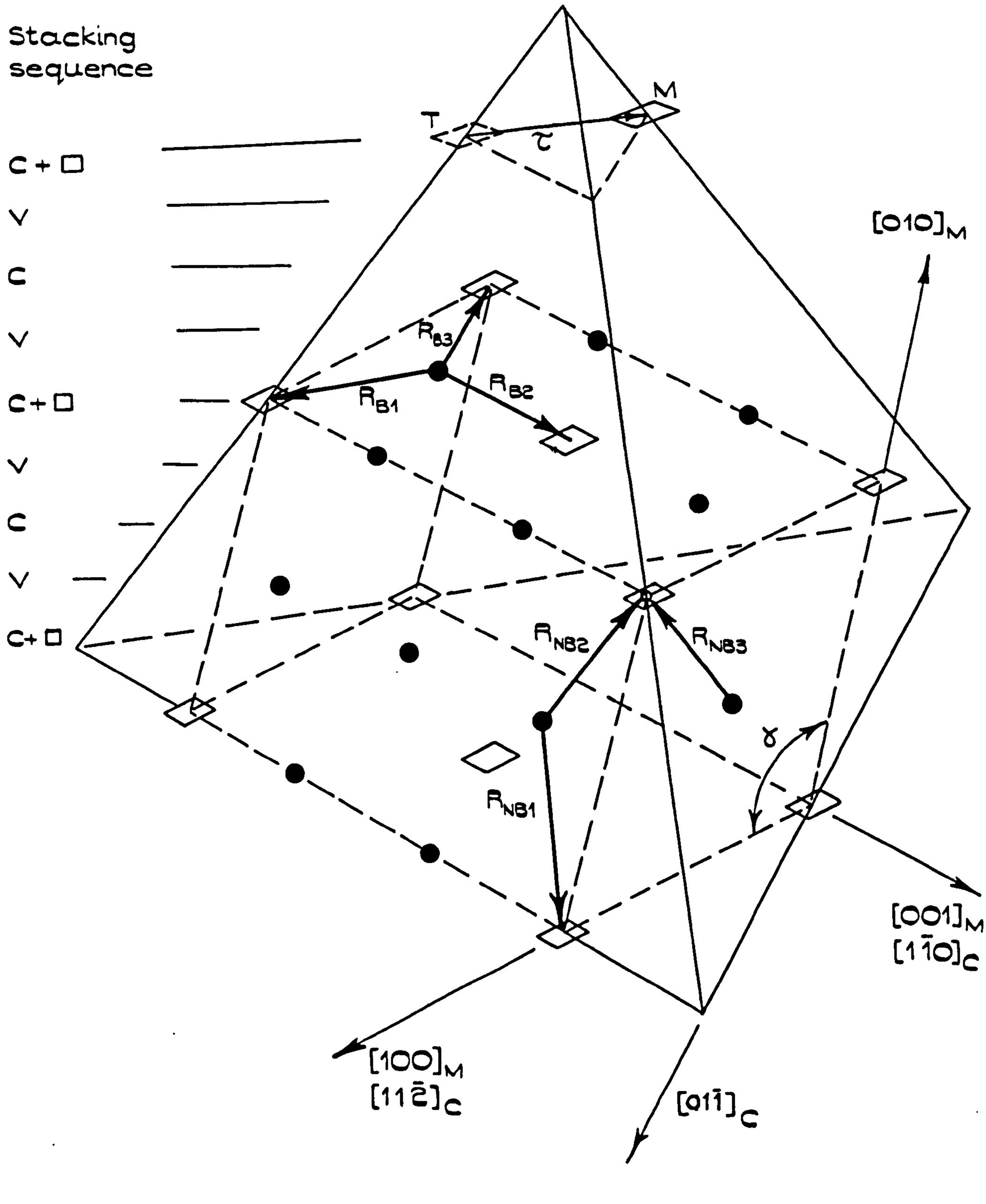


FIG. 4.5.12.

THE MONOCLINIC UNIT CELL.

(Carbon atom positions shown on 3 faces only.)

| | |
|---|---|
| a = 5·09 Å | α = 90° |
| b = 5·09 Å | β = 90° |
| c = 8·82 Å | γ = 109°47′ |

containing carbon layer that the structures differ.

Structure factors were calculated for the proposed atom distribution using the computer programme used by Venables[41] for the trigonal structure. This enabled reciprocal lattice sections to be constructed, which gave patterns in 112 sections similar to those observed in figs.4.5.10 and 4.5.11. Patterns similar to those in fig. 4.5.1, and also a 110 section having no superlattice spots i.e. a disordered pattern, were also obtained. No pattern similar to the highly symmetric (111) foil pattern 'd' (fig. 4.5.1), was however obtained. The existence of a monoclinic ordered structure was strongly indicated by the diffraction evidence combined with the suggested structural translation. However some additional spots not indicated by the structure factor calculations (of either structure), nor easily explicable in terms of double diffraction were obtained in certain 112 sections (cf figs.4.5.1 and 4.5.10). These spots may arise due to slight variations of order within the close packed layers. The trigonal structure was proposed to account for the threefold symmetric 111 diffraction pattern combined with the N.M.R.results, but both the N.M.R.results and all diffraction patterns except (111) 'd' in fig. 4.5.1 are explicable in terms of the monoclinic structure. Moreover, comparison of the carbon atom and vacancy distribution in fig. 4.5.12 for the monoclinic, and fig. 4.5.3 for the trigonal structures, shows that the analysis of possible A.P.B's presented in section 4.5.1 is equally applicable to both structures. Thus both structures can contain basal and non-basal faults as discussed earlier.

### 4.5.4 A Long Period Superlattice

Annealing led to both a reduction and rearrangement of the A.P.B's present as substructure in these alloys. In certain compositions and temperature ranges, alignment of the A.P.B. in a particular direction occurred in certain regions of the crystal resulting in the formation of a long period superlattice. Thus fig. 4.5.13 shows such a periodic array of A.P.B within a region corresponding to a particular orientation of superlattice in a $VC_{0.85}$ alloy annealed for 100 hours at 1070°C. The A.P.B. are aligned parallel to $\{110\}$ planes with respect to f.c.c. indices or $\{1\ \bar{2}10\}$ planes referred to the hexagonal indices (for $V_6C_5$ structure) i.e. the direction of the superperiod corresponds to the direction of nearest neighbour carbon -carbon atom separation in the basal plane of the superlattice.

Regular spaced interfaces inclined with respect to the foil surface can give rise to regularly spaced striations, but preclude the measurement of the fault spacings. The real spacing between fault planes can only be determined by tilting the specimen until the fault planes are edge on, when the spacing can be deduced from the diffraction pattern.

The superperiod of the structure can be measured from fig. 4.5.13 as approximately 50A, which agrees closely with the calculated periodicity from the separation of the split spots in the corresponding diffraction pattern which is also shown in fig. 4.5.13. The micrograph was taken in bright field with the small spots on either side of the main beam included in the objective aperture e.g. A in

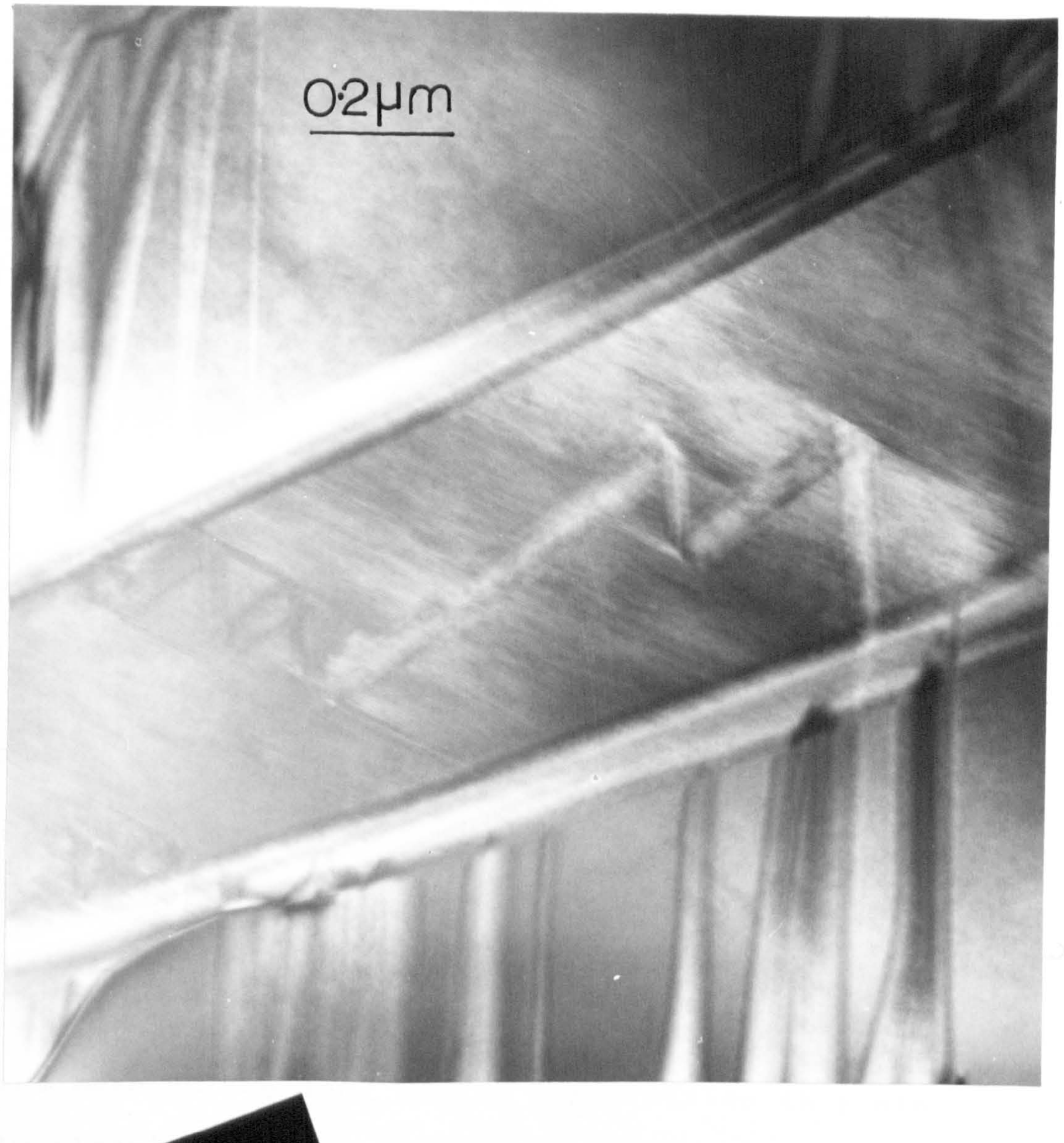


Fig. 4.5.13 Showing alignment of A.P.B's to form a long period superlattice in $VC_{0.85}$ annealed for 100 hrs. at 1070°C. The corresponding diffraction pattern containing the split-spots is also shown.

fig. 4.5.13. This technique has been used by Sato and Toth[42] as well as the more usual technique of taking beam tilted dark field micrographs using the split spots e.g. B in fig. 4.5.13.

A number of samples close to the $VC_{0.85}$ composition contained such structures after heat treatments in this temperature region, but no such structure could be resolved at lower carbon content e.g. $VC_{0.81}$ and $VC_{0.75}$, although splitting of the spots occurred in the diffraction patterns. Examination of the $VC_{0.85}$ alloy following an 800°C treatment indicated an intermediate type of structure (fig. 4.5.14). This showed a structure, composed of A.P.B'S whose vectors lie within the basal plane, made up of A.P.B's lying parallel to {111} planes, and in addition a number of boundaries lying approximately parallel to {110} planes as seen in the long period superlattice. When these latter boundaries make up the long period superlattice they are extremely closely spaced and strictly parallel. A regular arrangement of A.P.B's producing an extra periodicity in the lattice has been referred to as a long period superlattice[42] or a shear structure[43].

A shear structure has been described in Chapter 1, and results in the division of a parent structure into slabs or blocks by sets of crystallographic shear planes. Considerable confusion exists in the literature in the terminology used in characterising fault planes and A.P.B's, and Hyde and Bursill[44] recently tried to clarify the situation by suggesting that fault planes with slip vectors parallel to the plane be called anti-phase boundaries (A.P.B.),

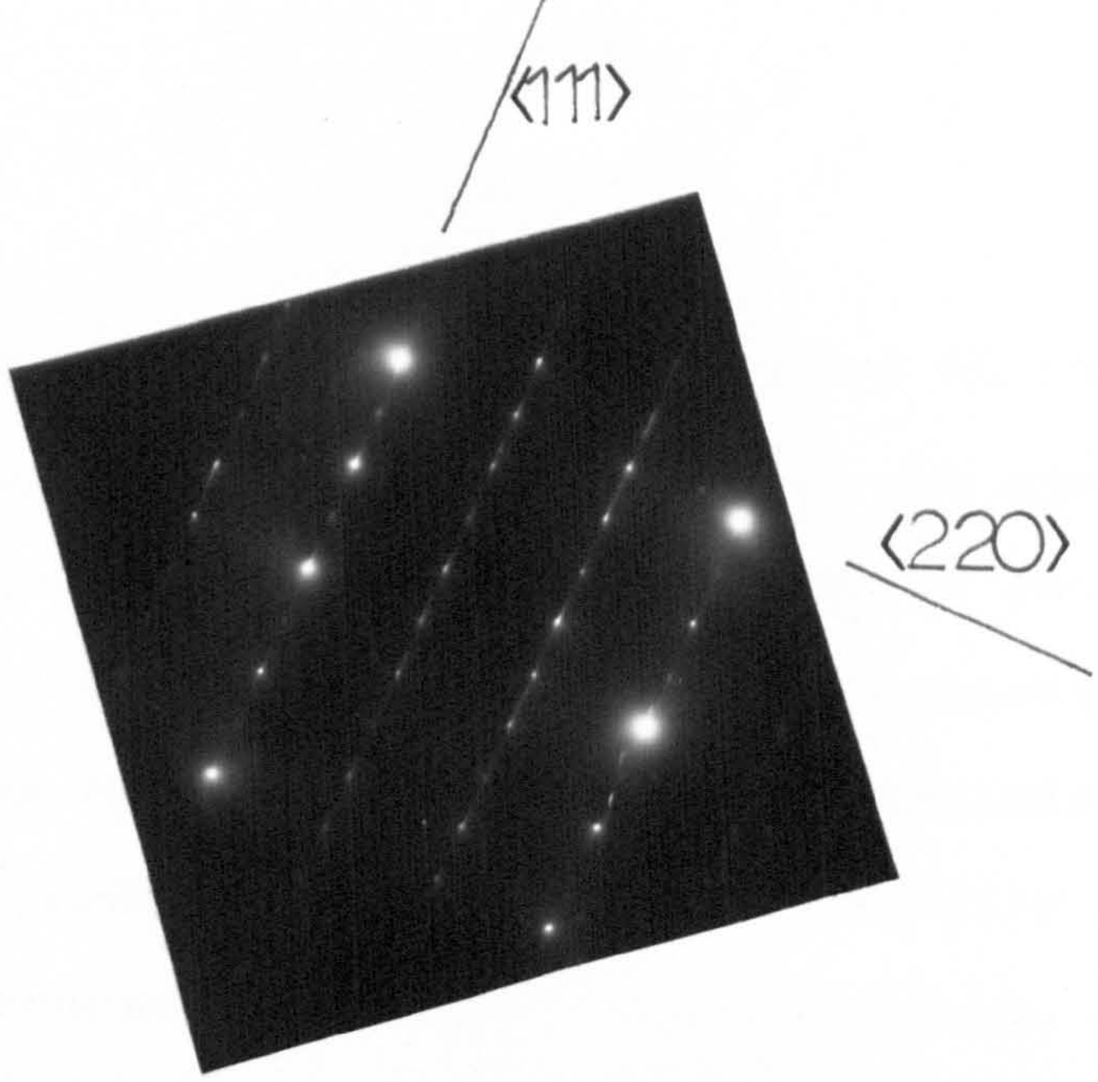


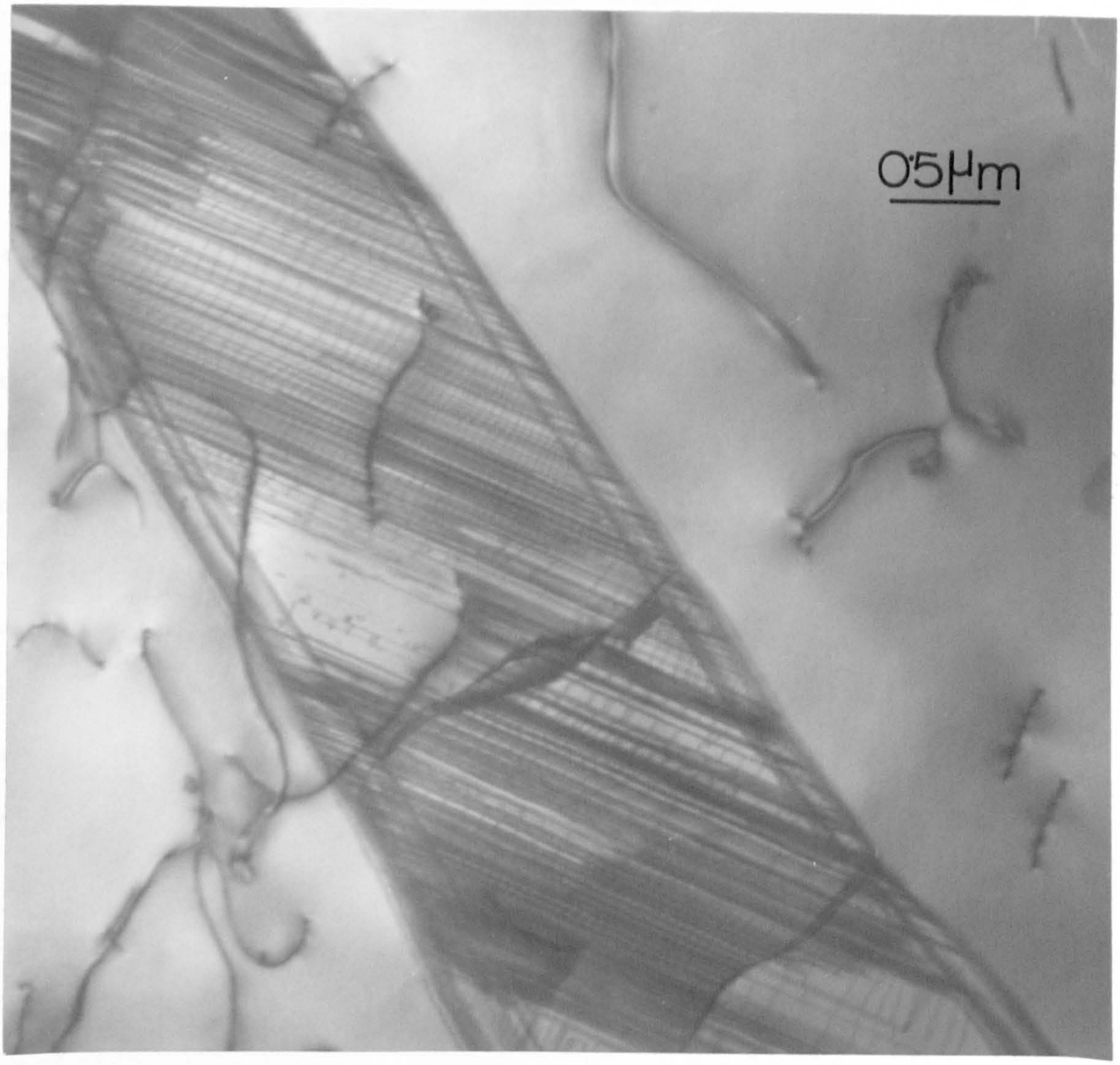


Fig. 4.5.14. Intermediate arrangements of A.P.B's in $VC_{0.85}$ annealed at 800°C. Streaking in diffraction patterns corresponds to alignments of A.P.B's on {111} planes.

and fault planes with slip vectors inclined to the fault planes crystallographic shear planes (CS). No compositional changes are associated with the first type of fault but they may be associated with the latter. Crystallographic shear planes have been seen in non-stoichiometric rutile $TiO_2$[45,46] and Cambini et al.[47] have recently reported a long period structure in vanadium oxide (3 wt. % oxygen). A structure with regular A.P.B's that are not strictly parallel has been reported in TiC[48] near to the lower phase boundary limit of $TiC_{0.5}$.

A long period superlattice is characterised by anti-phase domains of a definite size thus creating an extra periodicity in the lattice by their formation. They are equilibrium structures, and are found mostly in f.c.c. alloys having compositions around AB or $A_3B$. A one - dimensional long period structure means that the superperiod exists only in one direction in one particular region of the crystal. Such superstructures have now been found over a wide range of compositions in the Cu-Au[49,50] system. The best known of these is the Cu-Au II structure in which the anti-phase domain boundaries occur regularly at intervals of five unit cells along one cube edge, thus forming a one dimensional long period superlattice with periodicity ten unit cells. Many such structures are now known to occur especially in metallic systems containing noble metal constituents [51]. The stability of such structures is mainly associated with the A.P.B's producing a decreased electron energy in the system by producing a a Fermi surface contacting the Brillouin zone boundary.

The present superlattice forms with A.P.B's strictly parallel to {110} planes and such a structure is a shear structure formed in the manner indicated in fig. 4.5.15 by the translation indicated across a {110} boundary plane. This leads to a changed co-ordination in the boundary region which in the case shown has a lower carbon content corresponding to $V_4C_3$ instead of $V_6C_5$. As the number and proximity of these planes increases the composition becomes more and more carbon deficient. Calculation shows that in the present case the composition within such a region is modified from approximately $VC_{0.83}$ to $VC_{0.82}$ which is close to the limit of detection by the chemical analysis technique used. No analysis changes were detected.

4.5.5 Structural Variation With Composition And Temperature

The long range ordered domain size was found to be strongly dependent on composition, increasing with carbon content from approximately 0.1 μm at $VC_{0.75}$ to 1-3μm at $VC_{0.84}$. Grain and sub-grain boundaries are found to be preferential sites for domain formation. With the smaller domain sizes it was difficult to obtain a uniform electropolished surface because of preferential attack at the domain boundaries. These lower carbon alloys ($^C/_V < 0.8$) were also difficult to analyse because the domain sizes were too small to allow single domain orientations to be examined. These alloys were however useful in studying the early stages of the ordering process which will be described in a later section (4.5.6).

At all compositions where the domain size was large enough to permit careful examination of internal

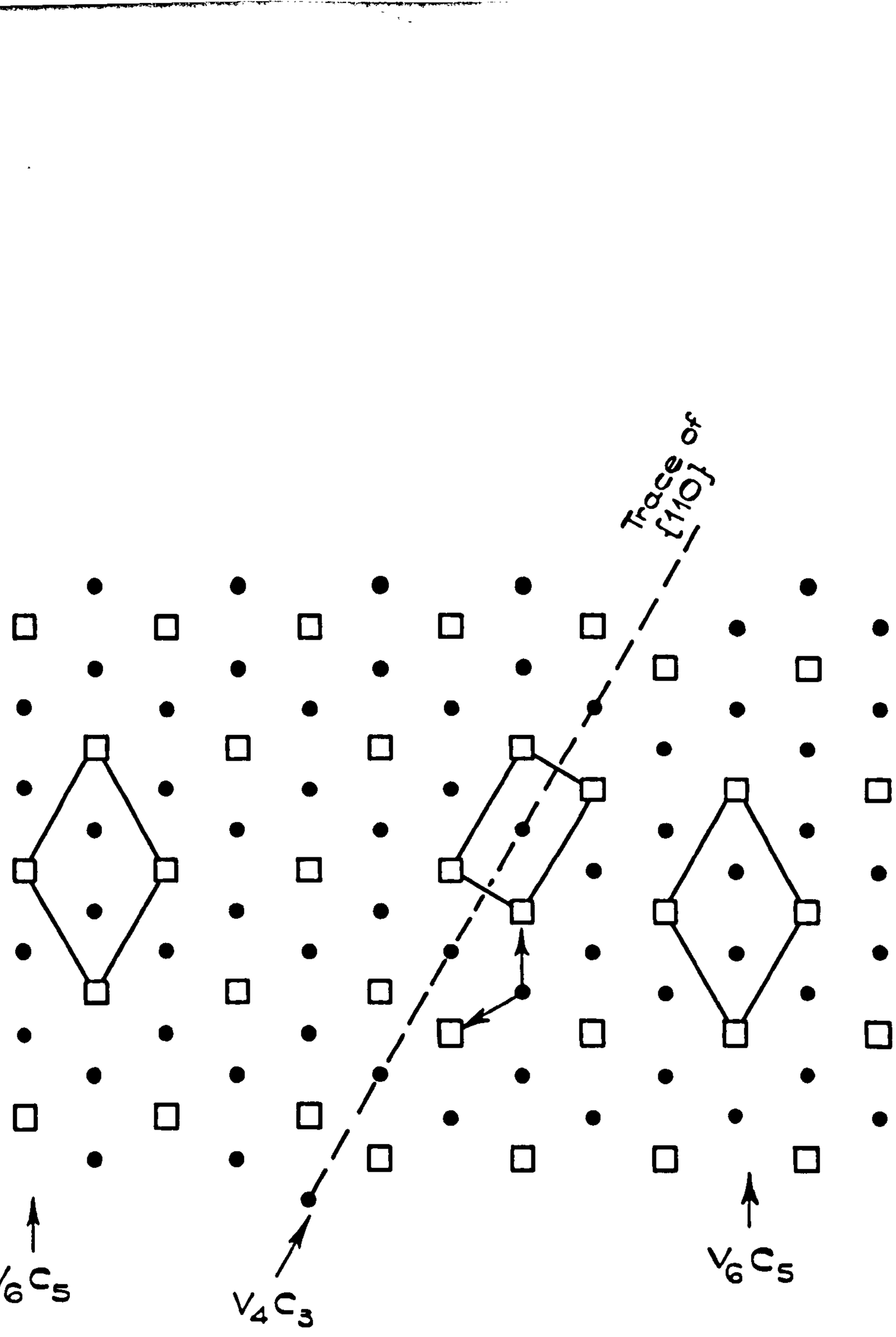


FIG. 4.5.15.

SHOWING HOW SHEAR STRUCTURE ARISES FROM INDICATED TRANSLATIONS. THE COMPOSITION IS MODIFIED IN THE REGION OF THE BOUNDARY.

structure a large amount of substructure was present within the ordered domains. This mainly consisted of A.P.B's lying within the basal planes of thc superlattice unit cell of sufficient density to cause profuse streaking in the diffraction patterns. The density of these faults was continuously reduced by annealing at temperatures above 800°C, but even following extensive anneals at temperatures near to the order-disorder temperature (1200°C) some faults were still present. The long period superstructure was seen in a number of alloys close to the $VC_{0.84}$ composition annealed in the temperature range 1000° to 1070°C. There was also some evidence for its formation at lower carbon compositions. It appeared to be destroyed by A.P.B. re-arrangement at lower temperatures.

Diffraction patterns in 112 sections showing both trigonal and monoclinic forms of ordered structure, were obtained throughout the entire compositional range, often from closely associated regions. In addition, although large numbers of heat treated samples were examined, neither of these forms of order could be solely associated with a particular temperature region within the range studied 600° to 1200°C. Thus it appeared that both ordered structures existed at all temperatures throughout thc composition range. Examination of the 'as grown' and low temperature annealed samples had shown duplex structures similar in appearance to two-phase microstructures. No separate regions were obtained however that were large enough to show only thc unique 112 monoclinic diffraction pattern. Thc samples annealed at higher temperatures ($>800^{o}C$) did contain distinct

regions giving only this type of diffraction pattern. They could be isolated within a region corresponding to one particular orientation of the superlattice. Thus fig.4.5.16 shows such a domain in $VC_{0.84}$ annealed at 1070°C, and the corresponding dark field micrographs are taken with super-lattice spots associated only with the monoclinic (fig.a) or the trigonal (fig.b) superlattice diffraction pattern. Thus it appears that the two forms of order can co-exist in a closely related manner throughout the crystal. The two forms of ordered $V_6C_5$ are structurally very closely related, and probably have similar energies of formation since one can form from the other by a simple shearing process. Thus it is expected that duplex structures containing both forms of order can easily be produced. The very high incidence of basal plane faults in both structures indicates a very low fault energy. Thus as normally produced $VC_{0.84}$ ($V_6C_5$) or closely related compositions, are composed of highly faulted structures containing both the trigonal and mono-clinic forms of carbon vacancy arrangement. Unless specifically stated in the text subsequent references to the $V_6C_5$ structure will refer to both types of order.

The destruction of the long period superlattice at lower temperatures mainly seems to occur by movement of the A.P.B's in a direction perpendicular to that of the periodic direction (see fig.4.5.5). Diffusion of carbon atoms is the most likely mechanism to bring about this structural re-organisation since no dislocations can be associated with the trailing A.P.B's.


(a) (b)

Fig.4.5.16 Dark field micrographs of $VC_{0.84}$ annealed at 1070 °C taken with diffraction spots only present in monoclinic (a) or trigonal (b) superlattice patterns.

### 4.5.6 Nucleation Of Long Range Ordered Phases

The early stages of the long range ordering process were clearly observed in the lower carbon alloys $VC_{0.75}$ to $VC_{0.78}$ by a series of annealing experiments. Alloys of the same composition were examined in the fully ordered, partially ordered, and S-state conditions by successively raising the temperature of the annealing treatment. Each alloy was annealed for periods of 50 to 200 hours and then rapidly cooled in an attempt to examine near equilibrium structures.

A partially transformed alloy, $VC_{0.78}$ annealed at 1000°C, is shown in fig. 4.5.17 to consist of a lenticular shaped ordered region, composed of a number of long range ordered domains, formed within the S-state matrix. The diffraction patterns from the ordered regions and the matrix are also shown in fig. 4.5.17. The matrix pattern consisted of diffuse bands discussed elsewhere (section 4.4) and the lenticular regions gave superlattice spots consistent with the $V_6C_5$ structure. The boundaries between the ordered domains are clearly shown as $\delta$ interfaces. Examination of these fringe profiles (fig. 4.5.17) clearly indicated that the sense of the fringe asymmetry changed on moving from one domain to the next. This, combined with examination of dark field micrographs taken with superlattice spots (fig. 4.5.18) indicated that the domains are twin related.

Growth in this twin related manner occurs as a means of reducing the interface strain caused by the transformation to a less symmetric structure. The situation shown schematically in fig. 4.5.19 shows the vanadium atom

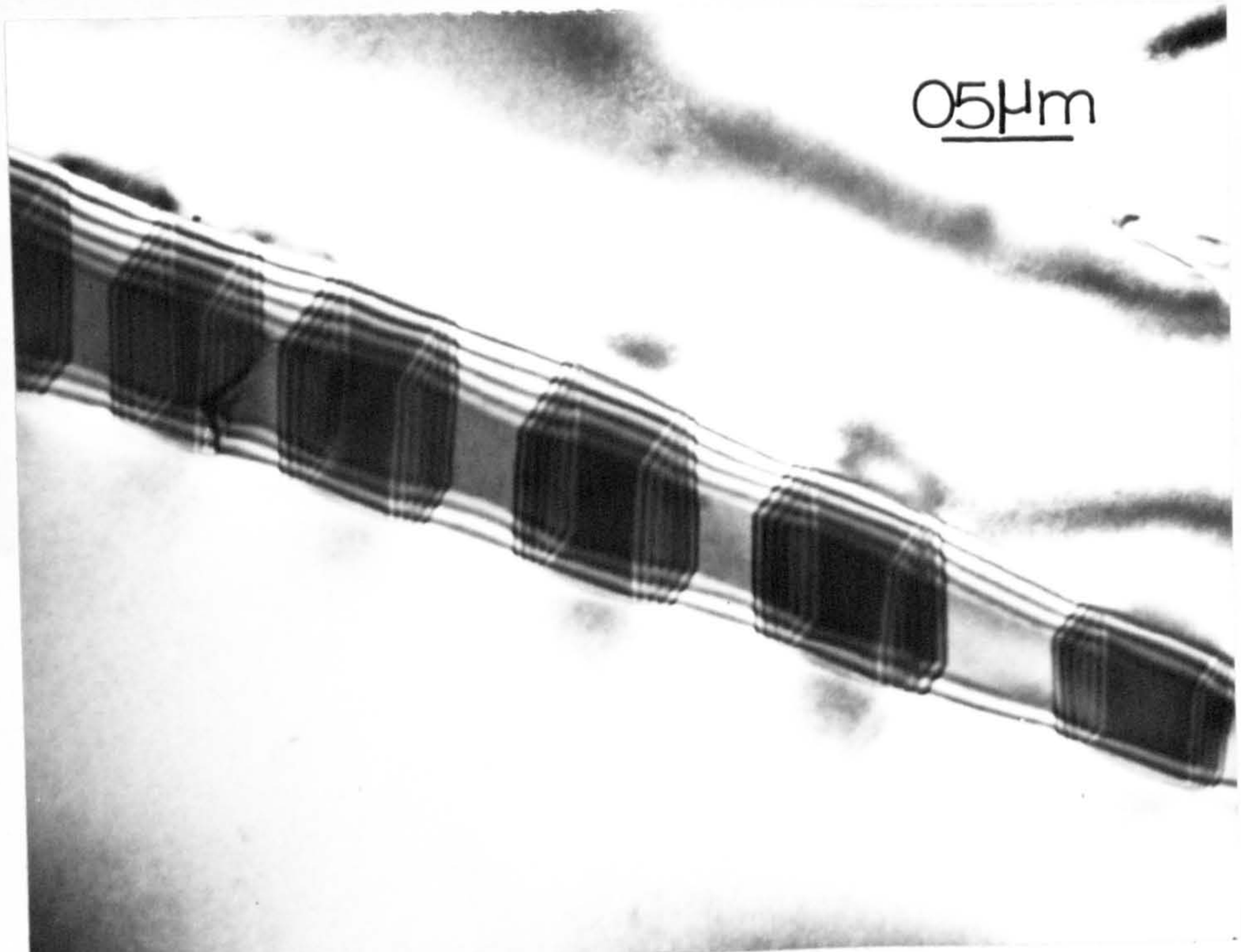


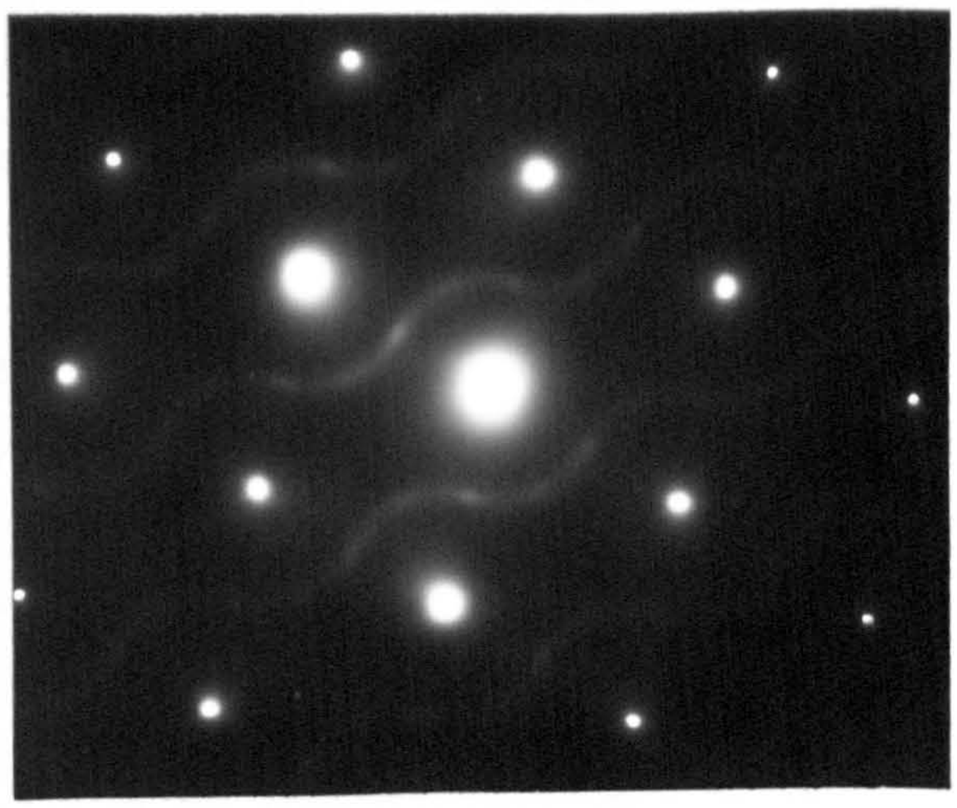

Fig. 4.5.17 Nucleation of ordered $V_6C_5$ domains in an S-state matrix. $VC_{0.78}$ annealed 100 hrs.at 1000°C. Note S interfaces between domains.

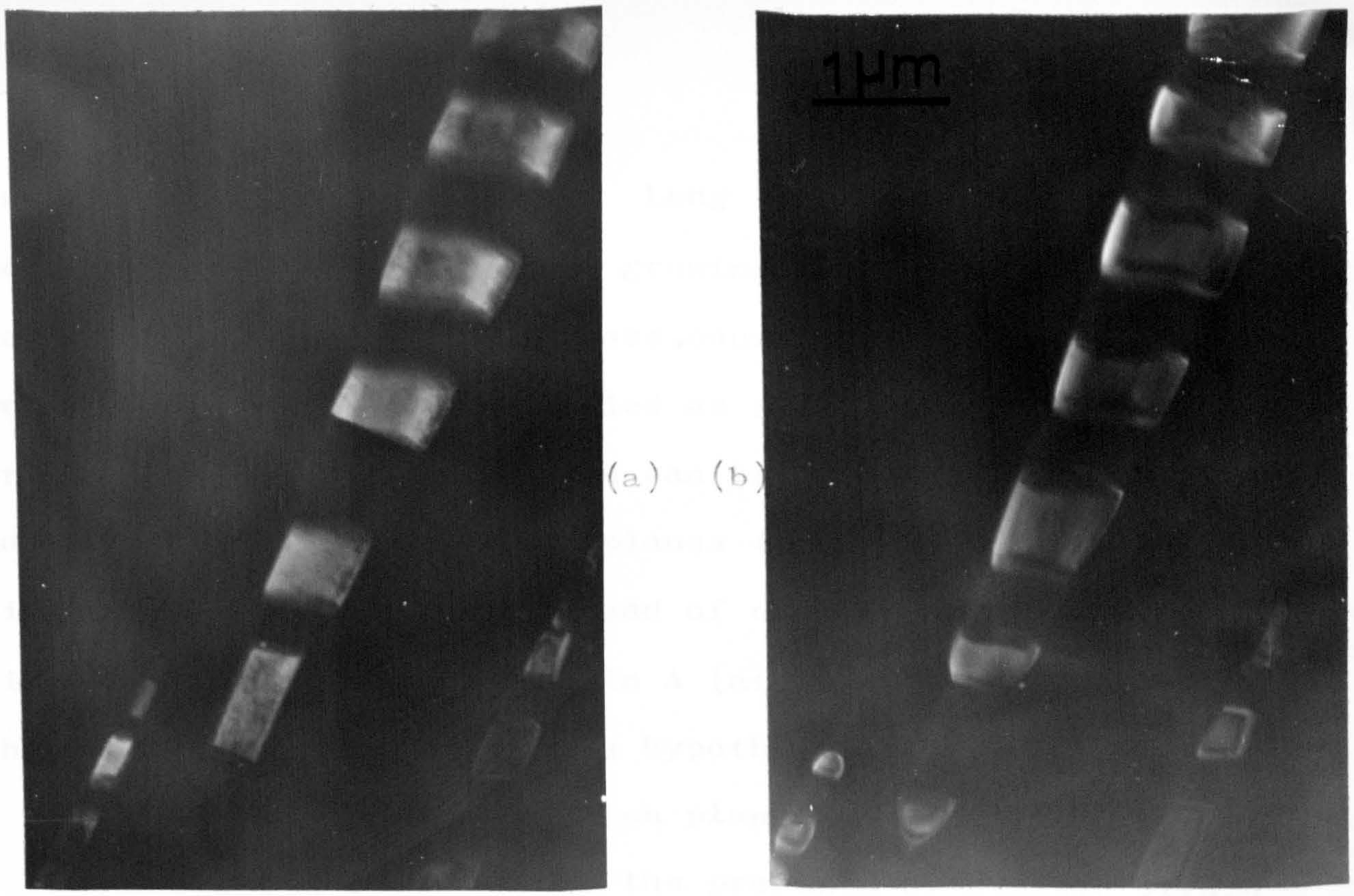


Fig.4.5.18 Dark field micrographs showing twin related superlattice domains. Foil normal 112. Micrographs taken with (a) $\frac{1}{2}$ (111) and (b) $\frac{1}{2}$ (311) reflections.

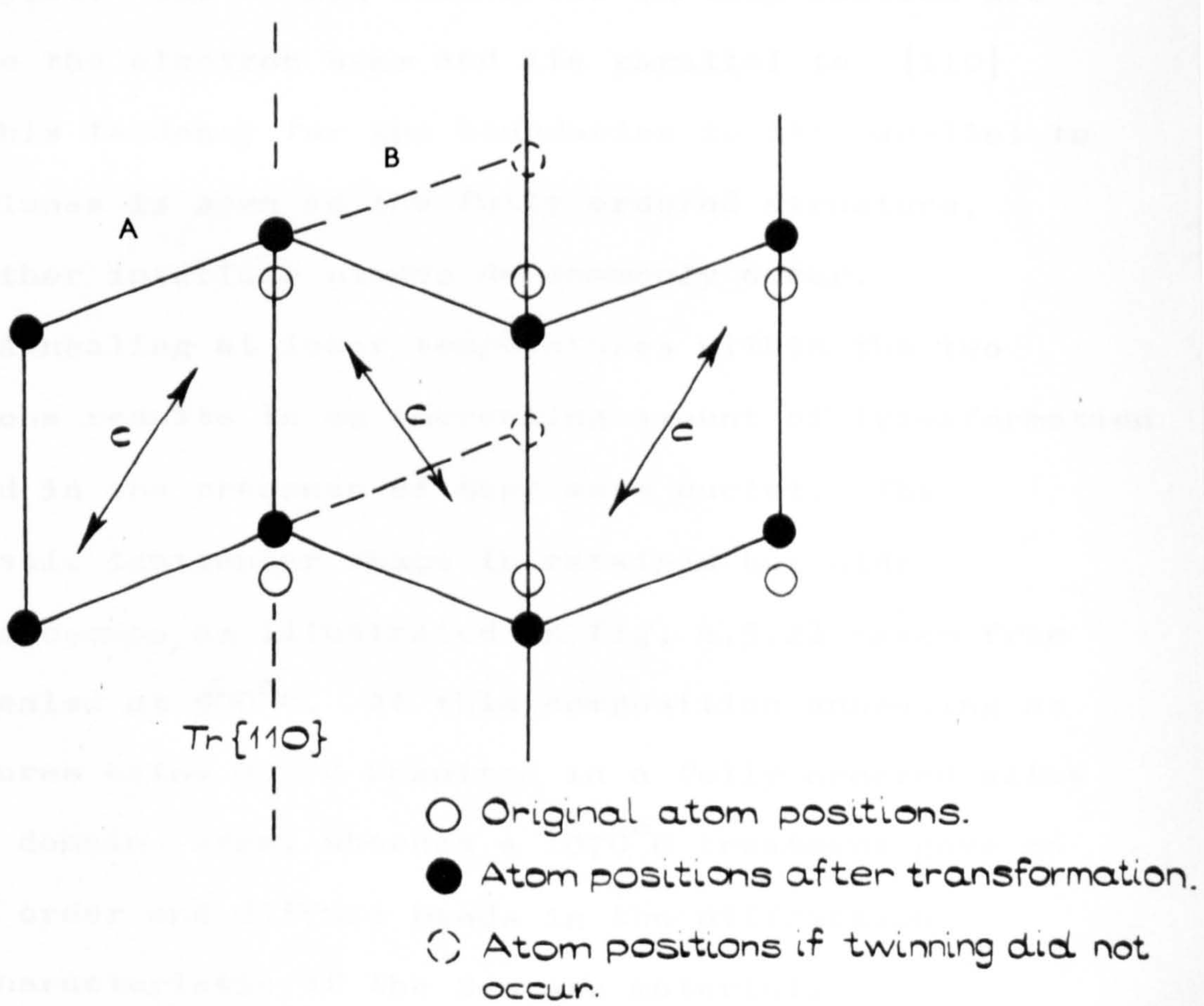


FIG. 4.5.19.

FORMATION OF TWIN RELATED DOMAINS.

positions on a {110} plane. Long range atomic displacements at the interface of the growing domains, during formation of the non-cubic phase, causes the atom positions bounding domain A to be modified as shown. The distortion produced by the transformation can be reduced if the material twins along {110} planes (i.e. forming domain B with a different c-axis) instead of continuing to grow with the fixed c-axis of domain A (atom positions dotted). The micrographs support such a hypothesis and indicate that {110} is the twin composition plane.

Direct evidence for the presence of elastic strain at the growing interface between ordered and S-state material is shown by the presence of elastic strain fields in fig. 4.5.20. The domain boundaries in this section are parallel to the electron beam and lie parallel to {110} planes. This tendency for the boundaries to lie parallel to {110} planes is seen in the fully ordered structure, although other interface planes do commonly occur.

Annealing at lower temperatures within the two phase regions results in an increasing amount of transformation product and in the presence of many more nuclei. The characteristic lenticular shape is retained but side branching is common, as illustrated in fig. 4.5.21 taken from $VC_{0.78}$ annealed at 900°C. At this composition annealing at temperatures below 800°C resulted in a fully ordered alloy with small domain size, whereas a 1070°C treatment gave no long range order and diffuse bands in the diffraction patterns characteristic of the S-state material.

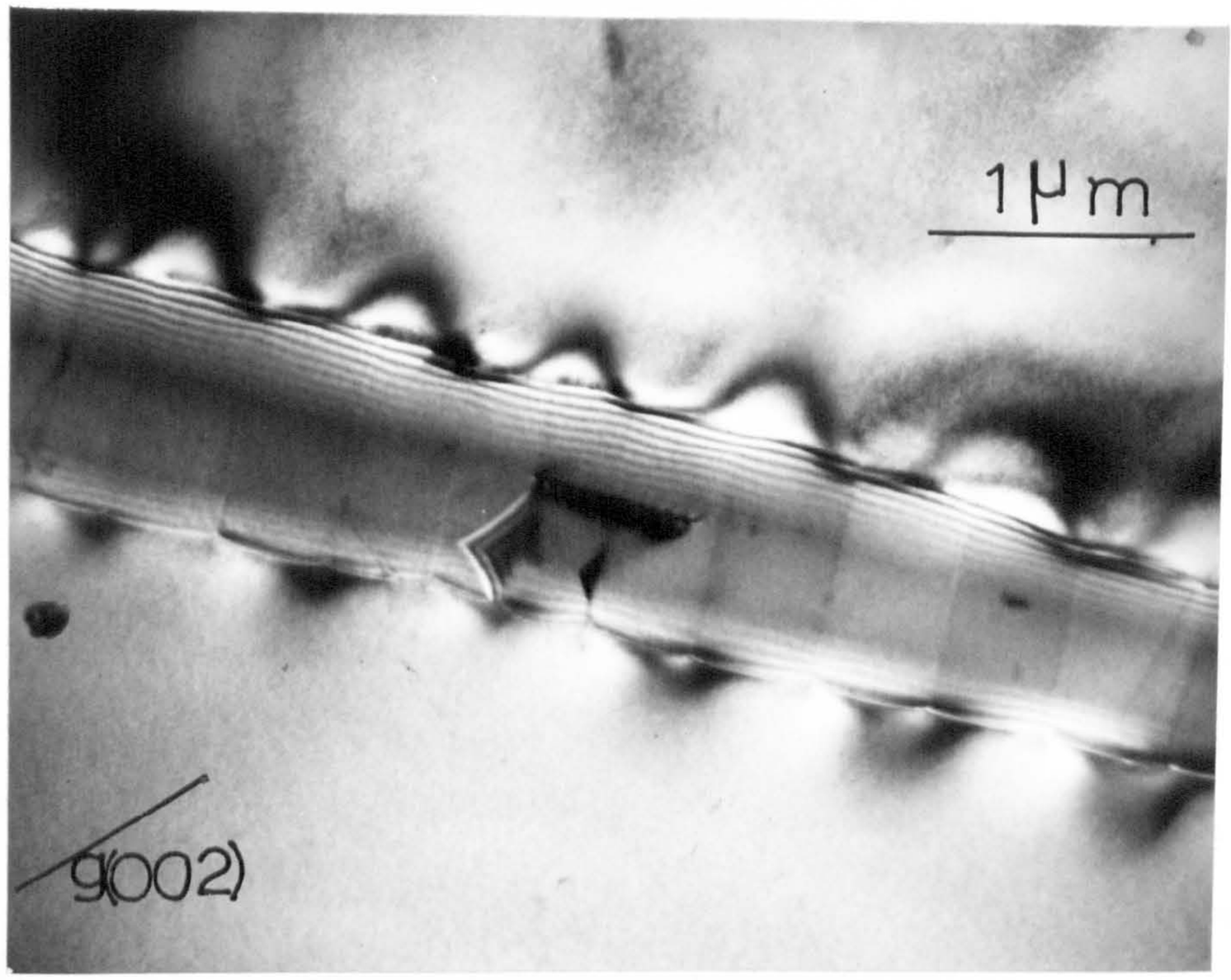


Fig. 4.5.20. Showing elastic strain fields in matrix at interface with ordered domains. $VC_{0.78}$ annealed at 1000°C. Domain boundaries are parrallel to {110} planes..

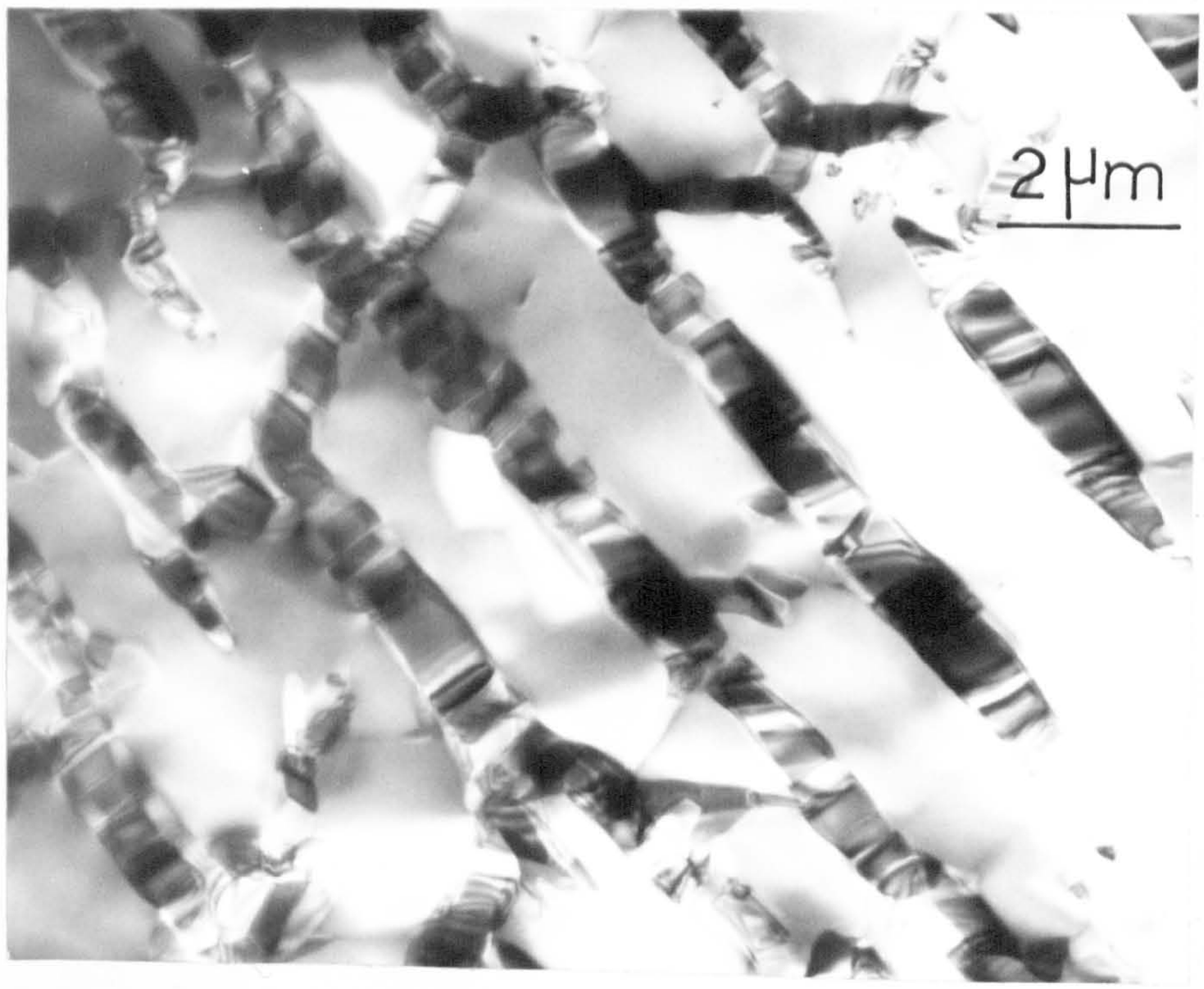


Fig. 4.5.21 Showing increased amount of transformed ordered phase on annealing at lower temperature. $VC_{0.78}$ annealed at 900°C.

The diffraction patterns from the ordered regions are consistent with the trigonal $V_6C_5$ structure except for the formation of additional spots along the 220 reciprocal lattice vector as illustrated in fig. 4.5.22(a). In $V_6C_5$ the superlattice spots form at one third spacings along this vector but neither of the spots shown here coincides with this position. The strongest spot does however form where the diffuse bands intersect the vector. Dark field images formed with these spots indicate a fringe structure within the domains (fig. 4.5.22(b)). It is possible that these two spots are indicative of an extra periodic structure similar to the long period superlattice reported in section 4.5.5 at higher carbon content, and if so the splitting of the spots indicates that the period would be approximately 23Å. It is unlikely that this spacing could be resolved using the large angle goniometer tilt stage, and with such a small amount of transformed product. The fringe spacing observed in fig. 4.5.22(b) is likely to be a Moiré effect due to overlying structures.

An alloy of composition $VC_{0.75}$ consisted of S-state material both in the 'as-grown' condition and following a number of annealing experiments in the temperature interval 700° to 1200°C. However long range order was detected following annealing at 630°C for 340 hours. The diffraction patterns show long range order spots coincident with the diffuse bands fig. 4.5.23(a), which are associated with small long range ordered regions as shown by the dark field micrograph (fig. 4.5.23(b) ). The average size of the ordered regions after this treatment is 600Å. This alloy $VC_{0.75}$ has

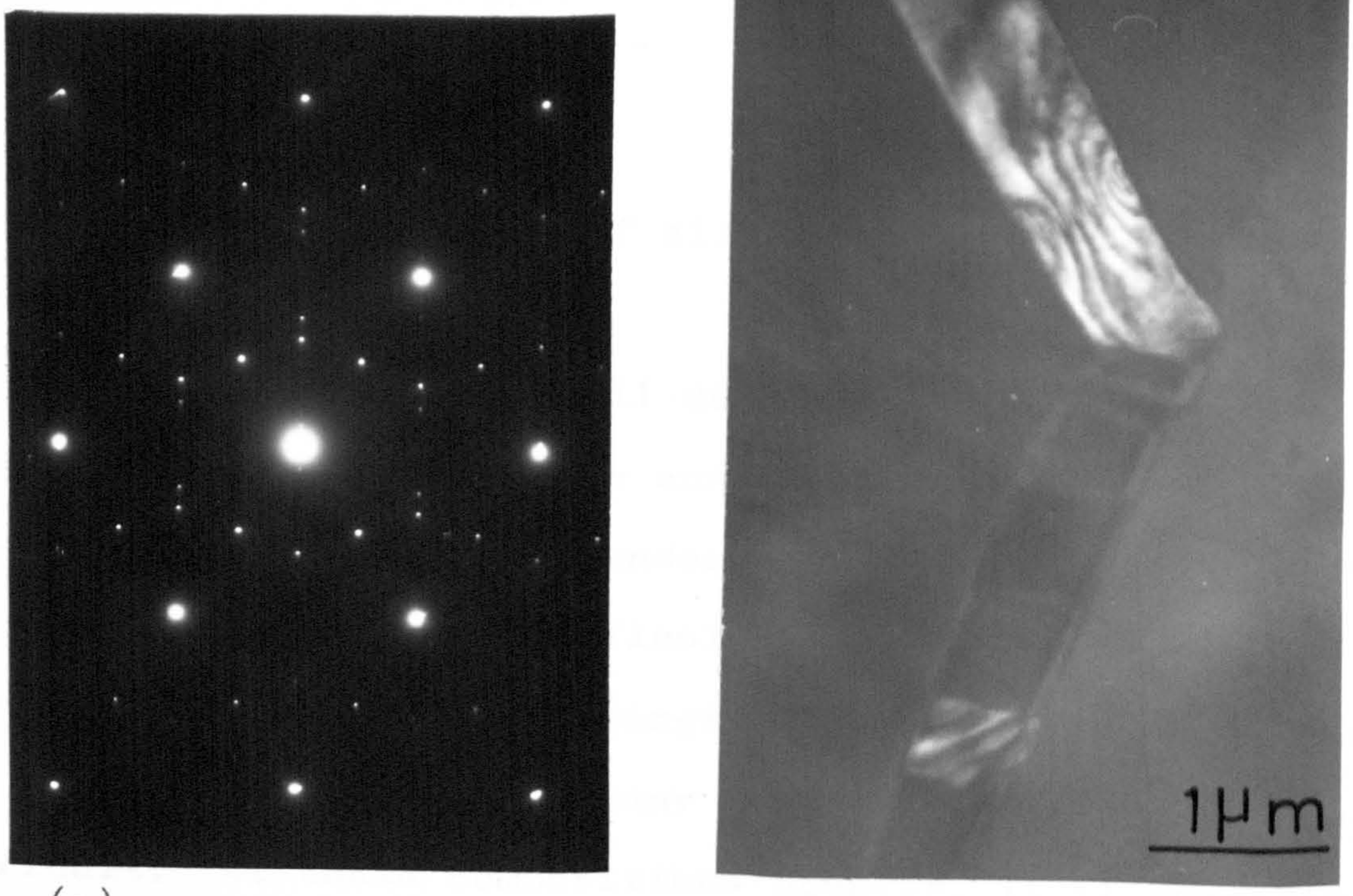


(a) (b)

Fig. 4.5.22 Diffraction pattern from transformed region $VC_{0.78}$ annealed at 900°C, and corresponding dark field image taken with $\frac{2}{3}$ $\frac{2}{3}$ 0 spot .

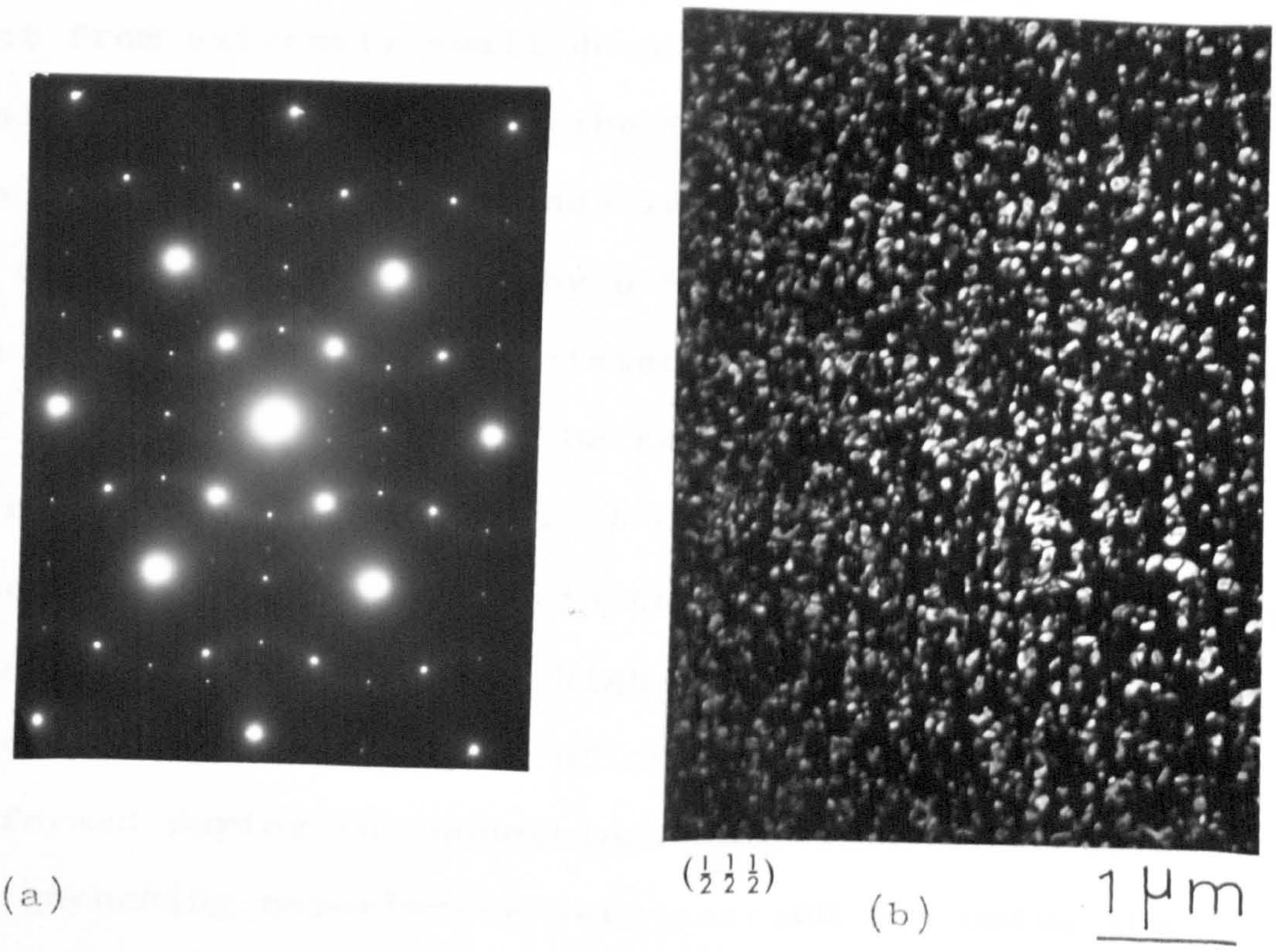


(a) (b)

Fig. 4.5.23 $VC_{0.75}$ annealed 340hrs at 630°C. Small long range ordered domains are shown in the dark field micrograph (fig.b). The domains are approximately 600A in size.

the lowest carbon content of all alloys in which long range ordered $V_6C_5$ was detected.

The relatively small domain size in all these alloys, even after extensive annealing treatments near to the ordering temperature, renders detailed examination of the structure much more difficult than at higher carbon contents. This is because single domain diffraction patterns are difficult to obtain and any tilting procedures become difficult. At these compositions however, it it possible to quench in the high temperature S-state which becomes increasingly difficult as the carbon content and ordering temperature increase.

A possible explanation of the diffuse banding in the S-state material is that it is due to a diffraction effect from extremely small domain sizes. Very long annealing times resulted in the formation of diffraction spots as well as diffuse bands in the diffraction patterns from the $VC_{0.75}$ alloys and by using dark field images the small domains could be associated with these spots. No very small domains could however be seen by dark field imaging with only the diffuse bands. A difficulty arises as to whether the diffuse banding is characteristic of a non-random arrangement of vacancies at high temperature or is only a consequence of the presence of an extremely fine domain size formed during the quenching. In order to resolve this, quenching experiments were carried out using the hot-stage attachment to the electron microscope. An alloy of composition $VC_{0.73}$ whose diffraction pattern consisted only of diffuse bands, was heated in situ in the electron

microscope, and the diffraction pattern observed at various temperatures. From observations of the order - disorder temperature of a number of other alloys of different composition (measured outside the microscope by annealing and quenching experiments) an ordering temperature below 700°C would be expected if such an alloy did order. Thus annealing at temperatures well above this should remove the S-state if it is due to the presence of extremely small domains formed during the quench. The alloy was heated slowly to 950°C and held at that temperature for an hour without any change taking place in the diffraction pattern i.e. the diffuse bands did not disappear. This result was also duplicated on a second specimen of slightly different composition $VC_{0.75}$. Thus it appears that the so called 'S'-state is not due to the quenching treatment but is a stable state in the system where the carbon vacancy arrangement is non-random. Moreover this state is stable at temperatures well above the order - disorder temperature.

At a composition of $VC_{0.78}$ the strain set up when material in the S-state transformed to a long range ordered phase manifested itself in two ways. Firstly elastic strain fields were set up in the material around the transformed regions and secondly the domains formed in a twin related manner. When much larger domains are formed under these conditions the displacements caused by the strain set up at the growing interface are too large to be accommodated.

in this manner, and are relieved instead by the formation of interface dislocations. Large numbers of such dis - locations are seen in fig. 4.5.24 in an alloy of composition $VC_{0.81}$ annealed at 1200°C for 100 hours. The structure consists of large ordered domains of $V_6C_5$ separated from regions showing darker mottled contrast by large numbers of interface dislocations. The darker mottled regions can be shown by suitable dark field imaging to consist of small ordered domains of $V_6C_5$ in a number of orientations (fig. 4.5.25).

These regions are thought to be S-state material at 1200°C and fig. 4.5.24 enables a direct measurement of volume fractions of long range ordered $V_6C_5$ and S-state material existing in equilibrium at 1200°C to be made. During cooling the S-state material becomes supersaturated with respect to the ordered phase, and nucleation of this phase occurs resulting in the formation of a number of domains in different orientations. In addition the large ordered domains surrounding the supersaturated region provide an easy nucleation site for further ordered phase formation, and this can clearly be seen in fig. 4.5.26, where the advancement of the interface into the S-state region is clearly defined by the A.P.B's trailing the dislocations.

Annealing the same alloy at 1070°C. produced similar effects but the regions of small domain size were fewer in number and of smaller size.

At these higher carbon compositions $VC_{0.81}$ to $VC._{0.83}$ the domain size following high temperature anneals



Fig. 4.5.24 Interface dislocations in $VC_{0.81}$ annealed for 100 hrs. at 1200°C.

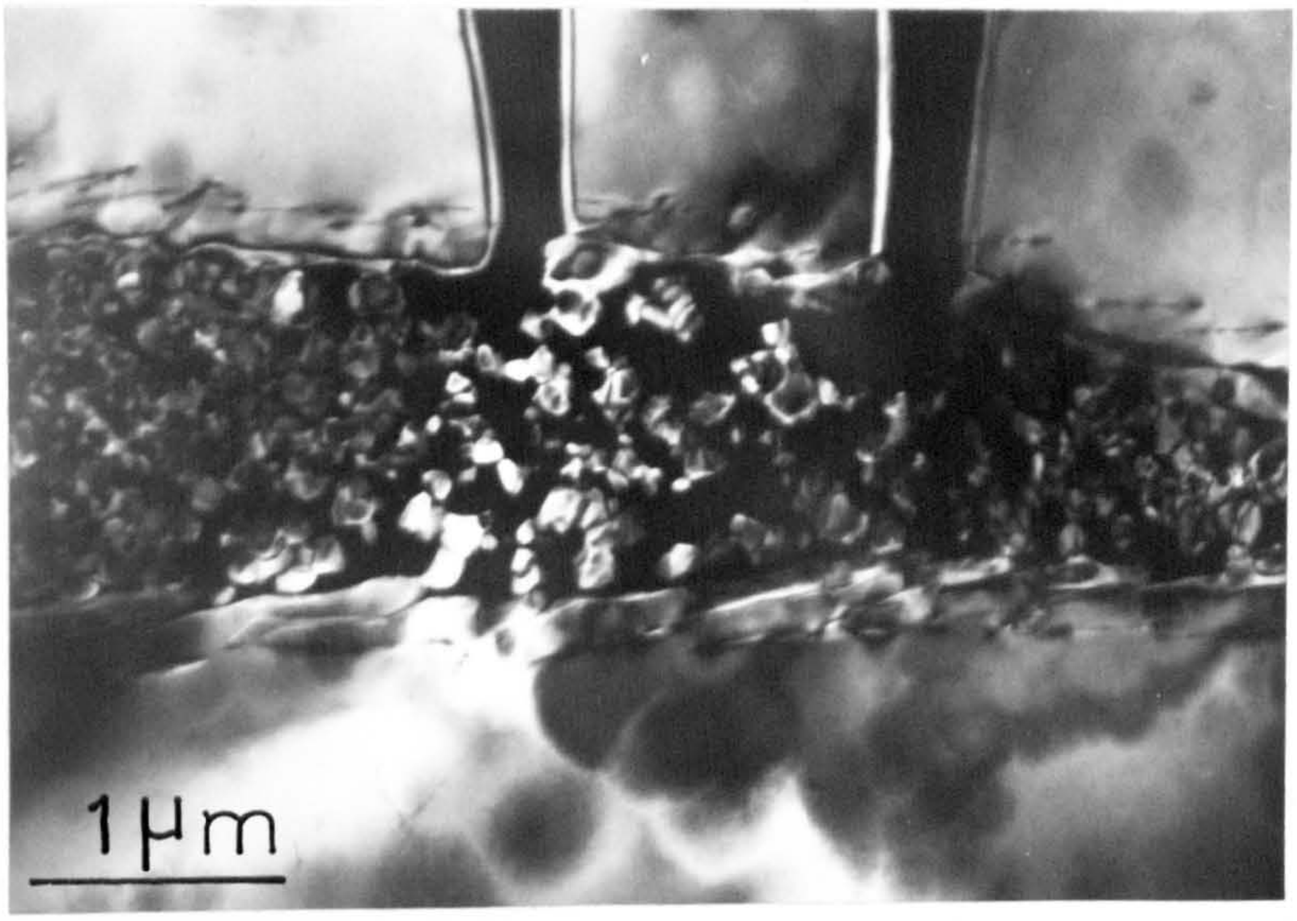


Fig.4.5.25 Dark field micrograph showing how the mottled regions in previous micrographs are composed of small ordered domains of $V_6C_5$ in a number of orientations,

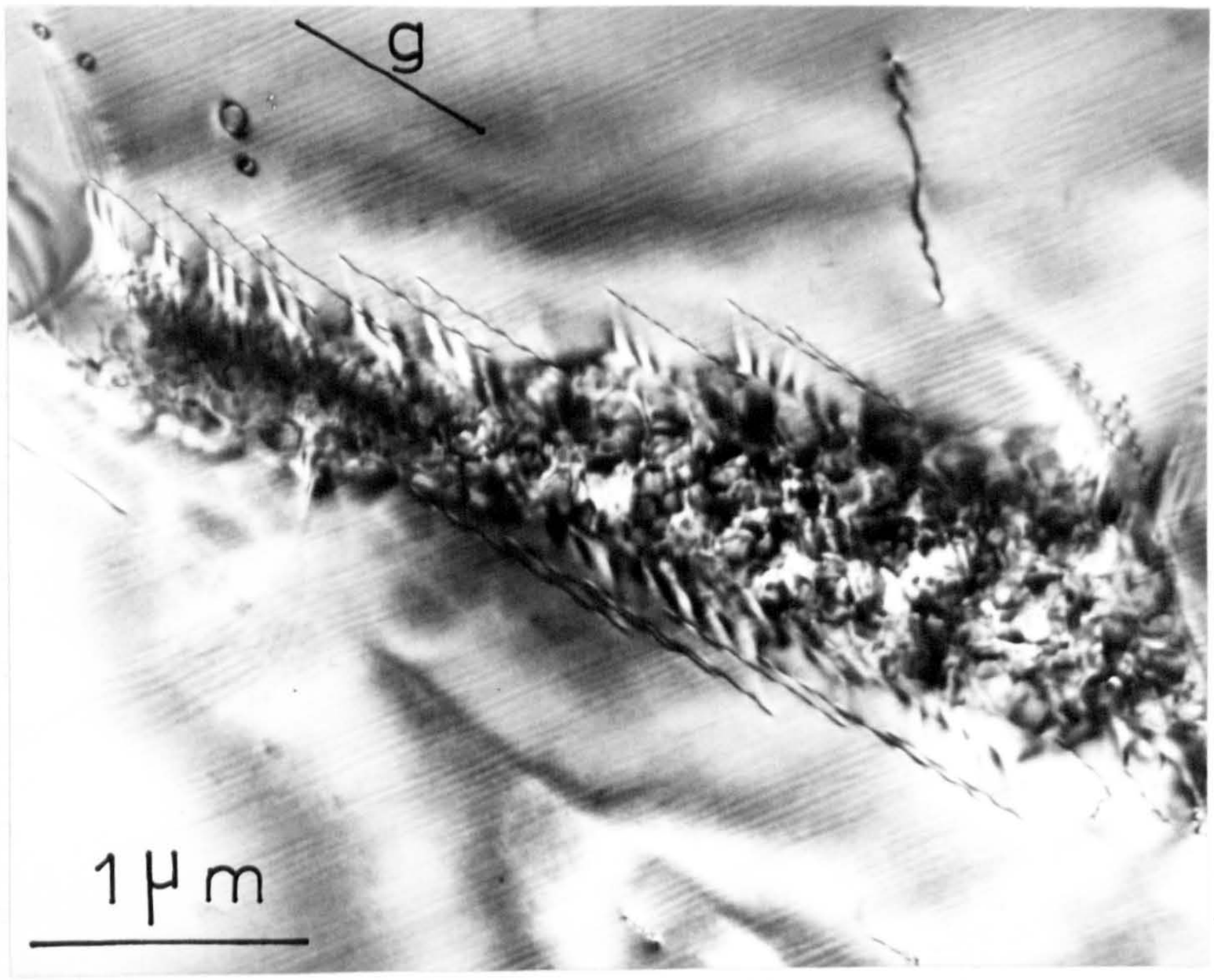


Fig. 4.5.26 Trailing A.P.B's indicating original interface at high temperature between ordered and S-state material. $VC_{0.81}$ annealed 100 hrs.1200°C.

was much larger than at $VC_{0.78}$ and appreciable amounts of substructure were noted (fig. 4.5.26). The S-state structure could not be retained at this composition with the cooling rates used, in contrast to the $VC_{0.78}$ alloys.

## 4.6 Co-Existence Of Two Ordered Phases

The present investigation has defined the composition limits within the monocarbide phase field where the previously determined ordered structures are stable. Thus the cubic $V_8C_7$ phase exists from $VC_{0.87}$ to $VC_{0.90}$ (described in section 4.3) and the trigonal and monoclinic duplex phase structure based on the composition $V_6C_5$ from $VC_{0.75}$ to $VC_{0.86}$ (described in section 4.5). Certain alloys, with compositions near to the composition limits of these two phases viz $VC_{0.85}$ to $VC_{0.87}$, were found to contain both the ordered cubic $V_8C_7$ and the duplex non-cubic ordered phases based on the composition $V_6C_5$.

The diffraction pattern from such an alloy showing superlattice spots associated with both ordered structures is shown in fig. 4.6.1. It is also possible to obtain patterns from regions associated with only one of the ordered phases by suitable positioning of the diffraction aperture (e.g. fig.4.6.1(b)and(c) ).Both the monoclinic and trigonal forms of $V_6C_5$ could be detected in some areas. The microstructure from such a region has the appearance of a two phase structure (fig. 4.6.2) and fringes are observed between the darker regions and the background. The fringes are $\delta$ fringes which is consistent with the precipitation of a cubic phase in a non-cubic matrix. Dark field micrographs taken with particular superlattice reflections(fig. 4.6.3)

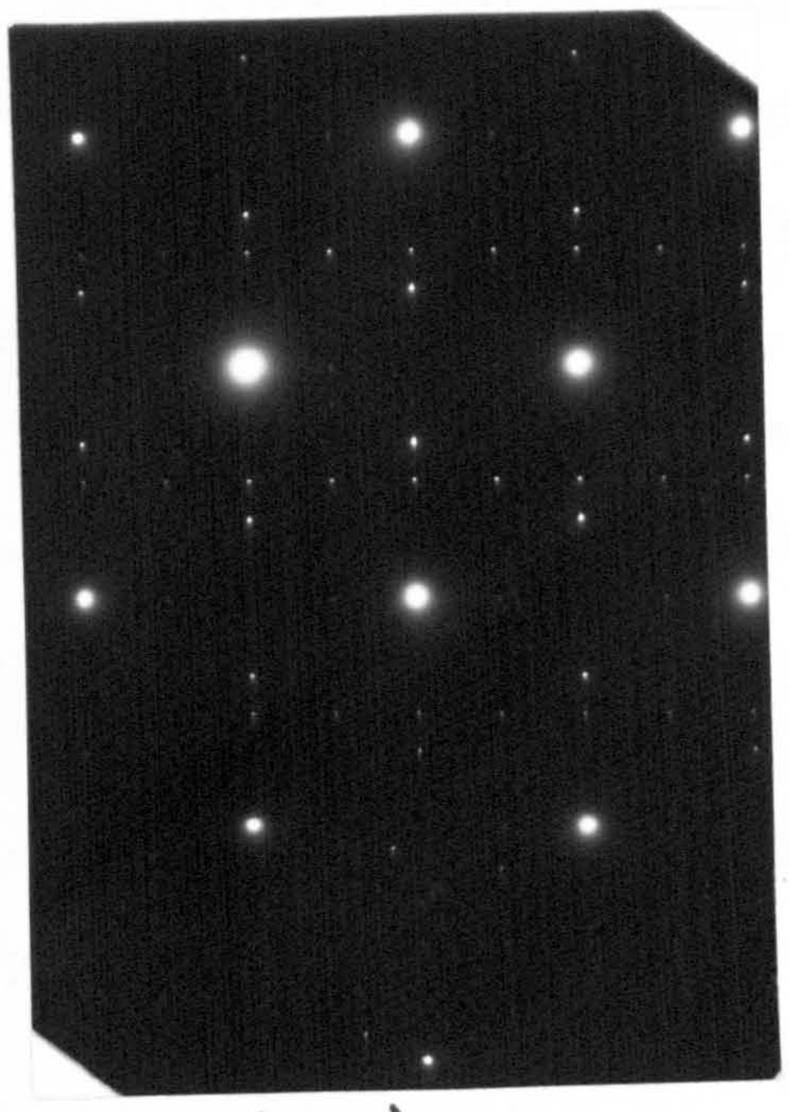

(110)

(a)

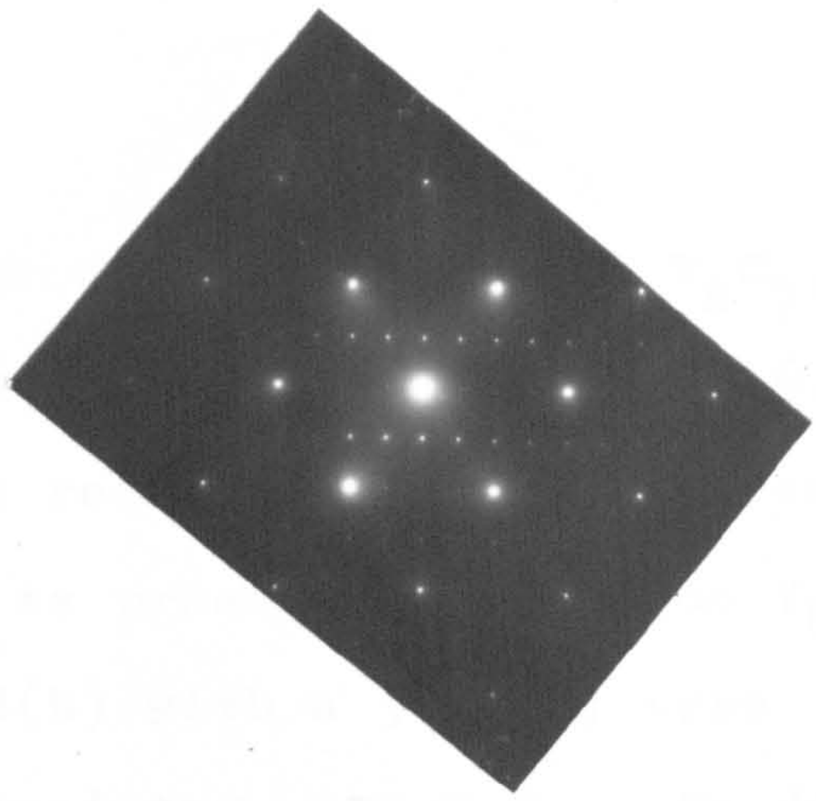

(b)

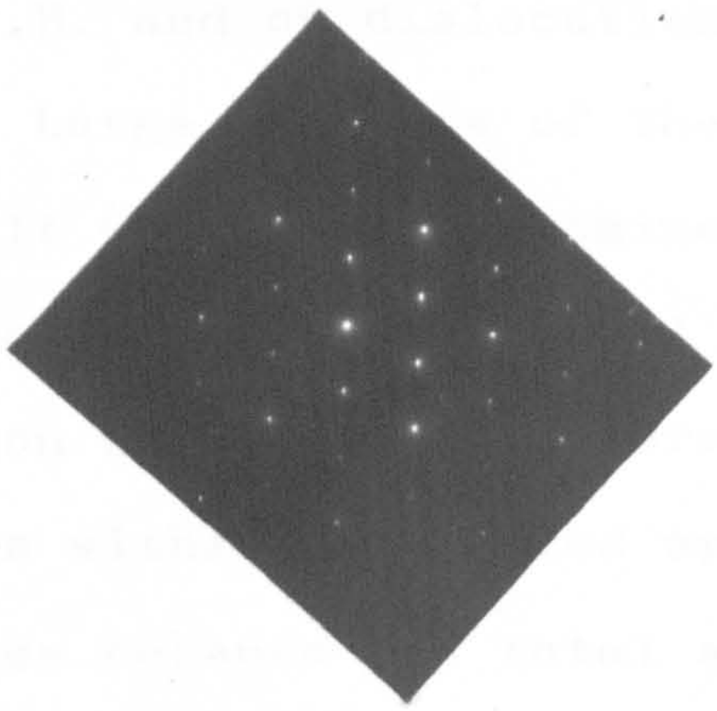

(c)

Fig. 4.6.1 Diffraction patterns from $VC_{0.86}$ alloy. The superlattice spots are consistent with the presence of both $V_8C_7$ and $V_6C_5$ in the structure, whereas Fig.(b) and (c) are from small regions consisting wholly of $V_8C_7$ and $V_6C_5$ respectively.


Fig.4.6.2. $VC_{0.85}$ annealed for 100 hrs. at 1000°C showing a two phase microstructure of $V_8C_7$ regions in a matrix $V_6C_5$

enables identification of the darker regions as $V_8C_7$, and the remaining lighter regions as $V_6C_5$. Thus fig.4.6.3(a) is taken with a $\frac{1}{4}$ (220) type reflection (with reference to the f.c.c. structure) which is present only in the $V_8C_7$ superlattice, and fig. 4.6.3(b) with a $\frac{1}{3}$ (311) type reflection which is only associated with $V_6C_5$. No dis - ordered regions appear to be present.

The $V_8C_7$ regions are preferentially nucleated on the irregular wavy type of A.P.B. and on dislocations within the $V_6C_5$ matrix (fig. 4.6.4). Large portions of these wavy A.P.B. usually have a fault vector not contained in the boundary, and are associated with compositional changes, which make them ideal.nucleation sites for transformations involving compositional changes within an ordered system. Dislocations are preferred sites because the total strain energy of the system can be minimised if transformations involving strain, viz from non-cubic $V_6C_5$ to cubic $V_8C_7$, occur at such sites.

The $V_8C_7$ shows no tendency to form with a particular interface plane relationship with the matrix, and since no dislocations are visible at such interfaces they are likely to be coherent with respect to the vanadium sublattice.

The reverse transformation in which $V_6C_5$ structures precipitated from $V_8C_7$ was observed in an alloy of composition $VC_{0.87}$. Diffraction patterns consistent with $V_8C_7$ reciprocal lattice sections were obtained from these alloys, but a number of additional low intensity spots were also present which could be indexed according to $V_6C_5$

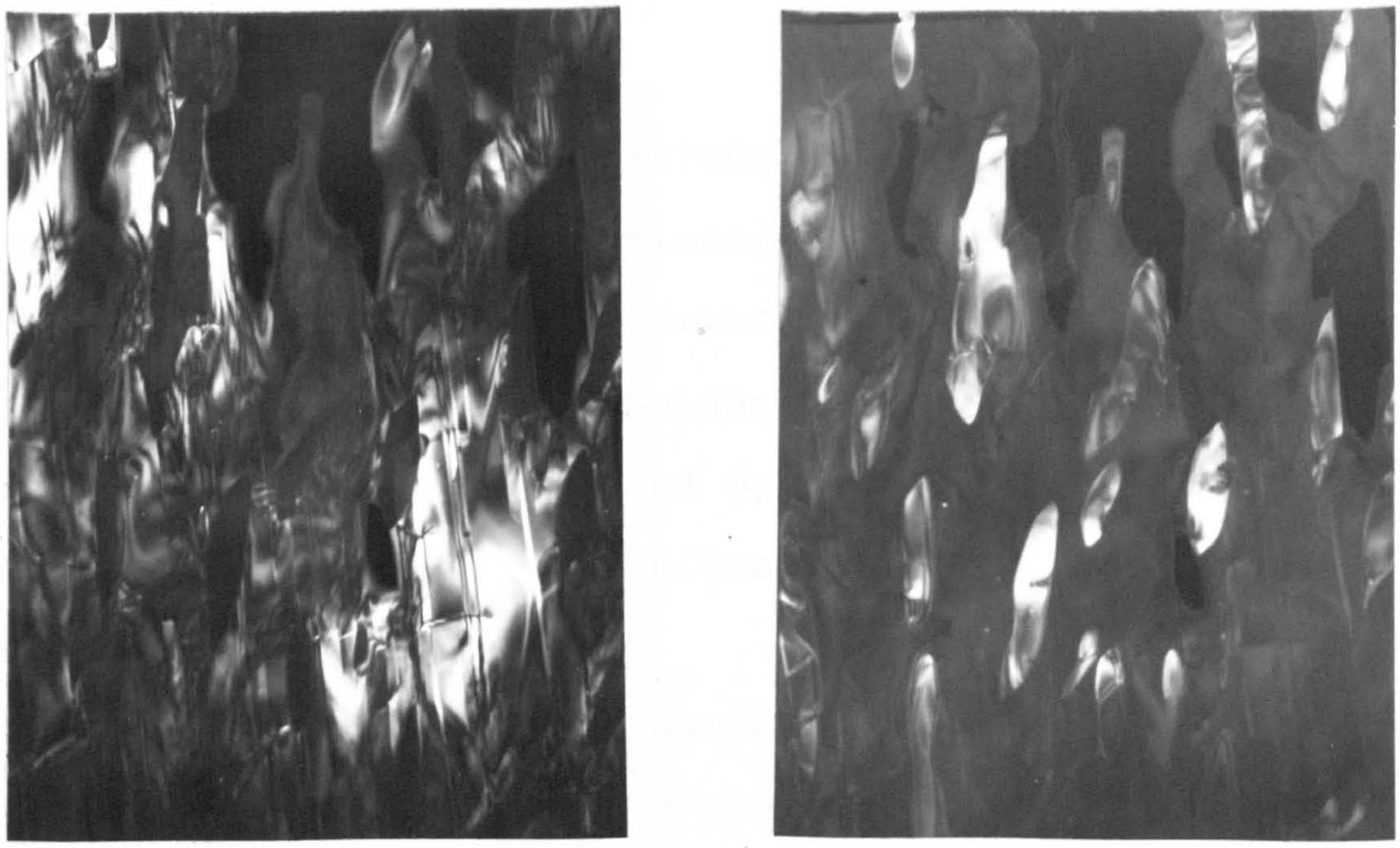


(a) (b)

Fig.4.6.3 Dark field micrographs from the same region of sample $VC_{0.86}$ taken with superlattice reflections consistent only with $V_6C_5$ (a) and $V_8C_7$ (b)

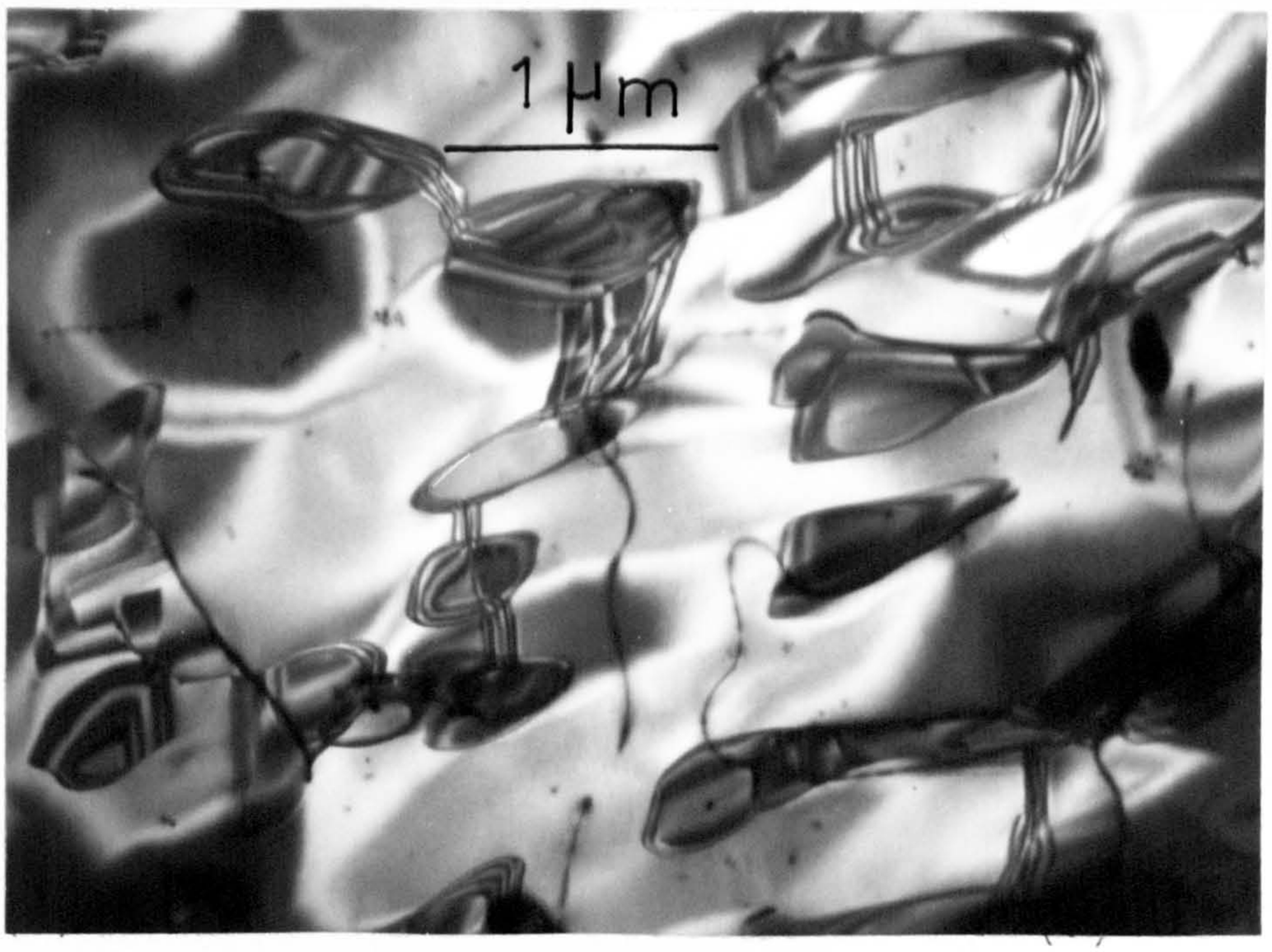


Fig. 4.6.4 Showing how dislocations and A.P.B's in the $V_6C_5$ structure act as nuclei for the formation of the $V_8C_7$ phase (darker regions).

(fig. 4.6.5(a). The low intensity of these additional spots and their close proximity to the much stronger $V_8C_7$ spots precluded positive correlation of their presence with $V_6C_5$ using dark field techniques. The bright field microstructures was characterised by the presence of small particles of second phase often associated with A.P.B's (fig. 4.6.5(b)).

Dark field examination with a $V_8C_7$ superlattice spot under almost two beam conditions, gave images as shown in fig. 4.6.6(a) where the smaller particles appeared dark against a bright background (due to $V_8C_7$). Thus these darker regions are not associated with $V_8C_7$ and are most probably particles of $V_6C_5$. Enhanced contrast at the particles is shown in fig. 4.6.6(b) taken in dark field with a $\frac{1}{2}$ (111) reflection which is common to both the $V_8C_7$ and $V_6C_5$ superlattices. The strong contrast shown by the particles indicates that the diffraction pattern from the particles includes this spot, which is consistent with the particles being $V_6C_5$. This diffraction contrast behaviour, combined with the electron diffraction and chemical composition evidence, strongly indicates that the particles are $V_6C_5$.

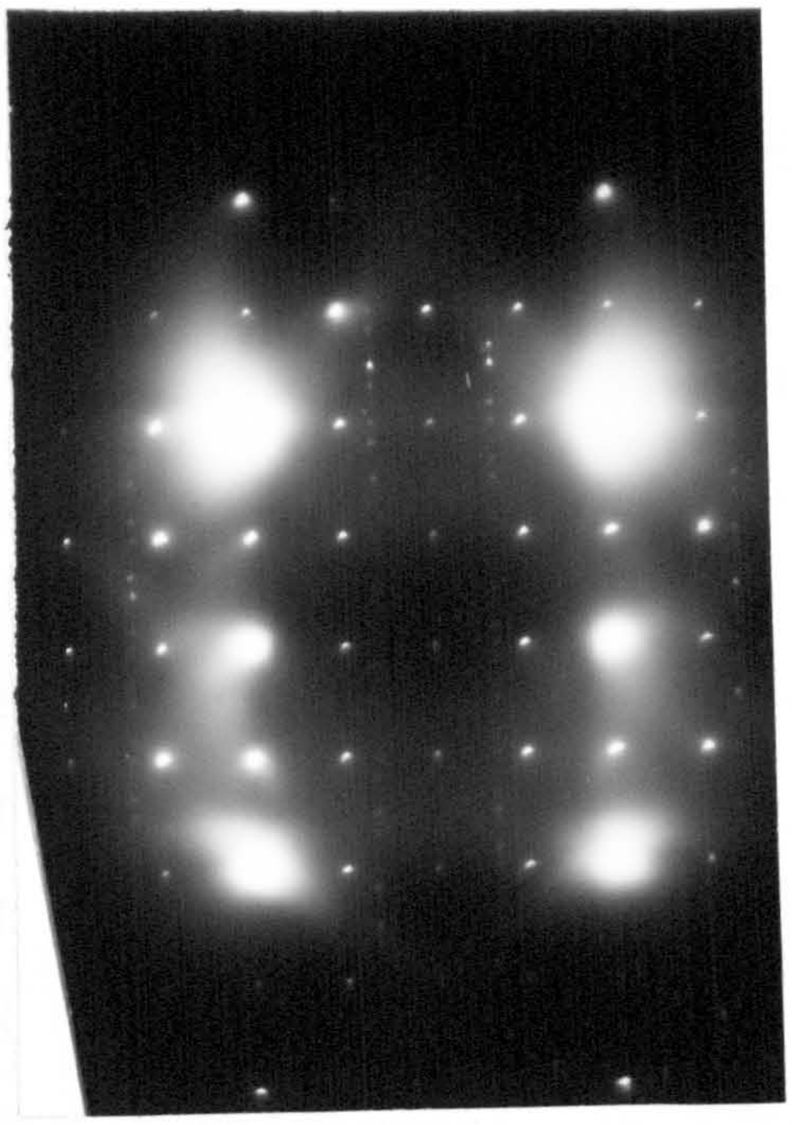

(a)

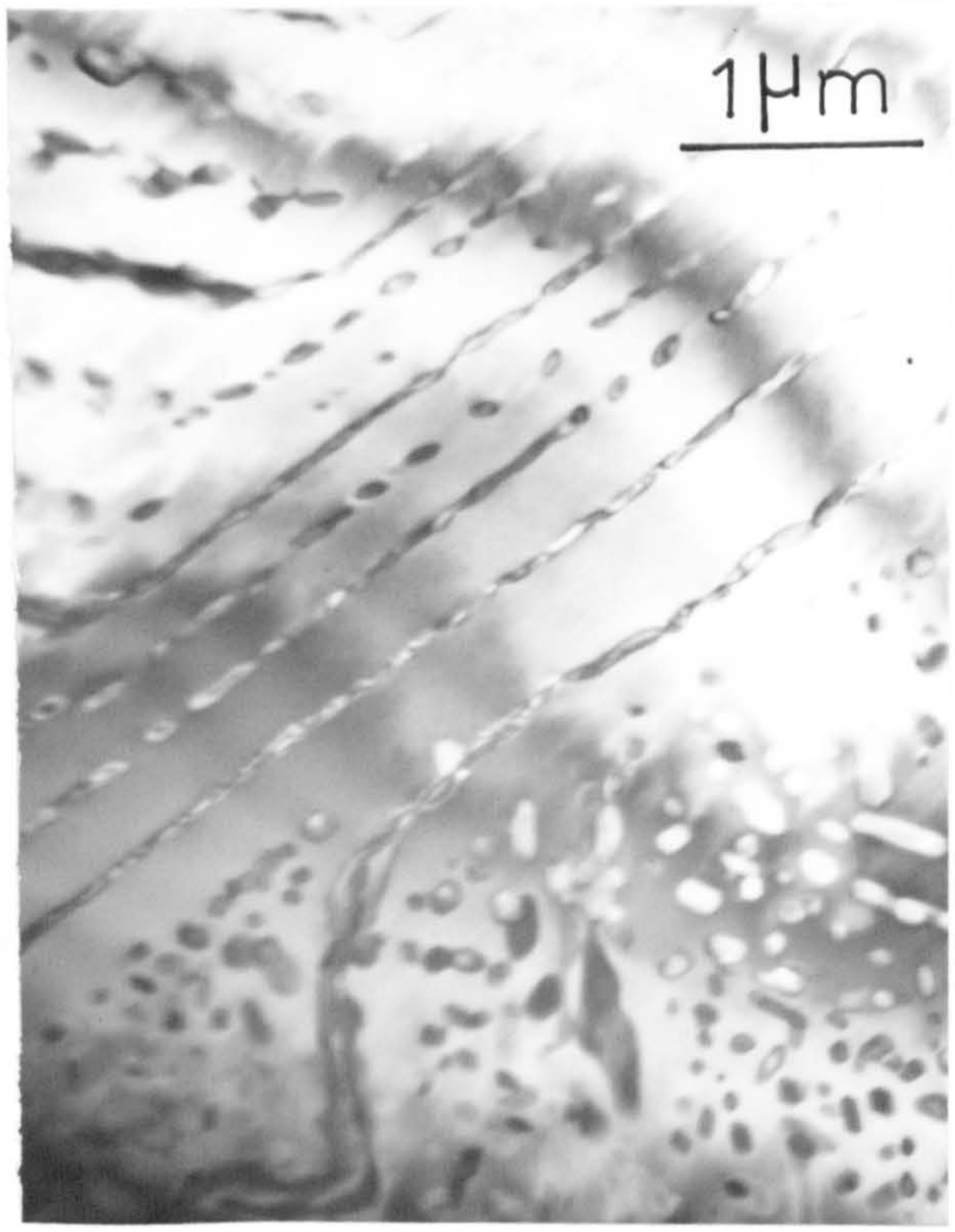


(b)

Fig. 4.6.5 Diffraction patterns from $VC_{0.87}$ alloy consisting of $V_8C_7$ spots plus additional weak spots consistent with both forms of $V_6C_5$. Fig.(b) shows the two phase appearance of the bright field microstructure of such an alloy.

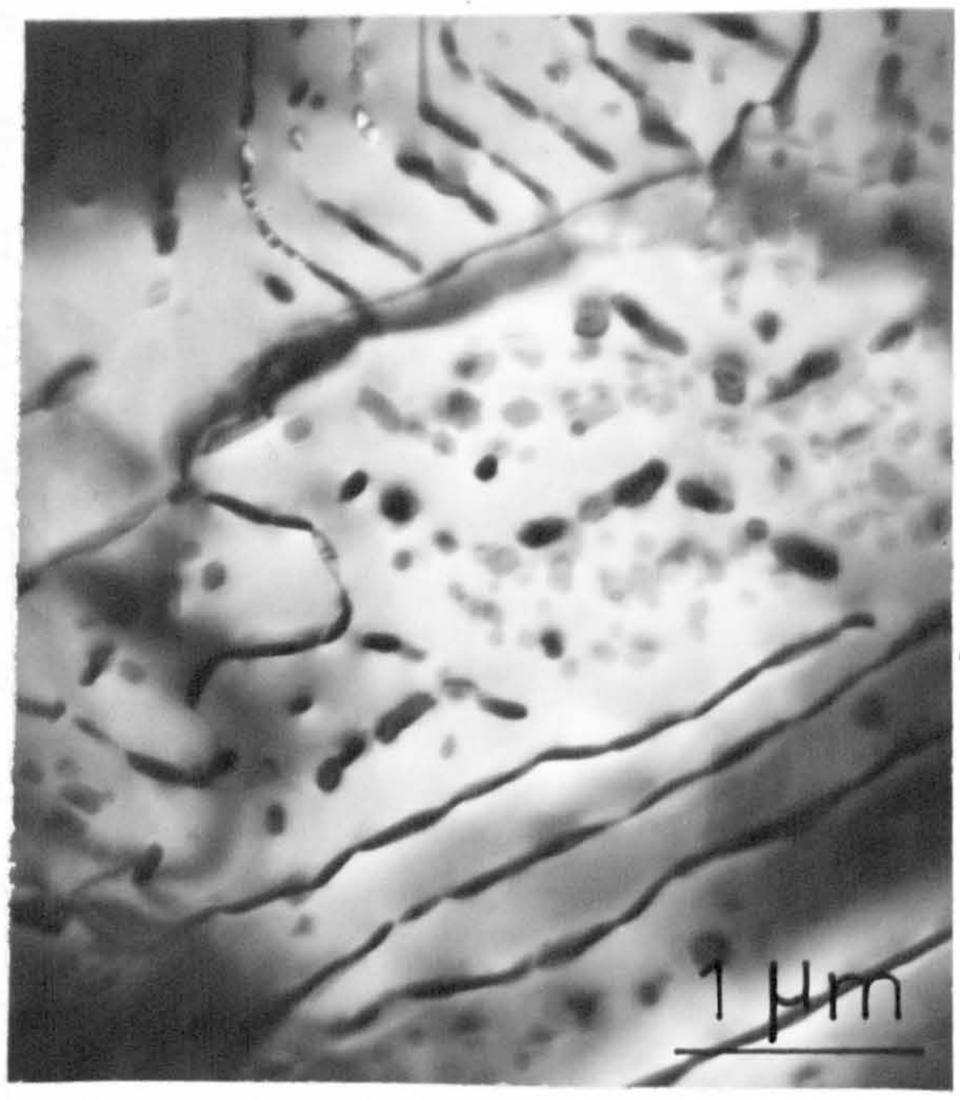


(a)


(b)

Fig. 4.6.6 Dark field microstructures of such $VC_{0.87}$ alloys. Fig.(a) $\frac{1}{4}$ (220) reflection consistent only with $V_8C_7$ superlattice. Fig.(b) $\frac{1}{2}$ (111) reflection consistent with both $V_8C_7$ and $V_6C_5$ superlattices.

## REFERENCES


1. T.Sahashi, Japan.J.Appl.Phys., 9 1, (1970)
2. J.D.Venables, D.Kahn and R.G.Lye,Phil.Mag., 18,177,(1968)
3. C.H.de Novion, R.Lorenzelli and P.Costa, C.R.Acad.Sci., Paris, 263, 775, (1966)
4. S.I.Alyamovskii, G.P.Shveikin, P.V.Gel'd and E.M.Shchetnikov, Russ.J.Inor.Chem., 13, 472, (1968)
5. H.Lipson, Prog.Met.Phy. 2, (B.Chalmers,ed.Interscience (1950)
6. M.J.Marcinkowski, in "Electron Microscopy and Strength of Crystals"(G.Thomas and J.Washburn,eds.Interscience,(1963)
7. R.M.Fisher and M.J.Marcinkowski, Phil.Mag., 6 1358, (1961)
8. M.J.Whelan and P.B.Hirsch, Phil.Mag., 2, 1121 and 1303 (1957)
9. W.L.Bragg and E.J.Williams,Proc.Roy.Soc.,(London).A145 ,699(1934)
10a. R.Gevers, J.Van Landuyt, S.Amelinckx, Phys.Stat.Sol., 9, 135, (1965)
10b. G.R.Booker and P.M.Hazzledine, Phil.Mag., 15, 523,(1967)
11. C.J.Humphreys, A.Howie and G.R.Booker, Phil.Mag., 15 507, (1967)
12. M.J.Marcinkowski and D.S.Miller, Phil.Mag., 6 871,(1961)
13. N.M.Volkova, P.V.Gel'd and S.I.Alyamovskii, Zh.Neorgan. Khim. 10, 1768, (1965)
14. P.S.Bell, Private Communication, University Of Warwick.
15. G.E.Hollox, J.D.Venables, Private Communication, R.I.A.S.
16. D.Watanabe,O.Terasaki,A.Jostsons and J.R.Castles,"The Mechanism of Phase Transformations in Crystalline Solids" Int.Symp.Inst.Metals,Manchester, 1968,P220.

17. E.Ruedl, P.Delavignette and S.Amelinckx, Phys.Stat.Sol., 28, 305, (1968)

18. G.E.Hollox, Private Communication , R.I.A.S.

19. P.B.Hirsch, A.Howie,R.B.Nicholson,D.W.Pashley and M.J.Whelan,"Electron Microscopy of Thin Crystals", (Butterworths, London, 1965)

20. H.Hashimoto,A.Howie and M.J.Whelan,Phil.Mag., 5,967,(1960)

21. R.Gevers, A.Art and S.Amelinckx,Phys.Stat.Sol., 2, 1563, (1963)

22. G.R.Booker and A.Howie, Appl.Phys.letters 3, No.9,156,(1963)

23. J.M.Silcock and W.J.Tunstall, Phil.Mag., 10,361, (1964)

24. G.E.Hollox and R.E.Smallman, J.Appl.Phys.,37, 818,(1966)

25. J.L.Martin,B.Jouffrey and P.Costa, Phys.Stat.Sol., 22 349, (1967)

26. J.D.Venables, Ibid. 15, 413, (1966)

27. E.K.Storms, "The Refractory Carbides",(Academic Press, New York, 1967)

28. K.Yvon and E.Parthe, Acta.Cryst., B26, 149, (1970)

29. J.L.Martin, Private Communication , O.N.E.R.A.

30. F.C.Frank and J.F.Nicholas, Phil.Mag., 44,1213, (1953)

31. A.Kelly and D.J.Rowcliffe, Phys.Stat.Sol., 14, K29, (1966)

32. M.L.Kronberg, Acta.Met. 5, 507, (1957)

33. E. Votava, Acta. Met. 8, 901, (1960); J. Inst.Metals, 90, 129, (1961).

34. J.A.Hren and G.Thomas, Trans. Met. Soc., AIME, 227 308, (1963)

35. G.Brauer and R.Lesser, Z.Metallk., 50, 8, (1959)

36. I.Zaplatynsky, J.Am.Ceram.Soc., 49, 109, (1966)

37. W.F.Brizes and J.M.Tobin, Ibid., 50, 115, (1967)

38. P.S.Bell and M.H.Lewis, Private Communication,Univ.of Warwick.

39. R.Gevers,J.Van Landuyt and S.Amelinckx, Phys.Stat.Sol. 11 689 (1965)

40. D.J.H.Cockayne, I.L.F.Ray and M.J.Whelan , Phil.Mag., 20, 1265, (1969)

41. J.D.Venables, PhD.Thesis,Warwick University,1970.

42. H.Sato and R.S.Toth, "Alloying Behavior and Effects in Concentrated Solid Solutions",Met.Soc.Conf. Vol.29 Cleveland,Ohio, 1963. (Gordon and Breach,New York,1965).

43. S. Anderssonand A.D. Wadsley, Nature,Lond,211,581, (1966)

44. B.G.Hyde and L.A.Bursill, "The Chemistry of Extended Defects in Non-Metallic Solids",.P.376, (North Holland, Amsterdam, 1970.)

45. A.Eikum and R.E.Smallman, Phil.Mag., 11, 627, (1965)

46. J.Van Landuyt and S.Amelinckx, Mat.Res.Bull, 5, 267, (1970)

47. M.Cambini,M.Heerschap and R.Gevers, Mat.Res.Bull, 4 , 633, (1969)

48. J.L.Chermant, P.Delavignette and A.Deschanvres, J. Less - Common Metals, 21, 89, (1970)

49. A.M.Hunt and B.W.Pashley,Le.Journal de Physique et le Radium 23, 846, (1962)

50. R.S.Toth and H.Sato, J.Appl.Phys. 33, 3250, (1962)

51. H.Sato, R.S.Toth and G.Hongo, J.Phys.Chem.Solids, 28 137, (1967)

# CHAPTER FIVE

# CORRELATION AND DISCUSSION OF PHASE STRUCTURES

## 5.1 The Vanadium-Carbon Equilibrium Diagram

In the previous Chapter the phase structure existing at compositions throughout the vanadium monocarbide phase field, and the effect of variations in temperature on the stability of the phases and of the defect structure contained within them, was discussed. During this work the examination of the microstructure of a large number of samples of known composition, which had been heat treated at different temperatures and rapidly cooled, enabled a new phase diagram to be constructed within the composition range $VC_{0.70}$ to $VC_{0.90}$. The order-disorder transformation temperature was determined at a number of compositions. Thus at high carbon contents it was determined by observing the change in the anti-phase domain size (section 4.3), and at lower carbon contents by the retention of the 'S' state in partially ordered structures (section 4.5).

These results, presented in the phase diagram fig. 5.1, show how the nominally cubic (rocksalt) phase field of vanadium monocarbide is modified at low temperatures by the formation of two ordered compounds corresponding to compositions $V_8C_7$ and $V_6C_5$. Both structures exist over a range of composition, particularly $V_6C_5$ which exists between $VC_{0.75}$ and $VC_{0.86}$. Within this wide homogeneity range two forms of ordered structure occur, corresponding to structures with trigonal and monoclinic symmetries (discussed in section 4.5). The two forms of ordered structure co-exist throughout the entire homogeneity range

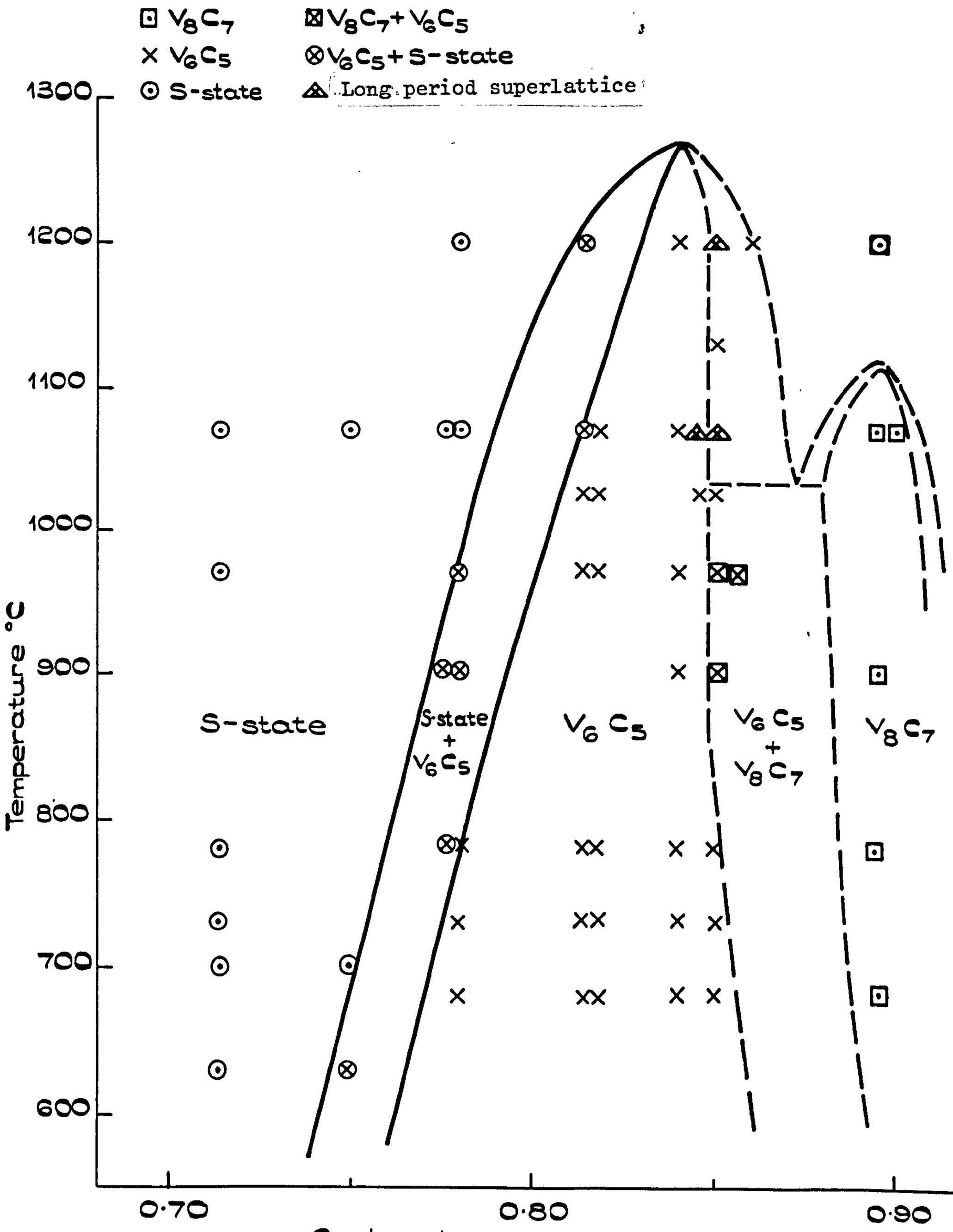


FIG. 5.1.

VANADIUM CARBON EQUILIBRIUM DIAGRAM.

homogeneity range at all temperatures studied. The region of the diagram between the $V_6C_5$ and $V_8C_7$ phase fields has been tentatively drawn showing eutectoid behaviour although no direct evidence for this was obtained. The positive identification of a two phase region at lower temperatures (section 4.6) containing both $V_6C_5$ and $V_8C_7$ phases, means that only two forms of diagrams are possible, one showing a eutectoid and the other a peritectoid reaction. In view of the small difference in the maximum ordering temperatures of these two phases, the eutectoid form is thought to be the most likely. The width of the two phase region, between the ordered and disordered (or S-state) regions, was estimated by the variation in the amount of partially transformed (ordered) phase present in the microstructure as a function of temperature and composition.

No additional ordered phases were detected at lower carbon contents e.g. $VC_{0.75}(V_4C_3)$ contrary to what had been envisaged when the study was initiated. Some diffraction patterns from alloys with carbon to vanadium atom ratios below 0.8 did indicate some possible variation from $V_6C_5$ (section 4.5), but no new phase could be identified. The long period structure described in section 4.5 was mainly observed at compositions near to $VC_{0.84}$ but evidence for its occurrence was obtained at other compositions and it is thought likely that it is present throughout this region as a means of accommodating compositional variations.

Fig. 5.1 is a considerable modification of published phase diagrams which show no modification to the cubic (rocksalt) phase field (see fig. 1.3 in Chapter 1),

and is believed to be one of the few studies where such a diagram has been constructed mainly from electron microscope observations. The allied facilities of electron microscopy and electron diffraction provide a most powerful technique for studies of this kind involving the examination of extremely small regions of differing crystal structure and/or orientation. Indeed no other technique could give such detailed information concerning the structures of such alloys. Other advantages of this method of study are: interactions between defects such as dislocations and particles can be observed, and estimates of the influence of such parameters as interface strain on transformations can be made. Dark field microscopy is an essential feature of such work.

It has been shown[1] that at low temperature (below 1200°C) the carbon vacancies in non-stoichiometric vanadium monocarbide are never distributed in a random manner. Thus between $VC_{0.75}$ and $VC_{0.90}$ long range order was detected in the carbon sublattice, and at lower carbon contents ($VC_{0.70}$ to $VC_{0.75}$) the S-state showed diffraction evidence for non-random arrangements. This result showed agreement with some earlier nuclear magnetic resonance studies by Froidevaux and Rossier[2] on a number of alloy compositions within this region produced by sintering pressed powders. They found evidence for some form of carbon vacancy-order existing throughout the monocarbide phase field, but did not ascribe any composition limits because the technique does not easily distinguish between long and short range order.

It must be emphasized that although these ordered compounds have different structures ($V_8C_7$ is cubic whereas

$V_6C_5$ is trigonal or monoclinic) it is only the carbon sublattice that is changed, the vanadium sublattice remains essentially unaltered throughout this entire region except for some small distortion. Thus only carbon atom displacements need be considered in any explanation of how transformations can occur.

## 5.2. Formation Of Ordered Compounds

At low temperatures, alloys within the monocarbide phase field of the vanadium-carbon system transform from disordered into ordered structures. These transformations have been observed to take place by nucleation and growth processes. The reason for the formation of such ordered phases can be rationalised by consideration of the electronic structure of alloys.

One electron calculations of the band structure have been made for TiC, TiN and TiO[3,4] and give a density of states function with considerable band overlap (hence the full metallic character) in which the Fermi level lies well above the uppermost bonding state. Changes in structure or stoichiometry that would decrease the occupation of states in the upper band, can therefore lower the free energy per atom of the compound. Perfect stoichiometry in TiN, TiO and vanadium carbide (but not in TiC) would involve electrons in anti-bonding states, and therefore the internal energy can be lowered by reducing the population of the uppermost states, and the configurational entropy increased by leaving non-metal sites vacant. Thus the non-existence of stoichiometric vanadium carbide and the existence of carbon compositional deficiencies can be qualitatively explained. The maximum occupancy of the bonding states in vanadium carbide

(the 3 d-states) has been shown by Lye[5] to occur when the carbon to metal atom ratio is close to $^{5}/_{6}$. Since these electronic interactions also effect the cohesive energy, he has proposed that the most stable structure will also occur at this composition when all the vanadium atoms have five nearest neighbour carbon atoms. A composition corresponding to this carbon to metal atom ratio (i.e.$V_6C_5$) will not satisfy this condition however, if the vacant sites are randomly distributed. Thus ordering of the vacant sites in such a way that this condition is fulfilled, is believed to be the driving force for the formation of the $V_6C_5$ structure. The proposed equilibrium diagram (fig. 5.1) with the maximum stability of the ordered phase occurring near $VC_{0.83}$ agrees with this hypothesis

Similar reasoning could apply to the formation of ordered $V_8C_7$ where again a much higher proportion of vanadium sites with five nearest neighbour carbon atoms occurs if the vacant sites are ordered than if they are randomly arranged. The overall stability of the phase is less in this case because some electrons must be present in anti-bonding d-states at this composition i.e. $VC_{0.875}$.

As the carbon content is lowered from $VC_{0.83}$ the tendency for the vanadium to retain five nearest neighbour carbon atoms is shown in that the structure remains ordered, but the driving force for ordering becomes less because not all bonding states can be occupied. The higher concentrations of vacancies in these low carbon alloys allows greater flexibility in their distribution hence resulting in a lessening in the driving force for long range order production.

This results in a suppression of the temperature at which ordering occurs, and above this temperature a retention of the S-state order only.

The ideas of Parthé and Yvon[6] concerning possible stacking sequences and ordered arrangements in the transition metal carbides have already been discussed in Chapter 1. However, some relevent points will be reconsidered in order to see how these ordered structures occur and how they are related to one another.

In the case of metal stacking c, if all the octahedral sites are occupied, only one structure type is possible the NaCl (B1) type. Most carbides however, including vanadium are carbon deficient, and at the present time four defect types are known[6] corresponding to formulae $T_8C_7$, $T_6C_5$ and two forms of $T_2C$, but others such as $T_3C_2$, or $T_8C_5$ are also considered possible. Within the composition limits imposed by the vanadium carbon phase diagram it would appear that only $V_8C_7$, $V_6C_5$, and possibly $V_3C_2$ could occur. $V_3C_2$ is of interest because it is the same structure type as $V_6C_5$ i.e. c $(C_3^2)$ and hence would show identical symmetry in diffraction patterns.

The $V_8C_7$ structure is the unusual case with respect to normal carbide behaviour, since it does not conform to the general rule that defects only occur in alternate carbon layers. Thus transformation of $V_8C_7$ to $V_6C_5$ and vice versa requires movement of carbon vacancies in all carbon layers. It is difficult for this to occur by crystallographic shear as in the production of shear structures, and the most likely mode of transformation is diffusion of carbon atoms and

vacancies to give the necessary distribution of vacant sites. Shear of $V_8C_7$ by removal of a full {110} carbon atom plane however, could produce regions of $V_6C_5$ separated by regions of different structure and composition. Diffusion of the vacancies in the intervening layers to these regions (so that vacancies are only present in alternate layers) results in the overall composition approaching that of $V_6C_5$, and the overall structure becoming a faulted $V_6C_5$ structure. Microstructural observations on the other hand shows that $V_6C_5$ is formed in $V_8C_7$ at A.P.B's which are regions associated with compositional variations, and it appears that the structure transforms by a nucleation and growth process which is controlled by diffusion of the carbon atoms and vacancies. Similarly the $V_8C_7$ formation in $V_6C_5$ is associated with the type of anti-phase boundary whose vector does not lie in the plane of the boundary (irregular boundaries) i.e. those usually associated with a compositional change. Thus again the transformation occurs by a nucleation and growth process which is controlled by carbon diffusion.

The ease of formation of an ordered structure in these alloys (the ordering cannot normally be suppressed by rapid cooling) indicates that the driving force for the ordering reaction is large. In certain regions of the $V_6C_5$ phase field however the formation of the long range ordered structure can be suppressed by rapid cooling ($^C/_V \simeq 0.78$). This agrees with Lye's ideas concerning the formation of the ordered phase and its stability variations with composition, indicating that in this system the ordering is largely controlled by electronic considerations.

The alloys within the $V_6C_5$ phase field showed a duplex structure in addition to the normal superlattice domain structure. As outlined previously, this arose because of the ease with which transformations could take place by a simple shearing mechanism between the trigonal and monoclinic ordered structures. Both regions of the duplex structure were highly striated due to the presence of large numbers of planar faults parallel to the basal plane of the superlattices.

These microstructures have a close resemblance to those produced by the massive transformation found in critical composition regions of alloys of copper with zinc, gallium, germanium etc. This type of reaction exhibits nucleation and growth rather than martensitic characteristics, and takes place by the transformation of solid solutions to produce material of the same composition as that of the original phase. It has been shown[7,8] that transformed Cu-Ga alloys consisted of a fine lamellar structure of h.c.p. or h.c.p. plus f.c.c. phases, and the adjoining plates were frequently twisted with respect to one another along the close packed planes of mutual contact. In the striated regions the (111) f.c.c. plane is parallel to the $(0001)_{\zeta_m}$ plane, and the close packed directions of the two phases are also parallel (this is identical to the situation occurring in the vanadium carbon alloys). The observed duplex structure is formed by whole groups of plates or blocks growing together during growth of the massive phase and this gives rise to the sub-structure.

## 5.3 Structure Above The Critical Temperature

The S-state which is characterised by a non-random arrangement of carbon vacancies is found in alloys with low carbon contents ($VC_{0.70}$ to $VC_{0.75}$) at all temperatures investigated (600 to 1200°C). This gives rise to characteristic diffuse bands in the diffraction patterns, the positions of which are closely related to the long range order spots occurring at higher carbon contents. It is likely that this state is also present at temperatures above the order-disorder temperatures for all compositions throughout the monocarbide range. Its detection is not possible in the higher carbon alloys because of the extremely rapid formation of the long range ordered structures following cooling through the transition temperature. However at compositions corresponding to $^{C}/_{V} < 0.8$ the S-state appears to be stable at temperatures above the disordering temperature, because it is retained in rapidly cooled microstructures. Conclusive proof of this hypothesis would require examination of the structures in the electron microscope at higher temperatures than is possible with the present 'hot stage' attachment.

The formation of diffuse spots in diffraction patterns due to short range ordering has been widely reported in many systems including TiC[9] $Ni_4Mo$[10] and $Au_3Mn$[11]. Diffuse banding, similar to that seen in the present experiment, has not been reported in the literature but has been seen in VC-TiC alloys[12], and in vanadium nitride[13] at correspondingly similar compositions near to the lower nitride phase boundary. Although the exact wavy form of

the banding cannot be explained it must be indicative of non-randomness in the carbon atom distribution. At slightly higher carbon contents, where a stable long range ordered structure exists, the diffuse bands co-exist with long range order spots, and one possibility is that the bands are composed of large numbers of diffuse spots due to the presence of a large number of very small domains in a number of different orientations. Although small long range ordered domains could be identified in the structure when these diffraction spots were present, (by the use of dark field imaging), no regions of enhanced contrast could be seen in dark field images formed from the most intense regions of the bands. Thus if the bands are caused by small long range ordered regions, these regions are extremely small.

The short range ordered state is usually considered by arising from either:

(i) a statistical non-random distribution of atom pair probabilities which is usually expressed[14] in terms of the Warren parameter $a_i$ which measures the probability of finding an A atom in the i-th co-ordination shell around a B atom in an alloy containing A and B atoms

(ii) the presence of microdomains where discrete regions or 'islands', having one structure and composition, are dispersed in a matrix of another structure and composition[15,16]

Cowley[17] proposed a modification to this second model whereby the alloy consisted of small domains of perfectly

ordered alloy separated by anti-phase boundaries. Thus splitting of the diffuse short range ordered spots in $CuAu_3$ has been observed by electron diffraction[18] and X-ray diffraction[19]. These splittings correspond to correlations over distances of approximately 30Å in the disordered lattice. This disagrees with the statistical model where correlation of lattice site occupancy decreases rapidly with distance and is insignificant after a few unit cells. Thus the idea of nuclei of the ordered phase present in the equilibrium state of temperatures well above the ordering temperatures can be postulated. Warlimont and Thomas[20] recently proposed a further variation whereby very small ordered particles (of diameter 10 to 70Å) exist in a disordered matrix. Their results were for iron aluminium alloys, but were also in agreement with work on $Ni_4Mo$ by Ruedl et al.[10], and by Blackburn on Ti-Al[21].

Nearly all studies of this type, including the present one, have involved quenching from above the critical temperature when it may not be possible to retain the short range ordered condition which might exist above the critical temperature. Thus high temperature electron diffraction and dark field imaging are required to completely investigate this condition. In the present experiment the banding could arise from effects occurring during the cooling and not be indicative of the conditions existing at high temperature where the material might show normal disordered diffraction patterns. Thus the formation of a very large number of extremely small long range ordered domains would cause diffuseness of the diffraction spots both by the

nature of their small size and the strain set up in the matrix by their formation. These small regions could be present in the disordered matrix and be prevented from further growth either because they are smaller than the critical nucleus size, or because they have an extremely low growth rate, due to the low driving force for the ordering reaction especially at the lower carbon compositions. A further possibility is that nucleation is easy and the structure consists of a complete assembly of very small long range ordered domains which do not grow because the driving force for growth, i.e. the possible reduction in interfacial energy, is very small.

There have been a number of investigations where the transformation from a fully ordered to a disordered structure may be quite progressive. Thus Okasaki[22] has shown that iron selenide becomes ordered through three successive stages each corresponding to a larger unit cell. Above 450°C the NiAs disordered state of $Fe_{1-x}Se$ is stable, whereas below 290°C the vacancies are ordered so that the formula is $Fe_7Se_8$ and the lattice becomes triclinic. Between these two temperatures intermediate states of order occur.

The present experiments are difficult to interpret in terms of either of the models since the S-state seems to exist at temperatures well above the critical temperature, e.g. 1200°C at $VC_{0.78}$, and also at compositions well below those associated with any long range order e.g. $VC_{0.72}$. The hot-stage experiments did however confirm that the S-state existed at elevated temperatures, and was not merely a diffraction effect caused by rapid cooling into an ordered

region. The close association of the position of the diffuse bands with long range order spots present at higher carbon contents indicates a close relationship between the carbon atom positions in the two structures. The S-state is thus a form of order, which can exist at temperatures well above the long range order-disorder critical temperature, in which the carbon atom vacancies are arranged in a non-random manner closely related to their arrangement in the ordered structure occurring at lower temperature and/or higher carbon contents. The stability of the S-state at temperatures well above the order-disorder temperature, e.g. 1070°C for $VC_{0.75}$ which orders at approximately 630°C, means that the statistical non-random distribution of nearest neighbours model does not adequately describe the state. Moreover the inability to obtain any dark field images associated with the diffuse bands indicates that if the microdomain theory is applicable the small ordered regions must be extremely small. However, the latter model is favoured with the state consisting of a number of small ordered domains in a disordered matrix. The low driving force for ordering is likely to be responsible for the retention of the state both in the rapidly cooled microstructures (near $VC_{0.78}$) and in the lower carbon containing alloys.

## 5.4 Transformation To Lower Carbides

Stacking faults were observed in the cubic vanadium carbide at compositions near to the lower phase boundary with the hexagonal dicarbide phase i.e. in material showing S-state diffraction behaviour. These faults were analysed as being of the intrinsic type and were bounded by Shockley partial dislocations. At slightly lower carbon contents the $\zeta$-phase which has a modified metal atom layer stacking sequence was identified although no composition or temperature limits could be assigned to its stability range. Consideration of the metal atom stacking sequence of the $\zeta$-phase, and of the increase in stacking fault density with decreasing carbon content suggested that such stacking faults could provide the nuclei for a transformation of the cubic carbide to the hexagonal $V_2C$ or $\zeta$-phase occurring at slightly lower carbon concentrations. The transformation involves a shear on every fourth {111} vanadium atom layer for the $\zeta$-phase and on alternate layers for the $V_2C$ phase, such as is produced by the glide of Shockley partial dislocations of similar Burgers vector on these respective layers.

The $\zeta$-phase has also been detected in the NbC[23], and TaC[24] systems, where stacking faults were also detected at $TaC_{0.75}$ in alloys prepared by carburisation of thin layers of tantalum. In a recent study of $\zeta$-phase in VC by Yvon and Parthé[25] the hexagonal $V_2C$ phase was always found in association with the $\zeta$-phase. Since this was not confirmed in the present study it is likely to be a consequence of their method of sample preparation (hot pressing of powders) and not a pre requisite for the $\zeta$-phase formation. Bell[26]

has observed similar large numbers of stacking faults in a matrix of vanadium mononitride showing diffuse banding near to the phase boundary with divanadium nitride, and it seems possible that the proposed transformation could be a general type for materials of this kind.

## 5.5 Correlation With Mechanical Properties

As outlined in Chapter 1 a large amount of early work on the carbides used polycrystalline material of unspecified purity which was usually prepared by pressing and sintering. The only comprehensive deformation study on high purity single crystal material has been made by Hollox[27] who studied the behaviour of three alloys $VC_{0.75}$, $VC_{0.84}$ ($V_6C_5$) and $VC_{0.88}$ ($V_8C_7$) over a range of temperature. He showed (see fig. 5.2) that the yield strength passed through a maximum as the carbon content was increased, the strength of $VC_{0.84}$ being higher than that of either $VC_{0.75}$ or $VC_{0.88}$. This contrasted with work on the titanium carbide system[28] where the strength increased monotonically with increasing carbon content throughout this composition range. He also plotted the dependence of the yield stress on temperature (see fig. 5.3) which indicated that the behaviour of the $VC_{0.84}$ and $VC_{0.88}$ alloys was similar and differed from that of $VC_{0.75}$. The latter showed identical behaviour to the disordered titanium carbide alloys. He interpreted the differences in these results as indicating that $VC_{0.75}$ was disordered, whereas $VC_{0.84}$ and $VC_{0.88}$ were ordered and became disordered at the temperature corresponding to the onset of ductility in the alloys i.e. 1250°C for

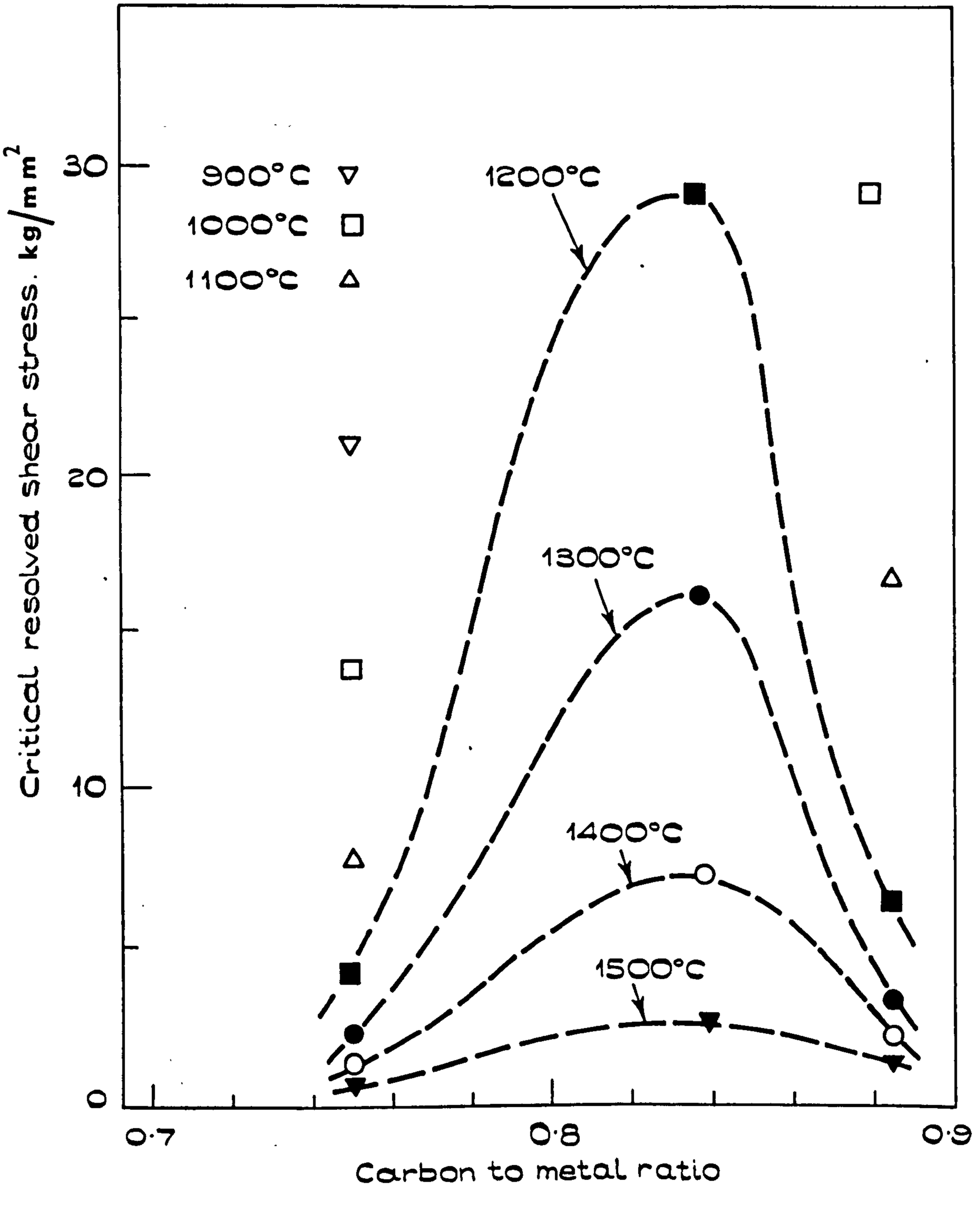


FIG. 5.2.

THE CRITICAL RESOLVED SHEAR STRESS FOR SLIP IN VC AS A FUNCTION OF CARBON CONTENT (AFTER HOLLOX[2]).

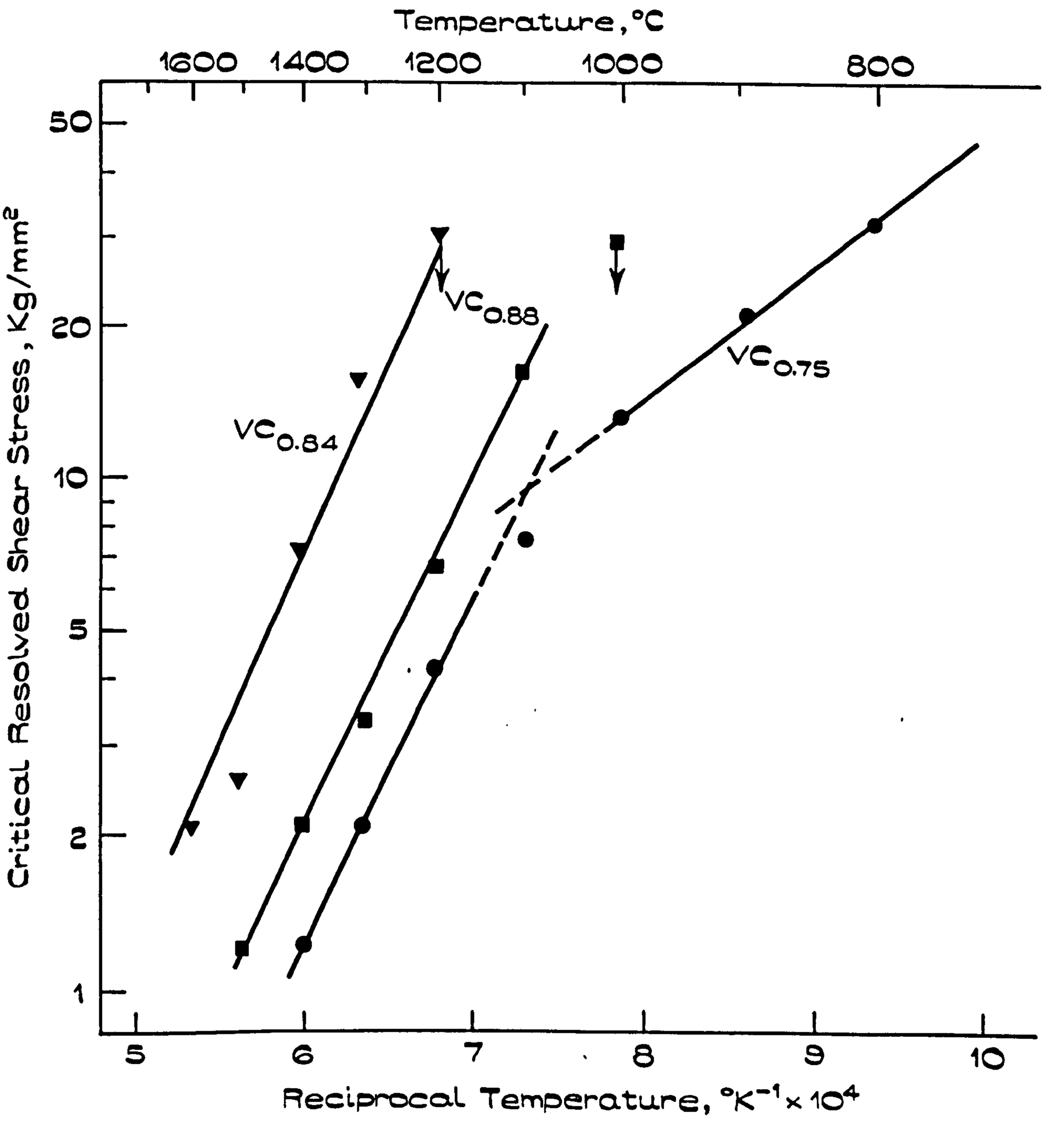


Fig. 5.3.

TEMPERATURE DEPENDENCE OF THE CRITICAL RESOLVED SHEAR STRESS FOR SLIP IN VC OF DIFFERENT CARBON TO METAL RATIOS (AFTER HOLLOX [2]).

$VC_{0.84}$ and 1100°C for $VC_{0.88}$. He used optical microscopical examination with polarised light to detect a change in domain size following a treatment at 1300°C which gave close agreement with the measured transition temperature.

This study has indicated that the transition temperature for $VC_{0.84}$ and $VC_{0.88}$ are approximately 1300°C and 1100°C respectively (see fig. 5.1) which agrees closely with the observed temperatures for the onset of ductility. The $VC_{0.75}$ alloy becomes ordered at low temperatures (≈630°C) only after extensive annealing treatments, and the deformation experiments were not continued to low enough temperatures to say whether the onset of ductility could be related to the order-disorder temperature at this composition. The presence of some ductility down to temperatures as low as 800°C in this alloy is however in accord with a much lower order-disorder temperature as is found by experiment.

Fig. 5.3 indicates that in the ordered alloys $VC_{0.84}$ and $VC_{0.88}$ only one thermally activated process controls the deformation behaviour above the transition temperature, whereas in the disordered alloy $VC_{0.75}$ two different processes apply within different temperature ranges. The latter behaviour is again similar to that shown by TiC where Williams[29] measured the activation energy for deformation above the critical temperatures as 3.0 eV and below the critical temperature, where it was also dependent on carbon content, as between 1.7 and 2.3 eV. He could not correlate these values with the measured self diffusion activation energies for titanium or carbon but did relate them to a value of 3.0 eV obtained for a pipe diffusion mechanism

deduced by annealing dislocation dipoles[29]. High temperature creep experiments[30] indicated an activation energy of between 5.0 and 7.0 which correlated well with the values reported for titanium self diffusion (5.1 eV from layer growth[31] and 5.25 from dislocation annealing experiments[29]. Thus at high temperatures the deformation appears to be controlled by metal vacancy diffusion, a result which is well established for metal systems. At lower temperatures there appears to be little correlation between the critical resolved shear stress and the self diffusion coefficients.

The behaviour of dislocations in this type of strong material is dependent on the diffusive motion of atoms, because the atoms must move together in order to preserve the structure during the motion of dislocations. This process known as synchro-shear and first postulated by Kronberg[32], has been used by Rowcliffe[33] to explain the deformation behaviour of transition metal carbides. Thus a single shear vector cannot be used to describe the unit of slip, the process depending on the synochronous movement of metal and carbon atoms, which may involve the diffusion of carbon atoms into tetrahedral or octahedral sites. The motion of the dislocation is then thermally activated, and controlled by the ease of carbon diffusion. Thus the dislocation mobility should be increased by thermal fluctuations leading to a strongly temperature dependent yield stress, a result which has been obtained. Other processess that might be important at high temperature e.g. debris formation, cross slip, dislocations interactions

are also likely to be influenced by the strong binding in the solid. Measured carbon diffusion data at high temperatures $>1500^{o}C$ gave activation energies of approximately 2.5 eV/atom[34], and Venables[35] recently obtained similar values (2.7 eV) at much lower temperatures by studying the kinetics of re-ordering material that was disordered by electron irradiation. Carbon atom diffusion is therefore rapid at similar temperatures to those involved in the deformation experiments. This emphasizes that the correlation between onset of ductility and onset of disorder is a valid one, and does not merely indicate that both processes are controlled by carbon atom diffusion and take place in the temperature range where this becomes rapid. Thus in a disordered structure carbon atom diffusion is sufficiently rapid at temperatures in the region of 800 - to $1000^{o}C$ for the synchro-shear mechanism to operate and for the alloy to deform. This is the condition existing in $VC_{0.75}$ and explains its ductility down to $800^{o}C$, and the ductility of the other alloys at higher temperatures.

At temperatures below the critical temperature where the structures were ordered, $VC_{0.84}$ and $VC_{0.88}$ would be expected to offer resistance to deformation because of the difficulty both in nucleating and moving dislocations through such structures. Dislocation motion is difficult because energy must be supplied to create the A.P.B's formed by the passage of dislocations, and in $VC_{0.84}$ in particular the presence of such a large amount of sub-structure causes additional strengthening due to the interactions that can take place.

The results in fig's. 5.2 and 5.3 indicate that $VC_{0.75}$ shows some ductility at 800°C and undergoes a change in deformation behaviour at approximately 1060°C. The alloy, certainly at the lower temperature, would have a structure corresponding to the S-state and this at 800°C might be expected to show some ductility (the temperature corresponds to 0.4 Tm for this lower melting point composition) by comparison with the other alloys which would have an ordered structure. It is possible that the change in mechanism near 1060°C could be due to the change from the S-state to a completely disordered state.

The increase in strength of $VC_{0.84}$ compared to the other compositions is greatest at 1200°C and decreases as the temperature is raised to 1500°C (fig. 5.2). The S-state is present at these compositions at elevated temperatures and it is likely that S-state behaviour is retained to higher temperatures at $VC_{0.84}$ which corresponds to the peak in the long range ordering curve (fig. 5.1). This structure would be expected to cause strengthening relative to the disordered structure because the dislocations would have to cut through or by-pass the S-state regions. Again this effect would be expected to be a maximum just above the order disorder temperature and decrease with increasing temperature which is the effect observed.

Room temperature microhardness which is an easily measurable property is often used to indicate the comparative high temperature deformation properties of materials on the simple concept that the hardest materials at room temperature are also the strongest at high temperature. This simple concept does not apply to the carbides where TiC has the highest room temperature microhardness[36] (2800 kg/mm2,

but is weaker than VC of similar composition at high temperatures, which is surprising also in view of its much higher melting point. This behaviour is obviously strongly affected by the ordering which takes place in the vanadium but not in the titanium carbon system. The effect of composition on the high temperature deformation behaviour of vanadium carbide is not indicated by room temperature microhardness measurements. Microhardness measured with a Knoop indentor at 200 gm load varied from 1800-2500 $kg/mm^2$ throughout the composition range $VC_{0.70}$ to $VC_{0.90}$. This contrasted with work in the other carbide systems where for titanium carbide the microhardness increased linearly with carbon content[37] (as did the high temperature strength) whereas for tantalum carbide[38] either a peak was obtained at intermediate composition, or the hardness decreased with increasing carbon contents[39]. A recent report by Hollox[40] where he reports that $VC_{0.75}$, $VC_{0.84}$ and $VC_{0.88}$ all have hardness value close to 2000 $kg/mm^2$ ($2000 \pm 200$ $kg/mm^2$) agrees with this work. Thus in a system where ordering occurs, room temperature microhardness does not appear to give any indication of high temperature deformation properties whereas in disordered systems such as TiC useful indications can be obtained. In this context it is interesting to note that Hannink[41] has recently obtained extremely high microhardness values of approximately 4000 $kg/mm^2$ in $VC_{0.84}$ which has been rapidly cooled through the order disorder temperature to produce an ordered alloy with an extremely fine domain size. Moreover he was able to obtain intermediate hardness values in the range 2000 to

4000 kg/mm$^2$ by varying the domain size by this quenching treatment. Similar extremely high hardness values of 4-5000 kg/mm$^2$ were reported recently by Rowcliffe and Warren[42] in tantalum carbide ($TaC_{0.85}$) produced by carburising thin sheets. The similarities in the equilibrium diagrams of VC and TaC (see fig. 1.1) particularly the maximum in the melting point near to the $MC_{0.85}$ composition, which is often indicative of ordering behaviour at lower temperature, indicates that a similar explanation for these extremely high hardness values could be possible. At the present time there has been no identification of ordered phases in tantalum carbide near this composition but the necessary electron or neutron diffraction experiments have not yet been carried out.

## REFERENCES


1. J.Billingham and M.H.Lewis, VII$^{th}$ Congrès International de Microscopie Électronique, Grenoble, Vol 2, 477, (1970)
2. C.Froidevaux and D.Rossier, J.Phys.Chem.Solids, 28, 1197 (1967)
3. H.Bilz, Z.Physik 153, 338, (1958)
4. S.P.Denker, Phys.Chem.Solids, 25, 1397, (1964)
5. R.G.Lye, Private communication in J.D.Venables Ph.D. thesis, University of Warwick, (1970)
6. E.Parthé and K.Yvon, Acta.Cryst., B26, 153, (1970)
7. L.Delaey, G.A.Sargent and T.B.Massalski, Phil.Mag., 17, 983, (1963).
8. L.Delaey, Phys.Stat.Sol., 25, 697,, (1968)
9. D.Watanabe, O.Terasaki, A.Jostsons and J.R.Castles, "The Mechanism of Phase Transformation in Crystalline Solids" Int.Symp.Inst.Metals, Manchester. P220, (1968)
10. E.Ruedl, P.Delavignette and S.Amelinckx, Phys.Stat.Sol., 28, 305, (1968)
11. L.E.Tanner, P.C.Clapp and R.S.Toth, Mat.Res.Bull.3, 855 (1968)
12. G.E.Hollox and J.D.Venables, Private communication
13. P.S.Bell, University of Warwick, Private communication
14. W.L.Bragg and E.J.Williams, Proc.Roy.Soc., A145, 699, (1934) A151, 540 (1935), E.J.Williams, Ibid A152, 231, (1935)
15. S.M.Ariya and YuG.Popov, J.Gen.Chem., U.S.S.R., 32, 2077, (1962)
16. J.S.Anderson, Proc.Chem.Soc., 166, (1964)
17. J.M.Cowley, J.Austra.Inst.Metals, 11, 258, (1966)
18. D.Watanabe and P.M.J.Fisher, J.Phys.Soc.Japan, 20, 2170, (1965)
19. S.C.Moss, Met.Soc.Conference, 36, Chicago, Feb, 1965, (Gordon and Breach, New York, 1966)
20. H.Warlimont and G.Thomas, Met.Sci.Journal, 4, 47, (1970)

21. M.J.Blackburn, Trans.Met.Soc., A.I.M.E. 239, 1200, (1967)

22. A.Okazaki, J.Phys.Soc.Japan, 14, 112, (1959)

23. G.Brauer and R.Lesser, Z.Metallk., 50, 8, (1959)

24. J.L.Martin, B.Jouffrey and P.Costa, Phys.Stat.Sol ,22, 349, (1967)

25. K.Yvon and E.Parthé, Acta.Cryst. 26, 149, (1970)

26. P.S.Bell, University of Warwick, Private communication.

27. G.E.Hollox, Mat.Sci.Eng. 3, 121, (1968)

28. W.S.Williams, J.Appl.Phys. 35, 1329, (1964)

29. G.E.Hollox and R.E.Smallman, Proc.Brit.Ceram.Soc. 1, 211, (1964)

30. F.Keihn and R.Kebler, J.Less.Common Metals, 6, 484, (1964)

31. D.L.Harrod and L.R.Fleischer, Proc.Int.Symp."Anisotropy in Single Crystal Refractory Compounds", ed.F.W.Vahidiek and S.A.Mersol, (Plenum Press, New York, 1968)

32. M.L.Kronberg, Acta.Met. 5, 507, (1957)

33, D.J.Rowcliffe, University of Cambridge, Ph.D.Thesis (1965)

34. L.M.Adelsberg and L.H.Cadoff, J.Am.Ceram.Soc., 51, 213, (1968)

35. J.D.Venables University of Warwick Ph.D.Thesis, (1970)

36. J.H.Westbrook and E.R.Stover, in "High Temperature Materials and Technology" eds.I.E.Campbell and E.M.Sherwood, Wiley, New York, 1967.

37. W.S.WilliamsInternational Conference on Semi-Metallic Compounds" Orsay France, 1965.

38. G.Santoro, Trans.A.I.M.E., 227, 1361, (1967)

39. R.Steinitz, in "Nuclear Applications Of Non-Fissionable Ceramics" Amer.Nucl.Soc., Illinois, 1966.

40. G.E.Hollox, D.L.Novak and R.D.Huntington, Second International Conference on "Strength of Metals and Alloys" Asilomar, 1970, to be published.

41. R.H.J.Hannink, University of Cambridge, Private communicatin

42. D.J.Rowcliffe and W.J.Warren, J.Mat.Sci., 5, 345, (1970)

# CHAPTER SIX

## CONCLUSIONS

(1) An apparatus has been designed and constructed for the growth of single crystals of high melting point materials utilising a floating zone technique operating under a pressurised inert atmosphere.

(2) Vanadium carbide single crystals have been grown using this apparatus at a number of compositions throughout the monocarbide phase field. Polycrystalline samples were also produced at a number of lower carbon compositions.

(3) Ordering of the non-stoichiometric carbon vacancies was detected throughout the entire cubic phase field of the vanadium carbon system from $VC_{0.70}$ to $VC_{0.90}$. The extent of the stability of the ordered compounds previously identified by other workers at $VC_{0.84}$ ($V_6C_5$) and $VC_{0.88}$ ($V_8C_7$) was determined with respect to composition and temperature. Although no other long range ordered structures were detected at lower carbon contents ($^C/_V < 0.75$) a characteristic form of non-random carbon atom distribution existed which was termed the S-state.

(4) At high carbon contents the presence of the cubic superlattice based on the ordered $V_8C_7$ compound, was confirmed between $VC_{0.87}$ and $VC_{0.90}$ and up to a temperature of approximately 1100°C. The microstructure of such alloys consisted of an irregular foam structure of anti-phase domain boundaries of the type $^a/_4 \langle 110 \rangle$.

(5) The S-state which was present at low carbon contents $^C/_V < 0.75$, and at other compositions at high temperature, was a structure characterised by diffuse banding in electron

diffraction patterns. It represents a stable state with carbon vacancy order intermediate between that in the long range ordered and disordered states, and is thought to consist of very small ordered regions in a disordered matrix.

(6) The ordered $V_6C_5$ compound, previously identified at $VC_{0.84}$, was found to be stable over a wide range of composition from $VC_{0.75}$ to $VC_{0.86}$. The order disorder temperature varied markedly with carbon content, decreasing from approximately 1250°C at $VC_{0.85}$ to 630°C at $VC_{0.75}$. The ordered structure was observed to form by a nucleation and growth mechanism from an S-state matrix.

(7) Two forms of ordered $V_6C_5$ were identified at compositions throughout the $V_6C_5$ phase field. The previously observed trigonal structure was confirmed, but in addition a closely related superlattice with monoclinic symmetry was identified. One structure can form from the other by a simple shearing process and as normally produced, alloys within this composition range have duplex structures containing both forms of order.

(8) A domain structure forms on ordering, and within each domain there are large numbers of planar faults. These are reduced by annealing at high temperatures and are identified as faults parallel to the basal plane of the superlattices with a $^a/_4$ ⟨110⟩ vector within this plane. Other faults with non-basal $^a/_4$ ⟨110⟩ vectors are less common and have an irregular form.

(9) A long period superlattice with 50Å spacing is formed at high temperatures ($\simeq 1070^{o}C$) in alloys near to the composition $VC_{0.84}$. This structure is a shear structure in which the A.P.B's are aligned parallel to {110} planes.

(10) At compositions between $VC_{0.84}$ and $VC_{0.87}$, alloys containing both the cubic $V_8C_7$ and the non-cubic $V_6C_5$ superlattices are obtained. Dislocations and A.P.B's are favoured sites for the transformation of one ordered phase to the other.

(11) The $\zeta$-phase, which has a complex 12 metal layer stacking sequence has been identified at $VC_{0.65}$, and a dislocation mechanism proposed for its formation, based on the observation of large intrinsic stacking faults at slightly higher carbon concentrations.

(12) A new vanadium carbon equilibrium diagram has been constructed based on the results obtained in this study. It shows the extent of non-stoichiometry in the ordered compounds and how this varies with respect to temperature and composition.

# APPENDIX

## BIBLIOGRAPHY


Adelsberg L.M. and Cadoff L.H., J.Am.Ceram.Soc., 51, 213, (1968)

Alyamovskii S.I., Shveikin G.P., Gel'd P.V. and Volkova N.M., Russ.J.Inor.Chem., 12, 301, (1967)

Alyamovskii S.I., Shveikin G.P., Gel'd P.V., Ibid, 12, 915, (1967).

Alyamovskii S.I., Shveikin G.P, Gel'd P.V. and Shchetnikov E.M., Ibid, 13, 472, (1968).

Anderson J.S., Proc.Chem.Soc., 166, (1964).

Andersson S. and Jahnberg L., Ark.Kemi., 21, 413, (1963).

Andersson S. and Wadsley A.D., Nature,Lond, 211, 581, (1966)

Ariya S.M. and Popov Yu.G., J.GenChem.,U.S.S.R.32, 2077,(1962).

Armstrong W.M. and Irvine W.R., J.Nuclear.Mat. 2, 1, (1963).

Ashbee K.H.G. and Smallman R.E., Proc.Roy.Soc.,A274,195,(1963)

Aust K.T., in "The Art And Science Of Growing Crystals", edited J.J.Gilman (John Wiley, New York, 1963)

Bartlett R.W., Halden F.A. and Fowler J.W., Rev.Sci.Instrum., 38, 1313, (1967)

Bartlett R.W. and Halden F.A., Stanford Research Institute NASA-49 (19), June 1967.

Bénard J., Inst.Interm.Chim.Solway Counseil Chim.,Brussels, 1956, 83, (1956).

Billingham J. and Lewis M.H., VII$^{th}$ Congrès International de Microscopie Electronique, Grenoble, Vol 2, 477, (1970)

Bilz H., Z.Physik, 153, 338, (1958).

Blackburn M.J., Trans.Met.Soc., A.I.M.E., 239, 1200, (1967)

Booker G.R. and Howie A., Appl.Phys.Letters 3, No.9 156,(1963).

Booker G.R. and Hazzledine P.M.,Phil.Mag., 15, 523, (1967)

Bowman A.L., Acta.Cryst. 19, 6, (1965).

Bowman A.L., Ibid, 21, 670, (1966).

Bradley A.J. and Taylor A., Proc.Roy.Soc.,A159, 56, (1937).

Bragg W.L. and Williams E.J., Ibid, A145, 699, (1934).

Bragg W.L. and Williams E.J., Ibid, A151, 540, (1935).

Brauer G. and Lesser R., Z.Metallk., 49, 622, (1958).

Brauer G. and Lesser R., Ibid, 50, 8, (1958).

Brizes W.F. and Tobin J.M., J.Am.Ceram.Soc., 50, 115, (1967).

Cambini M., Heerschap M. and Gevers R.,Mat.Res.Bull,4,633,(1969)

Campbell I.E., in "High Temperature Materials and Technology" eds., Campbell I.E. and Sherwood E.M.(Wiley,New York,1967).

Chermant J.L.,Delavignette P. and Deschanvres A., J.Less - Common Metals, 21, 39, (1970).

Cockayne B. and Ridley J.D., J.Sci.Instrum., 41, 647, (1964).

Cockayne D.J.H.,Ray I.L.F. and Whelan W.J.,Phil.Mag.20,1265(1969)

Cohen J.B., J.Mater.Sci., 4, 1012, (1969).

Cowley J.M., J.Austr.Inst.Met., 11, 258, (1966).

Dash J. and Otte H., Acta.Met., 11, 1169, (1963).

Denker S.P., Phys.Chem.Solids, 25, 1397, (1964).

Delaey L.,Sargent G.A.Massalski T.B., Phil.Mag.17, 983,(1968).

Delaey L.,Phys.Stat.Sol., 25,697, (1968)

de Novion C.H.,Lorenzelli R. and Costa P.,C.R.Acad.Sci., Paris, 263, 775, (1966).

Eikum A. and Smallman R.E., Phil.Mag., 11, 627, (1965).

Fisher R.M. and Marcinkowski M.J., Ibid 6, 1358, (1961).

Fleischer L.R. and Tobin J.M., Proceedings of Third International Symposium on High Temperature Technology, Asilomar, California, 1967, (Butterworths, London, 1969).

Frank F.C. and Nicholas J.F., Phil.Mag., 44, 1213, (1953).

Froidevaux C. and Rossier D., J.Phys.Chem.Solids,28,1197,(1967).

Gevers R., Art A. and Amelinckx S.,Phys.Stat.Sol.,2,1563,(1963).

Gevers R., Van Landuyt J.,Amelinckx S. Ibid, 9, 135, (1965).

Gevers R., Van Landuyt J.,Amelinckx S. Ibid, 11, 689, (1965).

Goldschmidt H.J.,"Interstitial Alloys",(Butterworths London 1967).

Gorbunov N.S.,Shishakov N.A. and Saidkov C.G.,Izv.Akad.Nauk. SSSR, 11, 2093, (1961).

Goretzki H., Phys.Stat.Sol., 20, K141, (1967).

Harrod D.L. and Fleischer L.R., Proc.Int.Symp."Anisotropy in Single Crystal Refractory Compounds", ed.Vahldiek F.W., and Mersol S.A. (Plenum Press, New York, 1968).

Hashimoto H., Howie A. and Whelan M.J.Phil.Mag.,5, 967, (1960).

Hirsch P.B., Howie A., Nicholson R.B.,Pashley D.W.and Whelan M.J. "Electron Microscopy Of Thin Crystals",(Butterworths Lon.1965)

Hollox G.E. and Smallman R.E., Proc.Brit.Ceram.Soc.1,211,(1964).

Hollox G.E. and Smallman R.E., J.Appl.Phys. 37, 818, (1966).

Hollox G.E., Mat.Sci. Eng., 3, 121, (1968).

Hollox G.E.,Novak D.L. and Huntington R.D., Second International Conference on "Strength Of Metals and Alloys" Asilomar, 1970, to be published.

Hren J.A. and Thomas G. Trans.Met.Soc.,A.I.M.E.,227,308,(1963).
Humphreys C.J.,Howie A. and Booker G.R.,Phil.Mag.15,507,(1967).
Hunt A.M. and Pashley B.W.,Le.Journal de Physique et le Radium 23, 846, (1962).
Hyde B.G. and Bursill L.A.,"The Chemistry Of Extended Defects in Non-Metallic Solids",P.376,(North Holland,Amersterdam 1970)
Jagodzinski H., Acta.Cryst., 7, 17, (1954).
Keck P.H., Grun M. and Polk M.L.,J.Appl.Phys.,24,1469,(1953).
Keihn F. and Kebler R., J.Less.Common Metals, 6, 484, (1964).
Kelly A. and Rowcliffe D.J., Phys.Stat.Sol.,14, K29, (1966).
Kieffer A.D.,Linde Co., private communication in paper by Williams W.S.and Schaal R.D.,J.Appl.Phy. 33, 955, (1962).
Kordes D. Phys.Stat.Sol., 26, K103, (1968).
Kronberg M.L., Acta.Met. 5, 507, (1957).
Libowitz G.G. in "Non-Stoichiometric Compounds",(Gould R.ed.) adv.chem. series., 39, (1963).
Linares R.C., J.Appl.Phys., 33, 1749, (1962).
Lipson H., Prog.Met.Phy. 2,(Chalmers B.ed.Interscience 1950).
Lye R.G.,Hollox G.E. and Venables J.D., Proceedings Of The International Symposium on "Anisotropy in Single-Crystal. Refractory Compounds",eds.Vahldiek F.W.,Mersol S.A. (Plenum Press, New York, 1968).
Magnéli A., Acta.Cryst., 6, 495, (1953).
Marcinkowski M.J. and Miller D.S.,Phil.Mag.,6, 871,(1961).
Marcinkowski M.J., in "Electron Microscopy and Strength Of Crystals" (Thomas G. and Washburn J.eds.Interscience,1963).
Martin J.L.,Jouffrey B. and Costa P., Phys.Stat.Sol.22,349,(1967)
Mason D.R. and Cook J.S.,J.Appl.Phys. 32, 475, (1961).
Moss S.C.,Met.Soc.Conferences,36, Chicago, Feb. 1965,(Gordon and Breach, New York, 1966).
Nishiyama A. and Kajiwara S., Japan,J.Appl.Phys.2,478, (1963).
Okazaki A., J.Phys.Soc. Japan, 14, 112, (1959).
Parthé E. and Yvon K., Acta.Cryst., 826, 153, (1970).
Pfann W.G., "Zone Melting" (John Wiley,New York, 1959).
Precht W. and Hollox G.E. J.Crystal Growth, 3,818, (1968)
Rowcliffe D.J., Ph.D.Thesis University Of Cambridge, (1965).
Rowcliffe D.J. and Warren W.J.,J.Mat.Sci., 5, 345, (1970) .
Rudy E.and Brukl C.E., J.Am.Ceram.Soc., 50, 265, (1967).

Rudy E.,Windisch S. and Brukl C.E.,Planseever, 16, 3, (1968).
Ruedl E., Delavignette P. and Amelinckx S., Phys.Stat.Sol., 28, 305, (1968).
Sahashi T., Japan, J.Appl.Phys. 9, 1, (1970).
Santoro G., Trans. A.I.M.E., 227, 1361, (1967).
Sato H. and Toth R.S., "Alloying Behaviour and Effects in Concentrated Solid Solutions",Met.Soc.Conf.Vol.29, Cleveland, Ohio, 1963,(Gordon and Breach,New York,1965).
Sato H., Toth R.S. and Hongo G.,J.Phys.Chem,Solids,28,137,(1967).
Schottky W. and Wagner C.,Z.Physik.Chem.(Leipzig)B11,163(1930).
Silcock J.M. and Tunstall W.J.,Phil.Mag., 10, 361, (1964).
Steinitz R., in "Nuclear Applications Of Non-Fissionable Ceramics", Amer.Nucl.Socl., Illinois, 1966.
Storms E.K. and McNeal R.J.,J.Phys.Chem.,66, 1401, (1962).
Storms E.K., "The Refractory Carbides",(Academic Press,New York, 1967).
Schwartskopf P. and Kieffer R., "Refractory Hard Metals", (MacMillan, London, 1953).
Takahaski T.,Sugiyama K. and Itoh H.,J.Electro Chem.Soc., 117, 541, (1970).
Tanner L.E.,Clapp P.C. and Toth R.S.,Mat.Res.Bull.,3,855,(1968).
Thomas G. and Villagrana R.E., Acta.Met. 14,1633, (1966).
Thomas G. and Villagrana R.E., Phys.Stat.Sol., 9, 499, (1965).
Toth R.S. and Sato H.,J.Appl.Phys. 33, 3250, (1962).
Van Landuyt J. and Amelinckx S. Mat.Res.Bull, 5, 267, (1970).
Venables J.D., Phys.Stat.Sol., 15, 413, (1966).
Venables J.D. Phil.Mag., 16, 143, (1967).
Venables J.D.,Kahn D. and Lye R.G., Ibid, 18, 177, (1968).
Venables J.D., Ph.D.Thesis, University Of Warwick, 1970.
Volkova N.M., Gel'd P.V., and Alyamovskii S.I., Zh.Neorgan. Khim., 10, 1768, (1965).
Votava E. Acta.Met., 8, 901, (1960).
Votava E.,J.Inst.Metals, 90, 129, (1961).
Wadsley A.D., Revs.Pure and Appl.Chem. (Australia) 5,165,(1955).
Wadsley A.D., in "Non-Stoichiometric Compounds",(L.Mandelcorn ed. Academic Press, New York, 1964).
Warlimont H. and Thomas G., Met.Sci.Journal, 4, 47, (1970).
Watanabe D. and Fisher P.M.J.,J.Phys.Soc.Japan,20,2170,(1965).

Wantanabe D., Terasaki O., Jostsons A. and Castles J.R.,"The Mechanism of Phase Transformations In Crystalline Solids", Int.Symp.Inst.Metals,Manchester, P220, 1968.

Wenkus J.F., Haggerty J.S. and Lee D.W.,Tech.Report. APML-TR-68-228, Sept. 1968.

Westbrook J.H., "Mechanical Properties Of Intermetallic Compounds" (Wiley, New York, 1960).

Westbrook J.H.,"Intermetallic Compounds" (Wiley,New York,1967).

Westbrook J.H. and Stover E.R., in "High Temperature Materials and Technology"eds.Campbell I.E. and Sherwood E.M., (Wiley, New York, 1967.)

Whelan M.J. and Hirsch P.B.,Phil.Mag. 2, 1121, and 1303,(1957).

Williams W.S.J.Appl.Phys. 32, 552, (1961)

Williams W.S. Ibid, 35, 1329, (1964).

Williams W.S.,"International Conference on Semi-Metallic Compounds" Orsay France, 1965.

Williams W.S., Trans.Met.Soc. A.I.M.E., 236, 211, (1966)

Williams E.J. Proc. Roy.Soc., A152, 231, (1935).

Yvon K. and Parthé E., Acta.Cryst., B26, 149, (1970).

Zaplatynsky I., J.Am.Ceram.Soc., 49, 109, (1966).

Zubkov V.G., Dubrovskaya.L.Gel'd P.V. Iskhai Y.A. and Dorafeev Y.A., Dokl.Akad.Nauk.SSSR, 184, 874, (1969).